Development of a New Electrochemical Glycosensor for the Detection of the *Vibrio cholera*e Toxin

by

CARLOS GUILLÉN POSTEGUILLO



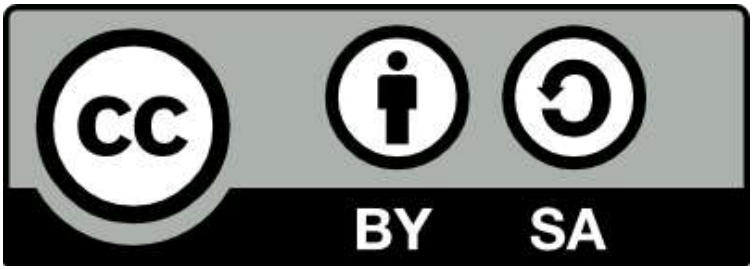
A thesis submitted to the University of Birmingham for the degree of
DOCTOR OF PHILOSOPHY

School of Chemistry
College of Engineering and Physical Sciences
University of Birmingham

April 2021

UNIVERSITY OF BIRMINGHAM

University of Birmingham Research Archive
e-theses repository



This unpublished thesis/dissertation is under a Creative Commons Attribution-ShareAlike 4.0 International (CC BY-SA 4.0) licence.

You are free to:

Share — copy and redistribute the material in any medium or format

Adapt — remix, transform, and build upon the material for any purpose, even commercially.

The licensor cannot revoke these freedoms as long as you follow the license terms.

Under the following terms:



Attribution — You must give appropriate credit, provide a link to the license, and indicate if changes were made. You may do so in any reasonable manner, but not in any way that suggests the licensor endorses you or your use.



ShareAlike — If you remix, transform, or build upon the material, you must distribute your contributions under the same license as the original.

No additional restrictions — You may not apply legal terms or technological measures that legally restrict others from doing anything the license permits.

Notices:

You do not have to comply with the license for elements of the material in the public domain or where your use is permitted by an applicable exception or limitation.

No warranties are given. The license may not give you all of the permissions necessary for your intended use. For example, other rights such as publicity, privacy, or moral rights may limit how you use the material.

Unless otherwise stated, any material in this thesis/dissertation that is cited to a third party source is not included in the terms of this licence. Please refer to the original source(s) for licencing conditions of any quotes, images or other material cited to a third party.

Abstract

Scarcity was during millennia the main concern to humans regarding food and water. Hunger and malnutrition are still a shameful reality of humankind but over 90% of the world's population has left this blight behind and human attention has shifted towards food quality. The most important feature of food quality is its safeness. And although most of us take the safety of what we eat and drink for granted, the World Health Organization estimates that every year hundreds of millions of people worldwide fall ill and near half a million die after ingesting poisoned food or water[1].

Pathogens are responsible for a majority of cases of foodborne diseases[2]. Many species of bacteria, capable of surviving outside the host for long periods of time, are especially dangerous[3]. Phenomena like climate change, increase in the consumption of processed food, world trade and the aging of the world population have only increased the risks of food/water biocontamination. Current methods to detect bacteria in food matrices have significant drawbacks, especially in the face of the challenges mentioned above. Electrochemical biosensors are an excellent alternative thanks to combining their high sensitivity with other features like simplicity, fastness, and portability.

Cholera, the illness caused by the bacterium *Vibrio cholerae*, is still a prevalent foodborne disease in some regions of the world. This thesis describes the efforts to develop a new electrochemistry biosensor based on saccharides to detect in water the toxin produced by *V. cholerae* and prevent cholera disease.

Abstract

Chapter 1 lays down the problem caused by cholera and the need to improve the detection of *V. cholerae*. It also explains the concept of electrochemical biosensors and includes examples of this technology to detect bacteria, in particular *V. cholerae*. **Chapter 2** sets the objectives of the thesis, while **Chapter 3** describes the principles of the experimental techniques used in this project.

The following four chapters constitute the experimental sections of the thesis *per se*. **Chapter 4** reports on the experimental procedures implemented and the chemicals used through the project. **Chapter 5** is devoted to synthesising small sulphur-containing hydrazide molecules to work as linkers between the sensor's transducer, a Au(poly) electrode, and the biorecognition element (BRE), a sugar. It also explains the difficulties of using these linkers to integrate both elements. In **Chapter 6** sulphur-containing polyhydrazides are employed as alternative linkers: following glycosylation with Gal and Lac, cyclic voltammetry (CV) demonstrates their successful adsorption on Au(poly) electrodes. Finally, **Chapter 7** describes the detection of cholera toxin subunit B (CTB) using Au(poly) electrodes modified with glycosylated polyhydrazides and different electrochemical techniques (*i.e.,* electrochemical impedance spectroscopy, EIS; and square-wave voltammetry, SWV). According to the preliminary results shown in this chapter, SWV would allow a qualitative detection of CTB in water whilst EIS also a quantitative analysis.

This text is completed with **Chapter 8**, which draws conclusions from the results obtained in previous chapters and discusses the next steps and future perspectives.

Abstract

This thesis demonstrates that polyhydrazides can be used as linkers to immobilise sugars on Au electrodes. It also shows some promising results to use this platform in electrochemical biosensors to detect the cholera toxin (CT).

A mi Familia

Acknowledgements

I would like to thank the people and institutions who accompanied and helped me through the challenge of doing a Ph.D. at the University of Birmingham. First, I want to express my gratitude to Dr. P. Rodríguez Pérez and Dr. F. Fernández Trillo for their supervision and help.

I also want to thank Prof. P. R. Unwin from University of Warwick and Prof. J. M. Feliu Martínez and Prof. E. Herrero Rodríguez from Instituto Universitario de Electroquímica (Universitat d'Alacant) for hosting me in their groups. These were privileged and a unique experiences for me, thank you very much.

I am also very grateful to Prof. C. Brett from Universidade de Coimbra for inviting me to his university in very complicated circumstances. It was a true pleasure to meet you and get engaged in regular discussions about the experiments and the way forward. It was also great to have the opportunity to know beautiful Coimbra and Portugal. Thank you so much, Professor Brett.

The PhD student colleagues, post-doctoral researchers and Master students I met in Birmingham, Warwick, Oxford, Alicante, Coimbra, and Leicester deserve an especial mention. Knowing you was the best part of my PhD experience, no doubt.

Finally, I would like to thank the BBSRC and the University of Birmingham for the MIBTP scholarship that allowed me to come to the UK to learn how to do research.

Acknowledgements

The people of Oxford University Innovation for their kindness and willingness to show me their work during my internship with them. The Royal Society of Chemistry for a research mobility grant to advance my project in Coimbra and a travel grant to show my work at the 2019 IUPAC Congress in Paris. And the people at the University of Birmingham, always eager to help with my experiments: Dr. Cécile Le Duff, Dr. Chi Tsang, Dr. Allen Bowden, and Dr. Louise Male.

Thank you very much All.

Table of Contents

List of Figures XI

List of Schemes XVIII

List of Tables XX

List of Abbreviations XXI

Chapter 1 : Introduction 1

1.1 Foodborne Disease 1

1.2 Bacteria and Food Safety 4

1.3 Current Detection of Bacteria in Food or Water 5

1.3.1 Cell Culture 5

1.3.2 Nucleic Acid-based Methods 6

1.3.3 Immunologically-based Methods 10

1.4 New Challenges for the Detection of Bacteria 12

1.5 Biosensors 13

1.5.1 Biorecognition Elements (BREs) 15

1.5.2 Transducers 23

1.5.3 Interfacing the BRE with the Transducer 26

1.6 Cholera 41

1.6.1 Historical and Geographical Remarks 41

1.6.2 The Cholera Disease 44

1.6.3 *Vibrio cholerae* Taxonomy 45

1.6.4 *Vibrio cholerae* Infection 46

1.6.5 Perspectives 57

Table of Contents

Chapter 2 : Aim and Objectives 59
2.1 Aim of the Thesis 59
2.2 Objectives 60
Chapter 3 : Experimental Electrochemical Techniques 61
3.1 The Electrochemical Cell 61
3.1.1. The Three-electrode Electrochemical Cell 63
3.2 The Electrochemical Process 64
3.2.1 Mass Transfer in Faradaic Electrode Processes 67
3.2.2 Non-faradaic Processes 69
3.2.3 A Microscopic Approach to Charge Transfer 71
3.3 Electrochemical Techniques 73
3.3.1 Voltammetry 74
3.3.2 Electrochemical Impedance Spectroscopy 79
Chapter 4 : Materials and Methods 85
4.1 Organic Chemistry 85
4.1.1 Chemicals and Materials 85
4.1.2 Methods of Compound Characterisation 87
4.1.3 Synthesis and Characterisation of Compounds 90
4.2 Electrochemistry 118
4.2.1 Chemicals and Materials 118
4.2.2 Instruments 119
4.2.3 Experimental Procedures 119

Chapter 5 : Synthesis of Small Molecular Linkers and Functionalisation of Polycrystalline Au Electrodes 123

5.1 Introduction 123

5.1.1 Galactose (Gal) as Biorecognition Element 125

5.1.2 Immobilisation of Gal on Electrodes 127

5.1.3 Self-assembled Monolayers (SAMs) Preparation 132

5.1.4 Electrode Conditioning 133

5.1.5 Electrochemical Characterisation 133

5.2 Results and Discussion 135

5.2.1 Asparagusic Acid as a Chemical Linker 135

5.2.2 3,3'-Disulfanediyldi(propanehydrazide) as a Chemical Linker . 140

5.3 Conclusions 170

5.4 Future work 171

Chapter 6 : Synthesis of Polymer Linkers and Functionalisation of Polycrystalline Au Electrodes with Galactose 173

6.1 Introduction 173

6.1.1 Polymers in Sensing 174

6.1.2 Glycopolymers 176

6.1.3 Synthesis of Glycopolymers 177

6.1.4 Glycopolymers with Gal and Lactose (Lac) 178

6.1.5 Modification of Au(poly) Electrodes with Gal 180

6.2 Results and Discussion 182

6.2.1 Modification of Au(poly) Electrodes with Poly(acryloyl) Hydrazide 182

6.2.2 Polymer Adsorption and Glycosylation with Gal 186

6.2.3 Post-polymerisation Glycosylation with Gal and Adsorption 189

6.2.4 Post-polymerisation Glycosylation with Lac and Adsorption 199

6.3 Conclusions 214

Table of Contents

Chapter 7 : Electrochemical Detection of the Subunit B of Cholera Toxin 217

7.1 Introduction 217

7.2 Results and Discussion 223

7.2.1 FcMeOH as Electrochemical Mediator 226

7.2.2 $[Fe(CN)_6]^{-3/-4}$ as Electrochemical Mediator 230

7.2.3 Optimisation of the Functionalisation of Au(poly) Electrodes with Glycosylated Poly(acryloyl) Hydrazide 232

7.2.4 Detection of Cholera Toxin Subunit B 236

7.3 Conclusions 243

Chapter 8 : Main Conclusions and Perspectives 245

8.1 Main Conclusions 246

8.2 Perspectives 248

References 251

List of Figures

Figure 1.1. Percentage of people practicing open defecation in the world in 2020 1

Figure 1.2. Human and economic costs caused by foodborne diseases (FBD).....3

Figure 1.3. Percentage of FBD cases in the UK in 2018 by pathogen 4

Figure 1.4. Steps to conduct PCR analysis on a DNA sample 9

Figure 1.5. Representation of an ELISA method in sandwich configuration.....11

Figure 1.6. Components and the general working mechanism of a biosensor.....14

Figure 1.7. Common monosaccharides found in vertebrates 18

Figure 1.8. General anomeric effect explained through Newman projections 20

Figure 1.9. Interaction between GBP proteins of a bacterium and saccharides.....22

Figure 1.10. Classification of electrochemical biosensors 25

Figure 1.11. Immobilisation methods of BREs on electrodes 27

Figure 1.12. Formation mechanisms of S-Au bonds in SAMs 34

Figure 1.13. Adsorption models of disulphides on Au electrodes.....35

Figure 1.14. Parts of a SAM 36

Figure 1.15. Examples of polymer molecules.....38

Figure 1.16. Examples of hydrazides 40

Figure 1.17. Images of *Vibrio cholerae* at different metabolic states. 42

List of Figures

Figure 1.18. Number of cholera cases in endemic countries in 2015 43

Figure 1.19. Classification of *Vibrio cholerae* strains 46

Figure 1.20. Stages of the *Vibrio cholerae* infection of humans 47

Figure 1.21. Representation of the human intestinal epithelium 48

Figure 1.22. Image of the glycocalyx of the capillary endothelium of a rat 49

Figure 1.23. Image of TCP pili from wild-type *Vibrio cholerae* 51

Figure 1.24. 3D crystal structure of the *Vibrio cholerae* toxin (CT) 53

Figure 1.25. Modes of CT penetration into host cells 54

Figure 3.1. Components of a basic electrochemical cell 62

Figure 3.2. Components of a three-electrode electrochemical cell 64

Figure 3.3. Model for an electrochemical double layer (EDL) 70

Figure 3.4. Mechanisms of electron transfer (ET): inner-sphere and outer-sphere mechanisms 72

Figure 3.5. Classification of electrochemical techniques used in electroanalysis 73

Figure 3.6. Electrical potential applied and voltammogram in CV 75

Figure 3.7. CV wave-shape and reversibility of electrochemical processes 76

Figure 3.8. Characteristic waveforms of several pulse voltammetry techniques 78

Figure 3.9. Randle equivalent circuit 81

Figure 3.10. Plots of EIS: Nyquist and Bode plots 82

List of Figures

Figure 4.1. TFA salt of 3,3'-disulfanediyldi(propanehydrazide) (DPA-HD) 99

Figure 4.2. HPLC chromatography of DPA-HD 100

Figure 4.3. ^{1}H-NMR spectrum of *tert*-butyl 2-acryloylhydrazinecarboxylate 105

Figure 4.4. ^{1}H-NMR spectrum of poly(*tert*-butyl-2-acryloylhydrazine-1-carboxylate) 107

Figure 4.5. GPC of poly(*tert*-butyl-2-acryloylhydrazine-1-carboxylate).....107

Figure 4.6. ^{1}H-NMR spectrum of poly(acryloyl hydrazide) (pAH_n).....109

Figure 4.7. GPC of pAH_n 109

Figure 4.8. GPC of *N'*-(2,3,5,6-tetrahydroxy-4-((galactopyranosyl)oxy)hexyl) poly(acryloyl) hydrazide.....117

Figure 5.1. Representation of the glycocalyx of a membrane cell 124

Figure 5.2. Interaction between saccharide units of GM1 and CTB 126

Figure 5.3. Integration of BRE and electrode with a chemical linker 130

Figure 5.4. Starting materials for the synthesis of chemical linkers for Gal 131

Figure 5.5. CV study of the electron transfer through a SAM of lipoic acid 136

Figure 5.6. XRD spectrum of 2,2-bis((tosyloxy)methyl)malonate 139

Figure 5.7. ^{1}H-NMR spectrum of DPA-HD.....141

Figure 5.8. CV study of the adsorption of hydrazides on Au surfaces.....143

Figure 5.9. Kinetics curve of DPA-HD adsorption on a sputtered Au surface obtained with *in situ* SEIRAS-ATR.....145

List of Figures

Figure 5.10. *In operando* ATR-SEIRAS spectra of the formation of a SAM of DPA-HD on a sputtered Au surface. 147

Figure 5.11. ATR-FTIR spectrum of acetohydrazide 148

Figure 5.12. CV on a SAM of DPA-HD..... 149

Figure 5.13. Comparison of the FTIR transmission and ATR-SEIRAS spectra of a sample of DPA-HD..... 150

Figure 5.14. ^{19}F-NMR spectrum of a sample of a TFA salt of DPA-HD 151

Figure 5.15. MS spectrum of the crude of the condensation product between DPA-HD and Gal..... 153

Figure 5.16. CV characterisation of a Au(poly) electrode modified with DMSO..... 154

Figure 5.17. ^{1}H-NMR spectrum of the DPA-HD crude product synthesised with HCl..... 156

Figure 5.18. ^{1}H-NMR spectrum of pure DPA-HD synthesised with HCl..... 157

Figure 5.19. ^{1}H-NMR spectra of the condensation reaction between DPA-DH and Gal at *ca.* 0 h. and 6 h..... 159

Figure 5.20. ^{1}H-NMR spectra of the condensation reaction between DPA-DH and Gal at *ca.* 0 h. and 6. h (low-field) 161

Figure 5.21. ^{1}H-NMR spectra of the condensation reaction between DPA-DH and Gal at *ca.* 0 h. and 6 h. (high field) 162

Figure 5.22. Yield calculation of the product of condensation between DPA-HD and Gal (DPA-HD-Gal)..... 164

Figure 5.23. TEM images of self-assembled bolaamphiphiles..... 166

List of Figures

Figure 5.24. ^{1}H-NMR spectrum of the reduction crude of DPA-HD-Gal 169

Figure 6.1. Drawbacks of using SAMs of small molecules for the integration of BREs with transducers 174

Figure 6.2. Recognition mechanism of a human cell by CT 175

Figure 6.3. General structure of pAH_n polymers 180

Figure 6.4. CV of a bare Au(poly) electrode in phosphate buffer (pH 7.4) 184

Figure 6.5. CV characterisation of a Au(poly) electrode modified with pAH_{20} 185

Figure 6.6. CV characterisation of a Au(poly) electrode modified with glycosylated pAH_{20} (Au-pAH_{20}-Gal) 188

Figure 6.7. ^{1}H-NMR spectra of the crude of the condensation between pAH_{50} and Gal using an excess of Gal (pAH_{50}-Gal_{33}) 191

Figure 6.8. CV characterisation of a Au(poly) electrode modified with the glycopolymer Au-pAH_{50}-Gal_{33} 193

Figure 6.9. CV characterisation of a Au(poly) electrode modified with Gal 194

Figure 6.10. ^{1}H-NMR spectra of the crude of the condensation between pAH_{50} and Gal using an excess of pAH_{50} (pAH_{50}-Gal_8) 200

Figure 6.11. CV study of a Au(poly) electrode modified with the glycopolymer pAH_{50}-Gal_8 198

Figure 6.12. ^{1}H-NMR spectra of the crude of the condensation between acetohydrazide and Lac (AcHD-Lac).....202

Figure 6.13. ^{1}H-NMR spectra of the crude of the reduction of AcHD-Lac with $NaBH_4$.....204

List of Figures

Figure 6.14. ^{1}H-NMR spectra of the crude of the reduction of AcHD-Lac with $PyBH_3$ 206

Figure 6.15. ^{1}H-NMR spectra of the crude of the reduction of AcHD-Lac with $Na(CN)BH_3$ 208

Figure 6.16. ^{1}H-NMR spectrum of the crude of the condensation between pAH_{50} and Lac (pAH_{50}-Lac_{15}) 210

Figure 6.17. ^{1}H-NMR spectrum of reduced pAH_{50}-Lac_{15} (pAH_{50}-RO-Gal_{15}) after purification 211

Figure 6.18. CV study of a Au(poly) electrode modified with the glycopolymer pAH_{50}-RO-Gal_{15} 213

Figure 7.1. Electrochemical mediators utilised in the thesis 218

Figure 7.2. Coordination between the hydrazide group and Fe 219

Figure 7.3. Origin of the analytical signal of the sensor of this thesis 221

Figure 7.4. Electrochemical characterisation of the redox couple $K_4Fe(CN)_6$ / $K_3Fe(CN)_6$ on a bare Au(poly) electrode 224

Figure 7.5. Electrochemical characterisation of the redox mediator FcMeOH on a bare Au(poly) electrode 225

Figure 7.6. Potential arrangements of a glycopolymer adsorbed on a Au(poly) electrode 227

Figure 7.7. Electrochemical study (CV and SWV) of the viability of using modified electrodes (Au-pAH_{50}-RO-Gal_{15}) with FcMeOH 228

Figure 7.8. Electrochemical effect of the interaction between FcMeOH molecules and carboxylic groups of a SAM 229

List of Figures

Figure 7.9. Electrochemical study (CV and SWV) of the viability of using modified electrodes (Au-pAH_{50}-RO-Gal_{15}) with $[Fe(CN)_6]^{-3/-4}$ 231

Figure 7.10. Effect of the functionalisation time of a Au(poly) electrode with pAH_{50}-RO-Gal_{15} on the $[Fe(CN)_6]^{-3/-4}$ response 233

Figure 7.11. SWV detection of CTB ($4.3 \cdot 10^{-5}$ M) with electrodes functionalised (Au-pAH_{50}-RO-Gal_{15}) at different times and $[Fe(CN)_6]^{-3/-4}$ 234

Figure 7.12. EIS detection of CTB ($4.3 \cdot 10^{-5}$ M) with electrodes functionalised (pAH_{50}-RO-Gal_{15}) at different times and $[Fe(CN)_6]^{-3/-4}$.....235

Figure 7.13. SWV and EIS detection of CTB ($4.3 \cdot 10^{-5}$ M) with a modified Au(poly) electrode (Au-pAH_{50}-RO-Gal_{15}) and $[Fe(CN)_6]^{-3/-4}$.....237

Figure 7.14. SWV and EIS detection of CTB at different concentrations with a modified Au(poly) electrode (Au-pAH_{50}-RO-Gal_{15}) and $[Fe(CN)_6]^{-3/-4}$ 238

Figure 7.15. SWV and EIS detection of CTB ($4.3 \cdot 10^{-5}$ M) with Au-pAH_{50}-Gal_{15} and $[Fe(CN)_6]^{-3/-4}$ after water incubation 240

Figure 7.16. SWV and EIS detection of CTB ($3.6 \cdot 10^{-9}$ M) with Au-pAH_{50}-Gal_{15} and $[Fe(CN)_6]^{-3/-4}$ after water incubation 241

Figure 7.17. Bode plot of the imaginary part of EIS experiments with Au-pAH_{50}-RO-Gal_{15} electrodes for the detection of CTB 242

List of Schemes

Scheme 1.1. Equilibrium of a hexopyranoside and the anomeric effect 19

Scheme 1.2. The glycosidic bond 21

Scheme 1.3. Hydrazone bond formation between hydrazide and aldehyde 41

Scheme 4.1. Synthetic route of asparagusic acid 90

Scheme 4.2. Preparation of diethyl 2,2-bis((tosyloxy)methyl)malonate 91

Scheme 4.3. Synthesis of diethyl 2,2-bis((acetylthio)methyl)malonate 94

Scheme 4.4. Synthetic route of DPA-HD 96

Scheme 4.5. Synthesis of di-*tert*-butyl 2,2'-(3,3'-disulfanediylbis(propanoyl)) bis(hydrazine-1-carboxylate) 97

Scheme 4.6. Preparation of DPA-HD 98

Scheme 4.7. Condensation reaction between DPH-HD and Gal 101

Scheme 4.8. Reaction conditions for the synthesis of DPH-HD-Gal 102

Scheme 4.9. General procedure for the preparation of pAH_n 103

Scheme 4.10. Preparation of *tert*-butyl 2-acryloylhydrazinecarboxylate 104

Scheme 4.11. Polymerisation conditions for the synthesis of poly(*tert*-butyl-2-acryloylhydrazine-1-carboxylate) (Boc-pAH_n) 105

Scheme 4.12. Preparation of pAH_n 108

Scheme 4.13. Post-polymerisation glycosylation of pAH_{20} with Gal 110

List of Schemes

Scheme 4.14. Post-polymerisation glycosylation of pAH_{50} with Gal 111

Scheme 4.15. Coupling of acetohydrazide with Lac and reduction 112

Scheme 4.16. Conditions for coupling acetohydrazide with Lac (AcHD-Lac).....113

Scheme 4.17. Reduction of AcHD-Lac to afford AcHD-RO-Gal 113

Scheme 4.18. Synthetic route of *N′*-(2,3,5,6-tetrahydroxy-4-((galactopyranosyl)oxy)hexyl) poly(acryloyl) hydrazide (pAH_{50}-RO-Gal) 115

Scheme 4.19. Coupling of Lac with pAH_{50} (pAH_{50}-Lac_{15}) 116

Scheme 4.20. Chemical reduction of pAH_{50}-Lac_{15} with $PyBH_3$.....116

Scheme 5.1. Transformation of organic acids into saccharide linkers.....128

Scheme 5.2. Interconversion of tautomers of Gal in aqueous media 129

Scheme 5.3. Two different strategies to attach Gal to a Au electrode.....134

Scheme 5.4. Representation of the S_N2 reaction mechanism 138

Scheme 5.5. Scheme of the reduction of DPA-HD-Gal with TCEP 167

Scheme 5.6. Alternative synthetic route to afford asparagusic acid 172

Scheme 6.1. Two different strategies for the synthesis of glycopolymers 178

Scheme 6.2. Different strategies to link Gal to pAH_n 179

Scheme 6.3. Different strategies to immobilise sugars (e.g. Gal) on a Au(poly) electrode using pAH_n as a linker.....181

List of Tables

Table 1.1. Main nucleic acid-based methods for detecting bacteria 7

Table 1.2. Principal immunological-based methods to detect bacteria 10

Table 1.3. Types of biosensors according to the nature of the BRE 16

Table 1.4. Physical methods of immobilisation of BREs on electrodes 28

Table 1.5. Chemical methods of immobilisation of BREs on electrodes 31

Table 1.6. Methods of immobilisation of BREs on electrodes with polymers 39

Table 4.1. XRD crystal data and structure refinement of diethyl-2,2-bis(tosyloxy)methyl)malonate 92

Table 4.2. Fractional atomic coordinates and equivalent isotropic displacement parameters of diethyl-2,2-bis(tosyloxy)methyl)malonate 93

Table 4.3. Reaction conditions attempted to synthesise diethyl 2,2-bis((acetylthio)methyl)malonate 95

Table 7.1. Physical and chemical characteristics of FcMeOH and $[Fe(CN)_6^{3-/4-}]$ 220

List of Abbreviations

AC	Adenylate Cyclase, Adenyl Cyclase, EC. 4.6.1.1
AcCN	Acetonitrile
AcHD	Acetohydrazide
AcHD-Lac	*N'*-(lactosyl)acetohydrazide
AcHD-RO-Gal	*N'*-(2,3,5,6-tetrahydroxy-4- -((galactopyranosyl)oxy)hexyl)acetohydrazide
ADP	Adenosine Diphosphate
ATP	Adenosine Triphosphate
ATR	Attenuated Total Reflectance
Au(poly)	Polycrystalline Gold
Boc	*tert*-Butyloxycarbonyl Protecting Group
Boc-pAH	Poly(*tert*-butyl-2-acryloylhydrazine-1-carboxylate)
BRE	Biorecognition Element
BSA	Bovine Serum Albumin
cAMP	Cyclic Adenosine Monophosphate
$CHCl_3$	Chloroform
CFTR	Cystic Fibrosis Transmembrane Conductance Regulator
CT	Cholera Toxin (Choleragen)
CTA	Cholera Toxin Subunit A
CTB	Cholera Toxin Subunit B
CV	Cyclic Voltammetry
DCM	Dichloromethane
DMF	Dimethylformamide
DMSO	Dimethyl Sulphoxide
DMSO-d_6	Deuterated Dimethyl Sulphoxide
D_2O	Deuterated Water
DP	Degree of Polymerisation
DPA	3,3'-Dithiodipropionic Acid
DPA-HD	3,3'-Disulfanediyldi(propanehydrazide)

List of Abbreviations

DPA-HD-Gal	D-Galactose 3,3'-Disulfanediyldi(propanehydrazone)
EDC	Ethyl-dimethyl-aminopropylcarbodiimide Hydrochloride
EDL	Electrochemical Double Layer
EIS	Electrochemical Impedance Spectroscopy
ER	Endoplasmic Reticulum
ET	Electron Transfer
Et_2O	Diethyl Ether
EtOAc	Ethyl Acetate
FBD	Foodborne Disease
FcMeOH	Ferrocenemethanol
Gal	Galactose
GBP	Glycan-binding Proteins
GDP	Guanosine Diphosphate
GM1	Monosialotetrahexosylganglioside
GPCR	G-protein-coupled Receptor
GTP	Guanosine Triphosphate
LA	Lipoic Acid, (±)-5-(1,2)Dithiolan-3-yl-pentanoic Acid, Thioctic acid
Lac	Lactose
$NaBH_4$	Sodium Borohydride
$NaBH_3CN$	Sodium Cyanoborohydride
pAH	Poly(acryloyl) Hydrazide
Py	Pyridine
$PyBH_3$	Borane Pyridine Complex
RAFT	Reversible Addition-fragmentation Chain Transfer Polymerisation
SAM	Self-assembled Monolayer
SEIRAS	Surface-enhanced Infrared Absorption Spectroscopy
SWV	Square Wave Voltammetry
TCEP	Tris(2-carboxyethyl)phosphine Hydrochloride
TCP	Toxin-coregulated Pilus
TFA	Trifluoroacetic Acid

List of Abbreviations

THF	Tetrahydrofuran
VA-044	2,2′-Azobis[2-(2-imidazolin-2-yl)propane] Dihydrochloride

Chapter 1

Introduction

1.1 Foodborne Disease

Human life is sustained upon four basic physiological activities: breathing, sleeping, eating/drinking, and excreting. In regard to significant progress been made in the last decades, today *ca.* 20% of the world population lack basic sanitation services, with 890 million practising open defecation **(Figure 1.1)**: they excrete outdoors (in the fields, bushes, rivers, canals, open bodies of water, beaches, and other open spaces) exposing themselves to infectious disease. Besides, more than 800 million do not have access to enough food or water[4]. These problems are concentrated in certain parts of Africa, Asia, and Latin America.

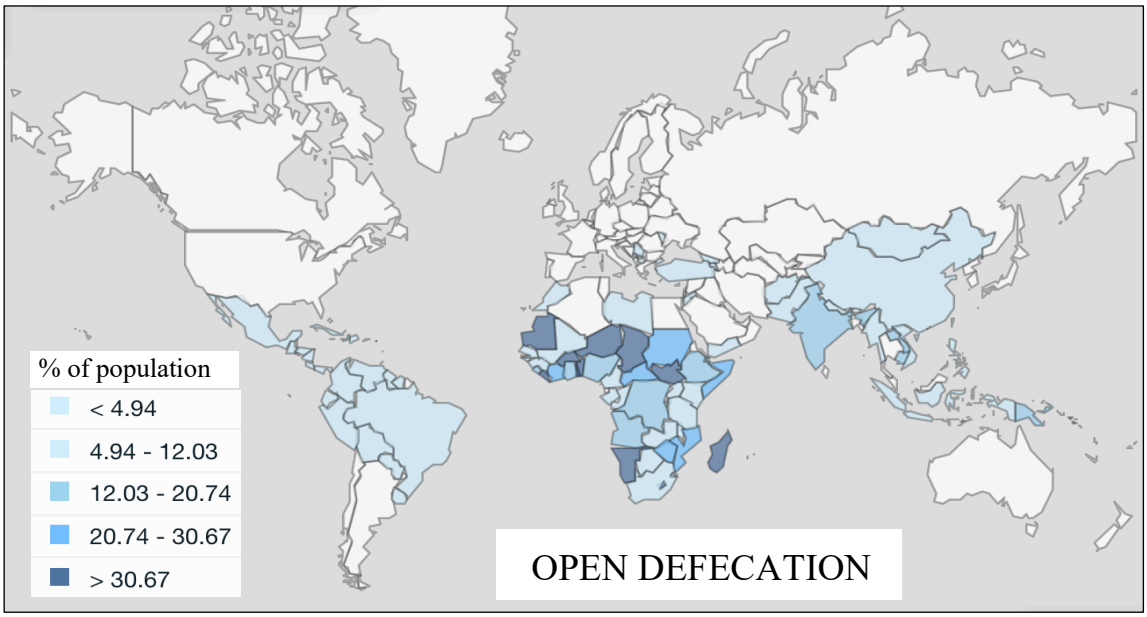


Figure 1.1. Map with the percentage of people practicing open defecation in the world in 2020 according to The World Bank[5].

Another issue related to food and water consumption affects every person on the planet: foodborne diseases (FBD). Humans can suffer from disease after ingesting food or water due to the presence of pathogens (bacteria, viruses, fungi, parasites), toxins, prions, chemicals, radioactivity or even physical agents[6]. According to the World Health Organization (WHO) near 1 in 10 people fall ill and around 400,000 die every year after being poisoned with food or water[1]. People with weakened immune systems -*i.e.* infants, young children, pregnant women[7] and old adults[8]- are most at risk[9], with children accounting for almost one-third of all deaths[10]. This is not only a concern in countries with weak health systems; estimates in the UK set at more than 500,000 per year the number of cases of FDB caused by known pathogens, more than 2 million overall[11-13]. These figures are just approximations since many individuals do not seek medical treatment and sometimes it is difficult to fully assess the contribution of consumption of poisoned food in chronic illnesses such as liver and kidney failure or cancer[9].

The impact of FBD does not only affect the wellbeing of individuals; it hinders the socio-economic development of populations with school and work absence and medical care costs[14, 15] **(Figure 1.2)**. Moreover, key economic sectors in many countries -*e.g.* tourism, agriculture, food industry and trade- are especially exposed to FBD[16]. Furthermore, contamination of food or water with microorganisms or their toxins can be used for terrorist purposes[17].

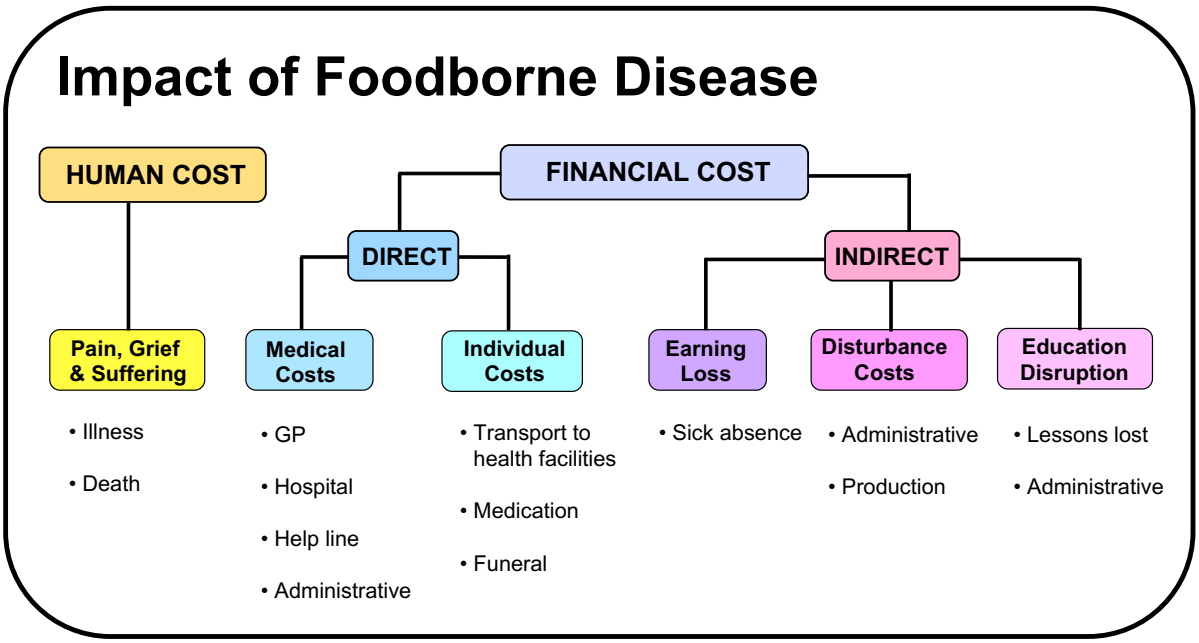


Figure 1.2. Diagram showing the human and economic costs caused by FBD[18]. Besides a human cost resulting from the worsening of an individual's wellbeing, FBD have a profoundly negative economic effect, either directly (medical and funeral costs) or indirectly (disturbance of educational and productive activities).

Food safety can be described as the 'activities to protect the food supply from microbial, chemical, allergenic and physical hazards that may occur during all stages of food production and handling'[19]. In most countries, local, regional and national infrastructures exist to guarantee food safety, like the Foods Standards Agency[20] (FSA) in the UK or the Food and Drug Administration[21] (FDA) in the USA. Globalisation, with a fast increment of the movement of people, goods and services, has also prompted the emergence of international food safety organisms like the European Food Safety Authority[22] (EFSA) in the EU.

1.2 Bacteria and Food Safety

One of the main vectors of foodborne illness are bacteria[23-25] **(Figure 1.3)**.

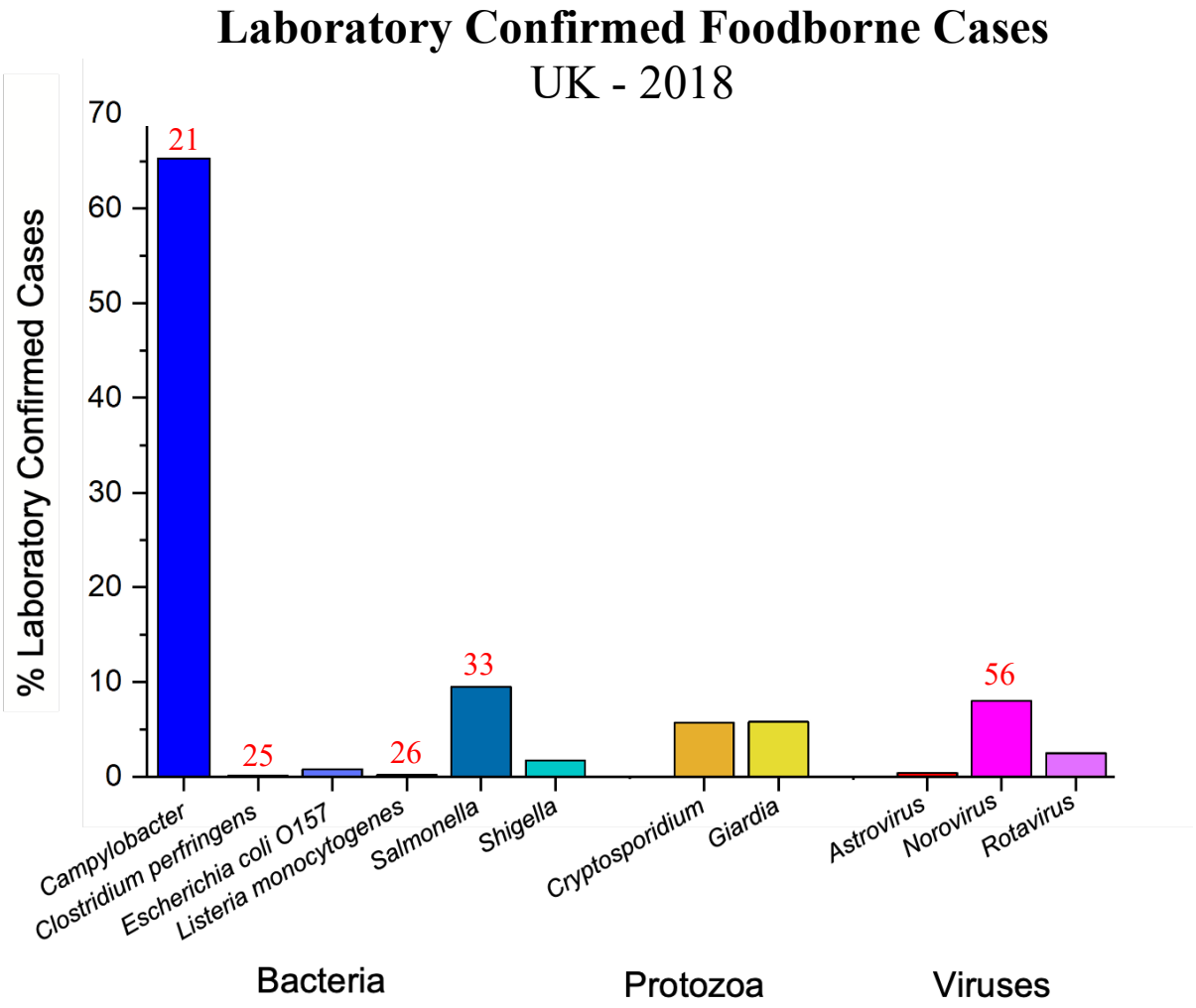


Figure 1.3. Percentage of FBD cases in the UK in 2018 by pathogen[26] and estimation of the yearly number of deaths (red figures on top of columns) caused by some key microorganisms dangerous to humans[27].

In the UK, *Campylobacter* bacteria, present in raw or undercooked meat and unpasteurised milk[28], is the leading cause of foodborne poisoning with more than 250,000 cases reported per year[29]. *Salmonella* (undercooked meat, raw eggs and dairy products) and *Escherichia coli* O157 (undercooked beef in mince, burgers,

meatballs and unpasteurised milk) cause the highest number of hospitalisations due to FBD[28]. *Listeria monocytogenes*, found in chilled, 'ready-to-eat' foods (like sandwiches) is a threat for people with weak immune systems causing death in the elderly and miscarriage in pregnant women[28, 30]. In developing countries, cholera, caused by the ingestion of water or food contaminated with the pathogen *V. cholerae* (strains *O1* or *O139*), is a primary vector of FBD.

1.3 Current Detection of Bacteria in Food or Water

Because of the importance of food safety, there has been a constant effort to improve the detection methods of pathogens in food and water. However, the detection of bacteria in food matrices presents significant challenges of sensitivity -a single pathogenic individual can cause disease- and specificity -the components of food, including other non-dangerous microorganisms, can act as interferents[31, 32]. The conventional methods for detecting foodborne pathogens are cell culture, nucleic acid-based methods, and immunological-based methods.

1.3.1 Cell Culture

The gold standard methods for bacterial detection in food and water, including *V. cholerae*[33], are based on cell culture[34]. They consist of leaving a potentially contaminated sample under ideal bacterial growth conditions and waiting to see if microorganisms develop. These methods overcome the beforementioned issues of sensitivity and specificity.

Nevertheless, although reliable, they present essential drawbacks. For example, the detection turnaround is too long (at least 1 to 3 days), which increases the risk of the spread of outbreaks. In addition, the process is laborious and requires specialised facilities making it impossible for an ideal point-of-care (POC) analysis. Finally, bacteria are not detectable if in their inactivation phase[35, 36].

These shortcomings are significant when pathogenic outbreaks occur in isolated or economically deprived areas[37] with a lack of robust health systems, as is the case of cholera disease[38, 39]. However, there are alternative methods to reduce the time of analysis[40-42], the so-called molecular methods[43] or rapid methods[31]. They can be divided into nucleic acids-based methods and immunological-based methods.

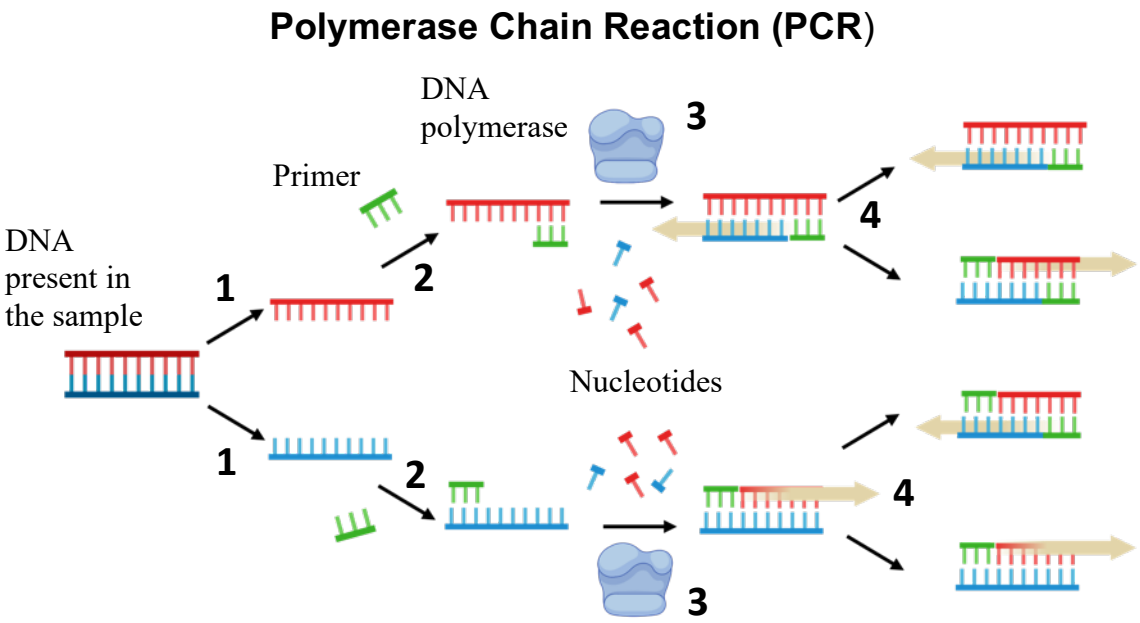
1.3.2 Nucleic Acid-based Methods

Nucleic acid-based methods **(Table 1.1)** detect bacteria -and other pathogens like viruses- through the presence of their genetic material in a sample.

Table 1.1. Main nucleic acid-based methods for detecting bacteria and their principle advantages and disadvantages.

Nucleic acid-based Methods	Advantages	Disadvantages
Simple PCR and Multiplex PCR	High sensitivity High specificity Reliable Automated	Expensive Non-portable Affected by PCR inhibitors Difficult to distinguish viable from non-viable cells
Real-time PCR	High sensitivity High specificity Reliable Automated Reproducible High speed Real-time analysis	Expensive Non-portable Difficult to distinguish viable from non-viable cells Affected by PCR inhibitors Requires expertise Potential cross--contamination
NASBA	Sensitive Specific Low cost	Requires viable organisms Complex (handling of RNA)
LAMP	High sensitivity High specificity Low cost Easy to operate	Complex (primer design)
Oligonucleotide DNA microarray	High sensitivity High specificity Simple Multiple pathogen detection	Expensive Requires expertise Complex Difficult to distinguish viable from non-viable cells

The most popular of them, polymerase chain reaction (PCR), uses the enzyme DNA polymerase to amplify the DNA of the microorganism **(Figure 1.4)**; the amplified DNA can then be detected with different techniques, for instance, staining with ethidium bromide and using electrophoresis[44]. PCR has been used to detect bacteria in food and water[45], including cholera[46]. Some examples of upgraded PCR that offer faster, more sensitive and specific analysis[31] are multiplex PCR[47] (mPCR) and real-time or quantitative PCR[47] (qPCR). Nucleic acid sequence-based amplification[48] (NASBA), loop-mediated isothermal amplification[49, 50] (LAMP), and oligonucleotide DNA microarray[51] are other nucleic acid methods utilised to detect bacteria. However, all present at least a substantial disadvantage: the inhibition of the enzyme in the case of PCR-based methods, a high price, expensive equipment, need of technical personnel, laborious preparation of samples (*e.g.* extraction of nucleic acids from a sample) and others[40].



Step 1: denaturation of DNA (95-96 ˚C)
Step 2: annealing (68 ˚C)
Step 3: elongation (72 ˚C)
Step 4: 20-40 repetitions of the 1-2-3 cycle

Figure 1.4. Steps to conduct PCR analysis on a DNA sample. In **Step 1** the two strands of the DNA double helix are separated by denaturation after applying high temperature. During **Step 2** the temperature is lowered and DNA primers are added to bind to the DNA strands (templates) obtained in the previous step. A DNA polymerase is added in **Step 3** to produce the complementary strands of the templates from the primers. **Step 4**, the last step, consists of a series of repeats of the three previous stages until enough genetic material is obtained for analysis (*e.g.* staining it with ethidium bromide and electrophoresis).

1.3.3 Immunologically-based Methods

Immunologically-based methods **(Table 1.2)** depend on the interaction between an antigen and its correspondent antibody.

Table 1.2. Principal immunological-based methods to detect bacteria and their advantages and disadvantages.

Immunological-based Methods	Advantages	Disadvantages
ELISA	Sensitive Automated Allows bacterial toxin detection	Low sensitivity False negatives Lack of specificity Requires expertise Complex
Lateral flow immunoassay	Low cost Sensitive Specific Easy to operate	Reliability issues

Enzyme-linked immunosorbent assay[52, 53] (ELISA) is the preferred amongst the immunologically-based methods to detect foodborne pathogens **(Figure 1.5)**. However sensitive and selective, ELISA requires trained personnel, specialised and expensive equipment and it is challenging to prepare a test[40, 54, 55].

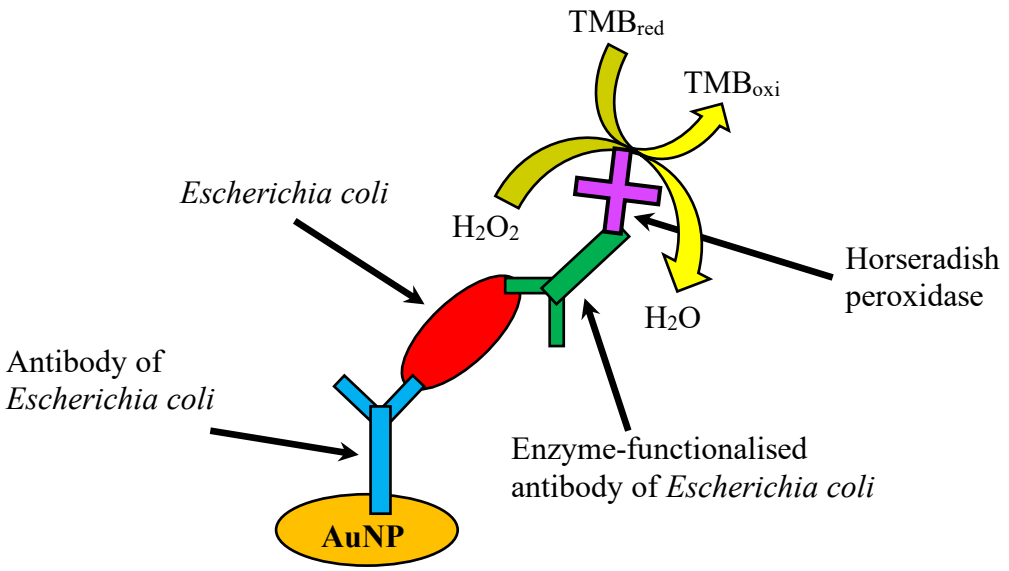


Figure 1.5. Schematic representation of an ELISA method in sandwich configuration[56]. A sample is put into contact with antibodies (blue) immobilised on a support (*e.g.* Au nanoparticles, AuNP). If the antigen is present in the sample (*e.g. E. choli*), it interacts with the antibodies allowing a second antibody (green) carrying an enzyme (*e.g.* horseradish peroxidase) to attach. The analytical signal is obtained measuring the product of an enzymatic reaction, in this case the oxidation of 3,3',5,5'-tetramethylbenzidine (TMB), in the presence of hydroxide peroxide (electron receptor).

Immunochromatographic methods, also known as lateral flow analysis[57], have circumvented some of these problems but at the cost of being less sensitive[58]. Moreover, if the matrix is complex, a pre-treatment of the sample requires labour-intensive work and equipment[59, 60]. Both ELISA and immunochromatographic methods, though, have been used to detect *V. cholerae*[61, 62].

Nucleic acid-based methods and immunologically-based methods significantly improve bacterial detection in food and aqueous matrices, especially by reducing the

turnaround. But although efficient and reliable, they have serious drawbacks[40] as shown during the Covid-19 pandemic in early 2020: they are complex[63], or expensive[64], or need specialised personnel and equipment[65] or lack sensitivity[58]. Therefore, if not impossible, their use is difficult in those regions most in need of advancing food and water safety, like developing countries and isolated areas. Furthermore, they are not helpful for applications where real-time and POC are priorities like food industry[66], healthcare[67] and defence[68].

1.4 New Challenges for the Detection of Bacteria

In the last decades, new phenomena have risen the threat to food safety, making necessary an upgrade of currently available methods. For example, the fast-growing and fast-ageing world population[9] augments the number of most vulnerable people, increasing the need for POC analysis. Since the 1980s urbanisation has worsened the situation with the formation of slums with poor water and food safety infrastructures that favour the emergence of FBD. In better-off city areas, the dependence on agribusiness (industrialisation of farming) can also result in the spread of this type of diseases[69]. Besides, the widespread use of antimicrobials in industrial agriculture[70] has increased the resistance of these microorganisms, making them a growing threat to food safety.

Globalisation[71] has been a game-changer in food consumption and poses a new threat regarding FBD. The food we put on our plates comes today from anywhere in the world, with severe implications to food safety like differences in quality controls in

origin and destiny countries; or more vulnerable food chains prone to contamination during transport. Furthermore, there is a change in the consumption habits: pre-processed, frozen and on-the-way foods are becoming prevalent and they are more susceptible to being infected by microorganisms[72, 73].

Climate change[74-76] is a considerable risk to food safety for many reasons. For a start, the increase of temperatures is forcing the review of food chain procedures to avoid contamination and also expanding the areas of the planet where pathogens thrive[77]. Besides, a higher number of natural disasters will put food chains and water supplies under strain, as happened in Mozambique in 2019 when the cyclone Idai ravaged the water infrastructure of the city of Beira[78].

These new factors have intensified the necessity to develop bacterial detection methods that are fast and reliable in terms of sensitivity and selectivity; but also simple to use, reproducible, reusable[79], robust, inexpensive and portable so they facilitate a broader use and the possibility of being employed whenever and wherever needed. This would particularly benefit populations at high risk in developing countries, isolated areas, regions affected by natural disasters, countries engulfed in violent conflicts; and also food production centres, food distributors and food retailers.

1.5 Biosensors

Biosensors are sensing devices with two main components: at least one biological or biological-derived element (*e.g.* a saccharide, nucleic acid, protein,

enzyme, cell, tissue), called biorecognition element (BRE) or bioreceptor; and a transducer[80]. The interaction between the BRE and an analyte produces a physicochemical change that is transformed by the transducer into a measurable signal, *e.g.* an electrical one. Then, the measurable signal is processed to generate a useful display for its interpretation **(Figure 1.6)**[81, 82].

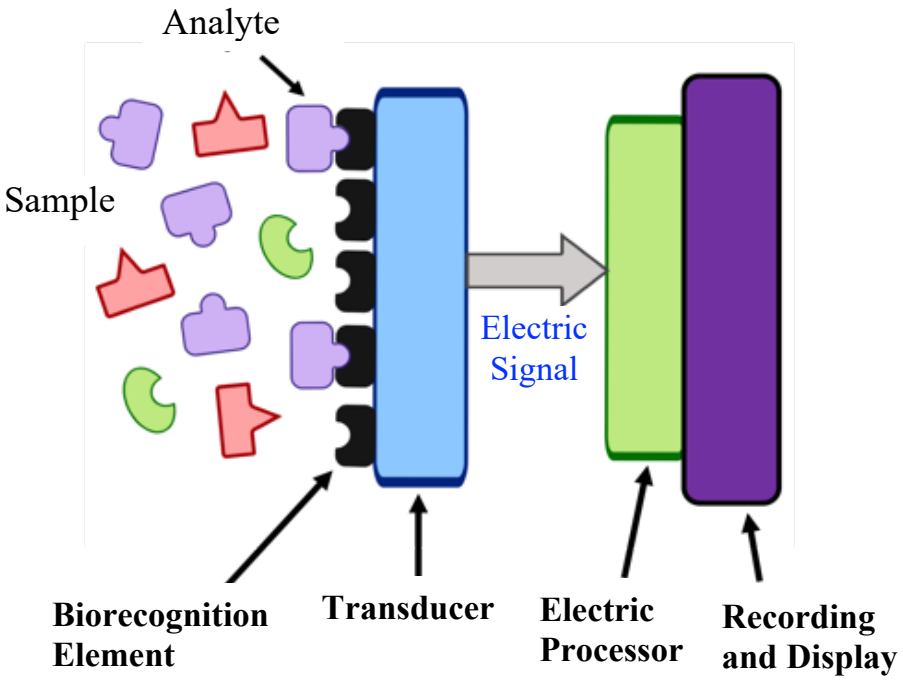


Figure 1.6. Essential components and the general working mechanism of a biosensor. In a biosensor, a BRE highly specific towards the analyte is immobilised on a transducer connected to an electric processor. The interaction between BRE and analyte generates a physicochemical change transformed into an electrical signal by the transducer and displayed as interpretable information following its treatment by the electric processor.

Since the 1980s there has been a growing interest in biosensors as analytical tools[83]. Already well established in clinical analysis, they have started to make inroads in other fields like environmental or food and water analysis, including sensing

microorganisms[84, 85]. Their potential in terms of sensitivity, fastness, simplicity, low cost, robustness, stability, portability, miniaturisation or simplification/elimination of sample preparation makes them an excellent alternative to previously commented methods[86].

1.5.1 Biorecognition Elements

The BRE is the principal component of a biosensor, ultimately defining the device's main capacities and overall design. Since the employment of an enzyme in the first biosensor[87], the list of BRE has continuously grown: small organic molecules, nucleic acids, proteins, lectins, saccharides, peptides, antibodies, polymers, organelles, tissues, whole cells, phages, and more. Biosensors can be classified according to the nature of this element **(Table 1.3)**.

Table 1.3. Types of biosensors according to their BRE and examples. The examples include the detection of the cholera toxin subunit B (CTB), an algae neurotoxin that accumulates in shellfish, sardines and anchovies (domoic acid), the neurotoxin tetrodotoxin[88] (present in some fish) and the botulinum neurotoxin type A (BoNT/A).

Type of Biosensor	BRE	Analyte	Reference
Immunosensor	Antibodies	CT	Chiriacò *et al.*[89] Khan *et al.*[90]
Genosensor	Nucleic acids	*V. cholerae (O1 and O139)*	Yu *et al.*
Aptasensor	Aptamer	CT	Bruno *et al.*[91]
Molecularly imprinted	Molecularly imprinted polymers	Domoic acid	Kubo *et al.*[92]
Enzymatic	Urease	Urea	Lakard *et al.*
Glycosensor	Saccharide	CTB	Jeong *et al.*[93]
Lipid-based	Lipid	CT CT CT	Tark *et al.*[94] Viswanathan *et al.*[95] Pan *et al.*[96]
Tissue-based	Tissue	Tetrodotoxin	Cheun *et al.*[97]
Cell-based (CBB)	Cell	CT	Lin *et al.*[98]
Peptide-based	Peptide	BoNT/A *Listeria* cells	Frisk *et al.*[99] Tolba *et al.*[100]

A priori, selectivity is the most important quality for a BRR. However, the final performance of a biosensor depends on many other factors that can make a highly selective BRE not the best option. For example, antibodies are amongst the most selective molecules in nature and have been used to detect FBD like cholera. Nevertheless they are expensive[101] and biosensors based on them are challenging to produce due to immobilisation and orientation issues[102, 103].

A. Saccharides

Saccharides, also known as carbohydrates or sugars, constitute one of the four classes of organic biomolecules together with proteins, nucleic acids, and lipids. They are the most ubiquitous and cellulose, a linear polymer of glucose, is the most abundant organic material on Earth[104].

The chemical composition of saccharides is homogeneous with most sugars containing only carbon, hydrogen and oxygen[105]. However, their structural diversity[106] and their association with other biomolecules (*i.e.* lipids, proteins) confer them critical roles in many biological functions such as energy supply, structural, cell recognition, cell signalling or immunology[107-110]. Saccharides are divided into monosaccharides **(Figure 1.7)**, oligosaccharides (up to ten monosaccharides linked by glycosidic bonds) and polysaccharides or glycans (more than ten monosaccharides joined by glycosidic bonds). All monosaccharides contain one carbonyl group, either an aldehyde (aldoses) or a ketone (ketoses); and at least one asymmetric carbon (except for dihydroxyacetone)[111]. Much of the enormous diversity of monosaccharides is due to the presence of chiral centres: 250 monosaccharides have been discovered in nature, almost all of them pentoses or hexoses[112].

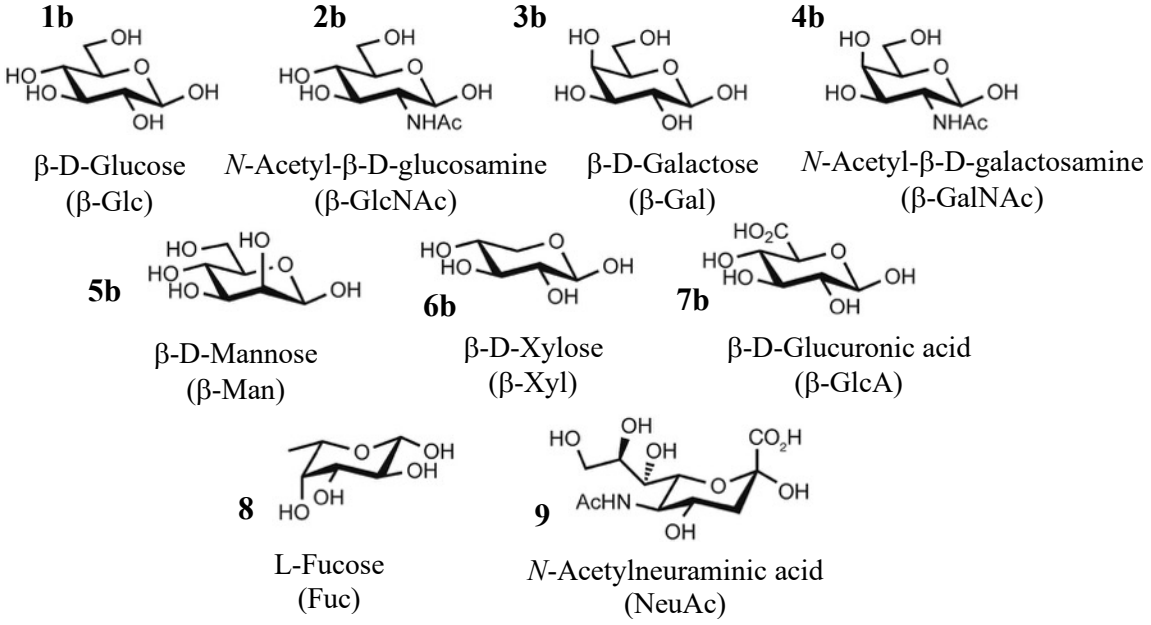
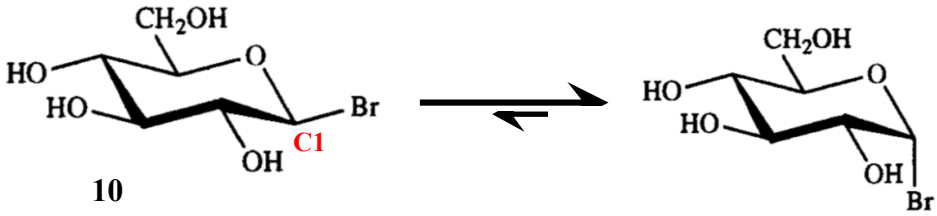


Figure 1.7. Some of the most common monosaccharides found in vertebrates shown in their cyclic form[113] (only one stereoisomer); NeuAc is the most common form of sialic acid. Most of these sugars are pentoses and hexoses and their chemical composition is almost exclusively made of C, H and O.

The cyclisation in aqueous media of monosaccharides of six or more carbons into rings of five or six atoms is paramount to explaining their physical and chemical properties. The rings are generated after one hydroxyl group of the open chain reacts with the carbonyl carbon, which becomes a new chiral centre and is called anomeric carbon. The cyclisation generates two hemiacetals, the conformers α and β. The instability of the cyclic forms makes the reaction reversible and the equilibrium between open and closed isomers is reached. This phenomenon is known as mutarotation[111]. The chemistry of the anomeric carbon is strongly influenced by the anomeric effect[114], originally described by the IUPAC as 'the thermodynamic preference for polar groups bonded to C1 (the anomeric carbon of a glycopyranosyl derivative) to take up an axial position'[115] **(Scheme 1.1)**.



Scheme 1.1. Equilibrium between two isomers of a hexopyranoside (**10**) with a polar group (Br) on carbon C1 (anomeric carbon)[115]. Due to the anomeric effect, a stereoelectronic effect, unfavourable Coulombic interactions between the unshared electrons of the ring O and the polar group Br force the latter to predominantly occupy the axial position.

This arrangement is contrary to the general chemical principle for which the most stable configuration of a non-conjugated six-member ring presents the substituent groups on equatorial position to avoid the steric hindrance between them when located in axial position. An axial orientation of the polar group on C1 (Br) would avoid electrostatic repulsive forces appearing between unshared electrons of the ring oxygen and the polar group. However, the phenomenon is not limited to the anomeric carbon of saccharides. A generalised anomeric effect has been described for the preference of gauche (synclinal) over antiperiplanar conformations in molecules with a C-X-C-Y segment, where X is an element with lone pairs of electrons and Y is a highly electronegative atom (*e.g.* O, N, halides)[115, 116] **(Figure 1.8)**. Although mainly explained by the accumulation of negative density of charge and the occurrence of Coulombic repulsive interactions, the anomeric effect is very complex and other factors must be considered for a complete explanation[117].

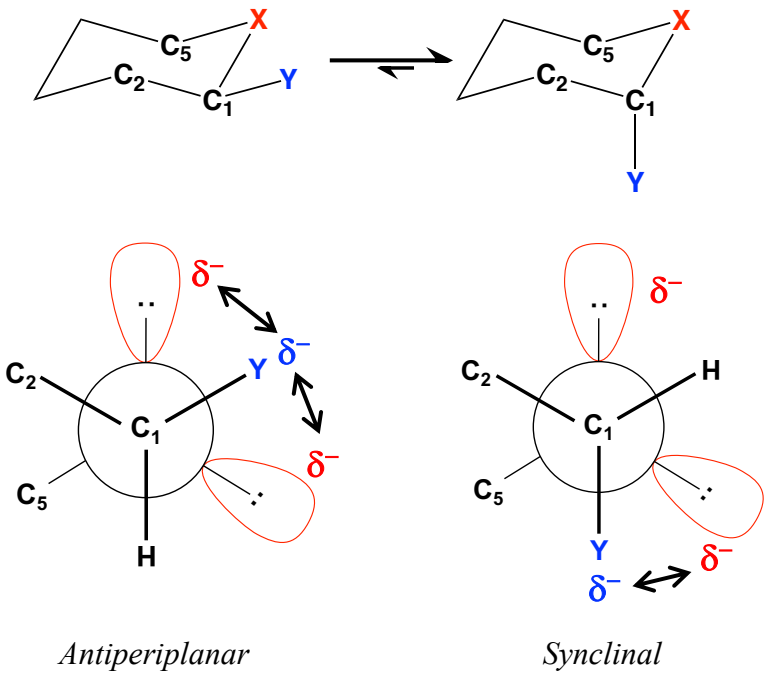
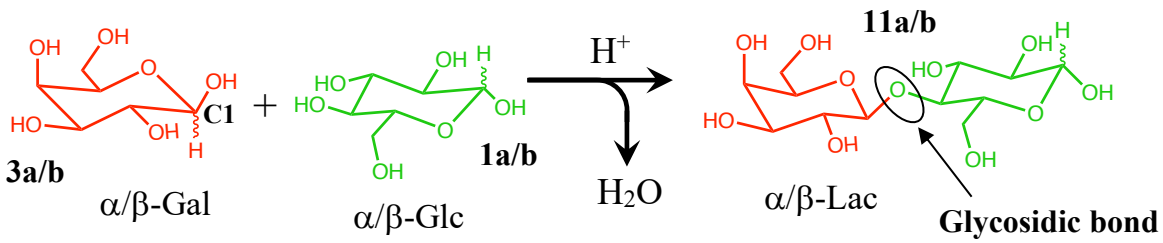


Figure 1.8. General anomeric effect explained through Newman projections. The initially more stable antiperiplanar conformation with the group **Y** occupying an equatorial orientation (left) is disfavoured due to more Coulombic repulsions (double arrows) between the cloud of electrons of **Y** (δ^-) and the unshared electrons of **X** (δ^-).

If the number of natural monosaccharides is enormous considering the limited number of elements of their composition and small carbon backbone, the bonding between them through the glycosidic bond **(Scheme 1.2)** explains the huge diversity of sugars. This bond, the essential linkage in all polysaccharides, forms when a hydroxyl group from one saccharide binds to the anomeric carbon (aldehyde or ketone) of another. Thus, in general, the bond and chemistry of glycans are deeply influenced by the early explained anomeric effect. Glycosidic bonds also form when the hydroxyl group pertains to another type of molecule, including biomolecules like proteins[118].



Scheme 1.2. Glycosidic bond between galactose (Gal) and glucose (Glc) to produce the disaccharide lactose (Lac)[113]. During the condensation reaction, the hydroxyl group of the anomeric carbon (C1) of Gal is lost as a water molecule due to the nucleophilic attack on C1 of a hydroxyl group of Glc and the formation of an acetal.

The involvement of many saccharides in functions like cell recognition, adherence and signalling, where they act as highly specific cellular receptors for other molecules, makes them attractive as BRE. Particularly abundant are glycan interactions with proteins called glycan-binding proteins (GBP)[119]. GBPs can be intrinsic, if they bind saccharides from the same organism, including sometimes from the same cell; or extrinsic, when the carbohydrate pertains to a pathogen or symbiont[107]. These interactions can be particularly useful for the design of biosensors for the detection of pathogens because many of them use saccharides as a target of the host cells **(Figure 1.9)**.

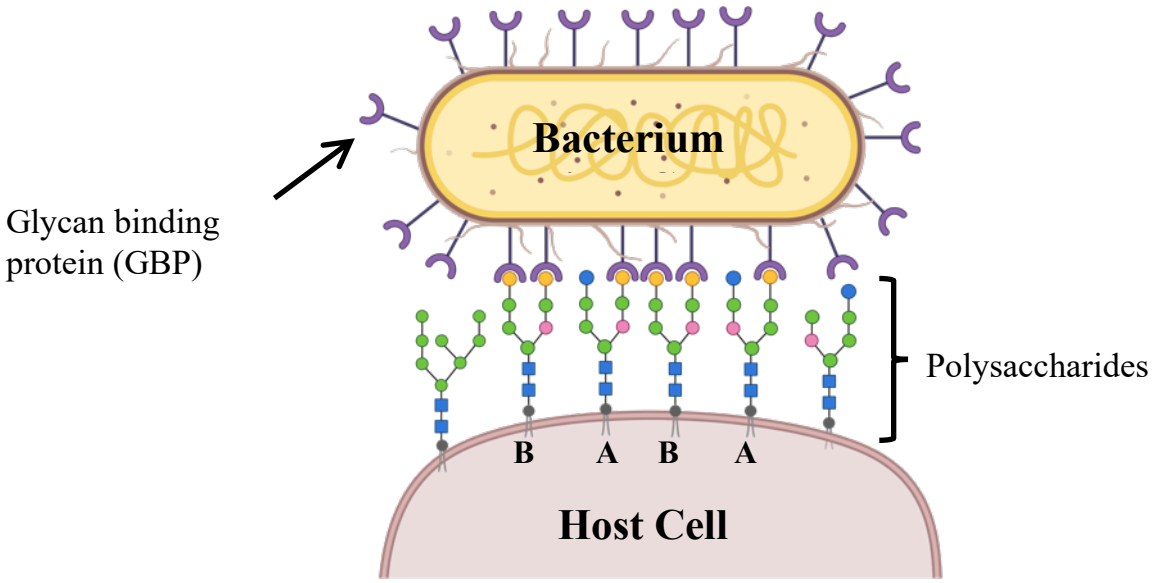


Figure 1.9. Interaction between the GBP proteins of a bacterium and the saccharides of a host cell. The interactions can be monovalent **(A)**, with a single protein binding a saccharide; or multivalent **(B)**, where various proteins bind the same sugar at a time[120].

The interaction is usually mediated by microbial GBPs, for example lectins containing a carbohydrate-recognition domain (CRD) for binding[111]. Bacterial lectins are commonly known as adhesins because of this function. Various bacterial toxins also depend on glycans to lock onto the cell membrane and start internalising their infectious domains, like CT of *V. cholerae* and the Shiga toxin of *Shigella dysenteriae*[121]. The normally low affinity of this type of interaction is compensated with multivalent binding[111].

Beyond the specificity of saccharides towards pathogens or their virulent agents, these biomolecules present multiple characteristics that give them an edge over other BRE. For instance, they are cheap and easy to obtain, a fundamental characteristic to develop a sensing platform aiming for wide use. They are also robust, important in

terms of durability and reproducibility; and are relatively easy to transform chemically and work with, essential to facilitate their incorporation into transducers.

Independently of the nature of the BRE, though, its final performance will be highly dependent on its integration with a transducer.

1.5.2 Transducers

Biosensors are often classified according to the type of transducer[122, 123] in electrochemical[124], piezoelectric[125], thermal[126, 127] (or calorimetric), magnetic[128] and optical[129].

Optical and electrochemical biosensors are the most popular for the detection of pathogens[123]. The former are based on how the interaction of the electromagnetic field (light) with a BRE changes when the latter interplays with an analyte[130]. They are highly sensitive and selective[123]; amongst their most significant disadvantages is the difficulty of making measurements in turbid samples[123]. Electrochemical biosensors offer high sensitivity, fastness, accuracy, portability and reliability at a lower cost than optical devices[123]. Their biggest challenge is to achieve high selectivity. The transducers of electrochemical biosensors, electrodes, are typically made of allotropes of C, such as graphite, glassy carbon or carbon nanotubes[131]; or metals, *e.g.* Au, Ag, Pt or Pd. More recently other platforms have also become popular, like conducting polymers (polyelectrolytes), metal oxides[132] like indium tin oxide[133] (ITO), or composite materials that combine different types of the above[95]. To improve the performance of transducers, a common strategy in electrochemical biosensors has been the

incorporation of nanomaterials onto the electrode like metallic nanoparticles[134], carbon nanotubes or graphene[135].[136]

A. Au Electrodes in Sensing

Au is regularly used in electrochemistry as electrode material. In terms of electrochemical sensing applications, in regards to limitations such as price and a short anodic range due to passivation[137], the noble metal offers many advantageous features: high conductivity; inertness -including to most pure electrolytes in a wide potential window (range)-; biocompatibility; big stable potential window in aqueous electrolytes -high over-potential for oxygen evolution reaction (OER) and low overpotential for hydrogen evolution reaction (HER); facile transformation into multiple forms: sputtered surfaces, nanostructures -*e.g.* nanoparticles, nanofibers, nanorods-, screen printed electrodes, arrays and others[138, 139]; compatibility with many surface characterisation techniques[140]. Au's most significant advantage for biosensor design is its easy chemical modification through diazonium salts and thiols. This topic is discussed in **section 1.5.3-B**.

B. Electrochemical Techniques in Biosensors

The analytical signal in electrochemical biosensors originates from changes that occur in an electrical current or an electrical potential following the interaction between a BRE and an analyte. Depending on the electrochemical signal observed[123, 141] electrochemical biosensors can be classified in voltammetric, amperometric, conductimetric[142] and impedimetric **(Figure 1.10)**.

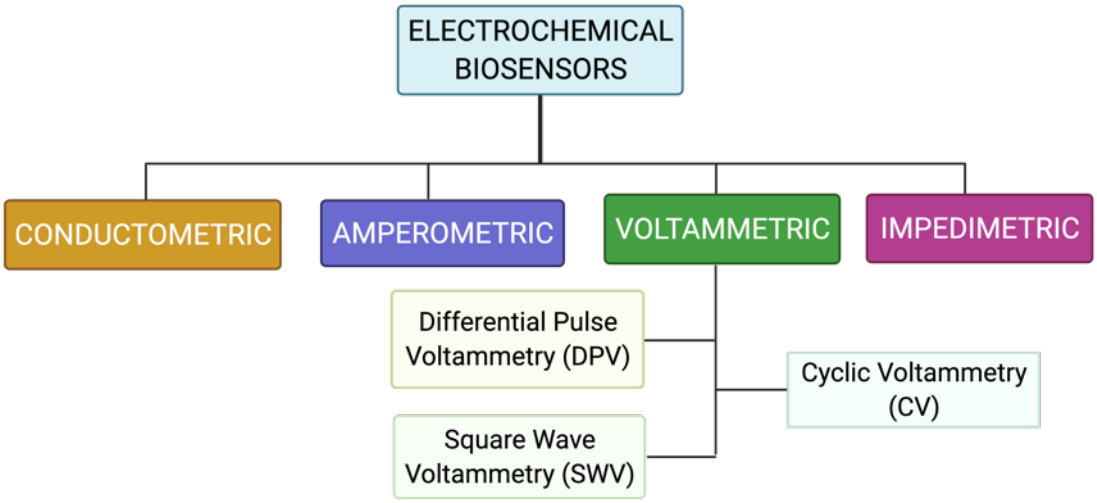


Figure 1.10. Types of electrochemical biosensors according to the electrochemical technique used. The analytical signal in conductometric biosensors originates from variations of the conductivity in the liquid sample analysed. Amperometric sensors measure changes in current intensity when a fixed potential is applied. Impedimetric biosensors record alterations of the impedance in the electrochemical cell. Finally, voltammetric sensing devices mesure the intensity of current when different voltage programmes are applied in the cell.

In voltammetric devices an electric current is measured in function of a changing potential, while in amperometric sensors the potential remains fixed. The electrochemical signal of conductimetric sensors is associated with the conductivity of the liquid sample measured[143]. Potentiometric sensors record changes in the potential and in impedimetric devices the analytical signal is the resistance generated in the biosensor when an alternating current is applied[144]. Further details of those techniques used in this work can be found in **Chapter 3**.

1.5.3 Interfacing the BRE with the Transducer

Whatever the importance of the BRE and the transducer of a biosensor, there is a crucial factor that determines its performance: how these two elements are integrated. The integration affects many of the essential properties of the device, from selectivity and sensitivity to lifespan and robustness[145]. In electrochemical biosensors the integration typically consists in binding a BRE onto the surface of the electrode, a process known as immobilisation. The main factor that conditions immobilisation is the nature of both elements. To obtain good sensing performance the immobilisation must provide an adequate loading of the BRE onto the electrode; avoid non-specific bindings; and produce a stable and durable modification of the electrode[146]. Occasionally, there are many other vital aspects to be considered: orientation or conformation of the BRE once fixed on the electrode (this would be essential when using enzymes and antibodies), reproducibility of the loading process or regeneration of the sensing surface[125].

A. Methods of Immobilisation

There exist many strategies for the immobilisation of bioreceptors onto electrodes. When the attachment cannot be directly achieved[147], which is in most instances, the biological element[148, 149] or the electrode surface[150-152] can be chemically modified to facilitate it. Although there are cases where good results have been obtained with this strategy, the use of linkers[153, 154], particularly chemical ones, is necessary in most cases. The many different ways of immobilising BREs onto

electrodes are often classed as physical and chemical methods depending on how BRE and transducer interact, often through a linker **(Figure 1.11)**.

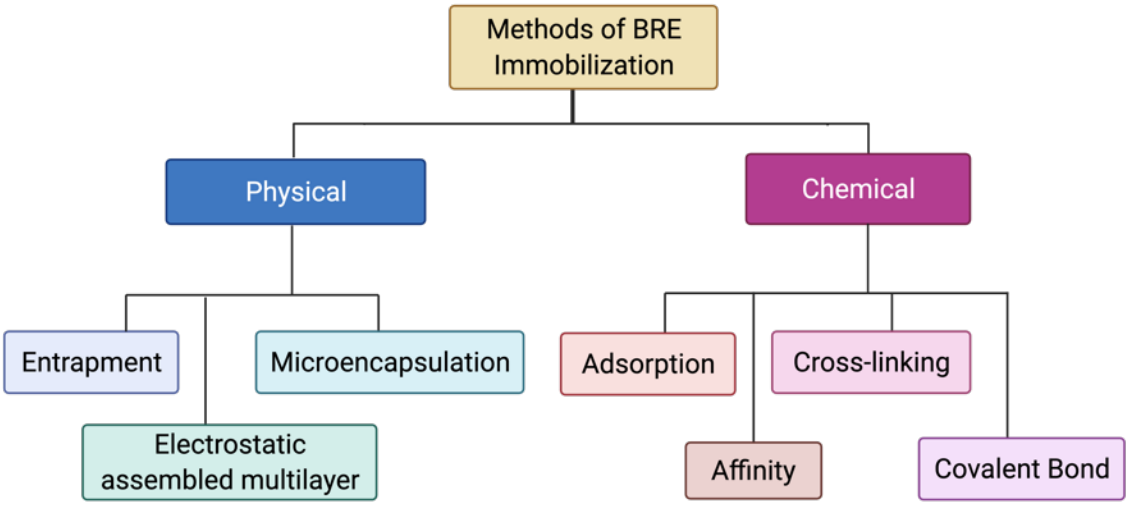


Figure 1.11. Different methods to immobilise BREs on electrode surfaces for electroanalysis. The methods are divided into physical and chemical methods, depending on the type of interaction that keeps the BRE attached to the transducer. The main physical methods are entrapment (the BRE is confined inside a solid attached to the electrode), microencapsulation (the BRE is immobilised in a membrane fixed to the transducer) and electrostatic assembled multilayer (the BRE is embedded in a multilayer grown from electrostatic interactions). The principal chemical methods are based on different chemical bonds between the BRE and the transducer, often mediated by a chemical linker.

A.1. Physical Methods

The principal physical methods to immobilise BREs are entrapment and microencapsulation **(Table 1.4)**. In entrapment the BRE is confined inside a solid with a porous matrix fixed on the electrode[145]. The nature of the matrix varies: polymers[155] (*e.g.* polyacrylamides, conducting polymers), sol-gels[156] (*e.g.* alginate), carbon paste[157], inks, resins[158], hydrogels[159],… Microencapsulation uses semipermeable membranes to hold the BRE onto the surface of the electrode, providing stability and

protection. Amongst those membranes used are cellulose acetate, polycarbonate (Nuclepore™), collagen, polytetrafluoroethylene (Teflon™) and Nafion™[160]. The less employed electrostatic assembled multilayer method successively deposits layers of oppositely charged molecules or polymers onto an electrode; since some BRE -*e.g.* enzymes- are charged, they can be incorporated as a layer of the multilayer construct[161].

Table 1.4. Physical methods of immobilisation of BREs in electrochemical biosensors[160, 162-164]. The table shows the main advantages and disadvantages of the principal methods of physical immobilisation.

Physical Method of Immobilisation	Advantages	Disadvantages
Entrapment	No BRE modification Moderately difficult Moderate cost Increased BRE stability Simple	Increase of response time Cost
Microencapsulation	No BRE modification Increased stability (*e.g.* pH, T, μ, E) Improved selectivity Longer lifetime Very flexible	Limited increase of response time
Electrostatic assembled multilayer	No BRE modification Very flexible	Time consuming Difficult implementation

A.2. Chemical Methods

This type of immobilisation requires chemical interaction between the BRE and the transducer or the linker that connects them. Well-known chemical methods are adsorption, bio-affinity, chelation or metal bonding, disulphide bond, covalent bonding, and cross-linking **(Table 1.5)**.

Adsorption is the simplest method of immobilisation. It is based on weak chemical interactions like hydrogen bonds, van der Waals forces and hydrophobic forces; or ionic bonds. An easy method to achieve this type of modification is drop-casting: a solution of the BRE is deposited on the electrode and the solvent is allowed to evaporate[163]. This functionalisation is highly dependent on the chemical and physical conditions under which it takes place, such as temperature, ionic force (μ), pH and concentration[145].

Bio-affinity immobilisation relies on the high affinity between different biomolecules like lectin-saccharide, antibody-antigen or biotin-avidin[162]. For all its advantages, it always requires the previous attachment of one of the elements of the pair onto the electrode; and, on occasions, the other has to be linked to the BRE too. Regularly employed examples are the streptavidin-biotin system and proteins A or G for the immobilisation of antibodies. Chelation or metal bonding is based on coordinating part of the BRE with a metal centre previously attached on the electrode[162, 165, 166].

The presence of disulphide bonds in BREs, like in antibodies and proteins, can be used for their immobilisation on electrodes. The *in situ* reduction of this bond into thiols can be followed by their interaction with the surface of the electrode, for example a Au electrode, resulting in specifically oriented and stable modifications[162, 167, 168].

The attachment of BREs onto electrodes through covalent bonds is a frequent approach. With rare exceptions, it requires an initial modification of the electrode to endow it with the chemical functional groups capable of reacting with the BRE. The process can require various steps; for example, carbon-based electrodes are electrochemically activated to introduce hydroxylic groups on their surface; then, a further chemical transformation provides them with the desired functions[163]. On occasions, this early modification is also necessary for the BRE. A critical issue during covalent immobilisation is to prevent that neither the aforementioned previous modification nor the final covalent union with the transducer gravely affects the specificity of the BRE towards the analyte. Most covalent immobilisations are based on reactions involving the following chemical groups present in BREs: primary amines (-NH_2), carboxylic groups (-COOH), ketones (-CO-), aldehydes (-CHO) and thiols (-SH)[162]. Cross-linking uses covalent bonds to connect two or more units of the BRE through bi- or multifunctional molecules called cross-linkers[163], *e.g.* glutaraldehyde and isocyanate[169, 170]. The resulting aggregates are then immobilised onto the surface of the electrode via further covalent interactions or any of the previously commented methods. An essential feature of some linkers employed with this method is the presence of long moieties or spacers that can help to modulate the final performance of the immobilisation[171].

Table 1.5. Chemical methods for the immobilisation of BREs in electrochemical biosensors[160, 162-164]. The table shows the main advantages and disadvantages of this type of methodology.

Chemical Method of Immobilisation	Advantages	Disadvantages
Adsorption	No BRE modification Simple Low cost Fast Easy electrode recovery	Weak binding Highly susceptible to the environment (*e.g.* pH, T, μ, E) Short lifetime Random BRE orientation
Bio-affinity	Controlled BRE orientation	Cost Difficult implementation Moderate binding BRE modification
Chelation	Simple	Moderate binding
Disulphide bond	Strong binding Easy electrode recovery	BRE modification
Covalent bonding	Strong binding Increased stability (*e.g.* pH, T, μ, E) Controlled BRE orientation Longer lifetime	BRE modification Complex implementation Cost Time consuming
Cross linking	Increased stability (*e.g.* pH, T, μ, E) Longer lifetime	BRE modification Increase of time of response Time consuming Moderate binding

Actually, many designs of electrochemical biosensors require the use of several immobilisation methods. Besides, when the direct immobilisation of the BRE onto the transducer is not possible or desirable, which is in most cases, chemical linkers must be used. A careful selection of this element can significantly improve the essential characteristics of a biosensor: lifetime, robustness, stability, electron transfer, BRE orientation, selectivity, signal/noise ratio, and others. The diversity of chemical linkers used in electrode surface modification is as ample as the field of chemistry. Herein are commented the two types of linkers employed in the experimental part: self-assembled monolayers (SAMs) and polymers.

B. Self-assembled Monolayers

Self-assembly can be defined as the autonomous spatially arrangement of the components of a system; the term was coined to describe the formation of the protein capsid of viruses[172, 173]. Self-assembly can be observed at all scales, from the growth of crystals at the nanoscale, to the formation of schools of fish in the seas or in the distribution of planets around stars[174, 175]. Processes essential to life, like the formation of lipidic bilayers[176], the folding of proteins[177] or the coiling of DNA[178], are dependent on self-assembly. Self-assembly is driven by Brownian motion and the physical or chemical interactions between the system components; thus, the importance of their structure and composition[172, 174]. The necessity of constant movement explains why the phenomenon is favoured in elements with Brownian motion and why it is more difficult to achieve as the number of components of the system increases[179]. Self-assembly can be modulated by the environment with the use of templates or augmenting the kinetics with stirring or temperature[174, 180].

One of the best-studied self-assembled systems in chemistry is the bidimensional arrangement of molecules adsorbed on liquid surfaces -Langmuir films- or adsorbed on solid surfaces -self-assembled monolayers (SAMs)[181]. When monolayers or multilayers formed on liquid surfaces are transferred onto a solid they are known as Langmuir-Blodgett films[182]. Because of their higher stability, SAMs have found multiple applications: protection of surfaces against corrosion, wetting control, tribology (mechanical wearing, lubrication, and reduction of friction), patterning, adhesion, and others[139, 181, 183]. SAMs are regularly used in biosensing as linkers to immobilise the BRE on the transducer thanks to their high stability, easy preparation, and flexibility. The two main components of any SAM are a solid substrate and the headgroup of adsorbed molecules that interact with it. The growth of SAMs can be achieved with molecules binding from gas phase, from dissolution[181] or even with drop casting[184]. When dissolutions are employed, the main factors that can determine the degree of coverage and packing are[139, 185] concentration of the adsorbate[186], solvent nature[187, 188], presence of O_2 in the solvent[189], temperature[190, 191], time of immersion[192] and pH[193]. Also, considering the substrate surface, its purity, free energy, crystallography/reconstruction, cleanness and roughness[185]. Although other SAM systems are used to construct biosensors, like organosilanes on hydroxylated conducting surfaces[194], organosulfur compounds on Au are overwhelmingly preferred. In this instance, the headgroup is usually a thiol that interacts with the metal to establish a covalent bond[192, 193, 195] (**1**).

$$R - SH + Au_n^0 \rightarrow RS - Au_n^0 + 1/2\, H_2 \qquad (1)$$

The strength and dynamics of the Au-S bond are very complex, with the adsorption mechanism depending on many conditions, including the oxidation state of Au[185, 196]. Two different mechanisms **(Figure 1.12)** have been proposed[193]: a coordination bond between Au and a S atom that is still protonated; and a covalent bond after the atom of S is deprotonated[197]. The reality is that, still today, there is no complete certainty about the dynamics of thiols on Au surfaces and where the proton goes after adsorption[198-201].

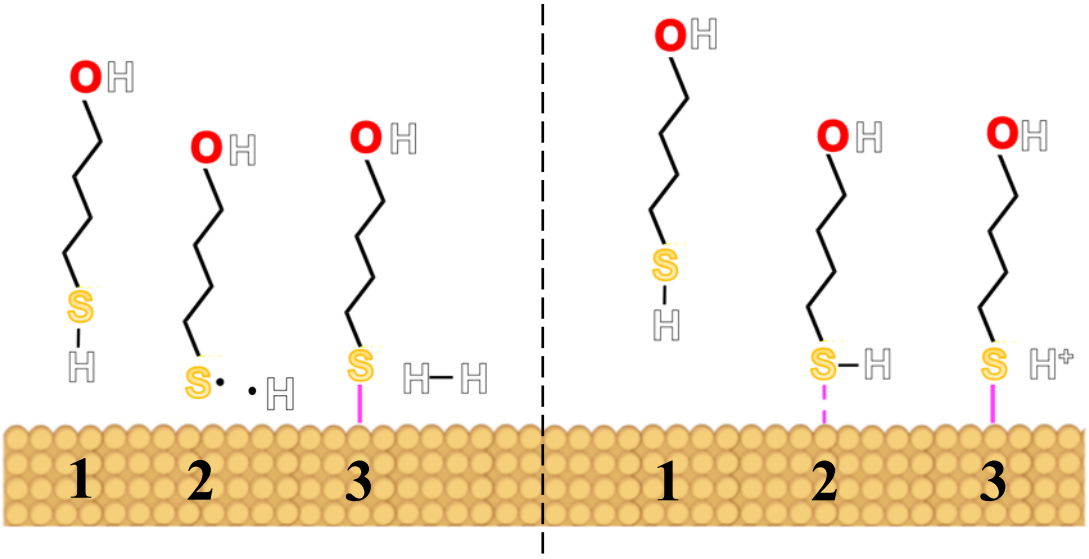


Figure 1.12. Two of the mechanisms proposed for the formation of S-Au bonds in SAMs. On the left, the chemisorption of the thiol proceeds through the previous formation of a thiolate radical; on the right, the protonated thiol adsorbs before the break up of the S-H bond.

The use of disulphides produces the same type of bond, although some reports point towards more perfect monolayers than when thiols are utilised. This is perhaps due to the higher steric hindrance offered by disulphides when they approach the surface to adsorb[202]. The binding mechanism of disulphides on Au proposed by Ulman[183] is:

$$RS - SR + Au_n^0 \rightarrow 2 \cdot RS - Au_n^0 \qquad (2)$$

The relative position of the S atoms in disulphides **(Figure 1.13)** seems to be crucial and dithiols and cyclic disulphides can show better stability than thiols[203].

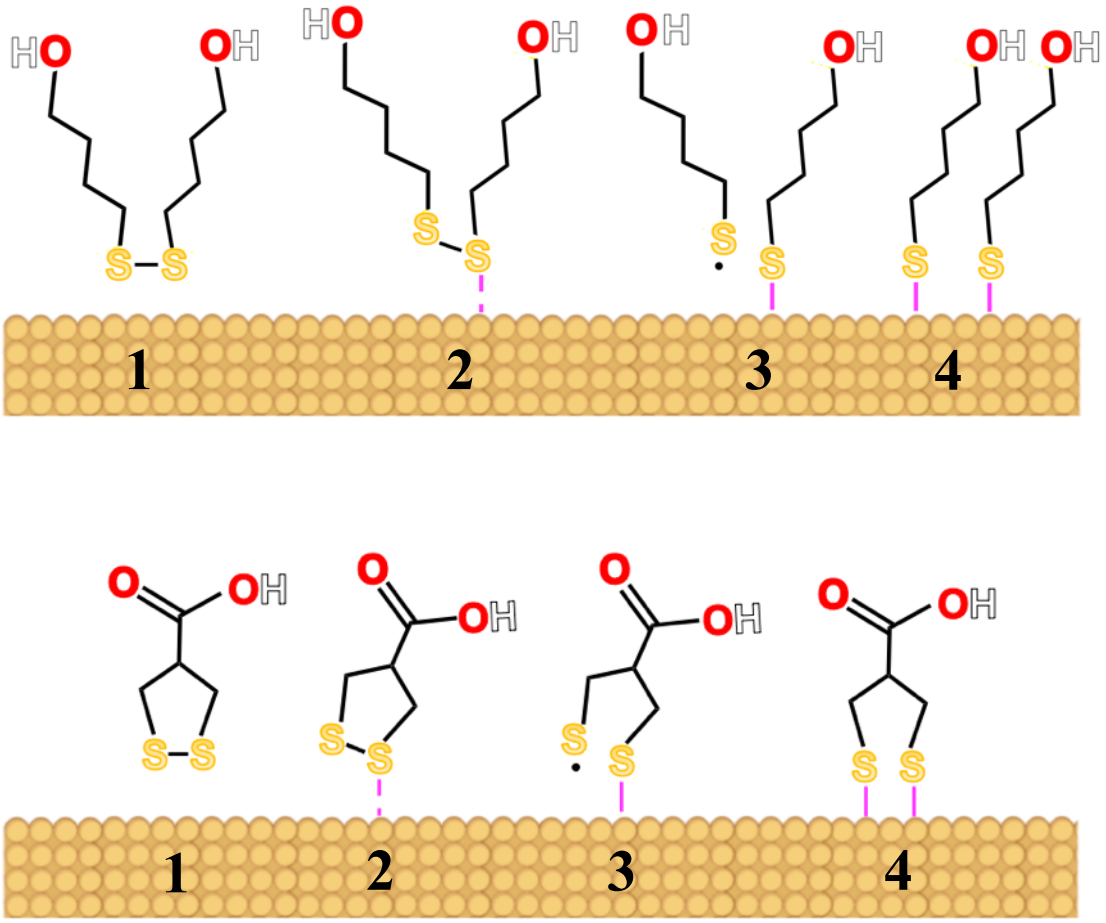


Figure 1.13. Proposed models for the adsorption on Au of different types of disulphides. On top, steps of the adsorption of a linear disulphide; at the bottom, stages of the adsorption of a cyclic disulphide.

Besides the head group, the other two parts of the adsorbate are also essential to determine SAMs' final configuration: the backbone or chain and the end group or tail group **(Figure 1.14)**[181].

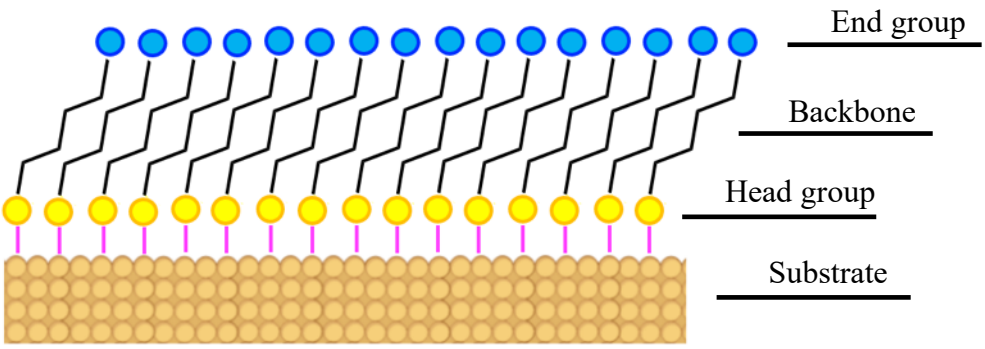


Figure 1.14. Representation of the molecules of a SAM[181]. The molecules adsorb on the substrate through chemical or physical interactions of their head group. The stability of the SAM is also highly dependant on lateral interactions between the backbone of the molecules. The molecules' end groups, which comprise the region of the SAM exposed to the environment, determine many of the properties of the SAM.

Significant aspects of a monolayer, like the degree of packing, tilting or its dynamics on the surface of the substrate, greatly depend on non-covalent interactions (*e.g.* van der Waals forces, hydrogen bonds or π-π stacking in aromatic species[204]) between the backbone of the molecules and between their end groups[205]; and on steric effects of these two parts of the adsorbates. Overall they are fundamental to explaining key properties of SAMs, like stability and wettability[181, 183]. The dual genesis of SAMs is confirmed by two different kinetics: one fast associated with the adsorption of the headgroup; another slow related to intermolecular interactions[183].

Since the adsorbates' end group is the part of the SAM exposed to the environment, it determines most of the physical and chemical properties of the layer. If SAMs are so useful in biosensing is because they can immobilise BREs to the end group through non-covalent or covalent forces[206]. In some cases it is impossible to do

it directly and a previous chemical transformation of the end groups (*e.g.* -COOH, -CHO, $-NH_2$, $-NHNH_2$, -OH) is necessary[207-209]. Methods other than organic chemistry, *e.g.* electrochemistry[210] and photoradiation[211], can also be used. This process may be laborious but bestows SAMs with an enormous versatility as platforms of biosensors.

In regards to their high stability, it cannot be forgotten that organosulfur SAMs on Au are dynamic systems with adsorbate displacement on the surface[199, 199, 212], reconstruction of atomic surfaces[213, 214] and desorption through the formation of disulphides -in well packed SAMs- or radicals -when the degree of coverage is smaller[215]-. Heterogeneous SAMs can also be obtained employing mixtures of thiols[216] (*e.g.* R-SH and R'-SH), asymmetrical disulphides[217] (R-S-S-R') or asymmetrical dialkylsulphides[218] (R-S-R').

C. Polymers

Polymer molecules are molecules of high relative molecular mass constituted by a repetition of one or various structural units called *monomer units*. The term polymer is regularly, and ambiguously, used to describe both polymer molecules and the substance they produce. The combination of monomer molecules to generate polymer molecules is called polymerisation[219].

Synthetic polymers have made inroads into biosensing thanks to their flexibility in terms of composition and structure **(Figure 1.15)**. Non-conducting polymers are popular linkers to immobilise BRE in an effective and stable way[220]; the conducting ones can also enhance the analytical signal[221]. With molecularly imprinted polymers

(MIP), polymer molecules have occupied the centre stage in biosensors becoming the BRE by themselves[222,223].

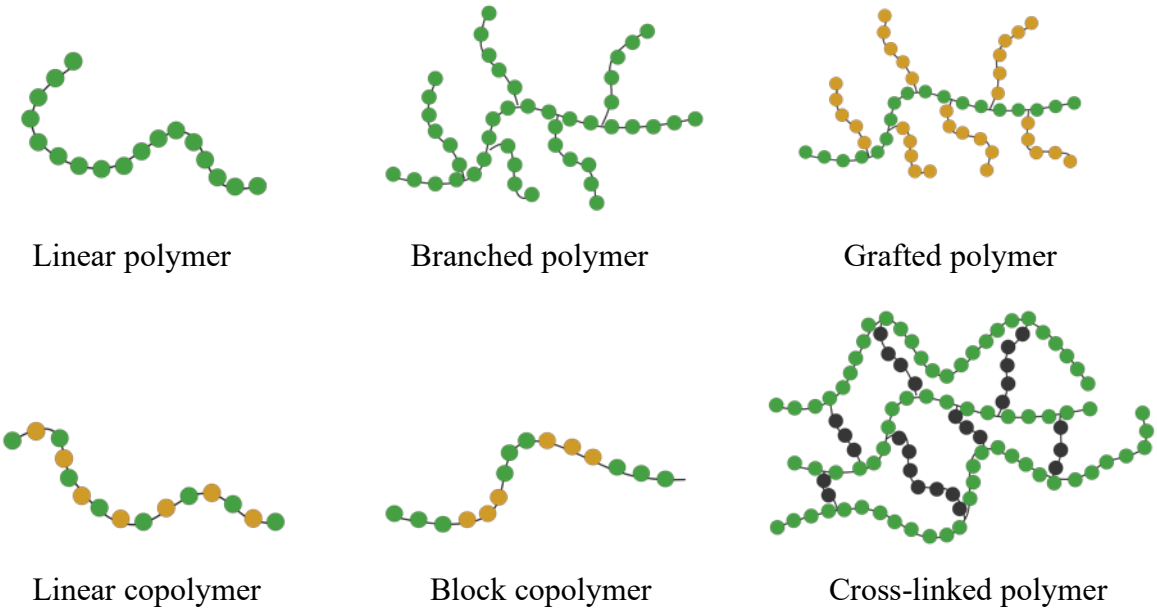


Figure 1.15. Examples of polymer molecules. In some instances, the polymers were obtained with more than one type of monomer (different coloured dots).

The main advantage of polymers *versus* SAMs is their greater robustness. In addition, the fact that some are conductors due to π-electron conjugation in their backbone[224] augments their attractiveness in electrochemical biosensors[225]. Another significant advantage is the possibility of an easy integration with other elements to enhance the performance of this type of device, for example nanotechnology (*e.g.* nanoparticles, nanotubes, and quantum dots)[226, 227].

The coupling or integration of BRE and polymer can be achieved at different times **(Table 1.6)**: simultaneously as the polymerisation takes place, for instance during electropolymerisation[228-230]; once the polymers have been obtained[231] (and before or

after they have been immobilised on the transducer), post-polymerisation; or the less frequent pre-polymerisation[232] if monomer molecules are already functionalised. As with SAMs, chemical modification of pendant groups of the polymer may be necessary for the linkage[229].

Table 1.6. Methods of immobilisation of BREs on electrodes with polymers[160, 162-164]. The BRE incorporation to the polymeric linker can be achieved before, during or after the synthesis of polymer molecules.

Immobilisation Method	BRE	Macromolecule	Analyte	References
Pre-polymerisation	Nucleotides	Polypyrrole	DNA	Livache *et al.*
Simultaneous polymerisation	Glucose oxidase (GOx)	Polypyrrole	H_2O_2	Umaña *et al.*
	Glucose oxidase (GOx)	Poly(phenols)	Glucose	Bartlett *et al.*
	Horseradish peroxidase (HRP)	Polypyrrole	H_2O_2	Wollenberger *et al.*
Post-polymerisation	Glucose oxidase (GOx)	Polypyrrole	Glucose	Schuhmann *et al.*[233]
	Antibody	Polypyrrole	*Listeria monocytogenes*	Minett *et al.*
	Oligonucleotide	Poly(thiophene) derivative	Oligonucleotide	Cha *et al.*

Amongst the functional groups of macromolecules that can be employed for post-polymerisation immobilisation is the hydrazide group.

D. Hydrazides

A hydrazide is a functional group consisting of two N atoms joined by a single covalent bond, with at least one of the four substituents being an acyl group

(Figure 1.16). The lone pair of electrons on the amine group confers hydrazides to their nucleophilic character. Its reactivity is enhanced by the presence of an electronegative atom with another unshared pair of electrons in an adjacent position (*viz.* α position): the phenomenon is known as the α-effect[234, 235]. The α-effect appears to be related to the stabilisation of the transition state[236] by the presence of a high charge density on the α position and increases when the atom on this location is found further to the right and further up in the periodic table[237].

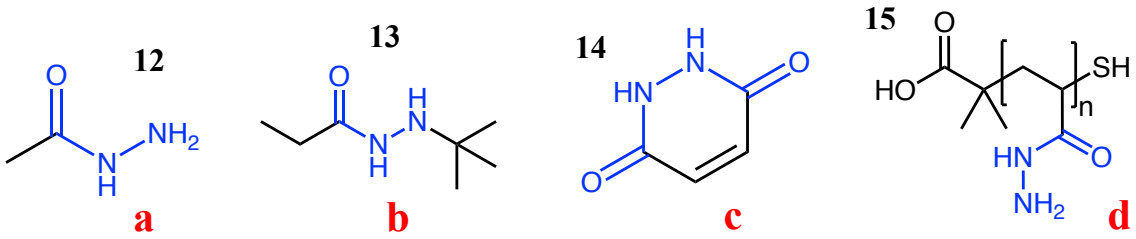
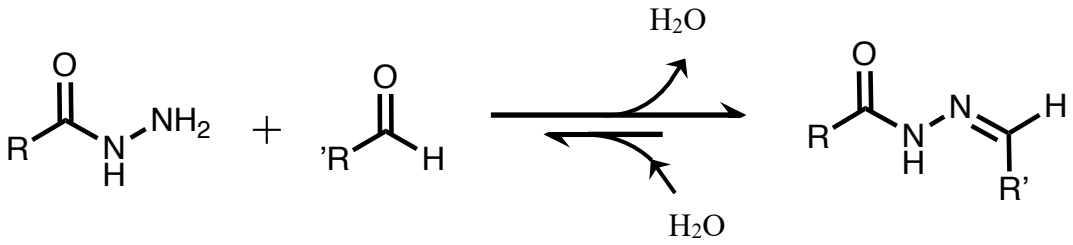


Figure 1.16. Examples of hydrazides**. (a)** Linear hydrazide, **(b)** substituted linear hydrazide, **(c)** cyclic hydrazide and **(d)** polymer hydrazide.

Hydrazides, like other N compounds like amines, hydrazines and hydroxylamines, can be used in nucleophilic additions on aldehydes and ketones. The only by-product is water and acidic conditions catalyse the reaction. The resulting C-N double bond is relatively stable because the reaction is reversible via hydrolysis[238, 239] **(Scheme 1.3)**. The final equilibrium depends on the pH of the medium[240] and the reaction rate on the concentration of aldehydes and ketones[241]. The advantage of using hydrazides versus the other nitrogenated compounds is superior stability rationalised through the existence of a higher number of resonance forms in the product, acylhydrazone**.** Only in strong acidic conditions (below pH 4) or at high

temperatures is the equilibrium displaced towards hydrolysis[242]. The presence of electron-withdrawing groups in the α position suppresses this possibility[242].



Scheme 1.3. Formation (forward) of a hydrazone bond between a hydrazide and an aldehyde by a condensation reaction; (backward) hydrolysis of the hydrazone.

In recent years hydrazides have become very handy in bioconjugation[238, 243, 244]. Tagging, labelling and immobilising biomolecules (*e.g.* proteins[245], saccharides[246], antibodies[247], and nucleic acids[248]) with hydrazides benefit from the facile formation of a covalent bond in biological conditions with reactions that can be easily reversed and whose only by-product is water.

1.6 Cholera

1.6.1 Historical and Geographical Remarks

The genus *Vibrio*[249] comprises more than 70 species of bacteria that live in shallow aqueous media, either in fresh water[250, 251] or salty environments like estuaries, coastlines and oceans[252, 253]. At least 11 *Vibrios* are pathogenic to humans[254] causing vibriosis[255], like *Vibrio parahaemolyticus* and *Vibrio alginolyticus*. Most vibriosis cases result from consuming raw or undercooked seafood and lead to watery diarrhoea accompanied by nausea, vomiting, fever and chills; full recovery usually takes place

within 3 days. Vibriosis caused by *Vibrio vulnificus* is far more dangerous: it can produce septicaemia (50% mortality rate) following the ingestion of contaminated food, or amputations when open wounds contact the brackish waters where the pathogen thrives[256]. The most notorious *Vibrio* species, though, is *Vibrio cholerae*, a comma-shaped, flagellated, gram-negative prokaryote **(Figure 1.17)**.

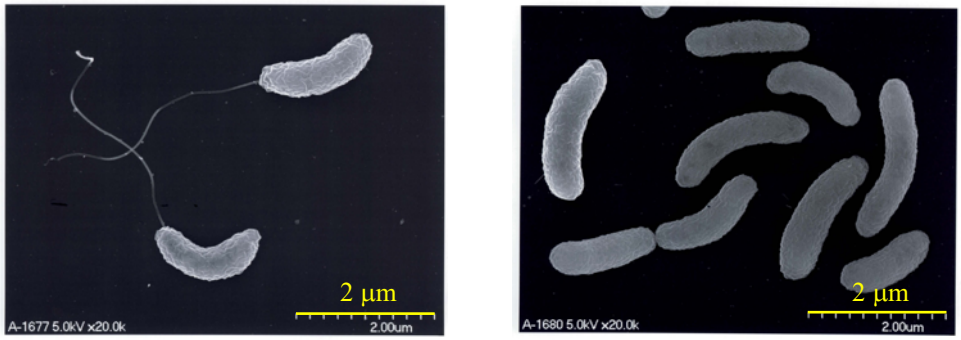


Figure 1.17. Scanning electron microscopy images of *V. cholerae* at different metabolic states[257]. On the left, *V. cholerae* microorganisms from an environmental isolate present a flagellum; on the right, *V. cholerae* bacteria from a patient suffering from cholera.

Humanity has suffered seven pandemics of cholera since the onset of the first in India[258] in 1817; the last started in Indonesia[259] in 1961 and is still active. Cholera is endemic[i] in some sub-Saharan Africa, Asia, and Haiti, showing seasonal patterns of outbreaks[39, 260, 261] **(Figure 1.18)**. Zimbabwe registered one of the latest episodes of cholera in 2018[262, 263]. *V. cholerae* is a halophilic bacteria autochthone of many coastal environments and can prosper in freshwater[264]; this means that even non-endemic countries are exposed to outbreaks if there is a massive displacement of population[265,

[i] *Endemic cholera:* the regular or seasonal presence of cases of human cholera.

[266] or water infrastructures are compromised. This happened, for example, during the current civil war in Yemen[267] or in the aftermath of natural disasters[268] (*e.g.* the 2010 earthquake in Haiti[269] or floods in Bangladesh[270]). In this regard, climate change is a factor that could increase the number of outbreaks of cholera[77, 271].

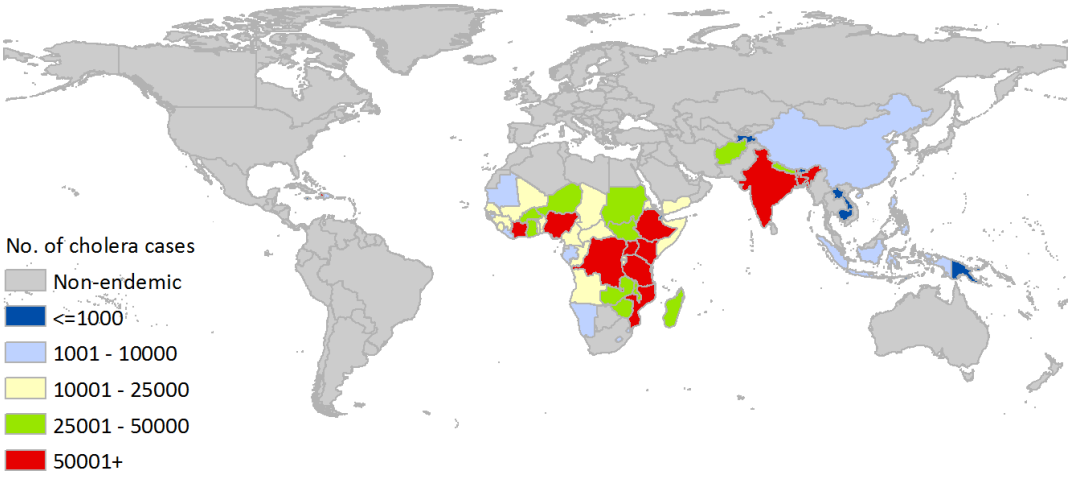


Figure 1.18. Number of cholera cases in endemic countries in 2015[39]. Most affected nations are found in sub-Saharan Africa and Asia.

It is difficult to establish the real burden of the disease[272] because many cases go unreported for different reasons: a majority of episodes are mild or moderate and, either no health help is sought, or they are identified with other causes of diarrhoea[273]; there is a lack of proper surveillance infrastructure[274]; countries fear bad reputation and sanctions[275] that can lead to economic loss, for example in tourism and trade. WHO estimates that every year in the world 3 to 5 million people are infected with *V. cholerae* and between 100,000 and 120,000 die[276].

1.6.2 The Cholera Disease

Cholera is a gastrointestinal illness characterised by mild-to-severe watery diarrhoea described as rice-water stools. The illness is regularly accompanied by vomiting and dehydration that produce initial intense thirst, fatigue, cramps in the legs and sunken eyes[277, 278]. Between 1% and 25% of those infected show signs of disease and, of them, only 10% to 20% experience severe illness[279] (cholera gravis) with extreme dehydration and risk of death. Cholera has an incubation period of between 18 h. and 5 days[278-280]. The symptoms can appear very fast, with the peak of watery stools being reached only after one day. Therefore, in acute cases, death from severe dehydration can take place in less than 24 h.[278, 281], particularly in infants and children, the elderly and immunosuppressed individuals. Without fast and proper rehydration, the death rate can reach 50%[278]. For the worst cases, a rapid intravenous supply of fluids is essential to replace the electrolyte loss. Antibiotics, ideally doxycycline, can reduce the volume of excretion, the symptoms and the convalescence time[282]. Their general use, though, is not recommendable since it barely stops the disease's spread and generates resistance[283]. Patients with milder symptoms can recover taking oral rehydration salts[284] (ORS), although their efficacy is reduced in the elderly and children[285].

Humans can contract cholera through the consumption of water or food that contains *V. cholerae*[33, 286]. This can occur in two different ways: primary and secondary transmission[287]. Primary transmissions originate from the reservoirs of the pathogen in nature and can happen, either through the consumption or use of non-clean water or seafood[288] (oysters, shrimp, clams, crabs, squid or even dry fish), especially when raw

or undercooked; or by ingestion of food in contact with contaminated water. Secondary transmission occurs if traces of the faeces of patients reach edibles or drinking water[269]. Therefore, the disease is linked to the lack of clean water and proper sanitation. With 850 million people who lack access to clean drinking water and 2.3 billion who lack basic sanitation, according to a WHO report[289] of 2017, there is still an enormous human population highly exposed to the disease. The minimum inoculum to cause the disease in individuals with normal acidic levels in their stomach is around $1 \cdot 10^8$ microorganisms; when the gastric acidity is lower, doses as low as $1 \cdot 10^3$ can become infectious[290]. The seriousness of the symptoms depends on many factors: bacilli strain, host factors like blood type[291], the quantity of bacteria ingested[292] and others.

1.6.3 *Vibrio cholerae* Taxonomy

V. cholerae strains **(Figure 1.19)** can be identified through different methods: traditional phenotypic strategies[293-295] (*e.g.* serological testing, biochemical tests, phage tests, antibiogram -susceptibility of a microorganism to different antibodies-), molecular methods[295, 296] (most of them based on analysis of short nucleic acid sequences) and whole-genome sequence (WGS). Accordingly, more than 200 serogroups have been recognised[293]. However, only strains of serogroups O1 and O139 have caused epidemics and pandemics. Until 1992 strains from serogroup O1 were solely responsible for severe episodes of cholera; since then a new infectious serogroup, O139, has become more prevalent. Based on phenotypic[293] and genotypic features[297], the serogroup O1 has been divided into two biotypes, El Classical and El Tor, of which the strains of the latter produce more acute cases of cholera[298].

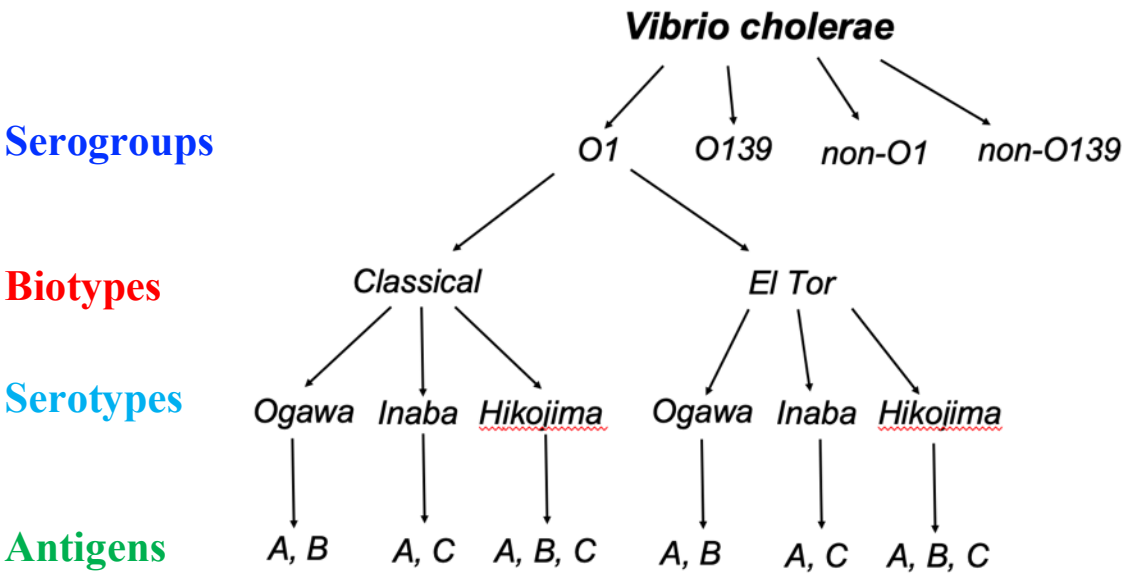


Figure 1.19. Classification of the strains of *V. cholerae*[299]. Based on bacterial antigens, the strains are classed as serogroups, of which only O1 and O139 include microorganisms that cause epidemics and pandemics. Depending on the variability of the antigens, serogroups are split into different serotypes. The serogroup O1 has been divided into biotypes according to genotypic and phenotypic features.

1.6.4 *Vibrio cholerae* Infection

Bacteria depend on virulent factors to enter their host, settle, replicate and disperse[300]. The infection of *V. cholerae* occurs in five stages **(Figure 1.20)**: invasion, colonisation, biofilm formation, toxin release, and shedding[301, 302]. The process, though, is very complex and is far from being completely understood[303]. Two virulence factors, a type IV toxin-coregulated pilus (TCP) and the cholera toxin (CT), play a central role. Here we describe some important aspects of each infectious stage, many of them studied in animal models (*e.g.* mouse and rabbit).

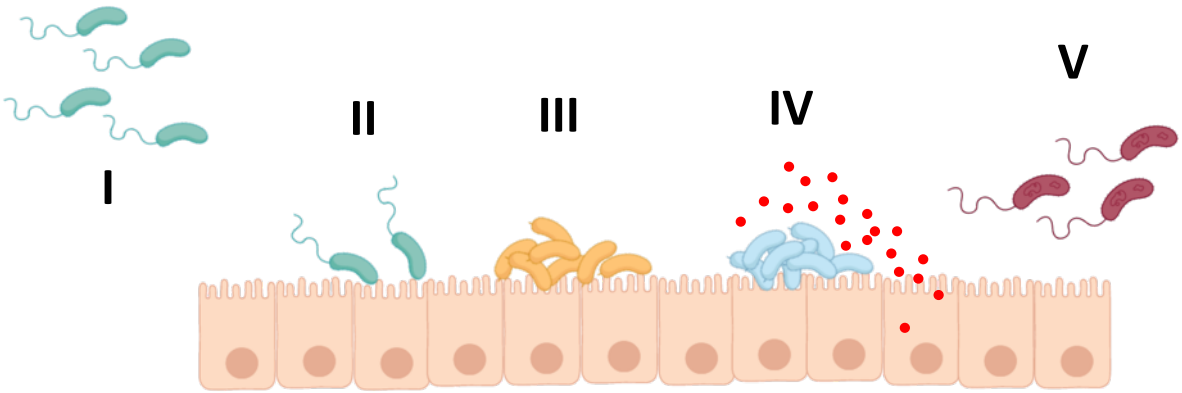


Figure 1.20. Proposal of the stages of *V. cholerae* infection of the human intestine: **(I)** invasion (food or water intake); **(II)** colonisation (bacterial arrival and recognition of intestine walls), **(III)** biofilm formation, **(IV)** toxin release and cell penetration and **(V)** shedding of bacteria.

A. Invasion

The infection of *V. cholerae* starts with thousands of microorganisms passing through the highly acidic human stomach. Since planktonic cells of the bacterium show little resistance to acidic media, the ingestion of hyper-infectious bacilli excreted by patients[304], biofilms[305, 306], viable but non-culturable cells (VBNC)[307] or even microcolonies[302] could favour this process[260].

The intestine still presents an adverse environment for *V. cholerae* with the presence of bile, high osmolarity, iron scarcity, commensals, antimicrobial peptides, and other factors[308]. To survive and colonise the intestine, the pathogen has developed mechanisms whose regulation is also connected to an increase of virulence[309, 310]. One of them is a single polar, sheathed flagellum[311] that gives it mobility **(Figure 1.17)**. *V.*

cholerae uses it, in conjunction probably with chemotaxis[ii], to move along the intestine and traverse a mucus layer of between 115 to 450 μm on its walls[312] **(Figure 1.21)**. However, there is still plenty of debate about how this happens[302, 311, 313, 314]. The microbes probably produce enzymes to break up the mucins, glycoproteins that are the main component of the mucus, to reach the layer of cells[302].

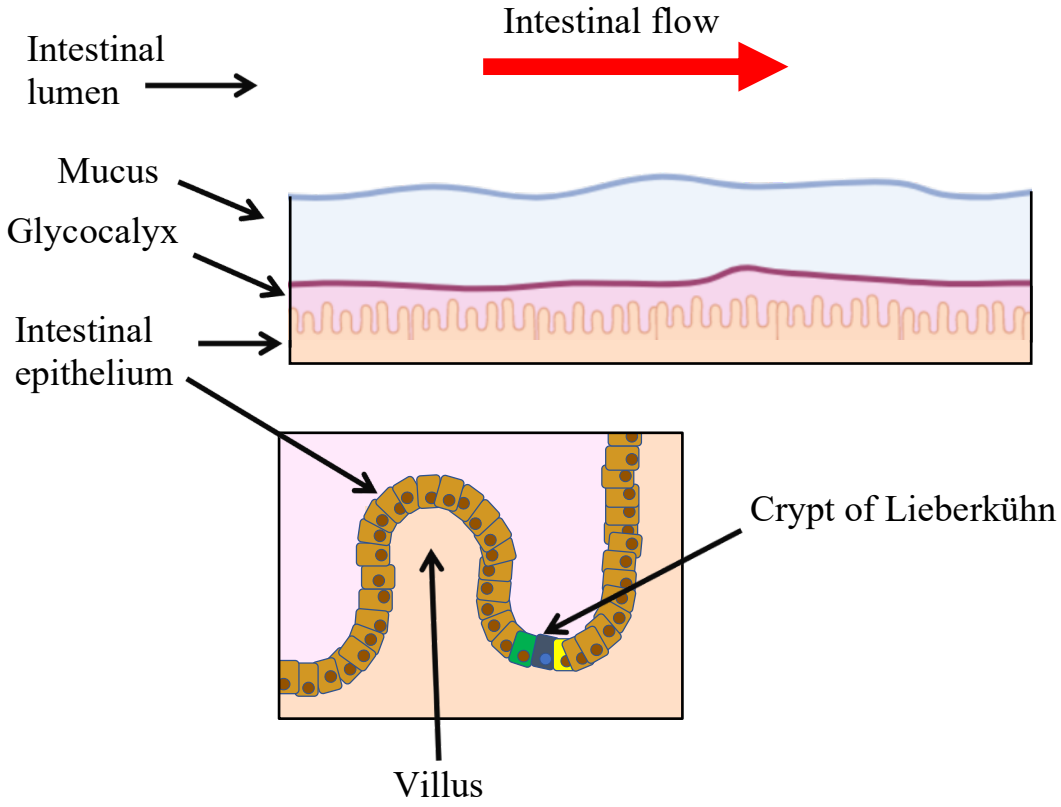


Figure 1.21. Representation of the human intestinal epithelium. The epithelium presents vascular projections, villi, that increase its surface area to absorb nutrients. At their base are found the crypts of Lieberkühn, regions of the epithelium with cells dedicated to different functions such as defence, signalling and regeneration. The epithelium is covered by a glycocalyx and a layer of mucus of glycoproteins.

[ii] *Chemotaxis:* displacement of an organism or part of it (*e.g.* a cell) induced by a chemical stimulus.

Pathogens must adhere to the epithelial cells to start their infection[313, 315]. The process is mediated by various adhesins, although it is still poorly understood given the difficulties to study the system *in vivo* in humans and the limitations of models like the infant mouse[316, 317]. One key adhesin is protein GbpA[318]. When GbpA binds *N*-acetylglucosamine (GlcNAc) residues of mucin, it upregulates host genes for mucin synthesis. An increase of mucin induces the bacillus to express GbpA further, guaranteeing its binding and helping its colonisation[319]. After passing the mucus, *V. cholerae* must overcome the glycocalyx **(Figure 1.22)** of the intestinal cells before adhering to them.

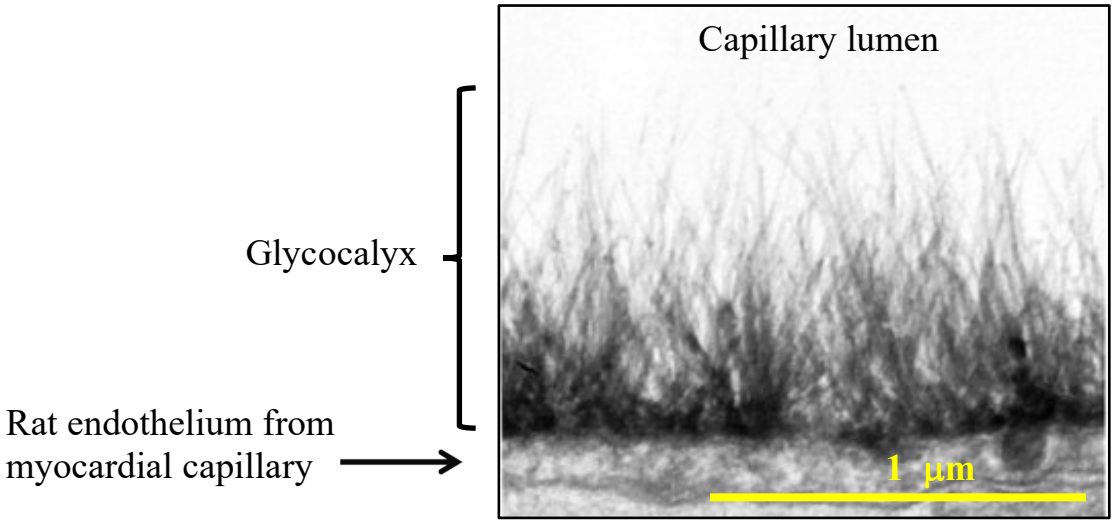


Figure 1.22. Microscopic image of the capillary endothelium of a rat and its glycocalyx according to van den Berg *et al.*[320]. The glycocalyx appears as a hairy layer coating the surface of the endothelium.

Once on the surface of the cells, the bacilli prefer to adhere to the crypts of Lieberkühn and the base of the villi[311, 313]; chemotaxis[321] could guide the process according to results obtained with a rabbit model. This location probably helps them

avoid the strong flow **(Figure 1.21)** produced by the peristaltic movements of the bowls that could end up in their early excretion.

New adhesins step in at this stage. The adhesin multivalence adhesion molecule MAM7 is an outer protein found in many gram-negative bacteria. It interacts with other proteins and with lipids on the surface of the epithelial cells during the first stages of attachment of *V. cholerae*[322]. The flagellum-regulated hemagglutinin A (FrhA) is another promoter of binding to epithelial cells and colony enhancer[315]. As its name indicates, it is regulated by genes associated with the flagellum expression. Thus, the flagellum, as it happens in other pathogens[323], not only propels *V. cholerae* inside the intestine but also helps it to settle on its walls[324, 325].

Pili are organelles that can also be involved in the adhesion of pathogens[326]. For example, in most infectious strains of *V. cholerae* (O139 and O1 biotype El Tor)[327], the mannose-sensitive hemagglutinin pilus (MSHA) combines with the movement of the flagellum to produce stable bindings onto the intestinal cells that become nuclei of growth of microcolonies[328]. Outside the host, the chitin-regulated pilus (ChiRP), another type IV pilus, is responsible for the attachment of the prokaryote to chitin surfaces, like that of crustaceans[329].

B. Colonisation

The colonisation process is mediated by many factors and has not been completely unravelled yet[35, 330]. The microcolonies of *V. cholerae* in the small intestine seem to start from a single bacterium[313] and grow with the production of clones only,

without other external, free bacilli joining. The TCP is the main virulent factor for developing and growing these colonies[331] **(Figure 1.23)**. TCP is a long (up to 7 microns *versus* the 1.5 microns of a *V. cholerae* cell), thin (less than 10 nm) and flexible pilus[332, 333]. Its constituent, the 20,5 kDa protein TcpA, is called pilin. The gene's transcription that expresses this protein (*tcpA*) seems to be somehow regulated by the loss of mobility of the bacterial flagellum[315, 334]. The pilins of TCP are ensembled in the inner membrane of *V. cholerae* before being extruded through the external membrane[335].

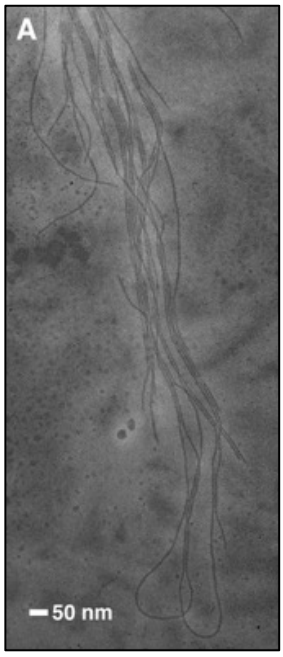


Figure 1.23. Transmission electron microscopy image of TCP pili from wild-type *V. cholerae.* TCP is one of the main colonisation factors of *V. cholerae*. Produced in the inner cell membrane, the microorganism extrudes TCPs to facilitate the colonisation of the host. The micrograph, reproduced from Li *et al.*[333], shows a high degree of bundling between pili.

TCP is associated with several aspects of *V. cholerae* virulence; its principal role is self-aggregate to hold together the newly produced cells from an attached bacillus

to form microcolonies[335, 336]. Its biogenesis is also linked to another important factor for the formation of microcolonies, the protein TcpF[316, 337, 338].

Many other elements are involved in the process of colonisation, such as other pili, proteins (*e.g.* outer membrane proteins, OMP), and hemagglutinins (glycoproteins). However, they are beyond the scope of this work[296].

C. Cholera Toxin: Choleragen

Bacterial infections disrupt the host's metabolism or kill its cells, either directly or indirectly (autoimmune response, *e.g.* sepsis). The process is modulated by virulence factors: bacterial adhesion to cells, invasion of cells or tissues and production of capsules, cell wall antigens, endotoxins or exotoxins[339]. Most exotoxins are proteins with enzymatic activity. There are three types of exotoxins based on their mode of action on eukaryotic cells: Type I, the toxin interferes in the transmembrane signalling; Type II, the protein directly modifies or damages the cytoplasmic membrane; and Type III, an enzymatic part of the toxin penetrates the cell[340].

The main virulent factor of *V. cholerae* is CT, a Type III exotoxin **(Figure 1.24)**. CT is responsible for the principal symptom of cholera disease, diarrhoea[341]. CT is a AB_5 hexameric protein with two subunits: subunit A has enzymatic activity (CTA) and subunit B (CTB), also known as choleragenoid, has binding functions[342, 343]. CTA is approximately 27 kDa[344] and, although synthesised as a single polypeptide, contains two differentiated segments or chains: a catalytic A1-chain and a A2-chain[345]. CTB is made up of five identical peptides of *ca.* 11.5 kDa each bound non-covalently into a

ring-shaped homopentamer with a central pore (10 Å diameter and 40 Å long)[345]. The helical chain A2 is embedded in this pore, anchoring CTA to CTB through its interactions with the 5 peptides of CTB[342].

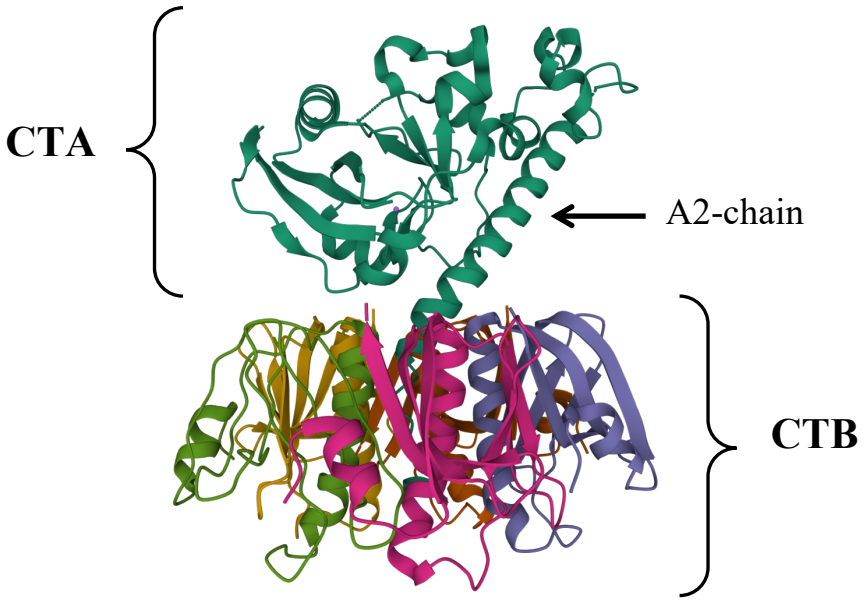


Figure 1.24. 3D crystal structure of the *V. cholerae* toxin published by O'Neal *et al*.[346] and reproduced from the Protein Data Base (PDB), structure code 1S5E. Two subunits constitute the endotoxin: subunit A (CTA, dark green) has enzymatic activity and induces the toxicity of CT; subunit B (CTB), a homopentamer (each peptide is coloured with a different hue), attaches to the surface of the host cell.

The monomer chains of CTA and CTB are synthesised in the cytoplasm of *V. cholerae* and translocated through the inner membrane into the periplasm, where they fold and ensemble to form CT[347, 348]. Afterwards, the whole holotoxin is secreted by the *Vibrio* bacillus through the outer membrane[349] into the lumen of the host. Then, CT suffers a pre-activation by an endoprotease synthesised and released by the own bacterium[350-352]. This enzyme cuts CTA on residue 192[348], physically separating chains A1 and A2; nevertheless, they still hold together by a di-sulphur bridge (Cys187=Cys199) and other weak interactions[342] ready to infect a cell.

D. Cholera Toxin Mode of Action

The CT produced by *V. cholerae* binds to monosialotetrahexosylganglioside (ganglioside GM1)[353-360], a sphingophospholipid, on the plasma membrane of the epithelial cells of the intestine. Evidence points to CT binding several GM1 at a time[361-363]. The complex CT-GM1 enters the cell in different ways[364] **(Figure 1.25)**: clathrin-dependent endocytosis[365], clathrin-independent endocytosis[366] (caveolae) and a third endocytosis mechanism[367], clathrin-independent carriers (CLIC), which does not involve clathrins[368] or caveolae[369, 370]. Some literature describes CT travelling to the Golgi apparatus inside endosomes, where it would split into CTA and CTB[345, 364, 371]. Nevertheless, growing evidence suggests CT crosses the cytoplasm embedded in lipid rafts and directly reaches the endoplasmic reticulum (ER)[372-374].

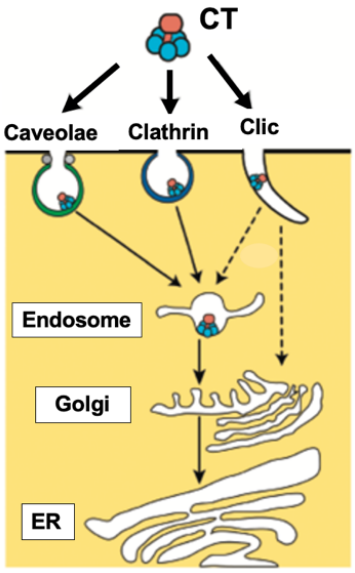


Figure 1.25. Modes of CT penetration into host cells and migration in the cytoplasm[364]. The entry of the toxin can occur via caveolar-dependent transport, by clathrin-dependent endocytosis or through clathrin-independent carriers (CLIC), where neither caveolae nor clathrins are involved. CT's transport mechanism and routes inside the cell are not entirely understood but it appears that the exotoxin reaches the ER directly as part of lipid rafts.

In the ER the chain A1 is disassembled from the rest of the toxin before being translocated back to the cytosol. The exact transport mechanism between the ER and the cytosol[348, 375, 376]is not completely known but seems to require the unfolding of A1 and the hijacking of the ER-associated protein degradation path (ERAD)[345, 376-380]. Once in the cytosol, A1 fragments are refolded and start disrupting the regulation of the transmembrane protein adenylate cyclase[381, 382] (AC). AC, also known as adenylyl cyclase [ATP diphosphate-lyase (cyclising; 3',5'-cyclic-AMP-forming), EC 4.6.1.1][381], is essential for the metabolism of the cell.

The regulation of the activity of AC is based on protein G_S, a type of membrane protein G[383]. G proteins are associated with G-protein-coupled receptors (GPCRs), another type of transmembrane protein responsible for signal transduction. The interaction of GPCRs with extracellular stimuli (*e.g.* neurotransmitters, hormones, ions, photons) provokes changes in their conformation and induces the activation of G proteins[384, 385]. In this particular case, when G_S is activated it releases a guanosine diphosphate (GDP) molecule from its alpha subunit ($G_{S\alpha}$-GDP) and takes in a guanosine triphosphate (GTP) molecule ($G_{S\alpha}$-GTP). The formation of $G_{S\alpha}$-GTP triggers its dissociation from the other G_S subunits[386, 387] ($G_{S\beta}$ and $G_{S\gamma}$) and its binding to AC[388]. The attachment of $G_{S\alpha}$-GTP to AC (AC-$G_{S\alpha}$-GTP) sets off the synthesis of cyclic adenosine monophosphate (cAMP)[389] from adenosine triphosphate (ATP). cAMP, a second messenger, activates protein kinase A (PKA) which, in turn, opens several ion-transport channels[390, 391, 392], including CFTR (cystic fibrosis transmembrane conductance regulator)[393-395]. One function of CFTR is to transport

chlorine ions out of the cell[396, 397]; to maintain the osmotic equilibrium, the exit of these ions is accompanied by the release of water from the cell[398].

However, $G_{S\alpha}$-GTP has a slow endogenous GTPase activity to hydrolyse[399] GTP into GDP. The hydrolysis regenerates $G_{S\alpha}$-GDP and, since $G_{S\alpha}$-GDP is not susceptible to remaining docked to AC, the enzyme is deactivated by the release of $G_{S\alpha}$-GDP and the CFTR channels close. The freed $G_{S\alpha}$-GDP associates again with the other G_S subunits to regenerate the original trimeric complex G_S[400].

When the subunit A1 of CTA is in the cytosol the metabolic path described above is disrupted. A1 is an ADP-ribosyltransferase[346] and uses the coenzyme NAD^+ to catalytically add ADP-ribose to $G_{S\alpha}$-GTP[382, 401, 402]. This inhibits the GTPase activity of $G_{S\alpha}$-GTP, preventing its hydrolysis into $G_{s\alpha}$-GDP and the subsequent dissociation of the complex AC-$G_{S\alpha}$-GTP. Therefore, the production of cAMP[403, 404] does not stop and the pumping of chloride through CFTR ion channels continues uninterrupted. As a result, the intestinal epithelial cells cannot stop releasing water to maintain the internal osmolarity. Because the blood capillaries that feed the epithelial tissue constantly replenish the lost water, eventually the intestine lumen is flooded with water and the excess of water provokes diarrhoea[278, 296, 405, 406].

E. Bacterial Shedding

Diarrhoea, the most characteristic symptom of cholera, serves *V. cholerae* to spread if humans consume water or food contaminated with faeces[407, 408]. Interestingly

enough, the virulence of human transmitted strains is much higher (up to 100 fold) than the virulence of strains found in the environment[290]. During episodes of cholera gravis the individual can defecate up to 1 L of fluid per hour[409, 410] releasing between 10^7 and 10^8 bacteria per gram of stool[411], well above the minimum inoculum. The stools contain planktonic bacteria and biofilm-like aggregates[305, 412] the pathogen forms in the intestine[301], to consolidate its colonies[413]. The biofilm-like structures in the water-rice stools contribute to the bacterium's survival and the formation of a reservoir[305]. The prokaryote also uses various mechanisms to promote the shedding: for example, expressing a hemagglutinin protease to detach from the intestinal walls[414, 415]; or using quorum sensing[332] to forward the transition between sessile and mobile forms in the bowels to disseminate better[301].

1.6.5 Perspectives

The abundance and diversity of *V. cholerae* strains in marine and coastal ecosystems, together with the increasing number of people living on the coast; the complexity of the microorganism's life cycle and gene recombination; the lack of vaccines that provide long-term immunisation; and the increasing bacterial resistance to antibiotics and their limited effect on the disease[416], all make it difficult to imagine a foreseeable future where cholera illness has been eradicated[417]. In this context, improving preventive measures, including early detection of the pathogen, becomes essential to reduce the burden it causes to humanity.

Chapter 2

Aim and Objectives

2.1 Aim of the Thesis

In the last four decades, electrochemical biosensors have emerged as a promising alternative in the analytical field, including the detection of microorganisms in food and water. However, despite thousands of scientific publications, most of them have struggled to see commercial success. The main factors to explain this disappointment are, on the one hand, the complexity or high price of the biorecognition elements employed; on the other, the difficulties for optimal integration with a transducer. This work aims at developing a new electrochemical biosensor for the detection of the *V. cholera* toxin in an aqueous medium. The device has been devised to use simple and inexpensive BREs, like Gal or Lac. Electrodes of polycrystalline Au, Au(poly), are chosen as transducing platforms because of their flexibility and easy recovery. The integration of both elements is attempted through bioconjugation of Gal and Lac with molecules and polymers that contain sulphur atoms and hydrazide groups. This allows the obtainment of a robust and adequate immobilisation of the Gal moiety onto electrodes. Direct and indirect (redox probe) electrochemical methods are employed to characterise the modified Au electrodes and test the effectiveness of the design for the detection of CTB in a biological medium.

2.2 Objectives

Several objectives were set to fulfil the aim of the project.

Objective I. Synthesis and glycosylation (Gal) of hydrazide disulphides and immobilisation on Au(poly) electrodes **(Chapter 5**).

Objective II. Synthesis of polymers with a thiol end-group and hydrazides as pendant groups; coupling of the polymers with sugars (Gal or Lac) through the pendant groups (bioconjugation); modification of Au(poly) electrodes with the bioconjugated polymers and electrochemical characterisation of the functionalised electrodes with cyclic voltammetry (CV) **(Chapter 6)**.

Objective III. Electrochemical detection of CTB **(Chapter 7)**: use of different electroanalytical techniques (*i.e.* square wave voltammetry, SWV, and electrochemical impedance spectroscopy, EIS) to sense the presence of CTB in aqueous solutions with Au(poly) electrodes modified with glycosylated polymers (Gal) and a redox mediator ($[Fe(CN)_6]^{-3/-4}$).

Chapter 3

Experimental Electrochemical Techniques

Electrochemistry is the part of chemistry focused on events where chemical and electrical phenomena are interrelated[418]; whether chemical reactions giving rise to electrical effects or the application of electricity into a system promotes chemical changes. Electrochemistry encompasses many different fields: the study of biological processes, corrosion, electrophoresis, energy conversion and storage, catalysis, organic synthesis, surface modification[419], materials, sensing, electrochromic devices, microfabrication[420], and others. This thesis is devoted to the use of electrochemistry for sensing purposes.

3.1 The Electrochemical Cell

The core of any electrochemical process is the transfer of charge through the interface of two chemical phases, most regularly an electrical conductor (electrode) and an ionic conductor (electrolyte)[421]. The charge exchange typically consists in the movement of electrons (or holes) in the solid electrode and of ions in the liquid electrolyte. The most elemental electrochemical cell may consist of two electrodes connected by an electrical conductor and separated by an electrolyte **(Figure 3.1)**. Away from the interface, electrical currents are transmitted by electrons in the external conductor and by ions through the electrolyte[422].

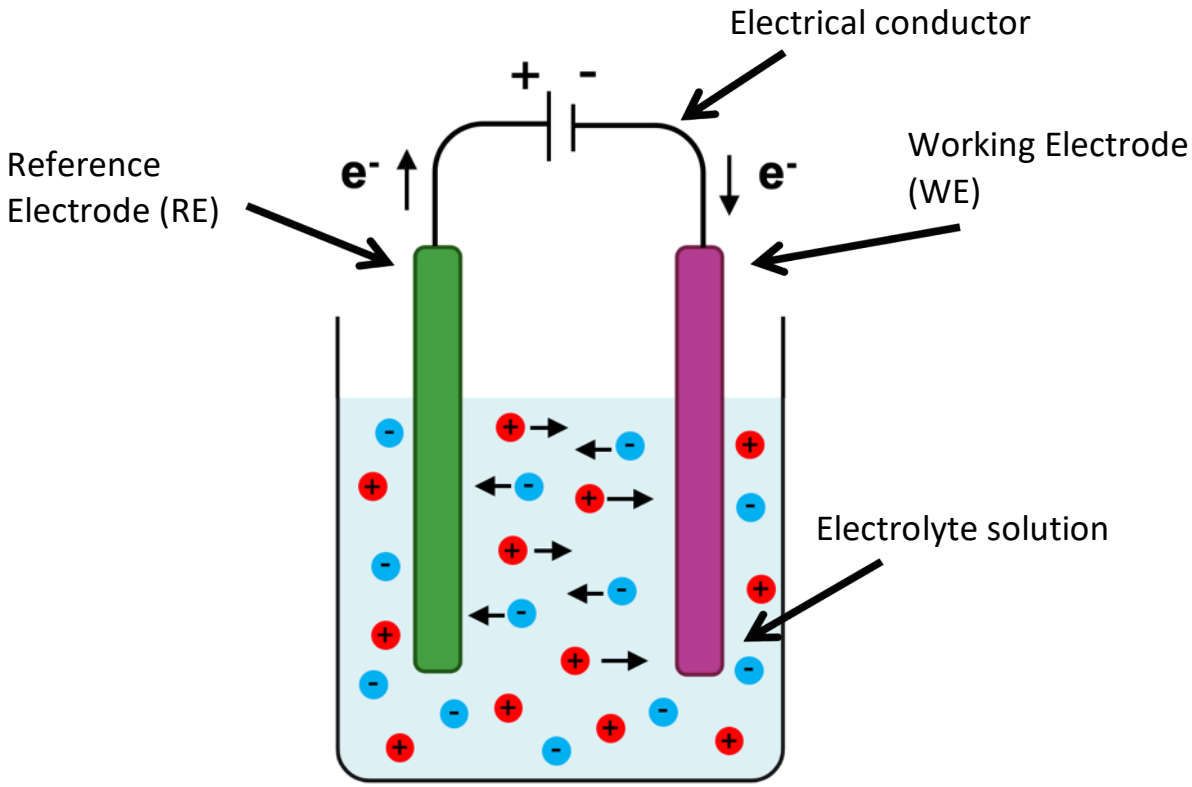


Figure 3.1. Components of the most basic electrochemical cell. A difference of potential between the WE and the RE (two conducting materials submerged in an electrolyte) generates a unidirectional movement of a charge constituted by electrons in the electrical conductor and ions in the electrolyte.

Amongst the materials more often used as electrodes are solid metals (*e.g.* Au, Ag, Pt, Pd), allotropes of carbon (*e.g.* graphite, graphene, single-walled carbon nanotubes), semiconductors (*e.g.* indium-tin-oxide, Si), liquid metals (*e.g.* Hg, amalgams), conducting polymers and others. Frequent electrolyte phases are aqueous solutions of ions like Na^+, K^+, H^+ and Cl^-. Other alternative electrolytes are melted salts[421] (*e.g.* molten NaCl-KCl eutectic), ionic liquids, ionically conductive polymers, and even solid electrolytes. Electrochemical cells can be divided into galvanic cells, also known as batteries or voltaic cells, and electrolytic cells. In galvanic

cells, spontaneous chemical reactions produce an electrical current, there is a generation of energy. In electrolytic cells, chemical reactions are induced through an externally applied potential, so there is a consumption of energy[423]. This type of cell is very useful for studying chemical systems and is employed throughout this project.

3.1.1 The Three-electrode Electrochemical Cell

In experimental electrochemistry the interest is generally focused on what happens in one of the electrodes, called working electrode (WE), while the other, the reference electrode (RE), is kept at a constant potential to serve as a reference. According to the Law of Ohm (**3**), the pass of current can alter the potential of an electrode:

$$V = I \cdot R \qquad (3)$$

with

$V = \text{potential [V]}$
$R = \text{resistance [}\Omega\text{]}$
$\text{I} = \text{intensity of current [A]}$

The potential variation produced by the pass of a current through the RE must be avoided for this electrode to be a good reference. Three-electrode electrolytic cells are usually employed to achieve so **(Figure 3.2)**.

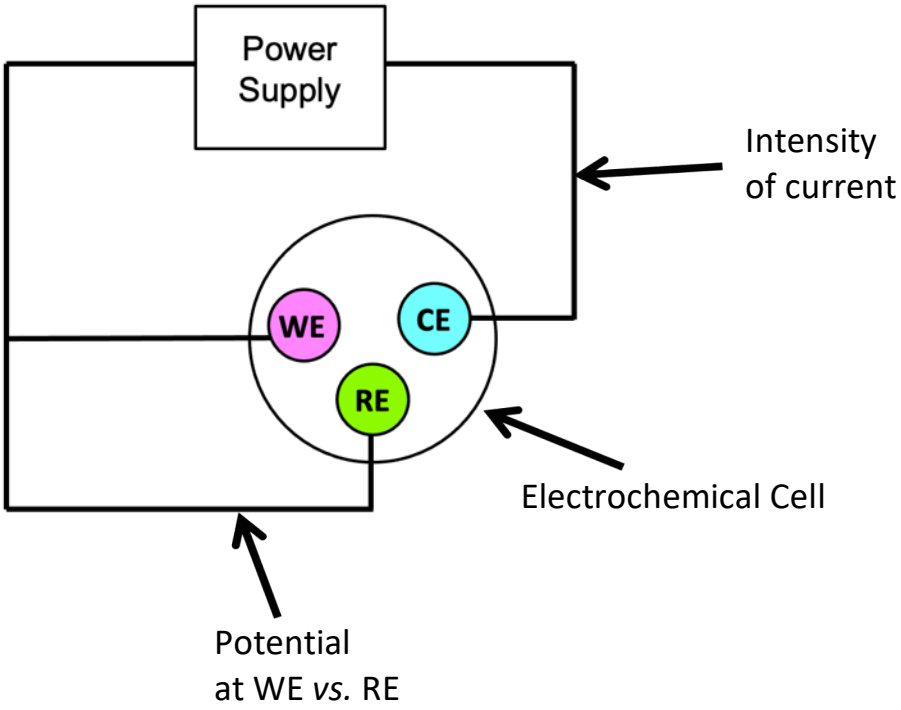


Figure 3.2. Components and configuration of a three-electrode electrochemical cell. The addition to the cell of a third electrode, the auxiliary or counter electrode (CE), permits to drive most of the electrical current away from the RE. This reduces the potential changes experienced by the RE and makes it a better reference of the potential applied to the WE.

The introduction of a third electrode, the CE, prevents the pass of most of the current through the RE keeping its high non-polarizability and, thus, guaranteeing the accuracy of the potentials measured in the WE.

3.2 The Electrochemical Process

The chemical reactions that characteristically take place in an electrochemical cell are redox reactions. In general, in a redox reaction a chemical species loses electrons (oxidised species) in favour of another (reduced species); in instances where

the same species loses and gains electrons the redox reaction is called disproportionation[424, 425].

In electrochemistry the redox reaction takes place through the interface electrode/electrolyte. Typically the electrode is a solid conductor and the species that are reduced or oxidised (electroactive species) are dissolved in a liquid electrolyte (**4**):

$$\mathrm{O}_{(aq.)} + \mathrm{n} \cdot e^-_{(elecrode)} \underset{k_{ox}}{\overset{k_{red}}{\rightleftarrows}} R_{(aq)} \qquad (4)$$

Species O and R constitute a redox couple and k_{ox} and k_{red} are the rate constants of oxidation and reduction, respectively.

When the electrochemical cell is at equilibrium, there is no flow of electrons through the interface (intensity of the current is null)[426]. In this situation the Nernst equation **(5)** defines the equilibrium potential (E_{eq}) of the electrode:

$$E_{eq} = E^{0\prime} + \left(\frac{RT}{nF}\right) \ln\left(\frac{\gamma_{red} \cdot C_{red}}{\gamma_{ox} \cdot C_{ox}}\right) \qquad (5)$$

being

$E^{0\prime}$ = formal electrode potential of the redox couple of interest [V]
R = gas constant ($8.314\ \mathrm{J \cdot K^{-1} \cdot mol^{-1}}$)
T = temperature of the electrolyte solution [K]
F = Faraday constant ($96{,}485\ \mathrm{C \cdot mol^{-1}}$)
n = number of electrons transferred per electroactive molecule/atom
γ = activity coefficients of the redox couple (1 if diluted solutions)
C_{ox} = concentration of species O at the electrode surfae [M]
C_{red} = concentration of species R at the electrode surface [M]

Under non-equilibrium conditions, the interface can experience a net transfer of charge if thermodynamically favourable, leading towards a chemical transformation. Faraday's Law (**6**) describes the relationship between the quantity of mass transformed and the electrical charge (*i*) that passes through the interface during an electrochemical reaction: hence, these are called faradaic processes[422, 427].

$$i = nFv \tag{6}$$

where:

$$i = \frac{dQ}{dt}$$

$$v = \frac{dN}{dt}$$

being

$i =$ current intensity [A]
$v =$ reaction velocity $[\text{mol} \cdot \text{s}^{-1}]$
$Q =$ electric charge [C]
$N =$ numbre of mols transformed [mol]
n = number of electrons transferred per mol of species
$F =$ Faraday constant $(96{,}485\ \text{C} \cdot \text{mol}^{-1})$

The above expression can be re-written in function of the area of the interface:

$$i = nFJA \tag{7}$$

considering:

$J =$ flux of the species in solution $[\text{mol} \cdot \text{cm}^{-2} \cdot \text{s}^{-1}]$
A = area of the interface $[\text{cm}^2]$

Because of the physical and chemical characteristics of the interface region, some changes like the adsorption and desorption of electrolyte ions can also give rise

to electrical currents[427, 428]. But, unlike in faradaic processes, no charge passes the interface: this behaviour is not governed by the Faraday's Law so these events are called non-faradaic processes.

3.2.1 The Importance of Mass Transfer in Faradaic Electrode Processes

For an ideally simple faradaic process (**4**) on the interface between a solid electrode and an electrolyte, the principal factors determining the reaction rate are the electron transfer (ET) at the electrode surface and the mass transfer. When the ET rate is not very fast, an electrochemical reaction outcome depends on the concentrations of the redox pair on the electrode's surface and in the bulk of the solution. Solutions are dynamic systems where the movement of matter is referred to as mass transfer or mass transport and can take place by three different mechanisms: diffusion, migration, and convection. Diffusion appears due to Brownian motion and due to a chemical gradient, for example a concentration gradient[429]. Migration can happen if a charged body is influenced by an electric field (*i.e.* a gradient of electric potential). Convection is generally caused by natural convection, like density gradients or thermal gradients; or also by forced convection through mechanical forces[430, 431] like a rotating disk electrode.

To facilitate the study of electrochemical processes, the mass transfer contribution to the reaction rate is experimentally simplified removing migration and convection[432]: Convection is avoided by leaving the electrolyte and electrode still during the experiment; and migration using a high concentration of an inert electrolyte

(called support electrolyte), usually ≥ 0.1 M for mM levels of analyte. When the only contributor to the mass transfer near the electrode/electrolyte interface is diffusion, the First Law of Fick describes the flux of mass of a species in function of its concentration (**8**)[430, 433]:

$$J_{i,d} = -D_i \nabla C_i \qquad (8)$$

being:

$J_{i,d} = \text{flux of species } i \text{ due to diffusion } [\text{mol} \cdot \text{s}^{-1} \cdot \text{cm}^{-2}]$
$D_i = \text{diffusion coefficient of species } i \ [\text{cm}^2 \cdot \text{s}^{-1}]$
$\nabla C_i = \text{Euclidian concentration gradient of species } i$

This expression reflects the proportionality between the flux of species i at a given position in the Euclidean space and its concentration gradient at a given time. If it is also necessary to consider variations in the concentration through time, then the Second Law of Fick (**9**)[430, 433] applies:

$$\frac{\partial C_i}{\partial t} = D_i \nabla^2 C_i \qquad (9)$$

When planar electrodes are employed, it can be considered that all flux occurs in a single direction x perpendicular to the surface of the electrode. The Second Law of Fick is then **(10)**[433, 434]:

$$\frac{\partial C_i(x,t)}{\partial t} = D_i \left(\frac{\partial^2 C_i(x,t)}{\partial x^2} \right) \qquad (10)$$

3.2.2 Non-faradaic Processes

The external currents (do not cross the interface) registered in an electrochemical cell have their origin in structural (*e.g.* electrode area), chemical (*e.g.* composition, concentration) or energetic changes (*e.g.* temperature) on the electrode arising from phenomena like absorption or desorption. The non-faradaic processes occur simultaneously with faradaic processes. Although the experimentalist will be interested most of the times in the latter, it is essential to understand the former for a correct interpretation of the results and the system[427].

A. The Electrical Double Layer

When a WE is submerged in an electrolyte, solvent molecules adsorb on its surface forming an inner layer. If a potential is applied to the electrode, it becomes positively or negatively charged with respect to the electrolyte, depending on the potential applied and the composition of the electrolyte. As a result, ions of opposite charge to the electrode arrange to compensate the new charge on the WE surface. Some ions can adsorb directly (specifically) on the surface, becoming part of the inner layer or plane; others are solvated so their interaction is non-specific and form an outer layer or plane **(Figure 3.3)**. The inner layer is also known as the compact, Helmholtz or Stern layer. The region between this layer and the bulk of the solution is called the diffuse layer because the electrolyte ions can move towards there. This configuration, which also includes oriented dipoles, is known as the electrical double layer (EDL)[422, 435].

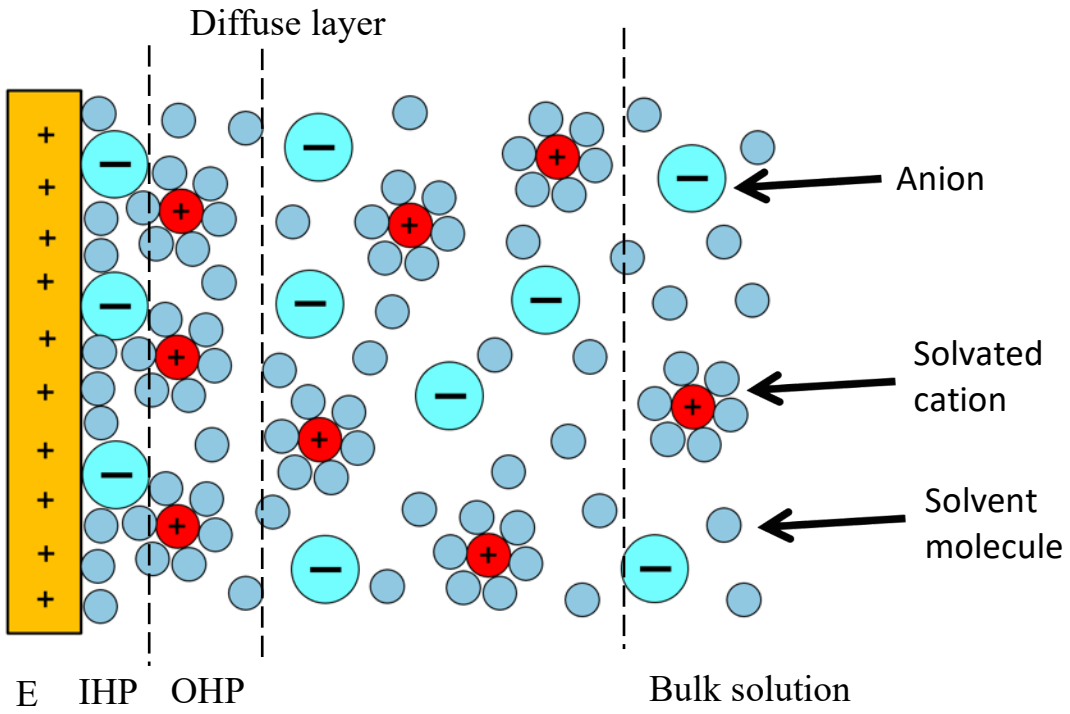


Figure 3.3. Model for an EDL formed on an electrode E where a positive potential is applied: E is the electrode, IHP is the inner Helmholtz plane and OHP is the outer Helmholtz plane.

This arrangement of charges on the interface resembles that of a parallel-plate capacitor[436] behaving as such. Equation (**11**) describes the behaviour of a parallel-plate capacitor:

$$C = \frac{\mathrm{q}}{\mathrm{E}} \qquad (11)$$

where

C = capacitance [F]
q = charge accumulated in the condensator [C]
E = potential between the plates of the condensator [V]

When a potential E is applied between a capacitor's plates, a current flows till the charge accumulated reaches the maximum capacitance C. The same effect takes place when a potential is applied to the WE. Since the species in the EDL are not electroactive, there is no ET but non-faradaic currents are produced to charge the capacitor constituted by the EDL. This capacitive current, called the EDL charge current, usually decays with time. The EDL capacitance is usually between 10 and 40 $F\mu \cdot cm^{-2}$[422]. The EDL thickness varies depending on the concentration of ions, with an estimated 100 Å for concentrations higher than 0.01 M[435]. It is evident that, beyond introducing capacitive effects, the presence of this EDL on the interface will affect any faradaic process, whether the redox species is adsorbed or remains in solution.

3.2.3 A Microscopic Approach to Charge Transfer

The microscopic treatment of the ET, like the work conducted by R. A. Marcus[437, 438], has established the concepts of inner-sphere ET reactions and outer-sphere ET reactions[439, 440]. In inner-sphere reactions, the ET only occurs if there is a specific adsorption on the electrode of either the reactant, the intermediate or the product of the reaction[439] **(Figure 3.4-A)**. In outer-sphere reactions, there is no direct or strong interaction between the electroactive species in the electrolyte and the electrode surface, with at least a layer of solvent molecules interposing them **(Figure 3.4-B)**.

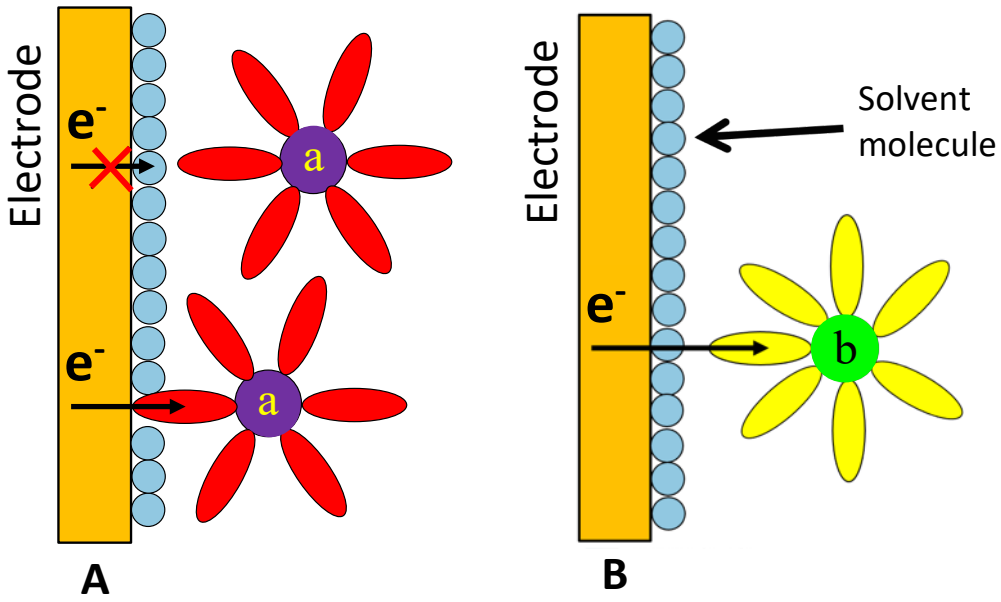


Figure 3.4. Mechanisms of ET. **(A)** Inner-sphere mechanism, with ET only occuring if there is a direct, physical contact between the electroactive species **a** and the electrode surface. **(B)** Outer-sphere ET where the electron exchange can happen even if there is no direct, physical contact between species **b** and the electrode.

A. Extended Charge Transfer

In outer-sphere reactions, the ET is generally interpreted as a quantum tunneling[441] of electrons between energy states of the electrode and molecular orbitals of the reactant[442]. However, sometimes there can be an insulating barrier between the reactant in solution and the electrode surface (other than the solvent or ions molecules adsorbed on the inner Helmholtz plane) that does not entirely prevent the electrons from reaching the electrode through tunnelling effect and generate a faradaic current. A good example is electrodes modified with organic SAMs for sensing applications[443, 444]. The study of this extended charge transfer is essential for developing

electrochemical sensors because of the critical importance of the relationship between distance and ET.

3.3 Electrochemical Techniques

The chemical analysis benefits from many electrochemical techniques **(Figure 3.5)**[445]. They may be divided into techniques used to measure processes related to the mobility of ions; and those related to processes taking place throughout an electrode interface. The latter can be classified as static -measurements are taken when the system has reached the equilibrium; and dynamic -the observations of interest imply pushing the system away from equilibrium. Dynamic techniques are the most popular in electroanalysis.

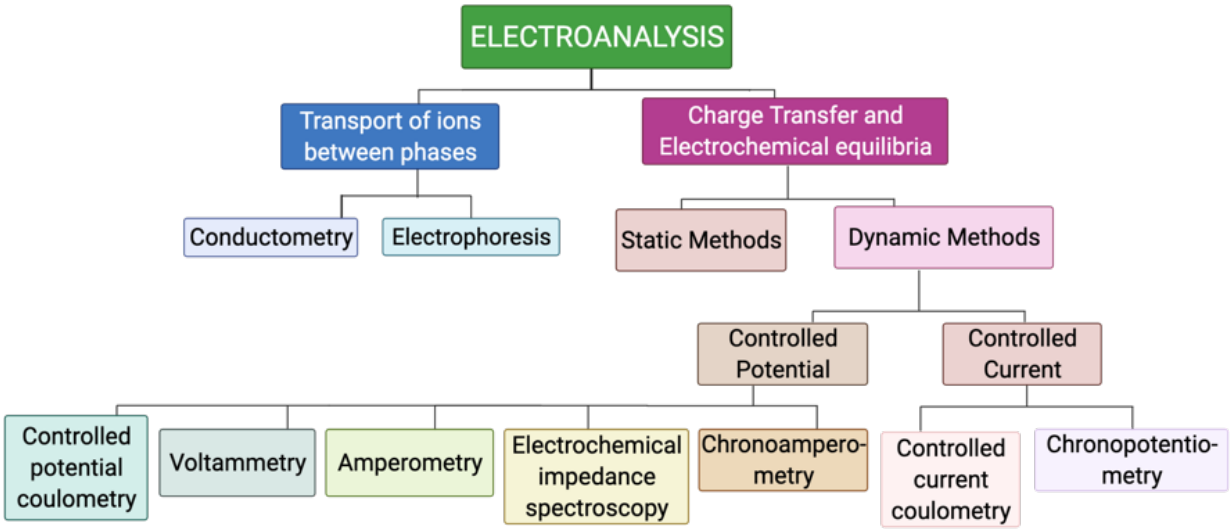


Figure 3.5. Diagram with a proposed classification of the most used electrochemical techniques in electroanalysis[445]. Techniques are divided into two big groups depending on the subject of study: the conduction in the electrolyte (charge transport of ions) or the charge transfer at the electrode/electrolyte interface. The latter group is subdivided into static techniques, where the electrochemical equilibrium at the electrode is not altered; and dynamic methods, in which an excitation is applied (*e.g.* a potential or a current) to displace the system from equilibrium.

3.3.1 Voltammetry

Voltammetry refers to electrochemical techniques where electrical currents (I) are measured while the potential (E) is controlled by an electronic device called potentiostat. The displays of voltammetric results, called voltammograms, show the relation I *vs.* E, I *vs.* time or E - I - time[446]. The ensuing description of voltammetry techniques corresponds to the experimental conditions employed in this thesis: the electroactive species are solved in the electrolyte; mass transport is exclusively driven by diffusion; planar electrodes (planar diffusion conditions) are used; and steady-state conditions are granted by a small electrode surface area and a high volume of electrolyte.[447]

A. Cyclic Voltammetry

CV is probably the most popular electrochemical technique thanks to its simplicity and the large amount of information that can be obtained from a studied system. A typical CV experiment consists in sweeping the voltage forth and back at a constant rate (scan rate) between two potentials, a starting potential (E_1) and a switching potential (E_2)[448] **(Figure 3.6-A)**. If a reversible electroactive species R is in the electrolyte, the recorded output of current intensity gives rise to the characteristic voltammogram of **Figure 3.6-B** associated with faradaic processes. Its main features are a couple of peaks corresponding to the successive oxidation (I_{ox}) and reduction (I_{red}) of the redox species.

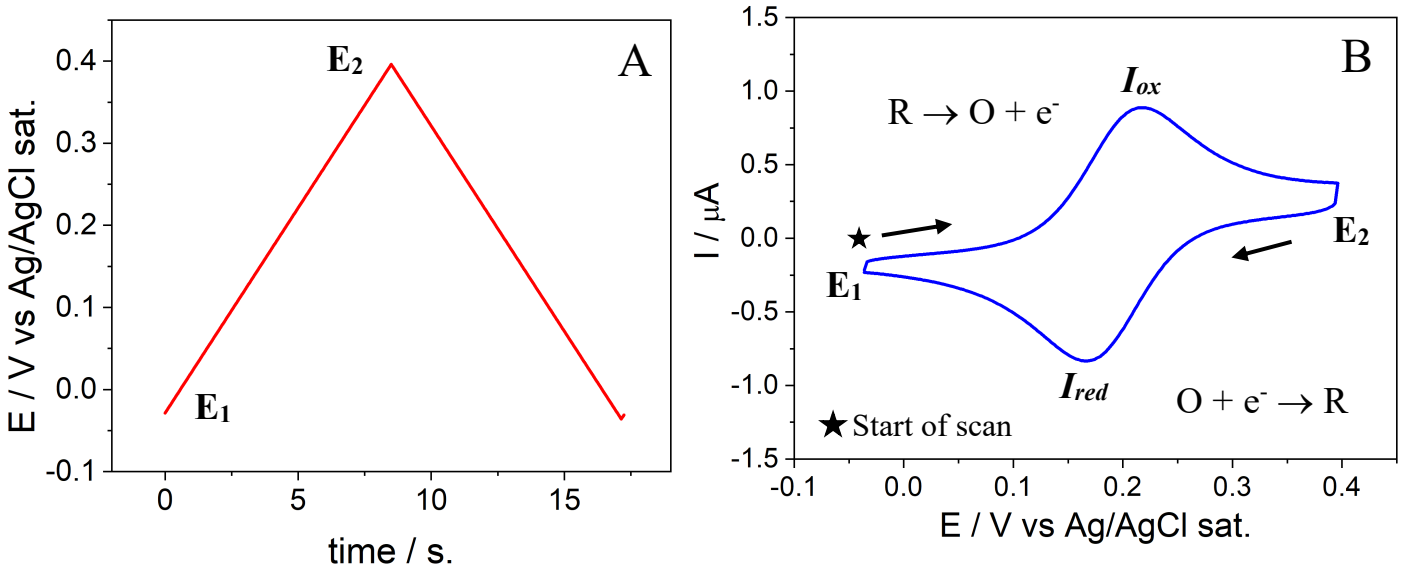


Figure 3.6. (A) Variation of the E applied during a CV experiment of one cycle with the starting potential (E_1) at -0.03 V and the switching potential (E_2) at +0.4 V. **(B)** CV voltammogram obtained with a redox probe R after the application of the E programme plotted on **(A)**. The appearance of oxidation and reduction peaks (I_{ox} and I_{red}) with very similar intensities and short separation indicates a reversible redox process.

The intensity of the peaks is the same and directly proportional to the concentration of the redox species in totally reversible reactions. When the electrochemical process is controlled by diffusion, the intensity increases with the square root of the scan rate according to the Randles-Sevćik Equation (**12**):

$$i_{pa} = 0.446\, nFAC^0 \left(\frac{\mathrm{nFv}D_R}{RT}\right)^{1/2} \qquad (12)$$

where

i_{pa} = peak of intensity during the anodic scan [A]
C^0 = concentration of R on the electrode $[\mathrm{mol} \cdot \mathrm{cm}^{-3}]$
A = electrode surface area $[\mathrm{cm}^2]$
v = scan rate $[\mathrm{V} \cdot \mathrm{s}^{-1}]$
D_R = diffusion coefficient of R $[\mathrm{cm}^2 \cdot \mathrm{s}^{-1}]$

The anodic and cathodic peak separation (ΔE_p) and their relative intensity are also important features of a CV voltammogram since they indicate the reversibility of an electrodic process **(Figure 3.7)**. For an ideally reversible redox reaction with 1 electron transferred, the I_{ox} and I_{red} are separated by 0.059 V.

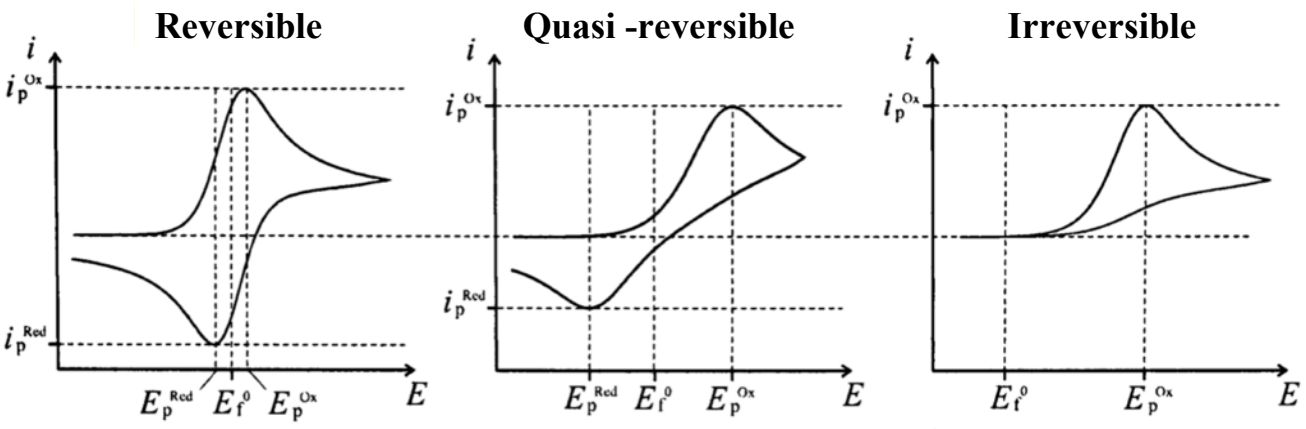


Figure 3.7. CV voltammograms of reversible, quasi-reversible and irreversible processes on a planar macroelectrode[449]. The differences in the relative intensity of the I_{ox} and I_{red} peaks and their separation show the degree of reversibility.

The versatility of CV facilitates the obtainment of lots of information from electrochemical systems: number and stability of the oxidation states of species[450, 451], formal redox potentials[452], kinetics[453, 454], mechanisms of surface adsorption[455, 456], polymerisation[457] and film deposition[458], surface characterisation[203, 459], coupled reactions[460] and quantitative analysis[461], amongst others.

The simplicity and capacity to study electrochemical systems have made CV one of the most popular techniques in electroanalysis. Nevertheless, CV is somehow limited in quantitative analysis: when the analyte is present at large concentrations it requires dilution[462]; besides, its detection limit usually only ranges between $1 \cdot 10^{-3}$ M

and 1 $\cdot 10^{-5}$ M[463]. And yet, CV can be very convenient for developing sensors, for example determining the potential window where an analyte is electroactive or characterising the modified surface of an electrode.

B. Square Wave Voltammetry

SWV is one of the so-called pulse voltammetry techniques **(Figure 3.8)**. They were devised to eliminate the contribution of charge currents, part of capacitive currents, in electrochemical measurements and obtain better faradaic signals. Pulse voltammetry is based on the difference in the decay rate between the faradaic and charge currents produced by applying a potential perturbation known as 'pulse'[464]. While charge currents decay exponentially, faradaic ones decrease at a much slower rate. Because the response to the pulse dies away due to the consumption of the electroactive species on the electrode surface[465], if the current generated by a pulse is measured at a specific time t after its application, only faradaic contributions would be recorded since the charge (non-faradaic) currents will have been already extinguished.

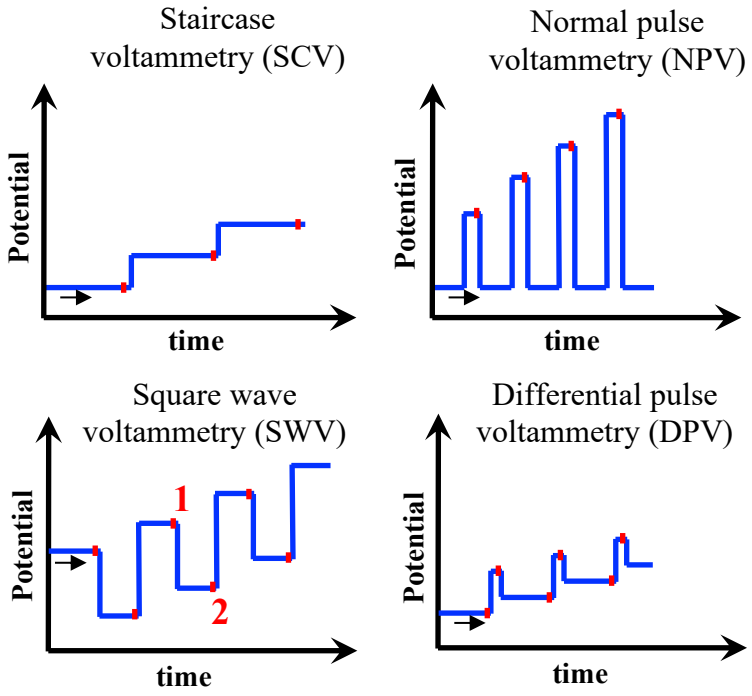


Figure 3.8. Characteristic waveforms of several pulse voltammetry techniques; red marks indicate the time at which the current is sampled. The techniques are characterised by different ways of applying the pulses, called waveforms, which in most cases are also superimposed on a staircase.

In SWV, the waveform is a square wave on a staircase and the currents are registered at the end of the forward (1) and reverse (2) pulses (red marks on **Figure 3.8**).[465] A significant advantage of SWV *versus* other pulse techniques is its fastness. In SWV the concentration of an analyte is proportional to the intensity of peak and limits of detection down to $1 \cdot 10^{-8}$ M can be achieved. Because SWV is faster than DPV, it requires a smaller analyte consumption and reduces the risk of fouling the electrolyte due to adsorption.

3.3.2 Electrochemical Impedance Spectroscopy

Impedance (Z) can be defined as the opposition a system presents to the pass of current. The opposition can have two different origins that determine the two components of impedance: resistance R and reactance X. Resistance appears because of the interaction between the charges of a current and the elements of the system through which passes. In the simplest case, an electrical circuit, interaction between the electrons of the current and the atoms of the conducting material. Reactance is produced by the capacitors (capacitive reactance, X_C) and inductors (inductive reactance, X_L) of the system.

$$Z = R + X = R + (X_L - X_C) \quad (13)$$

Reactance arises from the opposition presented by electric and magnetic fields generated by alternating currents (ac currents)[466]. In systems with only direct current (dc current) Z is reduced to resistance and is defined according to the Law of Ohm:

$$Z = R = \frac{V}{I} \quad (14)$$

being

$V =$ potential applied to the system [V]
$I =$ intensity of current circulating in the system [A]

Electrochemical cells can support the movement of charges of electrical currents, so that Z can occur in this type of system. To facilitate the study of Z in electrochemical cells, those components that can hinder the current pass are associated with traditional elements of electrical circuits: *e.g.* resistors, capacitors, and inductors. In this way, Z

in electrochemical cells is studied through electrical circuit models called equivalent circuits.

EIS is an electrochemical technique used to measure the Z in electrochemical cells when ac currents are applied. In other electrochemical techniques the response is obtained after considerable perturbations are imposed upon the system (*e.g.* set potential or current) that bring it out of equilibrium. In EIS, small alternating perturbations are utilised to follow the system's response through time while it remains in steady-state. This has significant advantages like allowing the conduction of high precision measurements (high sensitivity), linearisation of the response or measuring over a wide range of frequencies or times[467].

The most typical EIS method, known as faradaic impedance, consists of measuring Z in the presence of a redox probe. Usually, a single potential is set on the WE (the redox potential of the probe) while a program of ac frequencies is applied. This method permits the study of double-layer structures, electrode surface modification and heterogeneous ET[468].

A. Equivalent Circuit of a Cell

As previously mentioned, an electrochemical cell can be considered as a Z opposing a current generated by a small sinusoidal perturbation, an ac, and can be represented through an equivalent circuit. One of the simplest circuit models employed is the Randle equivalent circuit **(Figure 3.9)**.

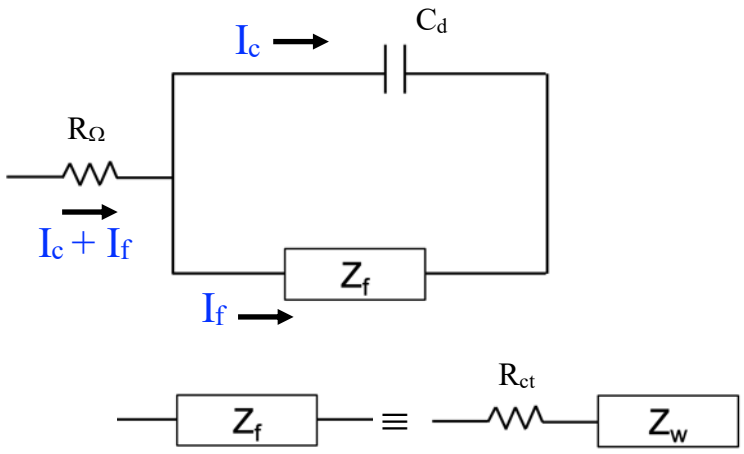


Figure 3.9. Randle equivalent circuit where R_Ω represents the opposition to the current presented by the electrolyte in the cell; C_d, a capacitor, denotes the capacitive currents of the EDL; while Z_f corresponds to the non-faradaic current. Z_f can be interpreted as the resistance to the ET on the interface of the electrode (R_{ct}) plus a kind of resistance to the mass transfer called Warburg impedance (Z_W).

By fitting the EIS results of an experiment to a circuit, the analysts can find a physicochemical interpretation of the phenomena occurring in the cell.

B. EIS Spectra

When the potentiostat that controls an EIS experiment applies a potential excitation on the WE with a particular frequency (a potential wave), the response is a current wave with the same frequency (because the former generates the latter) but with a time delay called phase angle (ϕ). From these two waves the software calculates Z, Z', Z'' and ϕ. The total impedance, Z, is the sum of the real impedance (Z'), originated from the resistance, and the imaginary impedance (Z''), associated with the reactance:

$$Z = Z' + Z'' \qquad (15)$$

The two most popular plots to represent EIS data are the Bode plot and the Nyquist plot **(Figure 3.10)**. The Bode plot is in reality a double representation, with the frequency set on the abscissa axis in the logarithmic scale and two different ordinate axis, one with the angle phase and the other with Z in the logarithm scale.

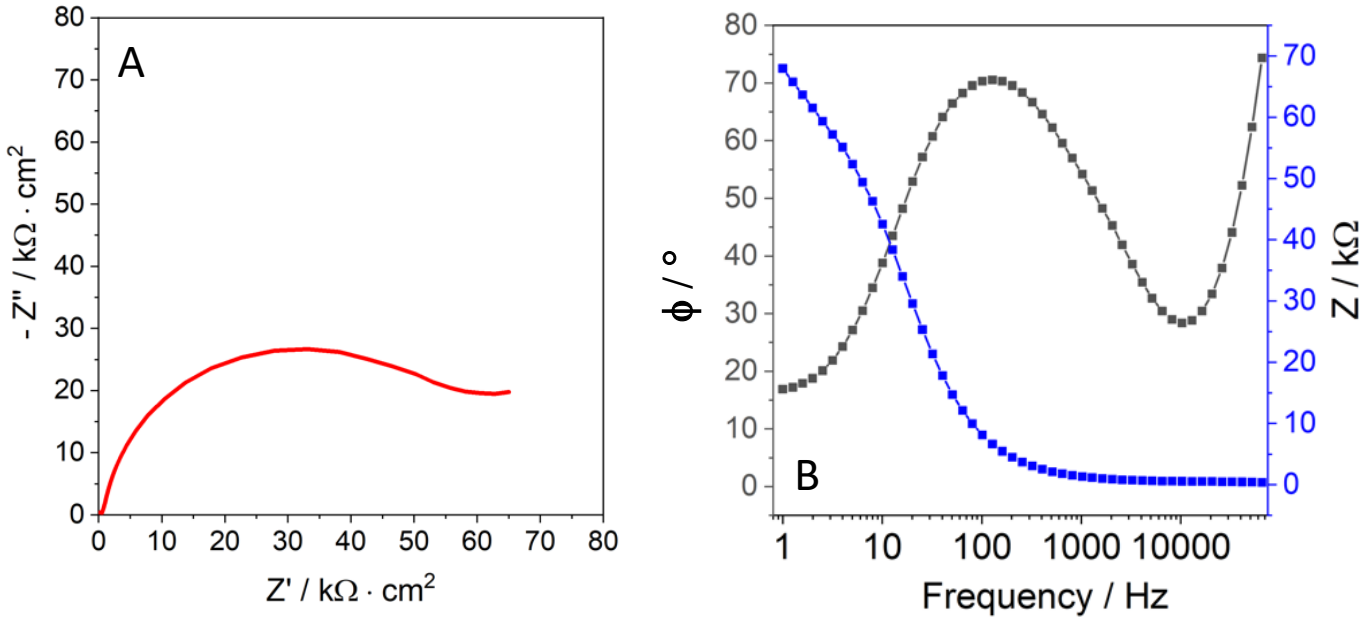


Figure 3.10. Two most popular ways of visualising EIS data. **(A)** Nyquist plot where the negative imaginary impedance (-Z'') is plotted *versus* the real impedance (Z'). **(B)** Bode plot of the same experiment, with the phase angle (ϕ) and the impedance (Z) are represented *versus* the frequencies applied.

C. EIS in Electroanalysis

EIS had traditionally been used for the study of materials, *e.g.* corrosion. Nevertheless, in the last decades, EIS has become increasingly popular for the development of biosensors. Not only for the characterisation of electrode-modified surfaces; but also to be used in label-free sensors. A typical impedimetric sensor consists of an electrode functionalised with a BRE. The interaction between the BRE

and the analyte provokes interfacial changes (ET changes, capacitance changes) that can be detected thanks to the high sensitivity of EIS[469]. In many cases, where the variation in the ET is related to the concentration of the analyte, the use of a redox probe helps enhance the analytical signal[470]. There is no doubt that one of the main strengths of impedimetric sensors is their extraordinary sensitivity, with concentrations below $1 \cdot 10^{-12}$ M being detected[132].

Chapter 4

Materials and Methods

4.1 Organic Chemistry

This section reports on the chemicals, materials, instruments, and methods used to synthesise and characterise the in-house organic compounds necessary to realise this thesis.

4.1.1 Chemicals and Materials

A. Solvents

All organic solvents used for synthesis, purification, and characterisation (D_2O, $CDCl_3$, DMSO-d_6) were of reagent grade or above and purchased from Fischer®, VWR® and Merck® (Sigma-Aldrich®). Deionised water (Milli-Q®, 18.2 MΩ · cm, 1 ppb total organic carbon) was employed for reactions, filtrations, and purifications with dialysis unless otherwise stated; HPLC grade water from Fischer Scientific® was used for chromatographic experiments.

B. Commercial Chemicals

Herein there is a list of the commercial chemical used in this thesis**.**

Diethyl 2,2-bis(hydroxymethyl)malonate was purchased from Sigma-Aldrich®; ***p*-toluenesulfonyl chloride** was delivered by Acrōs Organics®; **pyridine** was bought

from Fischer Scientific®; sodium carbonate **(Na_2CO_3)** was obtained from VWR® and anhydrous sodium sulphate **(Na_2SO_4)** and sodium acetate **(NaOAc)** from Sigma-Aldrich®; **thioacetic acid** was purchased from Sigma-Aldrich® and **potassium thioacetate** from Acrōs Organics®; DL-α-lipoic acid **(LA, thioctic acid)** was obtained from Alfa Aesar®; *N*-(3-dimethylaminopropyl)-*N'*-ethylcarbodiimide hydrochloride **(EDC)** and ***tert*-butyl carbazate** were received from Fluorochem®; trifluoroacetic acid **(TFA)** was acquired from Acrōs Organics®, hydrochloric acid **(HCl, 36%)** from Sigma Aldrich® and acetic acid glacial **(AcOH, 99.7%)** from Fischer®; D-(+)-galactose **(Gal)** was purchased from Acrōs Organics®, D-(+)-glucose **(Glc)** from Fischer Scientific® while D-(+)-mannose **(Man)** and α-D-lactose monohydrate **(Lac)** were delivered by Alfa Aesar®; acetohydrazide **(AcHD)** was received from Acrōs Organics®; sodium borohydride **($NaHB_4$, 98%)** and sodium cyanoborohydride **($Na(CN)BH_3$, 95%)** were requested from Alfa Aesar®, while borane pyridine complex **($PyBH_3$)** from Acrōs Organics®; tris(2-carboxyethyl)phosphine hydrochloride **(TCEP)** was ordered from Alfa Aesar® and also acrylic acid **(99%)**. For reversible addition-fragmentation chain transfer (RAFT) polymerisations, 2,2′-Azobis[2-(2-imidazolin-2-yl)propane] dihydrochloride **(VA-044)** from Fluorochem® was used as the initiator and in-house 2-((Ethylthio)carbonothioyl)thio-2-methylpropanoic acid as the chain transfer agent.

C. Other Materials

Organic reactions were monitored with thin layer chromatography (TLC) using silica gel 60 F_{254} aluminium plates from Merck® and resolving them with a $KMnO_4$ (Sigma-Aldrich®) solution and UV light (254 nm and 365 nm). Flash column chromatography purification was carried out with Geduran® 60 Å silica gel purchased

from VWR® and the reported solvent systems. The membranes used for polymer dialysis purification were Spectra/Por®6 Dialysis Membrane (pre-wetted RC Tubing, MWCO, 1kD). Filtration of polymer dissolutions were conducted with Millex®-LCR filters from Millipore® (0.45 μm, PTFE, hydrophile).

4.1.2 Methods of Compound Characterisation

The analytical techniques and equipment used to characterise the chemicals employed and synthesised in this project are herein briefly described.

NMR analysis was conducted at room temperature in a Bruker Avance® III (300 MHz), a Bruker Avance® NEO (400 MHz) or a Bruker Avance® III (400 MHz) spectrometer. Chemical shifts are reported in the delta scale (δ) in parts per million [ppm] downfield from tetramethylsilane (TMS, δ_H 0.0), and internally referenced to the residual proton of the deuterated solvent used: D_2O (δ_H 4.79); CDCl3 (δ_H 7.26, δ_C 77.16); DMSO-d_6 (δ_H 2.50). The multiplicity signal is annotated as: b = broad, s = singlet, d = doublet, t = triplet, q = quartet. Coupling constants (J) are given in Hertz [Hz]. The data of the spectra are reported in this thesis as follows: chemical shift, multiplicity, coupling constant, integration, and structural assignment.

MS spectra were obtained with an electrospray in positive mode (ES+) as the ionisation source and a time-of-flight (TOF) analyser. The assignment of molecular ion adducts was determined with the help of the tool developed by Huang *et al.*[471].

Several **Fourier transform infrared (FTIR)** techniques were used in this thesis. In all cases, absorption wavenumbers (υ) are reported in cm^{-1}; most significative bands are characterised as: weak (w), strong (s), broad (b); or also annotated as: ν_s = symmetric stretching, ν_{as} = asymmetric stretching, δ_s = symmetric bending, δ_{as} = asymmetric bending. Attenuated total reflectance (ATR or FTIR-ATR) experiments were conducted in a Cary 660 Spectrometer (Cary 600 series) from Agilent Technologies fitted with a MIRacle ATR accessory (PIKE Tech.); or a Nexus 8700 (Thermo Scientific) spectrometer equipped with a MCTA detector and a wire grid ZnSe polarised (PIKE Tech.). Transmission FTIR was also performed with a Nexus 8700 spectrometer. For dynamic *in situ* surface-enhanced infrared absorption spectroscopy (SEIRAS) under ATR conditions (SEIRAS-ATR), a spectroelectrochemical cell equipped with a Si window bevelled at 60˚ was placed at the top of a VeeMAX (PIKE Tech) reflectance accessory of a Nexus 8700 spectrometer. Previously, a Au thin film (*ca.* 25 nm) had been deposited on one of the faces of the low-oxygen content Si prism using a vacuum chamber of a PVD75 (Kurt J. Lesker Ltd.) coating system; a quartz microbalance IQCM was utilised to control the growth of the film. Spectra were collected with a resolution of 8 cm^{-1} (in ATR 4 cm^{-1}) and absorption intensities are presented in absorbance units (a.u.).

Analytical high performance liquid chromatography **(HPLC)** in reversed phase was conducted with a Kinetex 5 μm, EVO C18, 100A column (250 x 4.6 mm) fitted in an Agilent 1260 Infinity system with auto-sampler and a multi wavelength UV detector. HPLC purification of compounds was attained in a Kinetex 5 μm, C18, 100A, Axia packed preparative column (250 x 21.2 mm) fitted in a Agilent system with a UV

detector. Both chromatographic columns were acquired from Phenomenex Inc. (Macclesfield, UK) and the chromatographic systems controlled by Agilent OpenLAB software.

Gel permeation chromatography (GPC) analysis[472] was done in a Shimadzu Prominence LC-20A apparatus fitted with an SPD20A UV-vis detector (Shimadzu®) and a Refractomax 521 detector (ThermoFisher®). For the hydrophobic protected polymer poly(*tert*-butyl-2-acryloylhydrazine-1-carboxylate (Boc-pAH_n), the stationary phase consisted of a Polymer Labs PolarGel guard column (50 x7.5 mm, 5 μm) at 60 ˚C and the eluent used was 0.05 M of LiBr in DMF, 1 mL/min. flow rate. A standard calibration method employing polymethylmethacrylate was used for the calculation of molecular weights. For the hydrophilic deprotected polymer poly(acryloyl) hydrazide (pAH_n) the eluent used was Dulbecco's phosphate-buffered saline (DPBS) 0.0095 M without Ca^{2+} nor Mg^{2+} with a flow rate of 1 mL/min. In this case the column utilised was an Agilent PL aquagel-OH column (300 x 7.5 mm, 8 mm) run at 35 ˚C.

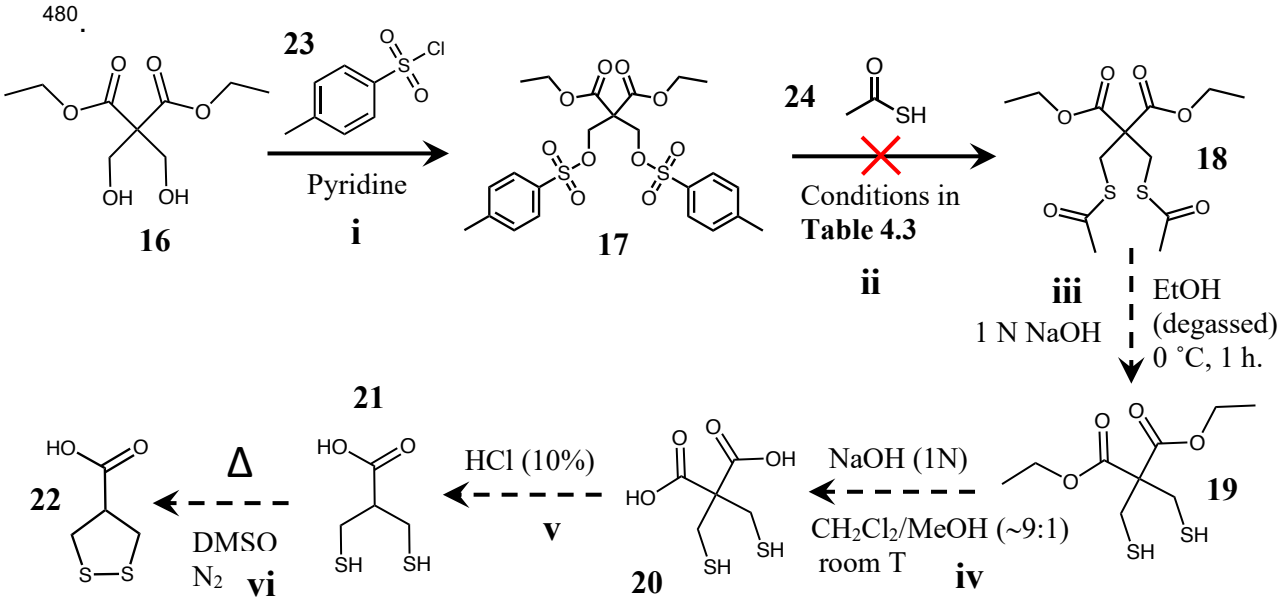
The **XRD** experiment was performed on a SuperNova, Dual, Cu at zero, Atlas diffractometer; during data collection, the crystal was maintained at 100.00 K. The analysis of the crystal was carried out with the Olex2[473] programme: the structure was solved with the ShelXS[474] structure solution program using Direct Methods, and refined with the ShelXL[475] refinement package using Least Square minimisation.

4.1.3 Synthesis and Characterisation of Compounds

The first goal of this thesis was the synthesis of chemical linkers containing S atoms and the hydrazide group. This would allow their coupling with saccharides and the modification of Au(poly) electrodes to detect CTB. Next are described the synthetic routes and methods attempted to achieve this objective.

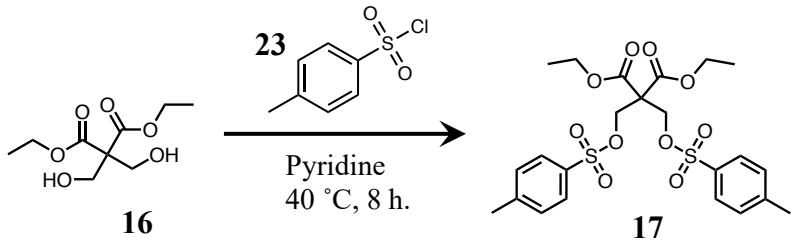
A. Synthesis of 1,2-Dithiolane-4-carboxylic Acid

1,2-Dithiolane-4-carboxylic acid (**7**), a cyclic disulphide known as asparagusic acid, was the first synthesis compound identified as a potential linker for the project. A synthetic route **(Scheme 4.1)** to produce it was designed according to the literature[476-480].



Scheme 4.1. Synthetic route to obtain asparagusic acid (**22**), a chemical linker, in 6 steps: **(i)** coupling of *p*-toluenesulphonyl chloride (**23**) with the dihydroxymethyl malonate **16**; **(ii)** nucleophilic substitution reaction (S_N2) of the tosylate groups of compound **17** by thioacetates to afford **18**; **(iii)** S_N2 at a carbonyl group to obtain dithiol **19**; **(iv)** hydrolysis of **19** to produce the malonic acid **20**; **(v)** decarboxylation of **20**; **(vi)** intramolecular reaction to produce asparagusic acid. Only the first step was completed after several unsuccessful attempts **(Table 4.3)** to synthesise **18**.

(**17**) *Diethyl-2,2-bis((tosyloxy)methyl)malonate*



Scheme 4.2. Preparation of diethyl 2,2-bis((tosyloxy)methyl)malonate (**17**) from 2,2-bis(hydroxymethyl)malonate (**16**) and *p*-toluenesulfonyl chloride (**23**). The reaction is the first step of the synthetic route shown in **Scheme 4.1** to obtain asparagusic acid (**22**).

2.004 g (9.1 mmol) of diethyl 2,2-bis(hydroxymethyl)malonate (**16**) were charged in a 25 mL round bottom flask and dissolved in 20 mL (248.29 mmol) of pyridine. While stirring, 10 g (18.92 mmol) of *p*-toluenesulfonyl chloride (**23**) were added in small portions to obtain a white, completely opaque suspension. The reaction was stirred at 1,500 rpm for 8 h. at 60 ℃. Afterwards, the reaction crude was poured into a crystalliser containing a mixture of water (130 mL), methanol (250 mL) and HCl 1 M (100mL) at 0 ℃ and left for 20 minutes for crystals to form. The white crystals of 2,2-bis((tosyloxy)methyl)malonate (**17**) were filtered with the help of a vacuum pump and washed 3 times with 50 mL of water. Further purification with flash chromatography (CH_2Cl_2, R_f = 0.50) afforded a pure compound in the form of a fine, white, crystalline powder (3.341 g, 69% yield). **^{1}H-NMR** (300 MHz, $CDCl_3$) δ 7.73 (d, 4H, C2-H), 7.35 (d, J = 8.0 Hz, 4H, C3-H), 4.42 (s, 4H, -SO_2-O-CH_2), 4.11 (q, J = 7.1 Hz, 2H, -CO-O-CH_2), 2.46 (s, 3H, C4-CH_3), 1.17 (t, J = 7.1 Hz, 3H, -CH_2-CH_3). **^{13}C-NMR** (400 MHz, $CDCl_3$) δ 165.05 (2C, C=O), 145.32 (2C, -C1-SO_3-), 132.01 (2C, C4), 130.01 (4C, C3), 128.02 (4C, C2), 66.18 (2C, -O-CH_2-CH_3), 62.72 (2C, -SO_2-O-CH_2-), 57.40 (1C, -C-(C=O)$_2$),

21.69 (2C, -C4-$\underline{C}H_3$), 13.76 (2C, -O-CH_2-$\underline{C}H_3$). **MS** (ESI+), m/z (%); $C_{23}H_{28}O_{10}S_2$, calculated: 528.11 ($[M]^+$); found: 551.1 ($[M + Na]^+$, 100%), 588.2 ($[M + IsoProp]^+$, 37%), 546.2 ($[M + NH_4]^+$, 27%). **XRD** Data shown in **Figure 5.6, Table 4.1** and **Table 4.2**.

Table 4.1. XRD crystal data and structure refinement for diethyl-2,2-bis(tosyloxy)methyl)malonate (**17**).

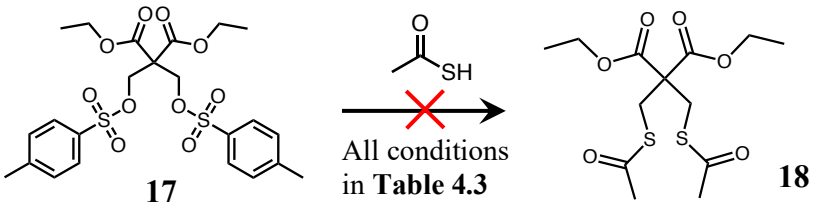
Empirical formula	$C_{23}H_{28}O_{10}S_2$
Formula weight	528.57
Temperature/K	100.00(10)
Crystal system	orthorhombic
Space group	$P2_12_12_1$
a/Å	8.4065(2)
b/Å	8.7660(3)
c/Å	34.0762(12)
α/°	90
β/°	90
γ/°	90
Volume/$Å^3$	2511.12(14)
Z	4
$\rho_{calc}g/cm^3$	1.398
μ/mm^{-1}	0.266
F(000)	1112.0
Crystal size/mm^3	0.273 × 0.227 × 0.163
Radiation	MoKα (λ = 0.71073)
2Θ range for data collection/°	6.67 to 52.722
Index ranges	-10 ≤ h ≤ 5, -10 ≤ k ≤ 10, -34 ≤ l ≤ 42
Reflections collected	14741
Independent reflections	5005 [R_{int} = 0.0402, R_{sigma} = 0.0471]
Data/restraints/parameters	5005/0/320
Goodness-of-fit on F^2	1.034
Final R indexes [I>=2σ (I)]	R_1 = 0.0361, wR_2 = 0.0791
Final R indexes [all data]	R_1 = 0.0412, wR_2 = 0.0824
Largest diff. peak/hole / e $Å^{-3}$	0.33/-0.36
Flack parameter	-0.05(4)

Table 4.2. Fractional atomic coordinates ($\times 10^4$) and equivalent isotropic displacement parameters ($Å^2 \times 10^3$) for diethyl-2,2-bis(tosyloxy)methyl)malonate (**17**). U_{eq} is defined as 1/3 of of the trace of the orthogonalised U_{IJ} tensor.

atom	X	Y	Z	U (eq)
C1	9424(3)	4798(3)	3715.9(8)	13.5(6)
C2	8769(3)	3181(3)	3659.3(8)	14.3(6)
C3	7798(4)	1000(3)	3992.4(9)	17.7(6)
C4	7344(4)	583(4)	4405.0(9)	26.9(8)
C5	8164(3)	5823(3)	3904.8(8)	14.4(6)
C6	5700(3)	7052(4)	3793.4(9)	20.4(6)
C7	4392(3)	7041(4)	3493.6(9)	23.8(7)
C8	9854(3)	5433(3)	3314.0(8)	14.3(6)
C9	8887(3)	8293(3)	2762.1(8)	13.0(6)
C10	8589(3)	7458(3)	2423.9(8)	17.4(6)
C11	7153(3)	7664(3)	2231.3(8)	18.6(7)
C12	6014(3)	8679(3)	2374.4(8)	17.6(6)
C13	6356(4)	9492(3)	2714.9(9)	19.9(7)
C14	7783(3)	9322(3)	2908.4(9)	18.2(6)
C15	4436(4)	8879(4)	2171.1(9)	24.8(7)
C16	10856(3)	4742(3)	3992.6(8)	16.2(6)
C17	12637(3)	1643(3)	4325.6(8)	17.3(6)
C18	12039(4)	387(3)	4127.1(9)	21.5(7)
C19	11413(4)	-807(4)	4340.6(9)	25.1(7)
C20	11366(4)	-769(4)	4748.3(9)	24.6(7)
C21	11983(4)	498(4)	4938.4(10)	29.0(8)
C22	12609(4)	1706(4)	4732.6(9)	24.1(7)
C23	10667(5)	-2079(4)	4978.6(11)	40.4(10)
O1	8641(2)	2559(2)	3347.1(6)	20.0(5)
O2	8390(2)	2571(2)	4007.1(6)	17.3(4)
O3	8322(2)	6446(2)	4215.9(6)	19.9(5)
O4	6916(2)	5971(2)	3667.2(6)	16.4(4)
O5	10220(2)	7036(2)	3384.5(5)	15.7(4)
O6	11759(2)	7183(2)	2775.6(6)	21.7(5)
O7	11175(2)	9451(2)	3185.1(6)	21.7(5)
O8	11996(2)	3747(2)	3800.7(6)	18.0(5)

O9	14522(3)	2571(3)	3770.7(7)	33.9(6)
O10	13939(3)	4329(3)	4318.1(7)	30.2(6)
S1	10690.4(8)	8047.7(9)	3011.6(2)	15.26(17)
S2	13452.4(8)	3151.3(9)	4055.0(2)	21.46(19)

(**18**) *Diethyl 2,2-bis((acetylthio)methyl)malonate*



Scheme 4.3. Reaction scheme for the synthesis of diethyl 2,2-bis((acetylthio)methyl)malonate (**18**), second step of the synthetic route to afford asparagusic acid (**22**). All attempts under different reaction conditions **(Table 4.3)** failed to produce **18**.

In a small vial, 500 mg (0.95 mmol) of 2,2-bis((tosyloxy)methyl)malonate (**17**) were suspended in 2.78 mL of water in ice-bath conditions with magnetic stirring (1,500 rpm). A solution of Na_2CO_3 (207 mg, 1.95 mmol) in water (0.83 mL) was added to guarantee a strong basic medium (pH>10). The suspension was set under Ar atmosphere and 148.24 mg (1.95 mmol) of thioacetic acid (**24**) were added in small portions with a syringe. The reaction was left to proceed until TLC evidenced that **17** had disappeared from the reaction medium. Afterwards, the suspension was acidified with 0.5 mL of HCl (1M) to obtain a white precipitate. The precipitate was extracted with EtOAc (3 x 25 mL) and the organic layer (EtOAc) was dried with Na_2SO_4. The rotary evaporator was used to remove the EtOAc to obtain a yellowish oil expected to be 2,2-bis((acetylthio)methyl)malonate (**18**). The oily crude product was purified with flash column chromatography (SiO_2) with eluent hexane/EtOAc 3:1 followed by

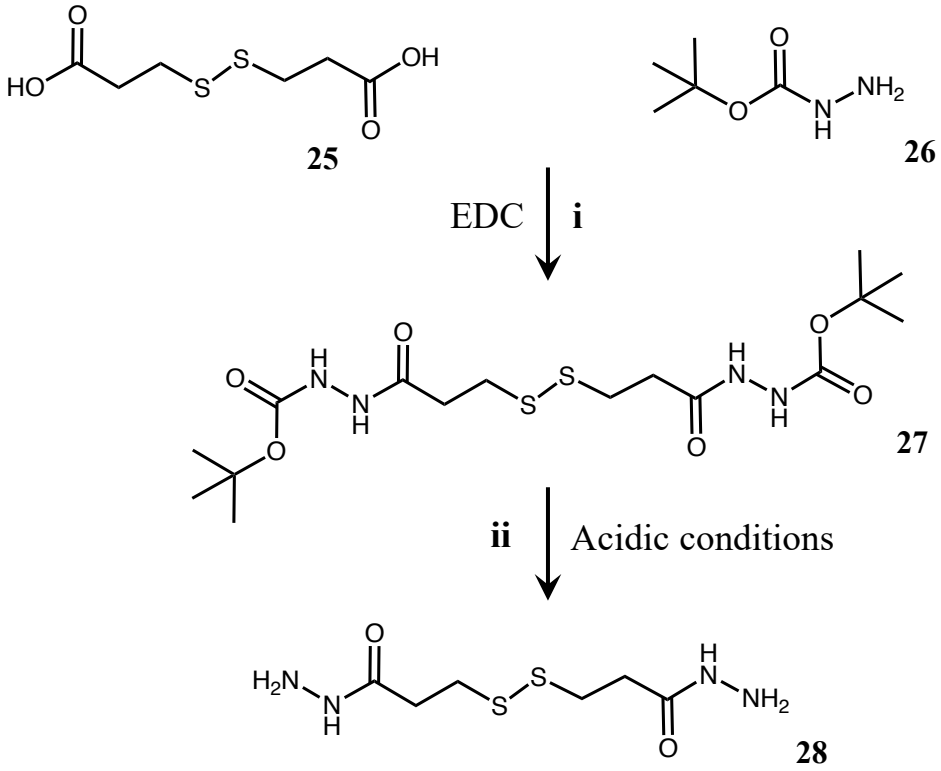
hexane/EtOAc 2:1. Characterisation of the oil showed that the synthesis was unsuccessful under the abovementioned conditions; therefore, new ones were attempted and are reported in **Table 4.3**.

Table 4.3. Reaction conditions attempted to synthesise diethyl 2,2-bis((acetylthio)methyl)malonate (**18**). Despite trying different solvents, temperature and atmosphere conditions, compound **18** could not be finally obtained. In entries with superscript 'a', T was left to reach room T after 8 h.; in those with superscript 'b', no Na_2CO_3 (aq.) was used.

Entry	Solvent	T (˚C)	Atmosphere	Time (h.)	Yield (%)
1[a]	water	0	air	24	0
2[b]	Py	0	air	24	0
3[a]	THF	0	air	24	0
4[a]	Py	0	Ar	24	0
5	THF	rt	Ar	24	0
6	AcCN	rt	Ar	24	0
7[b]	Py	rt	Ar	24	0
8	DMF	rt	Ar	24	0
9[b]	Py	rt	Ar	24	0

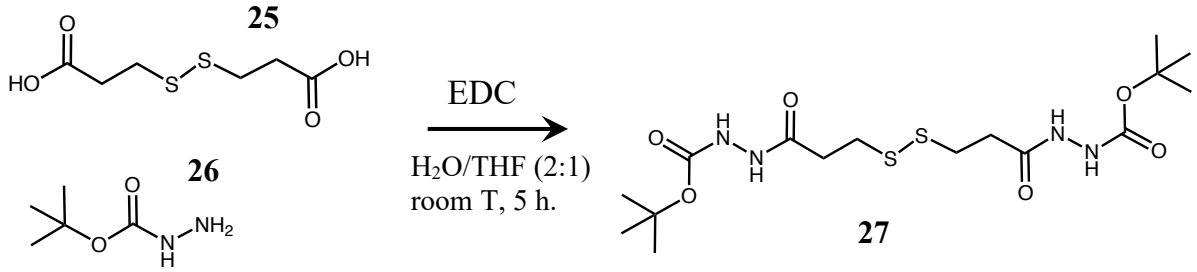
B. Preparation of 3,3'-Disulfanediyldi(propanehydrazide)

Following the unsuccessful efforts to synthesise asparagusic acid, the organodisulfur **28**, 3,3'-disulfanediyldi(propanehydrazide) (DPA-HD), was considered as a new linker for the project. The synthetic route drawn for this compound is shown in **Scheme 4.4**.



Scheme 4.4. Synthetic route for the preparation of DPA-HD (**28**) in 2 steps: first, the coupling agent EDC was used to introduce the amide group into diacid **25** with *tert*-butyl carbazate (**26**), obtaining di-*tert*-butyl 2,2'-(3,3'-disulfanediylbis(propanoyl))bis(hydrazine-1-carboxylate) (**27**); second, the deprotection of the *tert*-butoxycarbonyl (Boc) groups of **27** was achieved under acidic conditions (TFA or HCl).

(**27**) *Di-tert-butyl 2,2'-(3,3'-disulfanediylbis(propanoyl))bis(hydrazine-1--carboxylate)*

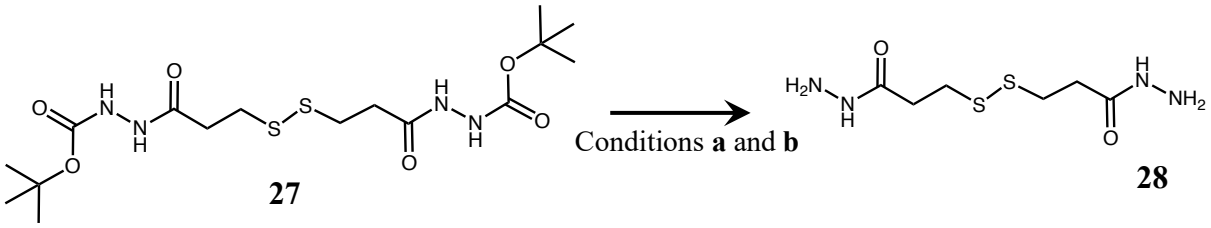


Scheme 4.5. Reaction conditions for the synthesis of di-*tert*-butyl 2,2'-(3,3'-disulfanediylbis(propanoyl))bis(hydrazine-1-carboxylate) (**27**), the first step to obtain **28** according to the synthetic route described in **Scheme 4.4**.

14.17 g (111.23 mmol) of *tert*-butyl carbazate (**26**) charged in a 500 mL RBF were dissolved in 200 mL of tap water with the help of stirring. 10.13 g (48.2 mmol) of 3,3'-dithiodipropionic acid (DPA, **25**) were also dissolved in 100 mL of THF in a 250 mL RBF with stirring. Then, both solutions were mixed and 21.16 g (110.15 mmol) of EDC were slowly added. The mixture, a perfect dissolution, was left reacting for 5 h. at room temperature. The product formed a white suspension that was filtered with vacuum and washed abundantly with water in the Buchner funnel to remove impurities. The pure di-*tert*-butyl 2,2'-(3,3'-disulfanediylbis(propanoyl))bis(hydrazine-1-carboxylate (**27**) obtained (7.47 g, 83% yield) was a white crystalline powder. **^{1}H-NMR** (400 MHz, $CDCl_3$) δ 8.89 (b, 2H, -O-CO-N<u>H</u>-NH), 6.66 (b, 2H, -O-CO-NH-N<u>H</u>-), 3.03 (t, J = 6.7 Hz, 4H, -CH_2-C<u>H</u>$_2$-S-), 2.68 (t, J = 6.7 Hz, 4H, -C<u>H</u>$_2$-CH_2-S-), 1.48 (s, 18H, -O-C-(C<u>H</u>$_3$)$_3$). **^{13}C-NMR** (400 MHz, $CDCl_3$) δ 235.56 (2C, -NH-<u>C</u>O-CH_2-), 170.86 (2C, -O-CO-NH-), 82.23 (2C, -O-<u>C</u>-(CH_3)$_3$, 34.24 (2C, -NH-CO-<u>C</u>H$_2$-), 33.20 (2C, -CH_2-<u>C</u>H$_2$-S), 28.17 (6C, -O-C-(<u>C</u>H$_3$)$_3$). **MS** (ESI+), m/z (%); $C_{16}H_{30}N_4O_6S_2$, calculated: 438.16 ($[M]^+$);

found: 461.15 ($[M + Na]^+$, 100%), 216.04 ($[M + 2AcN + 2H]^{2+}$, 8%). **FTIR** (ATR), υ (cm^{-1}) 3282 (b), 1747 (w, overtone, O-C=O), 1725 (s, O-C=O), 1660 (s, C-C=O), 1549 (w, N-H), 1502, 1365, 1236, 1157.

(**28**) *3,3'-disulfanediyldi(propanehydrazide), DPA-HD*

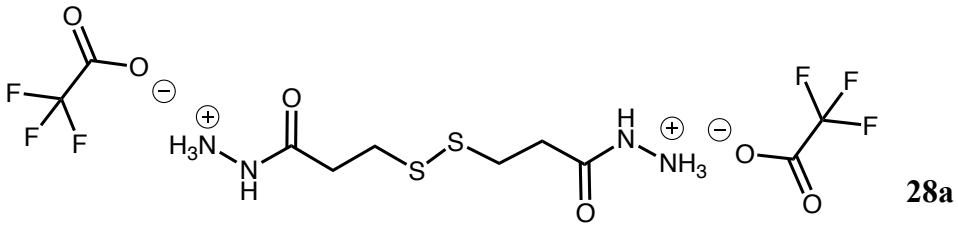


Scheme 4.6. Synthesis of DPA-HD (**28**) from di-*tert*-butyl 2,2'-(3,3'-disulfanediylbis(propanoyl))bis(hydrazine-1-carboxylate) (**27**). The removal of Boc groups from **27** was tried with two different acids: TFA (conditions **a**) and HCl (conditions **b**).

The synthesis of DPA-HD was attempted under two different acidic conditions:

Conditions a: in a 50 mL RBF containing 1.00 g (2.28 mmol) of **27** were added 2.5 mL (32.67 mmol) of TFA. The reaction was left stirring at room temperature for 3 h. Next, the excess of TFA in the crude was removed by bubbling Ar until the liquid product started to become viscous. Then, the crude was purified by precipitation (dropwise) into *ca.* 150 mL of Et_2O. Finally, the ether was removed with vacuum to afford 0.52 g (48.9% yield) of **28a,** a hygroscopic, fluffy, white solid that within minutes of being exposed to the atmosphere became very sticky **(Figure 4.1)**. **^{1}H-NMR** (400 MHz, D_2O) δ 2.94 (t, J = 6.7 Hz, 4H, -CH_2-CH_2-S-), 2.73 (t, J = 6.7 Hz, 4H, -CH_2-CH_2-S-) **(Figure 5.7)**. **^{13}C-NMR** (400 MHz, D_2O) δ172.16 (2C, -CO-), 32.48 (2C, -S-CH_2-

CH_2-), 32.05 (2C, -S-CH_2-$\underline{C}H_2$). **MS** (ESI+), m/z (%); $C_6H_{14}N_4O_2S_2$, calculated: 238.06 ($[M]^+$); found: 261.02 ($[M + Na]^+$, 100%), 239.04 ($[M + H]^+$, 58%). **FTIR-ATR**, υ (cm^{-1}) 1672 (s, C=O), 1531 (w, N-H), 1432 (w), 1196 (s), 1140 (s) **(Figure 5.13)**. **FTIR-transmission**, υ (cm^{-1}) 1745 (w, C=O), 1677 (s, C=O), 1640 (s, C=O), 1432 (w), 1200 (s, C-F), 1149 (s) **(Figure 5.13)**.



28a

Figure 4.1. TFA salt of DPA-HD (**28a**). The salt was obtained after deprotecting the Boc groups of **27** with TFA.

Conditions b: a 1 L RBF containing 8.03 g (18.31 mmol) of **27** was charged with 395 mL of HCl (1M); the suspension formed was left stirring vigorously overnight at 40 ˚C. The colourless crude obtained was lyophilised and purified with reversed phase preparative HPLC (eluent from AcCN/H_2O 1:19 to 20:0 in 20 min., 10 $mL \cdot min^{-1}$). 0.95 g (3.99 mmol, 21.8%) of pure **28 (Figure 4.2)** were obtained. **^{1}H-NMR** (400 MHz, D_2O) δ 2.96 (t, J = 6.8 Hz, 4H, -CH_2-$C\underline{H_2}$-S-), 2.63 (t, J = 6.8 Hz, 4H, -$C\underline{H_2}$-CH_2-S-) **(Figure 5.18)**. **^{13}C-NMR** (400 MHz, D_2O) δ173.05 (2C, -CO-), 33.02 (2C, -S-$\underline{C}H_2$-CH_2-), 32.96 (2C, -S-CH_2-$\underline{C}H_2$). **MS** (ESI+), m/z (%); $C_6H_{14}N_4O_2S_2$, calculated neutral DPA-HD: 238.06 ($[M]^+$); found: 261.05 ($[M + Na]^+$, 100%), 239.06 ($[M + H]^+$, 48%). **FTIR** (ATR), υ (cm^{-1}) 1682 (s, C=O), 1577 (w, N-H), 1525 (w), 1475 (s), 1410 (s), 1361 (w), 1248 (w), 1165 (s). **HPLC** (Kinetex 5 μm, C18, 100A, Axia packed; λ = 210.4 nm)

R_{t1} = 5.91 min., area = 6.3%; **R_{t2}** = 8.75 min., area = 57.9%; R_{t3} = 10.42 min., area = 31.3%; and R_{t4} = 12.82 min., area = 3.63% **(Figure 4.2)**.

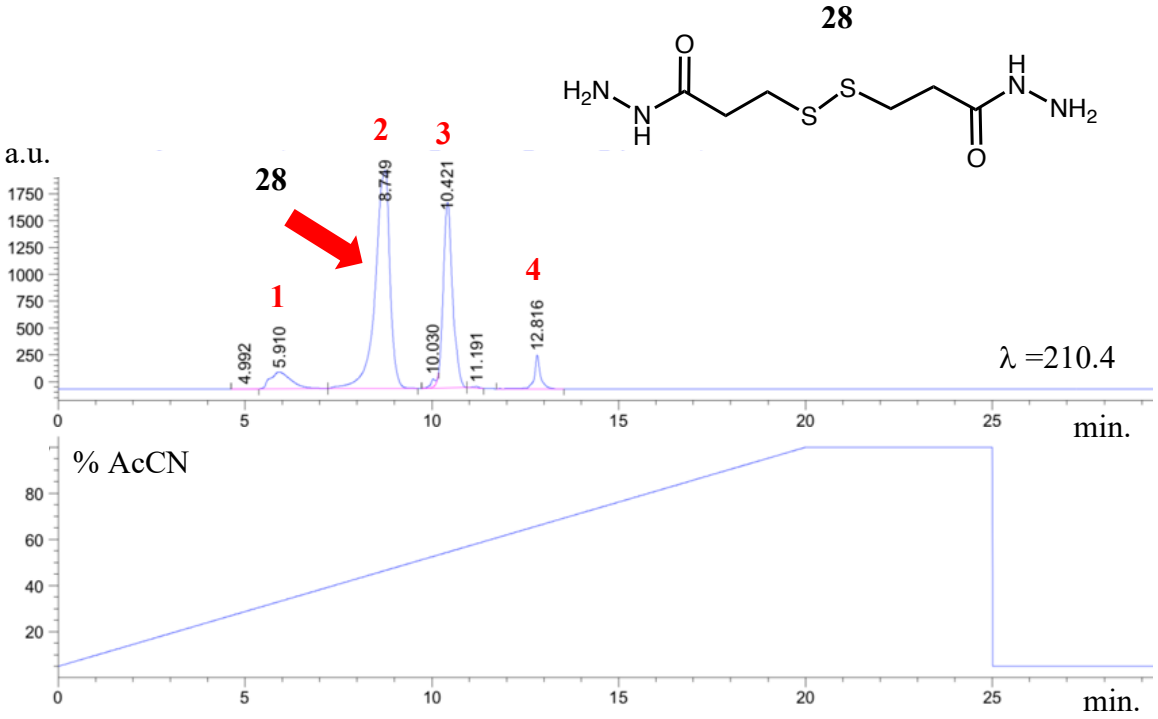
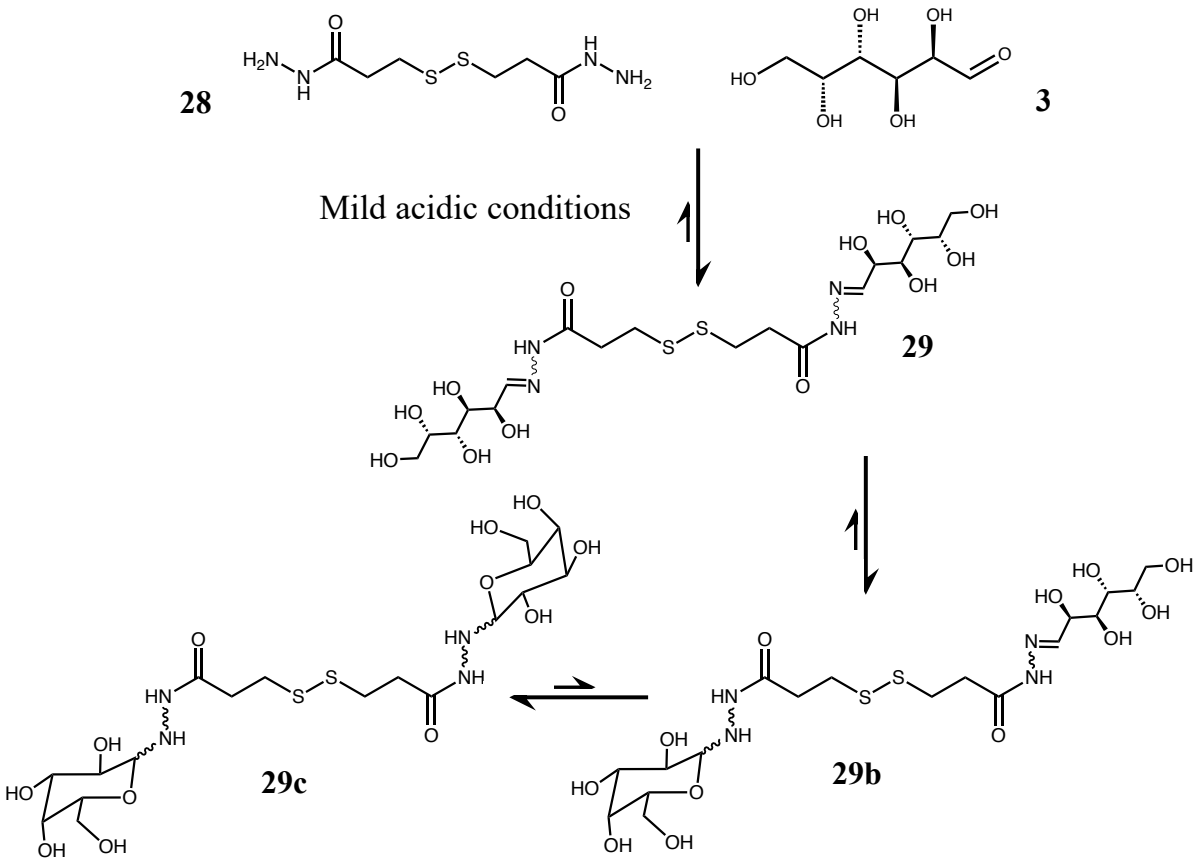


Figure 4.2. Prepartive HPLC chromatography of compound **28** in reverse phase. The retention time of pure **28** (red arrow) was 8.75 min. with an eluent ramp (bottom) from AcCN/H_2O 1:19 to 20:0 in 20 min. at 10 mL·min^{-1}. Retention times recorded with a UV detector at λ = 210.4 nm.=

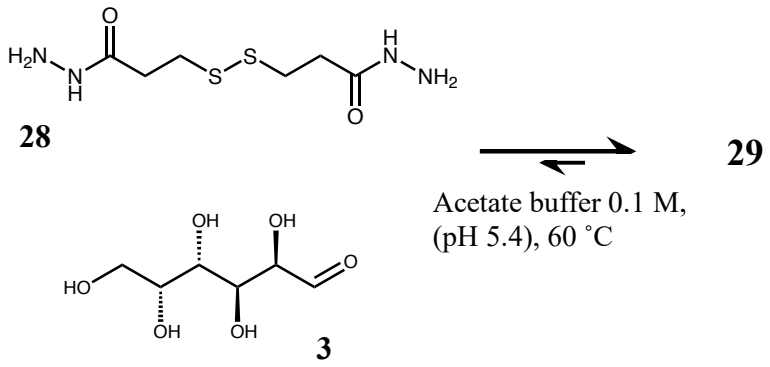
C. Coupling of 3,3'-Disulfanediyldi(propanehydrazide) with Galactose

The coupling of DPA-HD with Gal to obtain 3-((3-oxo-3-(2-((3R,4S,5R,6R)-3,4,5-trihydroxy-6-(hydroxymethyl)tetrahydro-2H-pyran-2-yl)hydrazineyl)propyl)disulfaneyl--N'-((3S,4R,5S,6S)-3,4,5-trihydroxy-6-(hydroxymethyl)tetrahydro-2H-pyran-2-yl)propanehydrazide (galactose 3,3'-disulfanediyldi(propanehydrazone), DPA-HD-Gal, **29**) is shown in **Scheme 4.7**.



Scheme 4.7. Condensation reaction to covalently couple DPH-HD (**28**) with Gal (**3**) for the obtainment of galactose 3,3'-disulfanediyldi(propanehydrazone) (**29**) where the monosaccharide was incorporated into a molecule prone to adsorb on Au electrodes through S atoms. The reaction was an equilibrium displaced towards the formation of hydrazones (**29**) under mildly acidic conditions. In aqueous media, due to the mutarotation of the sugar moieties, conformations with amines (**29b** and **29c**) were expected to be predominant.

(**29**) *Galactose 3,3'-disulfanediyldi(propanehydrazone), DPA-HD-Gal*

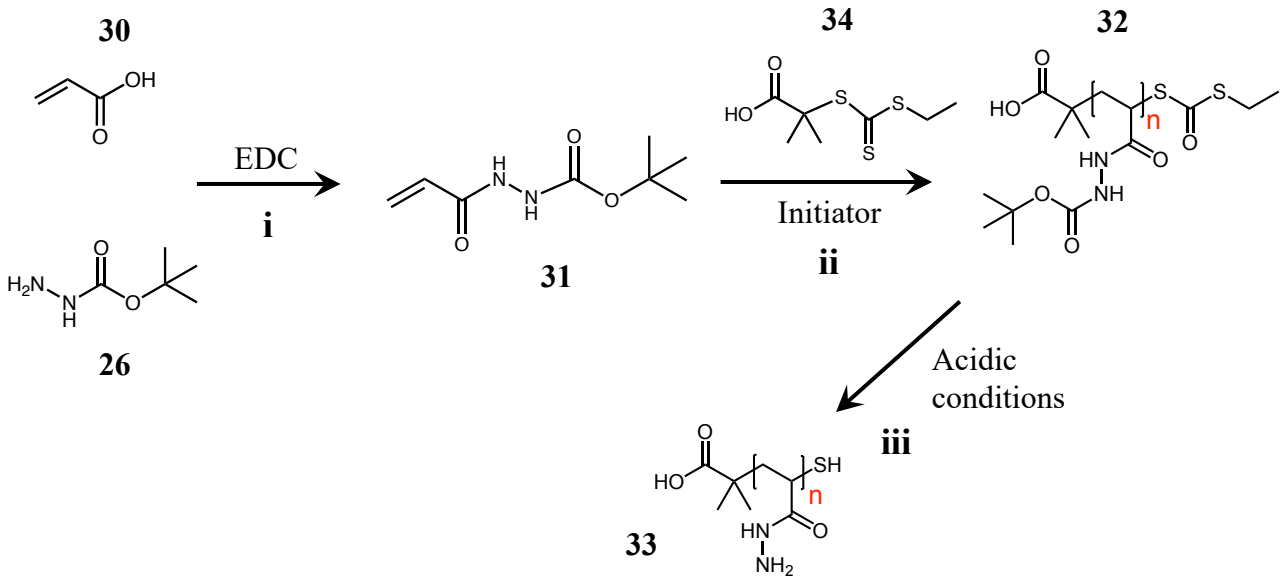


Scheme 4.8. Reaction conditions for the glycosylation of 3,3'-disulfanediyldi(propanehydrazide) (**28a** or **28**) with Gal (**3**). A slightly acidic medium of reaction and a mild temperature allowed the coupling of the di-hydrazide with the monosaccharide to obtain galactose 3,3'-disulfanediyldi(propanehydrazone) (**29**).

For a synthesis with the TFA salt of DPA-HD (**28a**) as starting material, 14.31 mg (0.060 mmol) of disulphide and 78.67 mg (0.44 mmol) of Gal were dissolved in acetate buffer (0.1 M, pH 5.5) prepared in D_2O and the mixture was left to react at 60 ˚C. The evolution of the reaction was followed by ^{1}H-NMR to determine its completion, although the formation of a thick suspension made it already impossible after 3 h. In fact, given the difficulties of dissolving the product with any mixture of solvents, no purification was conducted and only a tentative characterisation of the lyophilised crude (MS) was performed. **MS** (ESI+), m/z (%); $C_{18}H_{34}N_4O_{12}S_2$, calculated = 562.16 ($[M^+]$); found: 423.10 (100%), 585.15 ($[M + Na]^+$, 38%) **(Figure 5.15)**.

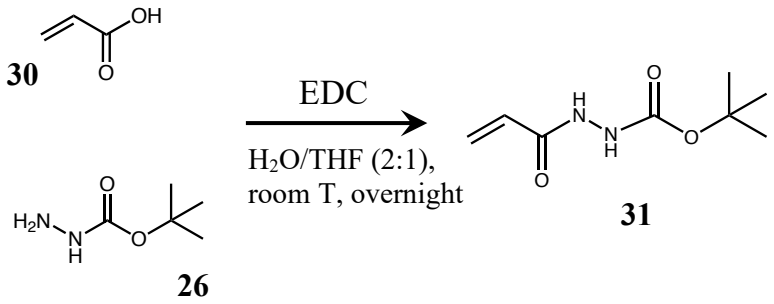
D. Synthesis of Poly(acryloyl) Hydrazide

The synthesis of poly(acryloyl) hydrazide (pAH_n) was accomplished in three steps **(Scheme 4.9)**.



Scheme 4.9. General procedure for the preparation of poly(acryloyl) hydrazide (pAH_n, **33**). First, monomer **31** was obtained by coupling acrylic acid (**30**) with *tert*-butyl carbazate (**26**); second, **31** was polymerised with the help of an initiator and the degree of polymerisation (DP) was controlled with 2-((ethylthio)carbonothioyl)thio-2-methylpropanoic acid (**34**); finally, the hydrazide group of the pendant groups of the polymer obtained (Boc-pAH_n, **32**) was deprotected under acidic conditions to obtain **33**.

(**15**) *Tert-butyl 2-acryloylhydrazinecarboxylate*



Scheme 4.10. Preparation of *tert*-butyl 2-acryloylhydrazinecarboxylate (**31**), the monomer of poly(*tert*-butyl-2-acryloylhydrazine-1-carboxylate) (**32**). The synthesis, first step of **Scheme 4.9**, required reacting acrylic acid (**30**) with *tert*-butyl carbazate (**26**) using EDC as a coupling agent.

12.02 g (90.95 mmol) of *tert*-butyl carbazate (**26**) were charged in a 500 mL RBF and dissolved in 240 mL of water. Once dissolved with stirring, 120 mL of THF were added. Finally, the RBF was also charged with 7.5 mL (109.91 mmol) of acrylic acid (**30**) to obtain an off-yellow dissolution that was stirred overnight. Product **31** was purified with a separation funnel: 5 x 50 mL of EtOAc, 2 x 50 mL of $NaHCO_3$ (sat.) and 1 x 50 mL of brine. The solid in the organic phase was dried with anhydrous Na_2SO_4 and then recrystalised from CH_2Cl_2 to afford 8.36 g (41.07% yield) of white crystalline monomer. **^{1}H-NMR** (400 MHz, DMSO-d_6) δ 9.78 (s, 1H, -O-CO-NH-), 8.82 (s, 1H, =CH-CO-N<u>H</u>-), 6.24-6.14 (m, 2H, -CO-CH=C<u>H</u>$_2$), 5.71-5.68 (m, 1H, -CO-C<u>H</u>=CH$_2$), 1.40 (s, 9H, -O-C-(CH$_3$)$_3$ **(Figure 4.3)**.

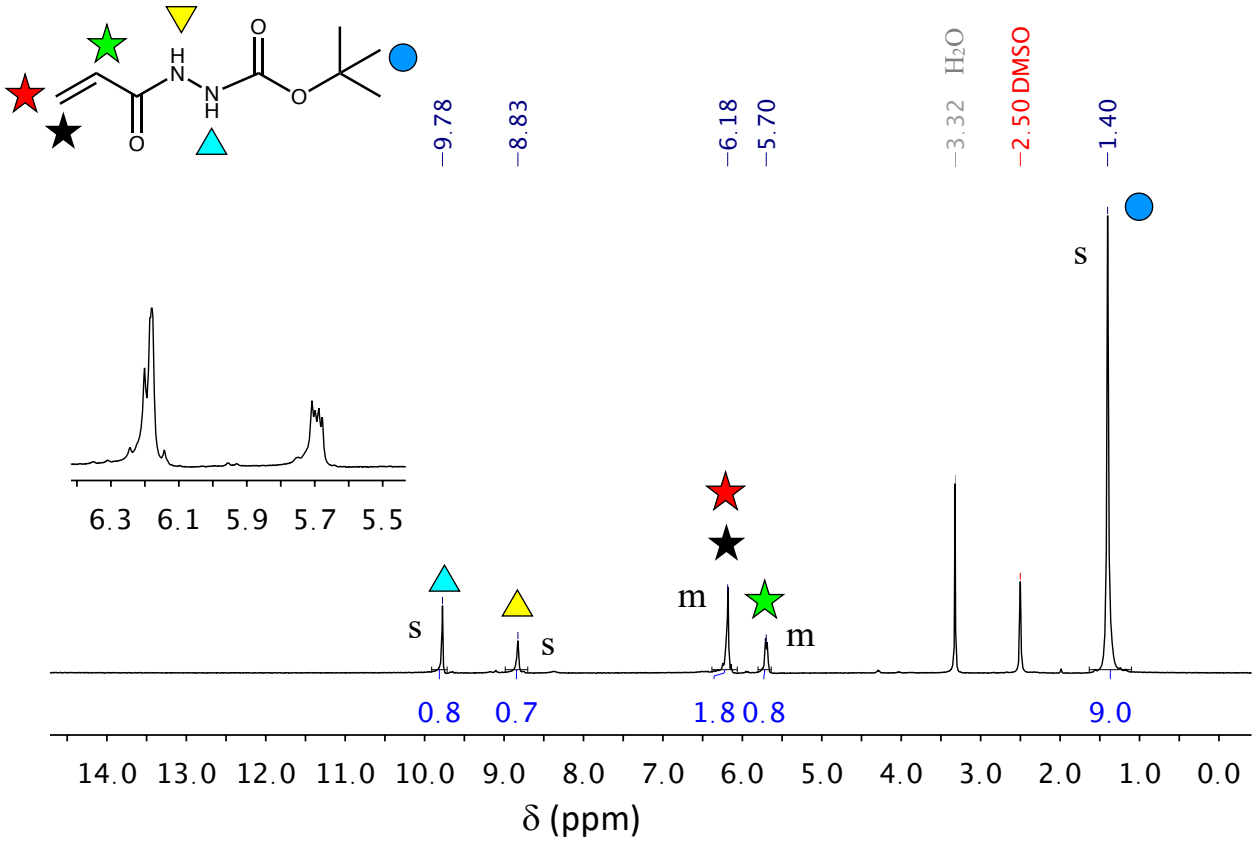
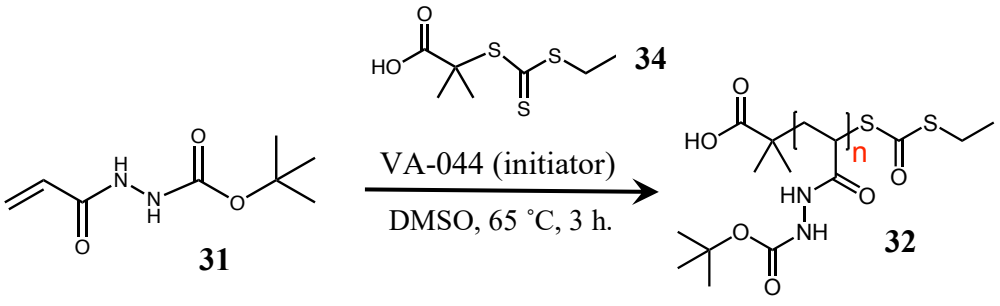


Figure 4.3. ^{1}H-NMR spectrum (400 MHz) of *tert*-butyl 2-acryloylhydrazinecarboxylate (**31**), the monomer used to produce pAH_n, in DMSO-d_6. The integration of the signals was normalised with the Boc group peak (blue dot) integral.

(**17**) *Poly(tert-butyl-2-acryloylhydrazine-1-carboxylate), Boc-pAH$_n$*



Scheme 4.11. Polymerisation conditions of *tert*-butyl 2-acryloylhydrazinecarboxylate (**31**) to afford poly(*tert*-butyl-2-acryloylhydrazine-1-carboxylate) (Boc-pAH_n, **32**). The synthesis, step ii of **Scheme 4.9**, employed the initiator VA-044 and 2-((ethylthio)carbonothioyl)thio-2-methylpropanoic acid as the chain transfer agent to control the DP of the polymer.

A test tube was charged with 2.012 g (10.8 mmol) of **31** (monomer) and 13.94 mg (0.043 mmol) of VA-044 (initiator); to obtain **32** with an approximate DP of 50 (DP50, Boc-pAH$_{50}$, **32a**), 48.21 mg (0.21 mmol) of 2-((ethylthio)carbonothioyl)thio-2-methylpropanoic acid (**34**, RAFT agent) were also added to the tube. Then, 2 mL of DMSO and a magnetic stirrer were also introduced before the tube was sealed with a septum and deaerated with Ar for 30 min. Next, the polymerisation was started by submerging the test tube in an oil bath at 65 ˚C for exactly 3 h.; the reaction was stopped opening the septum. The crude was left to cool down becoming a very viscous, yellow solid; then it was diluted in 4 mL of acetone and dropwise precipitated into 250 mL of EtOAc through a 0.45 μm filter. The supernatant was removed with centrifugation, grinded down with a mortar and the off-yellow fine powder obtained dried inside a desiccator. Finally, the dry product, 1.7213 g (83.49% monomer conversion for a Boc-pAH$_n$ polymer with DP50, **32a**) was characterised. **^{1}H-NMR** (400 MHz, DMSO-d$_6$) δ 9.17 (b, s, -O-CO-N<u>H</u>-), 8.57 (b, s, -<u>H</u>N-CO-CH-), 2.05 (b, -SH), 1.64 - 1.02 (b, 1H in -CO-CH-, 2H in -C<u>H$_2$</u>-CH- and 9H in C(CH$_3$)$_3$) **(Figure 4.4)**. **GPC** (eluent: 0.05 M of LiBr in DMF; 60 ˚C, flow rate of 1 mL/min) elution time 15.679 min **(Figure 4.5)**. **FTIR** (ATR), υ (cm^{-1}) 1717 (s, C=O), 1680 (s, C=O), 1481 (w, N-H), 1456 (w, N-H), 1393 (w), 1368 (w), 1246 (s), 1157 (s).

The procedure to synthesise the DP20 polymer (Boc-pAH$_{20}$, **32b**) was exactly the same but with the following quantities of chemicals: 2.000 g (10.74 mmol) of **31**, 120.49 mg (0.53 mmol) of RAFT agent **34** and 17.36 mg (0.053) of initiator VA-044.

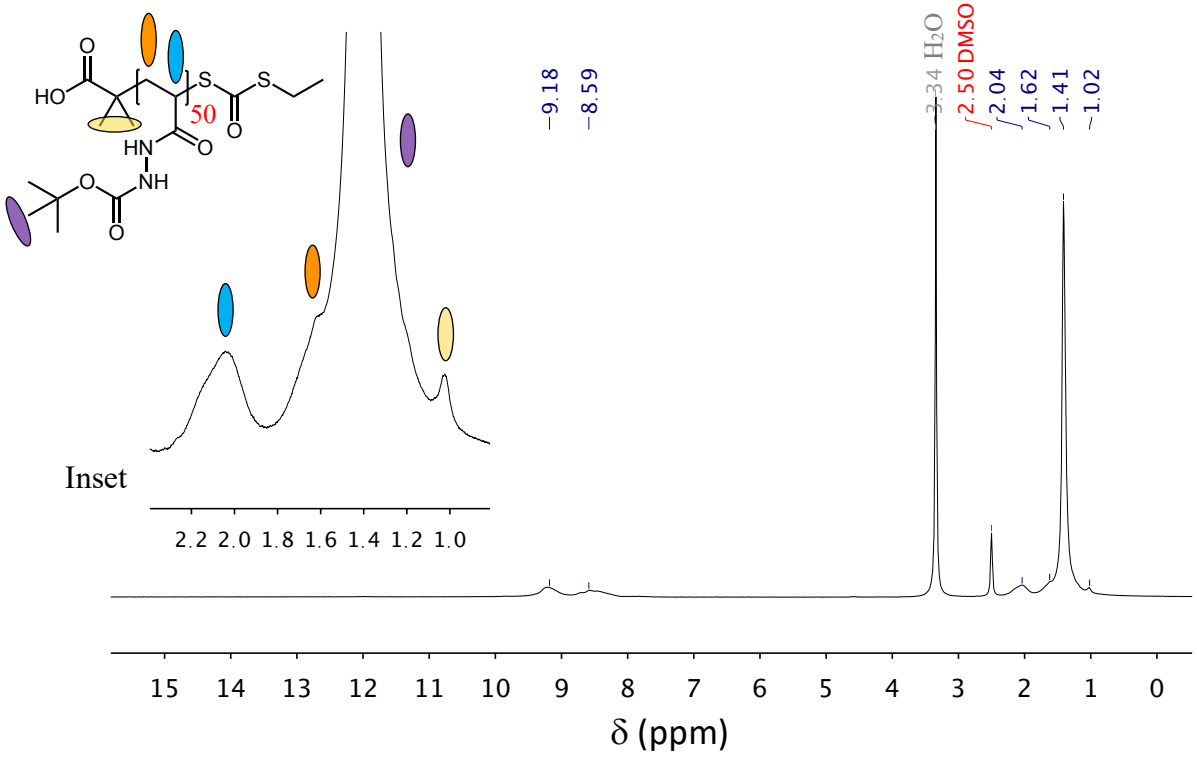


Figure 4.4. ^{1}H-NMR spectrum (300 MHz) of Boc-pAH$_{50}$ (**32a**) in DMSO-d_6. The broadness of the peaks confirmed the polymeric character of the sample. At low field (*ca.* 9 ppm) appeared the two signals of the protons on the N atoms.

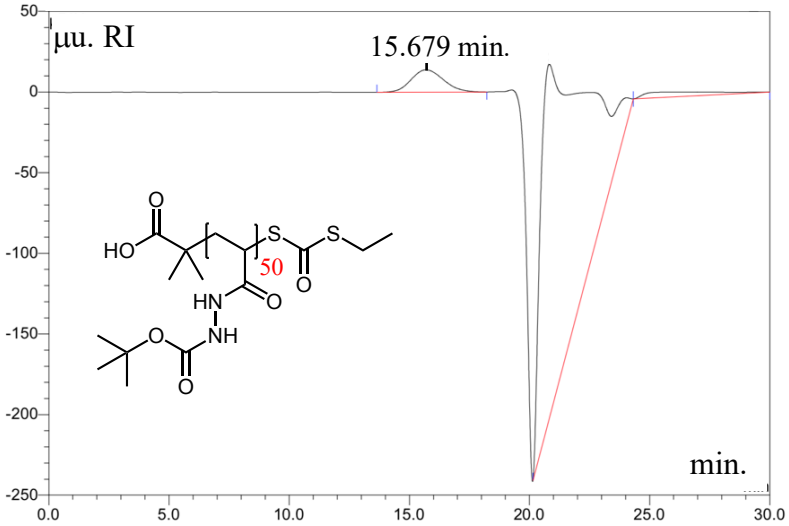
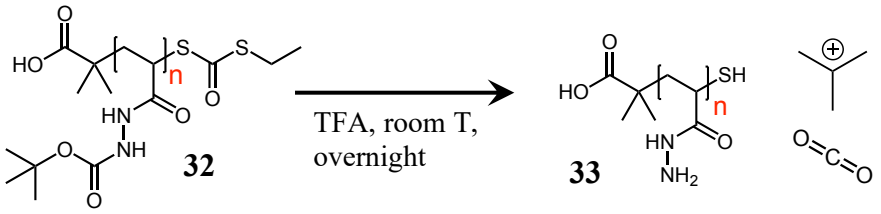


Figure 4.5. GPC of polymer **32a** (eluent: 0.05 M of LiBr in DMF; column at 60 ˚C, flow rate of 1 mL/min). The elution time according to the reflexion index detector occurred after 15.679 min. of the injection of the polymer sample.

(**18**) *Poly(acryloyl hydrazide), pAH$_n$*



Scheme 4.12. Synthesis of pAH$_n$ (**33**), step iii of **Scheme 4.9**. The deprotection in acidic conditions (TFA) of the Boc group of the pendant groups of **32** produced **33**.

The deprotection of Boc-pAH$_n$ requires its perfect dissolution in TFA and stirring at room temperature overnight followed by the removal of the excess of acid and a stage of purification. For example, 1.4480 g of Boc-pAH$_{50}$ were put in a 25 mL RBF with 9.05 mL of TFA; within 5 to 10 min. of stirring, the initial yellow suspension became a solution. After *ca*. 12 h., the excess of TFA (around 2/3 of the original volume) was removed bubbling Ar through the crude. Then, the crude was neutralised with saturated Na_2CO_3, dissolved in Milli-Q water, introduced in a dialysis membranes and dialysed for at least 3 days. Finally the polymer was lyophilised and left in a desiccator because of its high hygroscopicity. Once dry, the 0.5375 g of pAH$_{50}$ (**33a**) obtained (79.98% yield) were characterised. **^{1}H-NMR** (400 MHz, D_2O) δ 2.53 - 1.19 (b, 1H in -CO-CH-, 2H in -C$\underline{H_2}$-CH-), 0.99 (s, 3H, C-$(CH_3)_2$), 0.94 (s, 3H, C-$(CH_3)_2$) **(Figure 4.6)**. **GPC** (eluent: DPBS 0.0095 M without Ca^{2+} nor Mg^{2+}; flow rate 1 mL/min., column temperature 35 ˚C) elution time 15.458 min. **(Figure 4.7)**. **FTIR** (ATR), υ (cm^{-1}) 1603, 1515, 1445, 1390.

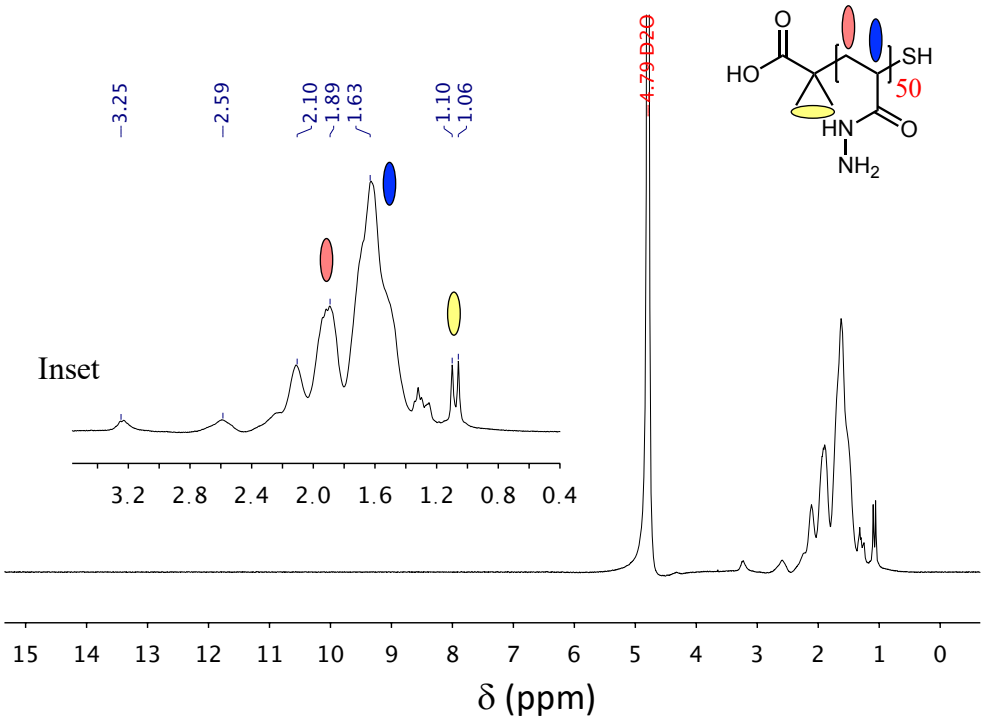


Figure 4.6. ^{1}H-NMR spectrum (300 MHz) of pAH_{50} (**33a**) in D_2O obtained after deprotection of Boc-pAH_{50} (**32a**) with TFA and dialysis.

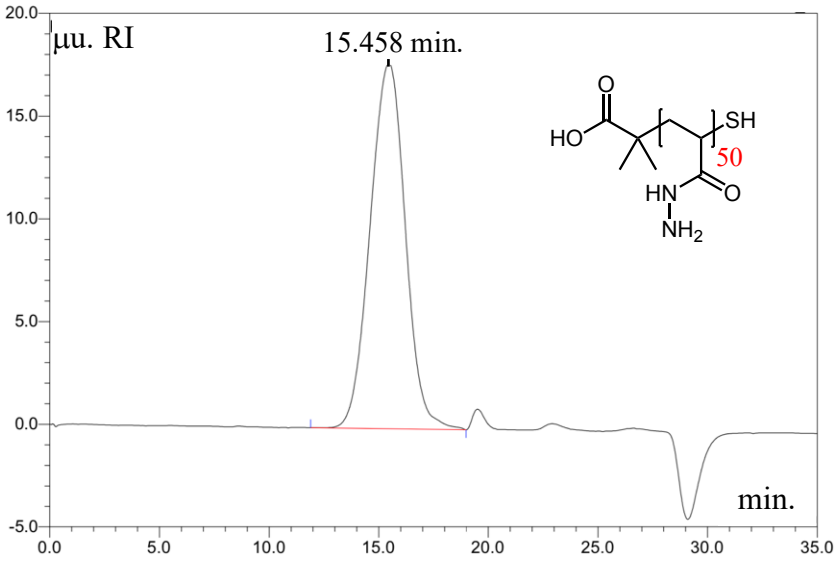
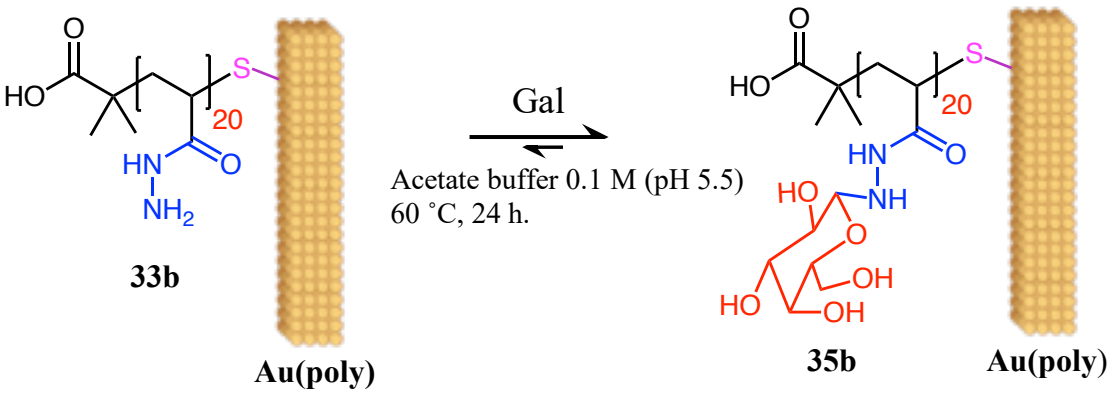


Figure 4.7. GPC of pAH_{50} (**33a**) (eluent: DPBS 0.0095 M without Ca^{2+} nor Mg^{2+}; flow rate 1 mL/min., column temperature 35 ˚C). The pure polymer eluted the chromatographic column at 15.458 min. according to the reflexion index detector.

E. Post-polymerisation Glycosylation of Poly(acryloyl) Hydrazide with Galactose in Heterogeneous Phase (Au-pAH$_{20}$-Gal)

After the immobilisation of pAH$_{20}$ on a Au electrode, the polymer was glycosylated with Gal **(Scheme 4.13)**.

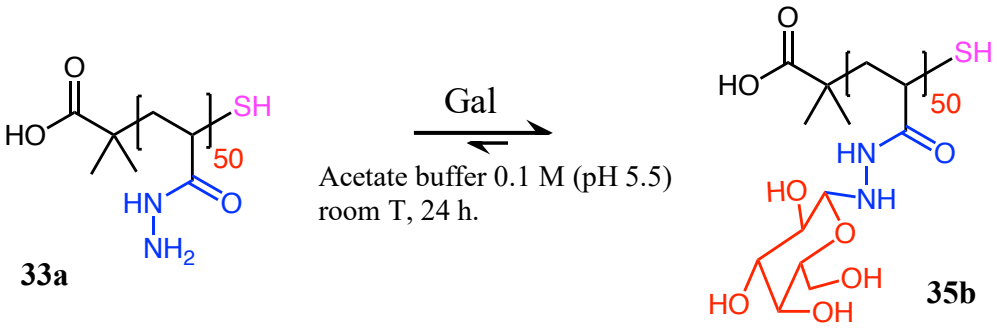


Scheme 4.13. Post-polymerisation glycosylation of pAH$_{20}$ (**33b**) with Gal in heterogeneous phase. Following the immobilisation of pAH$_{20}$ on a Au(poly) electrode, the immersion of the modified electrode in a 1.5 M Gal solution prepared in phosphate buffer 0.1 M allowed the coupling of the saccharide with the hydrazide pendant groups of the polymer.

A Au(poly) electrode modified **(section 4.2.3-D)** with pAH$_{20}$ (Au-pAH$_{20}$) was incubated in an acetate buffered solution (0.1 M, pH 5.5) with 1.5 M of Gal during 24 h. at 60 ˚C. The electrode surface was rinsed with Milli-Q water and electrochemically characterised **(Figure 6.6)**.

F. Post-polymerisation Glycosylation of Poly(acryloyl) Hydrazide with Galactose in Homogeneous Phase (pAH_{50}-Gal)

The **Scheme 4.14** shows the glycosylation in solution of pAH_{50} with Gal.

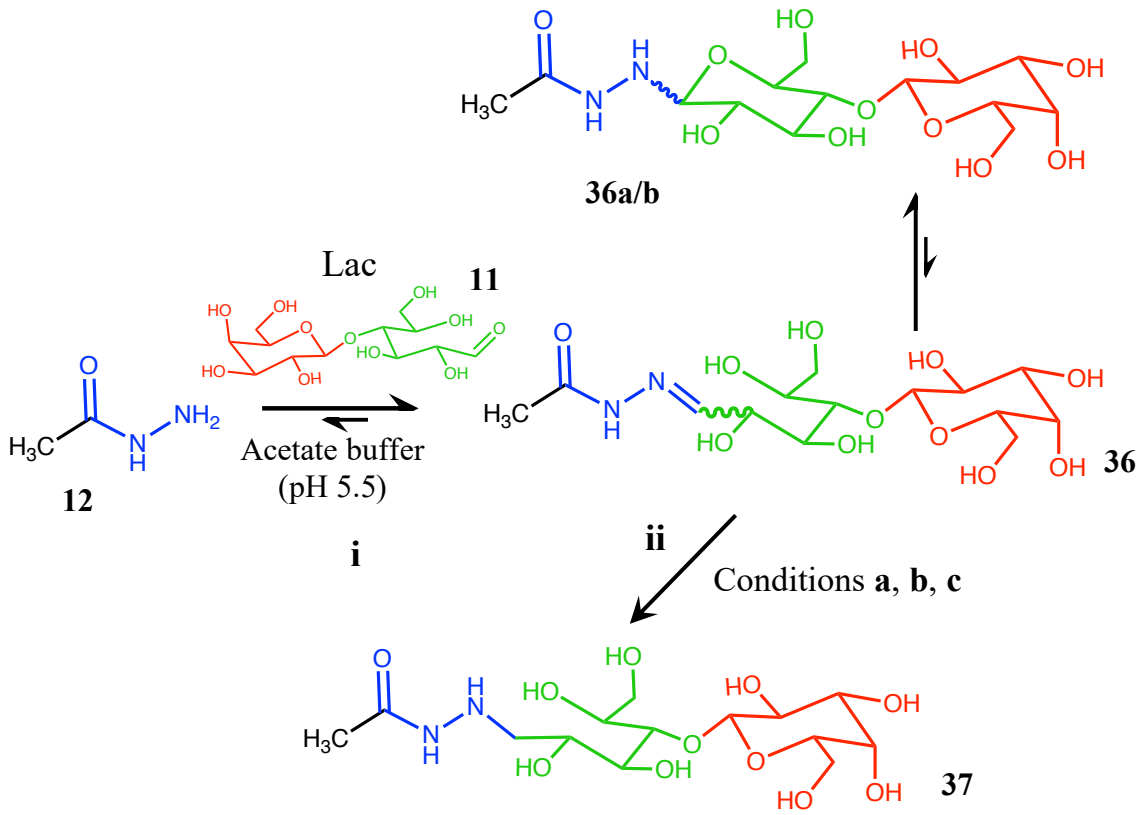


Scheme 4.14. Post-polymerisation glycosylation of pAH_{50} (**33a**) with Gal in homogeneous phase. To incorporate Gal into the hydrazide groups of pAH_{50}, the polymer was reacted with the sugar (pendant group/Gal, 1 : 2.1) in a mildly acidic medium at room temperature.

In a vial charged with 0.5 mL of acetate buffer (0.1 M, pH 5.5) prepared with D_2O were dissolved 22.3 mg of pAH_{50} and 100.4 mg (0.55 mmol) of Gal (hydrazide pendant group/Gal, 1 : 2.1) and left to react for 24 h. According to ^{1}H-NMR, *ca.* 66% of polymer loading with sugar (pAH_{50}-Gal_{33}) was achieved **(Figure 6.7)**. The crude product was employed for the modification of a Au(poly) electrode **(section 4.2.3-D)** that was then electrochemically characterised **(Figures 6.8)**. To reduce the loading of pAH_{50}, a synthesis with a smaller number of Gal equivalents (0.2) was carried out: in 0.5 mL of deuterated acetate buffer, 22.16 mg of pAH_{50} and 9.7 mg of Gal (0.054 mmol) were dissolved and the mixture was left to react at room temperature for 24 h. ^{1}H-NMR analysis **(Figure 6.10)** determined a saccharide loading of approximately 16% (pAH_{50}-Gal_8). The crude product was used to modify and characterise a Au(poly) electrode with CV **(Figure 6.11)**.

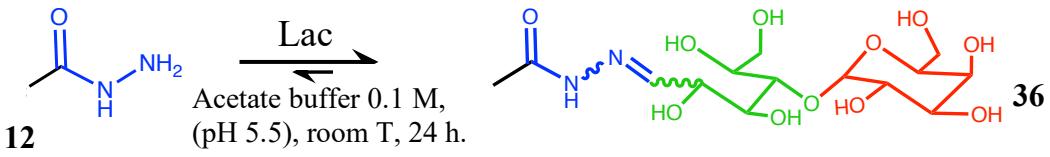
G. Glycosylation of Acetohydrazide with Lactose and Reduction (AcHD-RO-Gal)

AcHD was used to test the coupling of Lac with the hydrazide group and the reduction of the resulting hydrazone. **Scheme 4.15** shows the two steps of this synthetic route:



Scheme 4.15. Synthesis of *N'*-(2,3,5,6-tetrahydroxy-4--((galactopyranosyl)oxy)hexyl)acetohydrazide (AcHD-RO-Gal, **37**). After coupling acetohydrizide (**12**) with lactose (Lac, **11**) in a mild acidic medium to obtain *N'*-(lactosyl)acetohydrazide (**36**), different chemicals (conditions **a**, **b** and **c**) were used to reduce it into compound **37**.

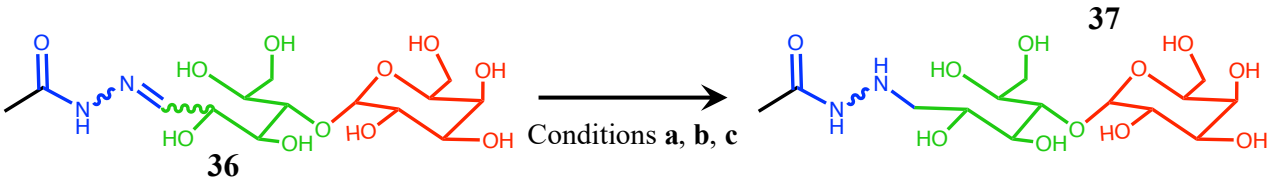
(**36a**) *N'-(lactosyl)acetohydrazide, AcHD-Lac*



Scheme 4.16. Reaction conditions to synthesising *N'*-(lactosyl)acetohydrazide (AcHD-Lac, **36**), the first step of **Scheme 4.15**. The coupling of AcHD with Lac proceeded in mildly acidic conditions at room temperature. The above scheme shows only the potential linear isomers (**36**) of the product.

First, 928.8 mg (2.58 mmoL) of Lac were weighed in a 10 mL RBF and mixed with 5 mL of acetate buffer (0.1 M, pH 5.5) prepared with D_2O; the mixture was mildly heated and stirred to obtain a perfect dissolution. Next, 93.53 mg (1.26 mmol) of AcHD were added to the Lac solution and left to react for 24 h. at room temperature. According to ^{1}H-NMR analysis of the crude product a yield of *ca.* 50% was afforded after 24 h. and 84% after 7 days **(Figure 6.12)**. The crude was directly employed for the synthesis of **37**.

(**22**) *N'-(2,3,5,6-tetrahydroxy-4-*
-((galactopyranosyl)oxy)hexyl)acetohydrazide, AcHD-RO-Gal



Scheme 4.17. Reduction of the linear tautomers of AcHD-Lac (**36**) to afford AcHD-RO-Gal (**37**), second step in the **Scheme 4.15**. The reduction of the hydrazones **36** was attempted using three different reaction conditions (**a**, **b** and **c**).

The reduction of AcHD-Lac (**36**) into AcHD-RO-Gal (**37**) was attempted using three different chemicals: $pyBH_3$, $NaBH_4$ and $NaBH_3CN$.

Conditions a:

For $NaBH_4$, 49 mg (1.30 mmol) of the salt were added to 1 mL of the crude obtained in the first step of **Scheme 4.15**. The reaction was left to react for 3 h. at 0˚C, and for another 12 h. at room temperature.

Conditions b:

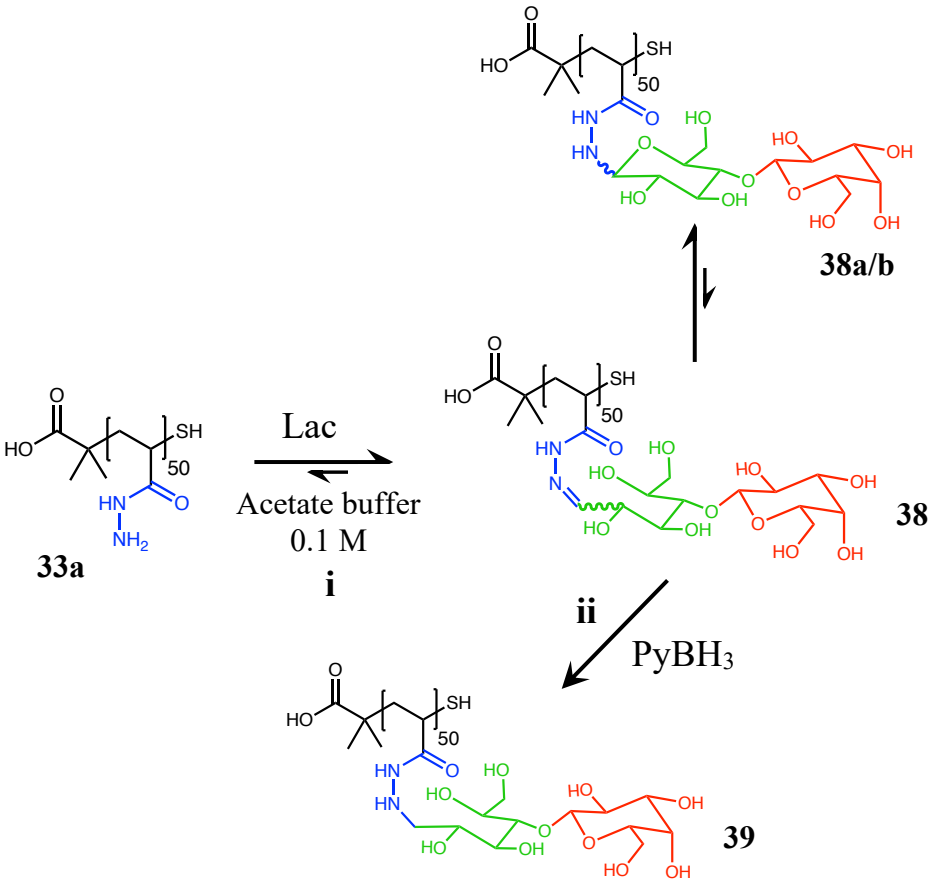
In the case of $pyBH_3$, 63 μL (3.49 mmol) of the complex were added to 1 mL of the crude product from the first step of the synthesis described in **Scheme 4.15**. Then, 23 μL of HCl (36%) were slowly added and the solution was stirred overnight at room temperature.

Conditions c:

Finally, when $NaBH_3CN$ was used, 35 mg (0.56 mmol) of borohydride were added to 1 mL of the crude afforded in the first step of **Scheme 4.15**. Afterwards, 15 μL of HCl (36%) were added dropwise and the mixture was left to react for 3 h. at 0˚C, and for 12 h. more at room temperature.

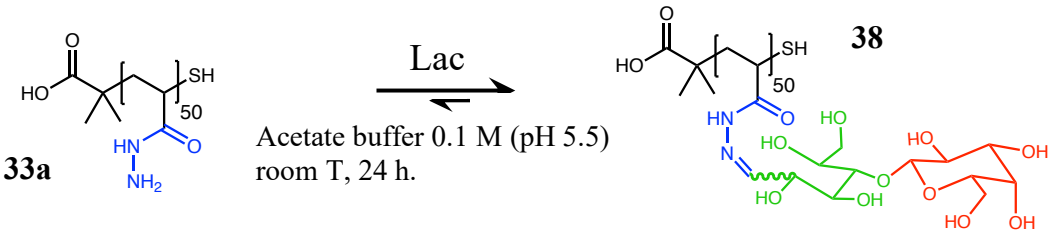
H. Post-polymerisation Glycosylation of Poly(acryloyl) Hydrazide with Lactose and Reduction

An alternative glycosylation of pAH_n with Gal was achieved in two steps using Lac **(Scheme 4.18)**:



Scheme 4.18. Synthetic route for the production of *N'*-(2,3,5,6-tetrahydroxy-4-((galactopyranosyl)oxy)hexyl) poly(acryloyl) hydrazide (pAH_{50}-RO-Gal_n, **39**). After the condensation of **33a** with Lac, isomers **38** were reduced with $pyBH_3$ in acidic conditions to obtain compound **39**.

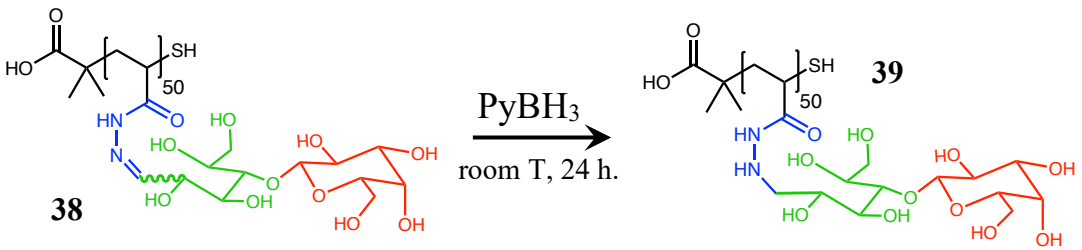
(**38a**) *N'-(lactosyl) poly(acryloyl) hydrazide, pAH$_{50}$-Lac*



Scheme 4.19. Coupling of Lac with pAH$_{50}$ in mildly acidic conditions at room temperature. The condensation reaction between disacharide and polymer was the first step **(Scheme 4.18)** to synthesise a glycopolymer (**39**) with Gal. The scheme shows a Lac molecule in its linear form linked to a pendant group of pAH$_{50}$.

First, 870.9 mg (4.42 mmoL) of Lac were dissolved in 4.4 mL of acetate buffer (0.1 M, pH 5.5) prepared in D_2O; the mixture was heated and stirred moderately to accelerate the formation of a dissolution. Then, the dissolution was added to a RBF charged with 100.1 mg of pAH$_{50}$ (22.73 mg/mL) and left to react for 24 h. at room temperature. According to ^{1}H-NMR ***(vid.* Figure 6.16)**, an approximate 30% loading was afforded (pAH$_{50}$-RO-Gal$_{15}$).

(**39**) *N'-(2,3,5,6-tetrahydroxy-4-((galactopyranosyl)oxy)hexyl) poly(acryloyl) hydrazide, pAH$_{50}$-Lac$_{15}$*



Scheme 4.20. Chemical reduction of the pendant groups of pAH$_{50}$-Lac$_{15}$ (**38**) with PyBH$_3$. The reduction of the hydrazone bond between Lac and polymer with PyBH$_3$ afforded a robust glycopolymer (pAH$_{50}$-RO-Gal$_{15}$, **39**) carrying Gal (red moiety).

0.29 mL (3.49 mmol) of $pyBH_3$ were added slowly to the crude product obtained in the first step of the synthesis shown in **Scheme 4.18** and that contained pAH_{50}-Lac_{15} (**38**); the mixture was left to react for 24 h. at room temperature. Afterwards, the new crude product was poured into a dialysis membrane and purified for 5 days, changing the water of the dialysis container (5 L) at least twice a day. Finally, the content of the membrane was lyophilised to obtain 0.353 g of pure, white polymer pAH_{50}-RO-Gal_{15} (**39**). **^{1}H-NMR** (400 MHz, D_2O) δ 4.43 (b, -R_3-CH(OR_2)-OR_1-), 3.91 (b), 3.83 (b), 3.68 (b), 3.58 (b), 3.55 (b), 3.46 (b), 2.98 (b), 2.84 (b) 1.89 (b, -CO-C<u>H</u>(R_1)-CH_2-R_2), 1.62 (b, -CO-CH(R_4)-C<u>H_2</u>-R_2), 1.19 and 0.97 (b, HO-CO-C(C<u>H_3</u>)$_2$-CH_2-) **(Figure 6.17)**. **GPC** (eluent: DPBS 0.0095 M without Ca^{2+} nor Mg^{2+}; 1 mL/min. flow rate, 35 ˚C column temperature) elution time 14.862 min. **(Figure 4.8)**.

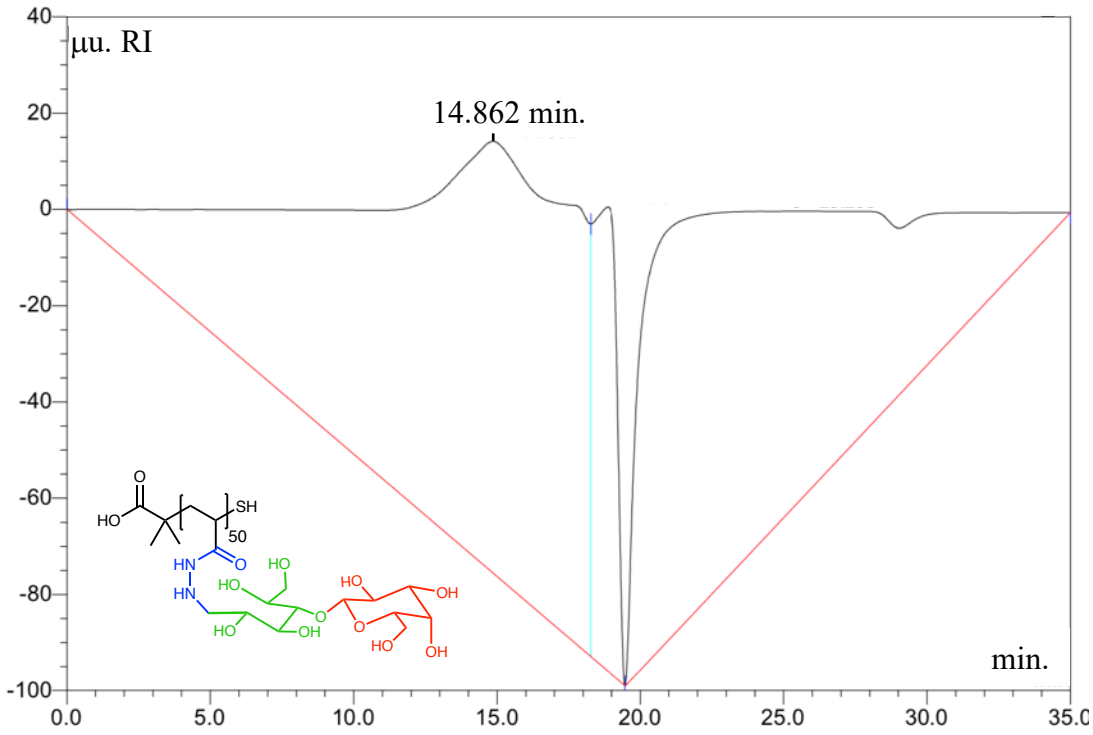


Figure 4.8. GPC of polymer **39** (eluent: DPBS 0.0095 M without Ca^{2+} nor Mg^{2+}; flow rate 1 mL/min., column temperature 35 ˚C). The reflexion index detector found the pure polymer leaving the chromatographic column after 14.862 min.

4.2 Electrochemistry

Herein are described the chemicals, instruments, materials, and procedures to perform the electrochemical experiments of the thesis.

4.2.1 Chemicals and Materials

All water used to carry out electrochemical experiments was Milli-Q® water (18.2 MΩ · cm, 1 ppb total organic carbon). To clean the glassware, aqueous acidic permanganate suspensions [**H_2SO_4** from VWR® and **$KMnO_4$** from Sigma-Aldrich® or E. Merck AG® (min. 99%)] and diluted piranha (**H_2O_2** from Merck®, **H_2SO_4**) were employed. All reagents used were of chemical grade. Polymer solutions were filtered with Millex®-LCR filters (13 mm, 0.45 μm, low protein hydrophilic PTFE membrane) purchased from Millipore®.

A. Commercial Chemicals

Different phosphate buffer solutions were used as electrolyte to reproduce physiological pH (7.4): DPBS, both commercial (Lonza®) and in-house preparations; and 0.1 M phosphate buffer solution. For the preparation of the in-house DPBS the following salts were used: **KCl** (99.999%), **NaCl** (99.99%) and **KH_2PO_4** (99.995%) from Merck®; and **Na_2HPO_4** (99.95%) from Sigma Aldrich®. The 0.1 M phosphate buffer solutions were obtained with **KH_2PO_4** from Sigma Aldrich® (≥ 99.0%) or Riedel-de Haën; **K_2HPO_4** (> 98%) from Acrōs Organics®; and **$K_2HPO_4 \cdot 3\ H_2O$** (98 – 100.5%) from Panreac®.

Two different redox probes were used in the electrochemical experiments: ferrocenemethanol (**FcMeOH**, > 95.0%) purchased from TCI-Tokyo Chemical Industry®; and the redox couple $[Fe(CN)_6]^{-3/-4}$ obtained from different salts: potassium ferricyanide **$[K_3Fe(CN_6)]$** from Merck's Reagenzien® or Acrōs Organics® (>99%); and potassium ferrocyanide trihydrate **$[K_4Fe(CN_6) \cdot 3H_2O]$** purchased from Fluka® (> 99.5%) or Alfa Aesar® (98.5-102.0%). Bovine serum albumin **(BSA)** was used to modify a Au(poly) electrode.

4.2.2 Instruments

The electrical potential applied during the measurements was controlled with several instruments: AutoLab potentiats (Metrohm®) managed by GPES and Nova 2.1.3 software (Metrohm®); e-DAQ® potentiostats coupled to waveform generators (Model 175 Universal Programmer, EG&G Princeton Applied Research®) and data recording and analysis systems (e-corder 401, e-DAQ®); and an IVIUM CompactStat analyser (Ivium Technologies®) controlled by IviumSoft software (IviumSoft®).

4.2.3 Experimental Procedures

A. Cleaning of the Electrochemical Cell and Glassware

Previous to any electrochemical experiment, to assure cleanness, the glassware was dipped in a slightly acidic potassium permanganate suspension (3 L water, 3 g $KMnO_4$ and 1 mL of pure H_2SO_4) overnight; then, rinsed with diluted piranha solution (1 L water, 3 mL H_2O_2 and 1 mL of pure H_2SO_4) to remove any traces of permanganate; and finally boiled in water 5 times to eliminate remnants of sulphates[481].

B. Cleaning of Au(poly) Electrodes

All electrochemical experiments reported in this text were carried out with high purity Au(poly) disk electrodes (Au ≥ 99.999%) after producing a hanging meniscus on the surface of the electrolyte. The surface of the electrode was cleaned after each experiment under a flame (flame-annealing) and cooled down for *ca.* 1 min. in an Ar atmosphere before further use or modification. In case of surface contamination, electrodes were polished with sandpaper, sonicated for 3 min. in water and flame-annealed.

C. Electrochemical Measurements

An electrochemical cell with a three-electrode configuration was used in all experiments. A big surface area of Au(poly) was employed as CE whilst saturated calomel electrodes (SCE), reversible hydrogen electrodes (RHE) and Ag/AgCl (sat.) electrodes were used, indistinctively, as a RE. All electrochemical results presented throughout the thesis have been converted into the Ag/AgCl (sat.) scale for the sake of consistency. As stated before, the electrolyte used in the experiments was DPBS or 0.1 M phosphate (pH 7.4). Unless otherwise reported, the scan rate of all CV was 50 $mV \cdot s^{-1}$. In the case of SWV, a frequency of 5 Hz, a step E of 5 mV and an amplitude of 25 mV were employed. Finally, in EIS experiments, a range of frequencies between 65,535 and 1 Hz was used with the E set at 148 mV and the amplitude at 10 mV. Two electrochemical mediators dissolved in the electrolyte were employed in the thesis: FcMeOH (0.5 mM) or $[Fe(CN)_6]^{-3/-4}$ (0.5 mM). Before starting the experiments, the cell was deaerated bubbling an inert gas (Ar or N_2) through the electrolyte for at least 20 minutes to prevent the reaction of O_2 with the Au surface; this way, all measurements

were conducted under an inert atmosphere. All experiments were carried out at room temperature (15 - 30 ± 1 ˚C).

D. Modification of Electrodes

Au(poly) electrodes were modified with SAM forming compounds and polymers (pAH_n, pAH_n-Gal, pAH_n-Lac, pAH_n-RO-Gal) by dipping them in aqueous solutions of the referred chemicals at several concentrations for different periods of time and at room temperature. Before each modification, electrodes were cleaned with flame-annealing and cooled down under Ar atmosphere for 1 min. After surface modification, before electrochemical characterisation or measurement, the electrodes were abundantly rinsed with water.

E. Dynamic *in situ* SEIRAS under ATR Conditions

For dynamic *in situ* SEIRAS under ATR conditions (SEIRAS-ATR) experiments, a spectroelectrochemical cell equipped with a Si window (Pastec Ltd., Japan) bevelled at 60° was placed at the top of a VeeMAX (PIKE Tech.) reflectance accessory of a Nicolet 8700 spectrometer (Thermo Scientific). Previously, Au (99.999%, Kurt J. Lesker Ltd.) thin films (*ca.* 25 nm) had been thermally evaporated and deposited on one of the faces of the low-oxygen content Si prism. The physical vapour deposition through sputtering was carried out in a vacuum chamber of a PVD75 (Kurt J. Lesker Ltd.) coating system at a base pressure of *ca.* 6-10 Torr; a quartz microbalance (QCM) was used to control the growth of the film. After setting the Au thin-film-modified prism in the cell, in-house DPBS (electrolyte) was added and a CV blank of the metal surface was obtained to assure its cleanness. The FTIR measurements in ATR configuration

were conducted in the already mentioned spectrometer, equipped with a liquidN2-cooled MCT-A detector and a wire grid ZnSe polariser (Pike Tech.), and controlled by OMNIC software. The spectra were collected with a 4 cm^{-1} resolution and are presented in absorbance units (a.u.). For the study of the formation of SAMs of DPA-HD on Au sputtered films, a concentrated solution of the disulphide was added to the cell containing the electrolyte for a final concentration of *ca.* 10 mM. For FTIR transmission experiments in the same cell, a final concentrations of *ca.* 50 mM was used instead.

Chapter 5

Synthesis of Small Molecular Linkers and Functionalisation of Polycrystalline Au Electrodes

5.1 Introduction

The cell membrane is the organelle that defines the boundaries of a cell, separating its interior from the environment. A physical barrier, it protects the cell and regulates the exchange of substances with the exterior. The scaffold of the cell membrane is a lipidic bilayer made of glycerophospholipids; its composition includes other lipids (*e.g.* cholesterol) and proteins whose function depends in many cases on sugars attached to them. The outward projection of these glycosylated macromolecules from the bilayer determines much of the composition and functions of the outer cell surface. One of these functions is the interrelation between cell and environment, including the communication with other cells and interactions with organisms. These saccharide structures constitute the glycocalyx of the cell[482] **(Figure. 5.1)**.

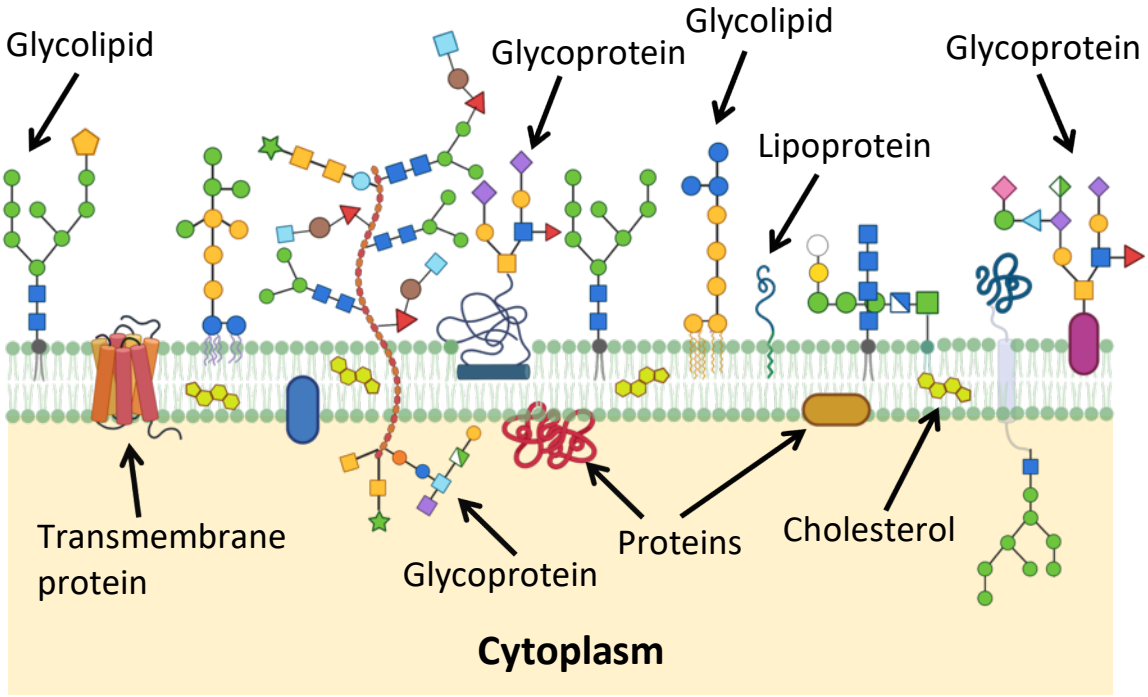


Figure 5.1. Cellular membrane with the glycocalyx on its outer face. The glycocalyx is a layer of saccharides attached to the lipidic bilayer through lipids and proteins (glycolipids and glycoproteins). Amongst the glycocalyx functions are structural - barrier between cell and environment-, cell-to-cell interaction and cell communication.

Many bacterial infections start when the pathogens or their toxins[483-486] recognise the glycocalyx of the host, like in the case of *V. cholerae* **(section 1.6.4)**; hence the enormous interest in studying cell-surface interactions. However, the task, both *in vivo* and *in vitro*, finds enormous difficulties, if only because of the structural complexity of sugars[487]. Amongst the strategies used to immobilise saccharides on surfaces[488-490] and make it possible are SAMs. SAMs allow the selective immobilisation of molecules and cells on surfaces[491-493] to investigate their layout and interactions[494, 495]. This same scheme is widely applied in sensing where the BRE of a biosensor is attached on different types of supports[496-502].

Biosensors with saccharides are known as glycosensors or glycobiosensors[503]. The recurrent interaction in nature between a pathogen and the glycocalyx of its host is an excellent opportunity to use sugars to detect bacteria. However, few cases of glycosensors of pathogens are reported in the literature, most of them electrochemical[93, 504, 505]. This thesis aims at the electrochemical detection of the presence of the *V. cholerae* bacterium through its toxin; to avoid the manipulation of the hazardous toxin, CTB (commercial and innocuous) is used in the first stages of development of the sensor, as it is also regularly done in the literature. This chapter describes the efforts made to complete the first step for developing the new glycosensor: the immobilisation of Gal, the BRE, on a Au(poly) disk electrode, the transducer.

5.1.1 Galactose as Biorecognition Element

Because of the enormous impact of cholera disease on human populations, CT's toxicity mechanism has been deeply studied **(section 1.6.4-C-D)**. The infection starts with the binding of the toxin to the cell membrane of the intestinal epithelium cells. The attachment mainly relies on the interaction between CTB and the glycan part of GM1[363, 506]. It has been described as a two-finger grip[361] and is based on weak forces (hydrogen bonds) between monosaccharides of GM1 and the CTB binding site reinforced by a structural fit **(Figure 5.2)**. The affinity of the toxin towards the cell membrane is augmented because it can bind it simultaneously through several of the 5 pentamers of its CTB. A secondary binding site has also been recently described[507].

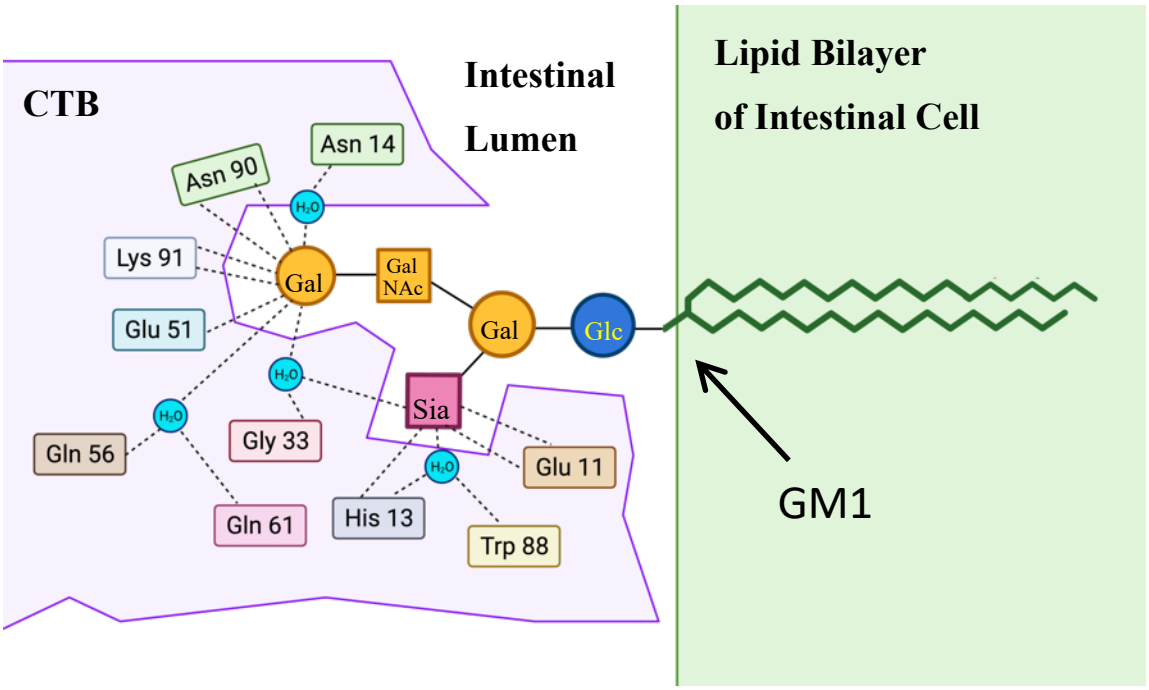


Figure 5.2. Schematic representation of the interaction between the saccharide units of GM1 and the amino acids of one of the pentamers of CTB according to Merritt *et al.*[361] Dotted lines represent hydrogen-bond interactions, with molecules of water (small light blue dots) acting in some instances as mediators.

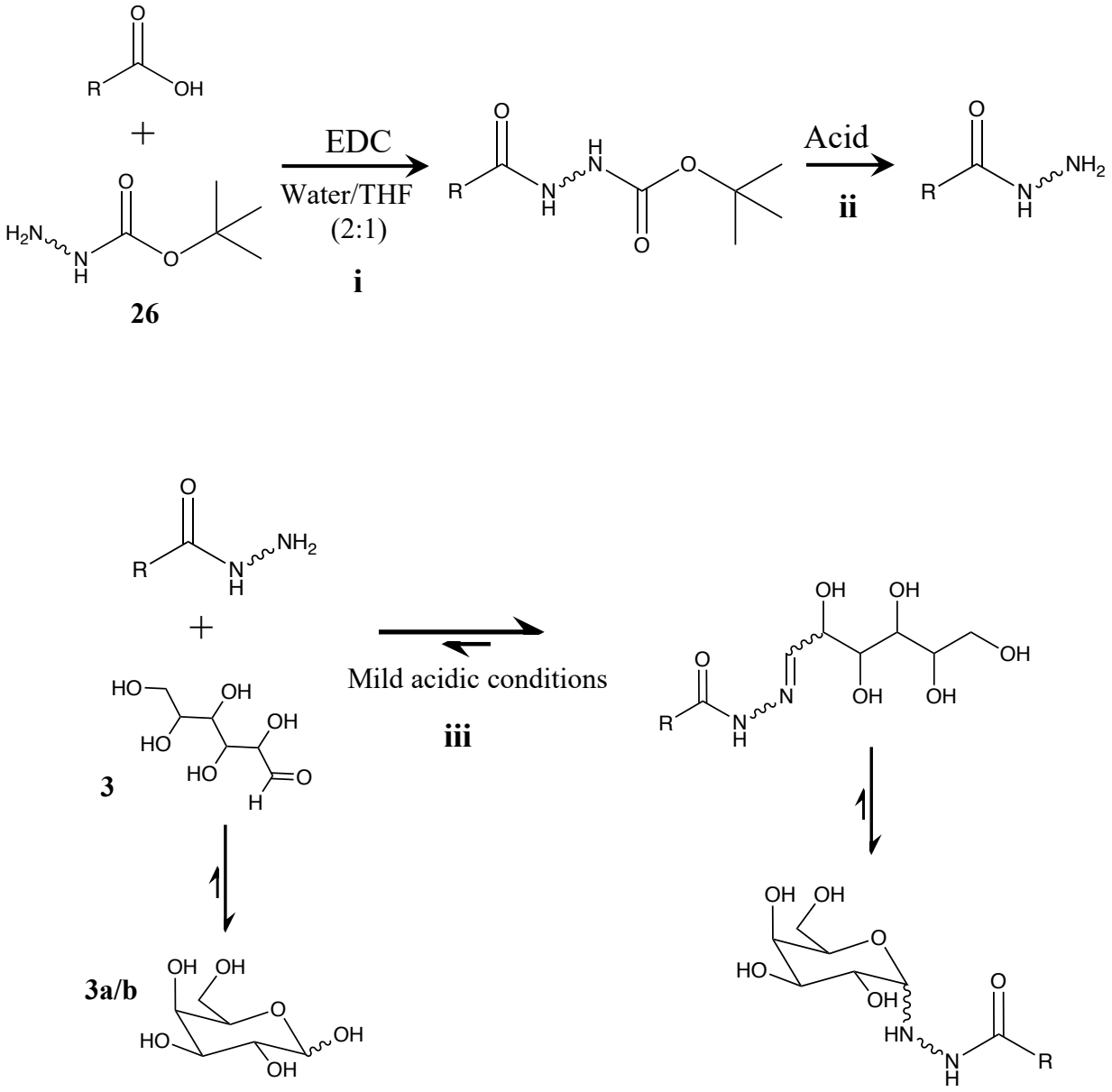
GM1 has been utilised in many biosensors as BRE[96, 508-511]; but its complexity and partial lipidic nature make it very unstable and difficult to integrate into electrodes. Due to its preeminent role in the interaction GM1-toxin[506, 512, 513], Gal, one of the monosaccharides of GM1, is a good alternative.

The use of Gal is also favoured for being a relatively simple, robust, and inexpensive molecule. The primary constraint in electrochemical biosensors is how to bind the BRE to what are, in most cases, carbonaceous or metallic electrodes. Because direct immobilisation is either impossible or too unstable, linkers become the

best option for their integration[93]. The coupling of a linker with Gal must secure the attachment of the sugar onto the electrode and guarantee that its 3D structure, essential for the recognition of CTB, remains unaltered. The terminal Gal monosaccharide of GM1, key in the interaction with CTB, presents a cyclic form. Gal in biological (aqueous) media is in equilibria between open and closed forms. Therefore, whatever the linker employed, it is critical that its coupling with Gal preserves the monosaccharide's cyclic conformation.

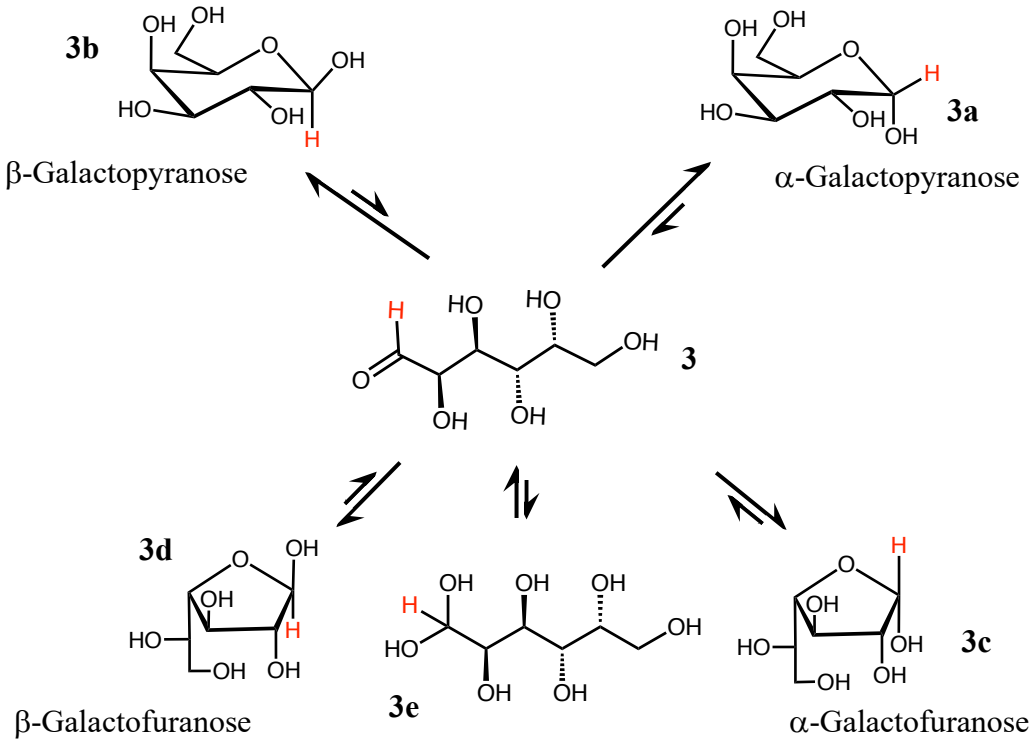
5.1.2 Immobilisation of Galactose on Electrodes

The linker used to immobilise Gal onto the electrode must secure strong and stable interactions with the sugar and the transducer. Linkers with a hydrazide group are very convenient because this group smoothly reacts with Gal thanks to the high reactivity of α-heteroatom nucleophiles towards the carbonyl group of reducing sugars[514] **(Scheme 5.1, step iii)**. Hydrazides can be easily synthesised from organic acids[488]; for example, reacting the carboxylic group with *tert*-butyl carbazate, followed by an acidic deprotection of the Boc protecting group[472] **(Scheme 5.1, steps i and ii)**.



Scheme 5.1. Chemistry to transform organic acids into linkers of saccharides: **(i)** coupling of carboxylic acids with *tert*-butyl carbazate using the coupling agent EDC; **(ii)** deprotection of the Boc group under acidic conditions for the obtainment of hydrazides; **(iii)** glycosylation of hydrazides with aldehyde saccharides in mild acidic media.

During biosensor construction, the BRE coupling with a linker must preserve the physical and chemical properties that allow the BRE to interact with the analyte. In solution, reducing monosaccharides are found in equilibria between different isomers[515] (tautomers). Gal in aqueous media mainly presents an open (acyclic) form (**3**), with an aldehyde group occupying one end of a 6-carbon backbone chain; and four cyclic isomers, two of them rings of four C atoms (furanosides) and two other rings of five C (pyranosides)[516-518] **(Scheme 5.2)**. At room temperature, over 98% of Gal molecules are either the α-galactopyranoside or the β-galactopyranoside tautomer.



Scheme 5.2. Interconversion equilibria between the different tautomers of Gal in aqueous media, according to Wertz *et al.*[518] The intramolecular nucleophilic attack in the linear Gal (**3**) of the hydroxyl group of C5 or C4 on the aldehyde group allows the formation of more stable, cyclic isomers in aqueous media. Nevertheless, hydrolysis makes these condensation reactions reversible. The reversible incorporation of a hydroxyl group into the carbonyl of **3** can produce the hydrate of Gal (**3e**), the least stable of all tautomers.

The constant and fast interconversion between the ring isomers of Gal via the linear aldehyde tautomer allows the interaction of hydrazides with this carbohydrate to form hydrazones. Notably, the bond formed still permits the equilibrium between the open and cyclic forms of the saccharide[519]. This is essential for the functioning of the biosensor since CTB only interacts with the pyranosides of Gal. However, the reaction is reversible and the hydrazone is hydrolysed, with an equilibrium being eventually reached **(Scheme 5.1, step iii)**.

Au(poly) electrodes were chosen as transducers for this work because of the easiness of preparing SAMs on this metal **(Figure 5.3)** and their flexibility. The strategy of using SAMs of organic molecules that contain atoms of S as linkers abounds in the literature[520-522]; several types of organosulfur compounds (thiols, aromatic thiols, dithiols, disulphides, and sulphonates) can be employed, although linear thiols are the most popular.

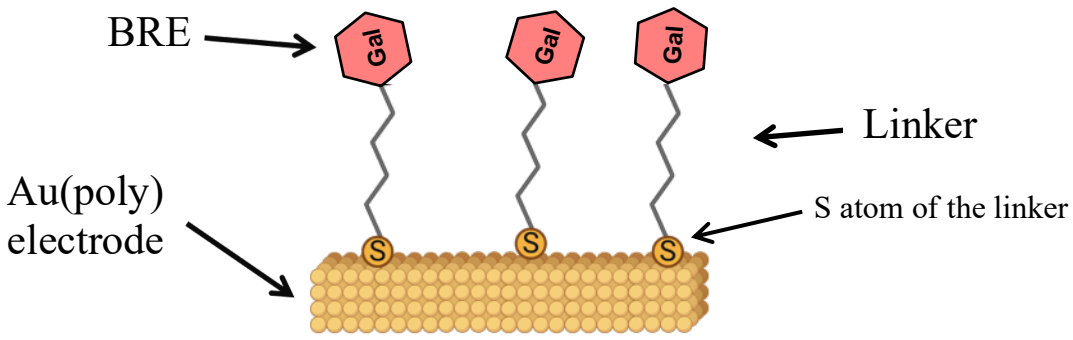
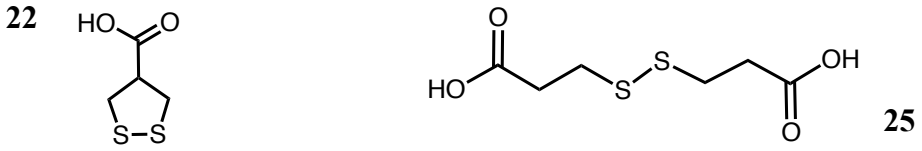


Figure 5.3. Integration of the transducer (electrode) and the BRE (Gal) of a glycosensor via chemical linkers with S. Molecules containing atoms of S adsorb easily and fast from solution on Au surfaces due to stable S-Au covalent bonds. The possibility of having different functional groups that can be connected to a BRE confers these molecules great potential as linkers.

For this project, two carboxylic acid disulphides were identified as starting materials of linkers **(Figure 5.4)**: asparagusic acid[523] (1,2-dithiolane-4-carboxylic acid); and 3,3'-dithiodipropionic acid (DPA). These molecules can strongly adsorb on Au(poly) via Au-S covalent bonds. Besides, they contain a carboxylic group that can be easily chemically transformed into a hydrazide group. Given the high reactivity between hydrazides and aldehydes, and being Gal an aldehyde, disulphide acids are very convenient starting materials to obtain linkers for this project.



Asparagusic acid

3,3'-Dithiodipropionic acid (DPA)

Figure 5.4. Starting materials used in **Chapter 5** for the synthesis of chemical linkers for Gal. The presence in these molecules of the carboxylic acid group and S atoms permitted, on the one hand, their transformation into hydrazides for the coupling with the sugar; on the other, their attachment to Au(poly) disk electrodes for the final construction of the glycosensor.

Surface coverage and stability are fundamental for the performance of biosensors. The stability can affect the analytical signal of the sensor and the robustness and durability of the device. The degree of coverage is of utmost importance: any area of the transducer not covered by the SAM could interact with any species of the sample other than the analyte (non-specific interactions) and generate noise. Several strategies can be used to block the uncovered surface, *e.g.* the adsorption of other thiols[524] or BSA[525].

5.1.3 Self-assembled Monolayers Preparation

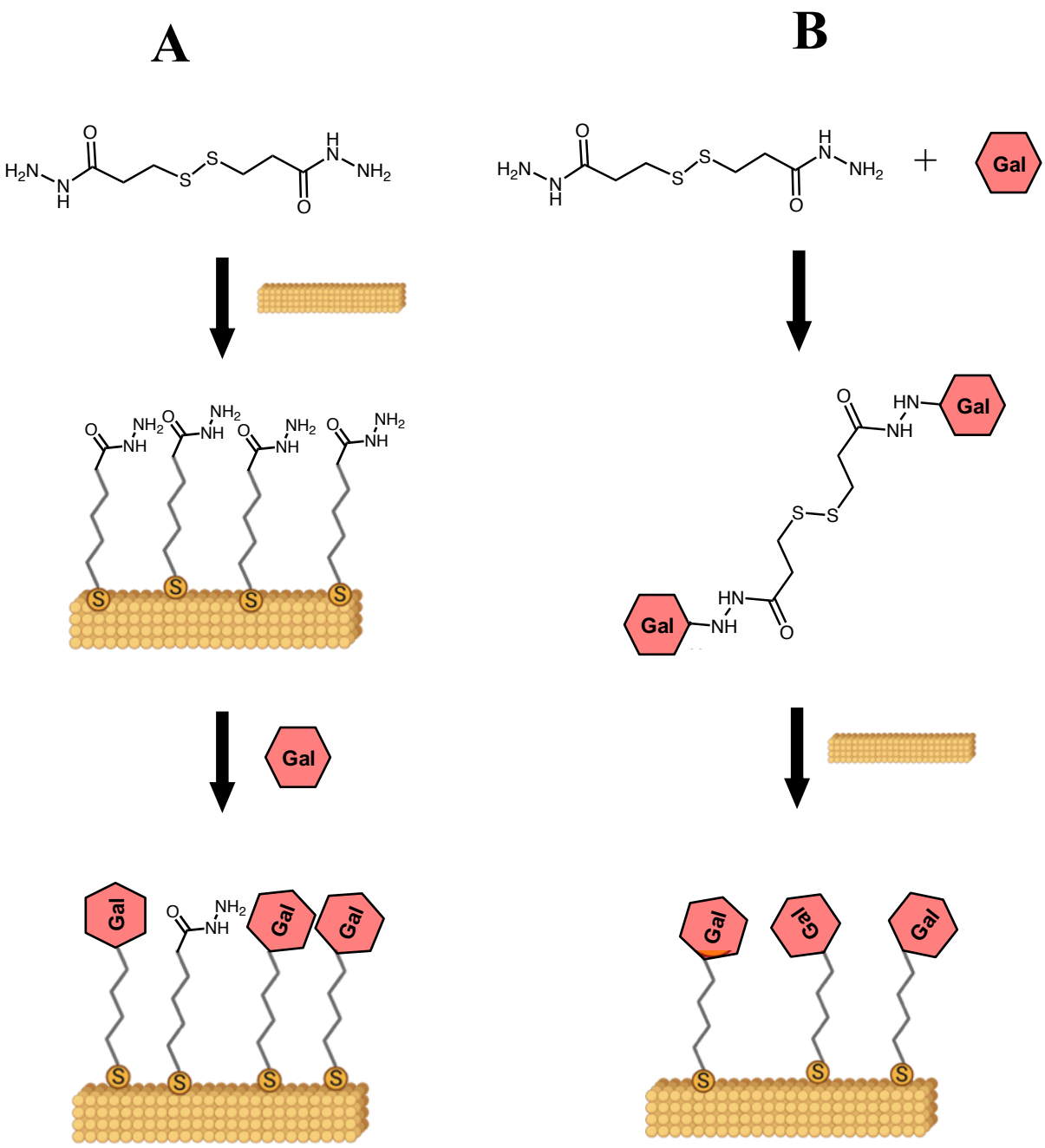
The main factors that determine the quality of a SAM were described in **Chapter 1**, like the preparation procedure. SAMs were obtained in this project from solution because it is simpler than producing them from gas phase or drop-casting. Therefore, the solvent employed was very relevant. For a start, it is highly recommendable that the organosulfur be perfectly dissolved to favour the mechanisms of self-assembly. Besides, it must be considered that solvent molecules can affect the process by interacting themselves with the electrode's surface. When possible, aqueous solutions of disulphides were used throughout this chapter to avoid the more volatile and polluting organic solvents. Another critical factor is the concentration of organic molecules in the solution, which must be high enough to guarantee a complete surface coverage in a reasonable period of time[526, 527]. Concentrations in the range of 1 mM to 100 mM were studied following the experience accumulated in the group[203] and in the literature[528]. Finally, the time of immobilisation, the period during which the electrode surface is in contact with the organosulfur solution, is also of great importance. As a starting point, similar times of those early used in Dr. Rodríguez's group[203] were considered and ATR-SEIRAS experiments confirmed them as optimal.

5.1.4 Electrode Conditioning

The modification of Au electrodes with organosulfurs with sensing purposes requires the close examination of aspects like cleanness, roughness, and the presence of impurities in the surface of the metal. Conditioning is relevant, not only for electrode modification, but also for sensing features like reusability and the increase of the commercial potential of a device. The inertness of Au, and the possibility of easy and fast regeneration of its surfaces, made of Au(poly) disks an advantageous election as transducers for the development of this sensor.

5.1.5 Electrochemical Characterisation

CV was employed for the characterisation of the SAMs produced on Au(poly) disk electrodes. The technique offered a simple means to confirm the modification of the surface and permitted the obtainment of essential information about the films, particularly their stability in potential windows where the detection of CTB is feasible. Although a disulphide dihydrazone was obtained as a linker (DPA-HD, **28**)**,** according to electrochemical characterisation, difficulties arose when trying to obtain SAMs of the compound from solution **(Scheme 5.3-A)**, preventing the glycosylation of its SAMs. Therefore, experiments to explore the possibility of first glycosylating DPA-HD (DPA-HD-Gal, **29**) before preparing SAMs were carried out **(Scheme 5.3-B)**.



Scheme 5.3. Two different strategies to attach Gal, the BRE of the glycosensor, to a Au(poly) disk electrode. **(A)** Formation of a SAM of hydrazides on an electrode, followed by the coupling with Gal. **(B)** Coupling a hydrazide linker with Gal, then preparing a SAM on a Au disk.

5.2 Results and Discussion

5.2.1 Asparagusic Acid as a Chemical Linker

The first disulphide identified as a potential suitable linker for the project was LA because it contained a hydroxylic group that could be easily transformed into a hydrazide. When a redox probe, $K_4Fe(CN)_6$, was used to characterise an electrode modified with a SAM of LA and test the extended charge transfer through it **(Figure 5.5-A)**, a substantial signal attenuation (solid red curve, Scan 1) was observed. After opening the potential window **(Figure 5.5-B)**, the characteristic reductive stripping of molecules appeared at *ca.* -0.70 V (solid blue curve, Scan 2). The fact that, after molecule desorption, there still was a significant attenuation of the redox probe in the following scan (dashed blue curve, Scan 3) indicated a fast re-adsorption of LA, confirmed by a smaller reduction peak in this same scan at *ca.* -0.75 V.

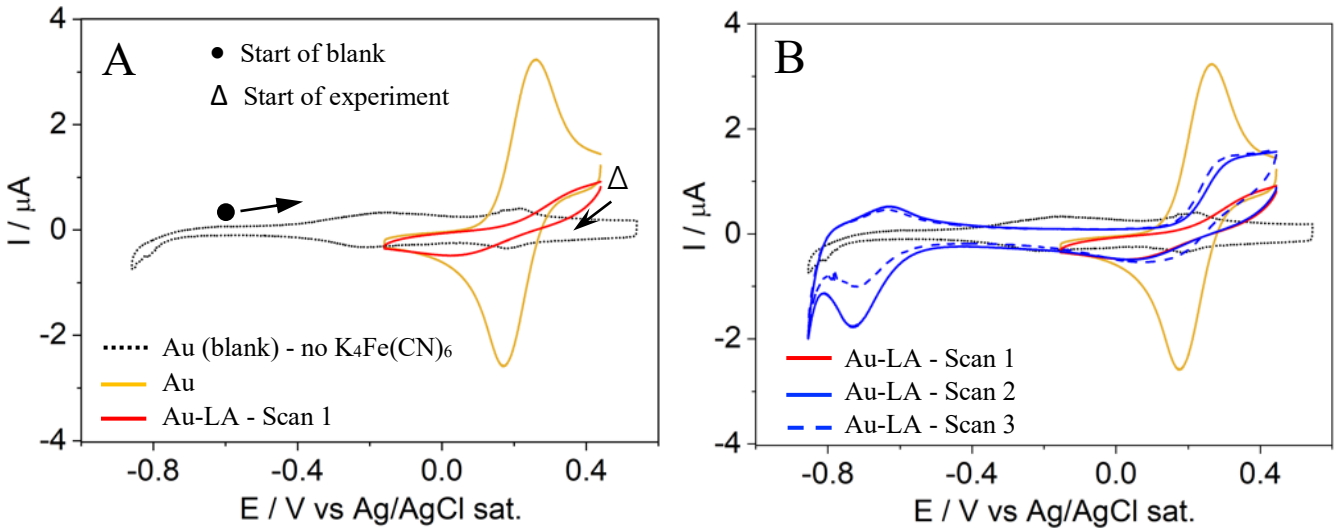


Figure 5.5. CV study with the redox complex $K_4Fe(CN)_6$ at 0.5 mM of the electron transfer through a SAM of LA formed on a Au(poly) electrode. (Dotted black line) CV on a bare Au(poly) electrode with phosphate buffer (pH 7.4) as electrolyte (blank); (solid gold line) CV scan on the electrode after $K_4Fe(CN)_6$ had been added to the electrolyte. **(A)** (Solid red line, Scan 1) After a SAM of LA had formed on the electrode surface, the CV response of $K_4Fe(CN)_6$ between -0.30 V and +0.45 V was attenuated. **(B)** (Solid blue line, Scan 2) When lower potentials were reached (-0.85 V), the reductive stripping of the SAM molecules was observed at *ca.* -0.75 V. A further scan (dotted blue line, Scan 3) evidenced a partial readsorption of LA molecules with a smaller reduction peak at *ca.* -0.75 V. (•) Start of the blank; (Δ) start of an experiment with the electrode surface modified. The scan rate of the sweeps was 50 $mV \cdot s^{-1}$.

The result demonstrated the formation of a SAM of LA on the electrode surface and pointed towards an inner-sphere electron exchange with a severe cancellation of the redox probe signal. This blockage could increase if LA were transformed into a hydrazide (LA-HD) and then coupled with Gal. CTB is not electroactive, so an electrochemical mediator was necessary to detect CTB **(Chapter 7)**. Therefore, considering that SAMs of glycosylated LA could even block outer-sphere mediators,

asparagusic acid, a molecule with a shorter backbone, was chosen as an alternative **(Scheme 4.1)**.

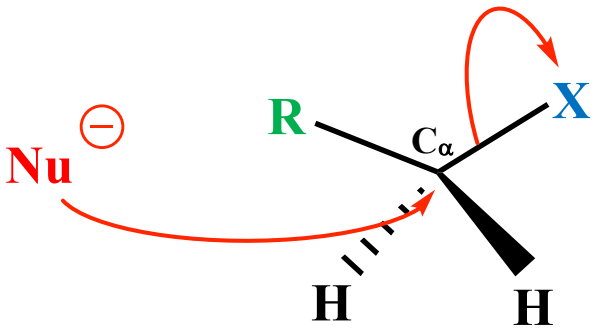
A. Synthesis of 1,2-Dithiolane-4-carboxylic Acid (Asparagusic Acid)

A synthetic route for asparagusic acid **(Scheme 4.1)** was designed according to the literature[476, 478, 529-534]. Diethyl 2,2-bis(hydroxymethyl)malonate (**16**) has been regularly utilised in organic chemistry as a starting material for synthesising different types of heterocycles[535-537] thanks to the reactivity of its two hydroxyl groups. To produce rings containing S atoms, the goal was to substitute them with the sulphur equivalent, the thiol group. On **step i** of the scheme mentioned above, compound **16** reacted with *p*-toluenesulphonyl chloride (**23**) under mild conditions to produce compound **17,** a crystalline, white solid (yield 69%) **(Section 4.1.3-A)**. This is a popular strategy to transform alcohols (poor leaving groups due to the strong basicity of the hydroxyl anion, HO-H $pK_a \sim 14$ in aqueous media[538]) into good leaving groups like the tosylate group (*p*-toluene sulphonic acid $pK_a \sim -3$ in aqueous media[539]) to get them engaged in S_N2 processes[540]. Other good alternatives are methanesulfonyl chloride (mesylate group, Oms)[541] and trifluoromethanesulfonyl chloride (triflate group, Tf)[542].

Step ii was designed to introduce S atoms in species **17** through an S_N2 nucleophilic substitution. Thioacetic acid was used as the sulphur-baring nucleophile[533, 534] and, to forward the reaction, basic conditions -aqueous Na_2CO_3- were employed. The first attempt **(entry 1, Table 4.3)**, based on work done by Roy et *al.*[533], was unsuccessful. Thus, other relevant parameters in the reactivity of S_N2

reactions were changed: solvent[543], temperature and the use of an inert atmosphere to prevent any potential oxidation of thioacetate[544].

Any of the conditions described by the entries of **Table 4.3** did work, so the K salt of thioctic acid was employed to enhance the nucleophilicity, although without positive results. The explanation could be the neopentyl effect[545-547]. According to the S_N2 reaction mechanism on saturated carbons[546] **(Scheme 5.4)**, a big substituent (**R**) in the reaction centre (α-carbon) can block the backside attack of the nucleophile (**Nu⁻**), hindering the substitution of the leaving group (**X**). If the steric hindrance is due to a tertiary β-carbon in the electrophile, then the phenomenon is known as the neopentyl effect.



Scheme 5.4. Representation of the S_N2 reaction mechanism, with the backside approach of a nucleophile **Nu⁻** to the reaction centre (α-carbon) of an electrophile and the ensuing substitution of a leaving group **X**. A big **R** group can hinder, and ultimately block, the nucleophile's access to the reaction centre. When the branching of a tertiary β-carbon causes the steric hindrance that stops the approach of the nucleophile, the phenomenon is called the neopentyl effect.

The single-crystal XRD spectrum of compound **17** shown in **Figure 5.6** hints at this possibility: the branching (green area) of C1 (β-carbon) would make difficult the

access of the nucleophile to the reaction centre (C8, red area) to induce the departure of the leaving group (blue area).

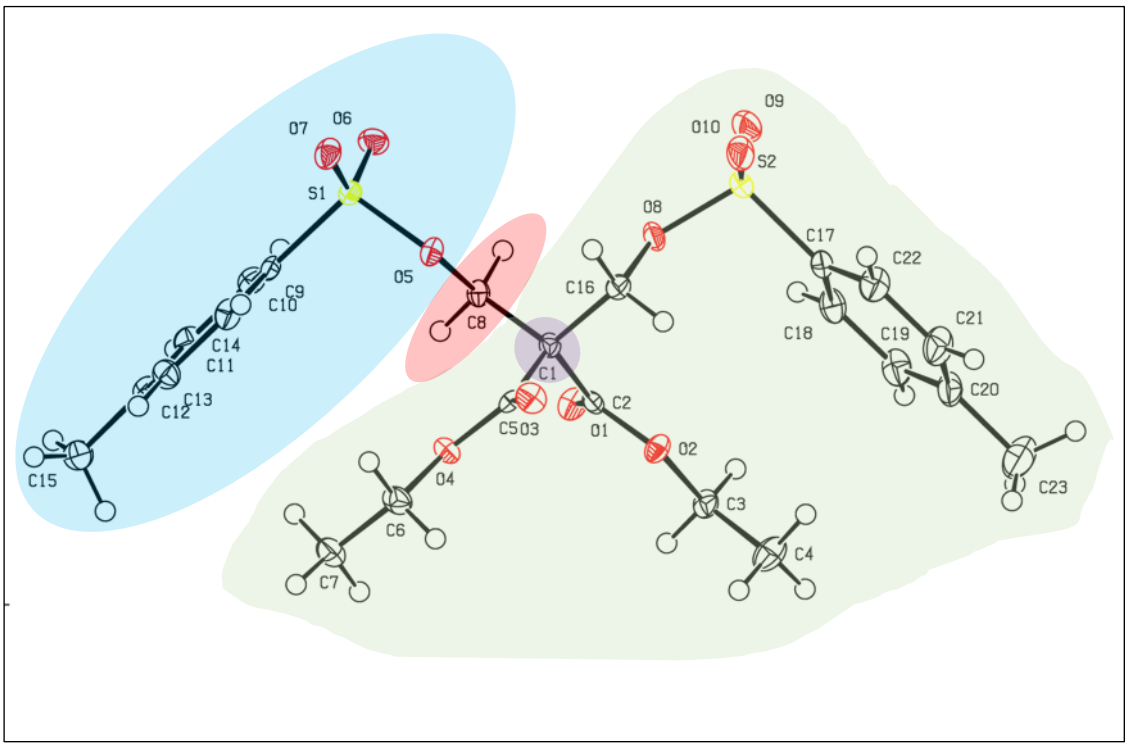


Figure 5.6. XRD spectrum of a monocrystal of compound **17**. Although the *p*-toluenesulphonyl group (blue area) is an excellent leaving group, the presence of a tertiary β-carbon (purple area, C1) with its substituents (green area) generated a high steric hindrance that blocked any nucleophile from reaching the reaction centre (C8, red area) and prompting an S_N2 reaction.

At this point, after different attempts to complete **step ii** of the synthetic route of asparagusic acid and deeming the neopentyl effect as the determinant factor for the negative outcome, it was decided the synthesis of a new linker from DPA.

5.2.2 3,3'-Disulfanediyldi(propanehydrazide) as a Chemical Linker

3,3'-Disulfanediyldi(propanehydrazide) (DPA-HD, **28**) was selected as a linker because it presented a short backbone and its synthesis had been previously done in one of the groups where this project was being carried out.

A. Synthesis of 3,3'-Disulfanediyldi(propanehydrazide)

The transformation of DPA (**25**) into DPA-HD was attempted in two steps described in **(Scheme 4.4)**: first, DPA was coupled with *tert*-butyl carbazate (**26**) using a carbodiimide, EDC, as coupling agent[548], to obtain compound **27** (Boc-DPA) **(Scheme 4.5)**; second, the Boc group was removed with TFA **(Scheme 4.6, conditions a)**. ^{1}H-NMR characterisation **(Figure 5.7)** suggested that there was no need for product purification with two very well resolved and expected triplets.

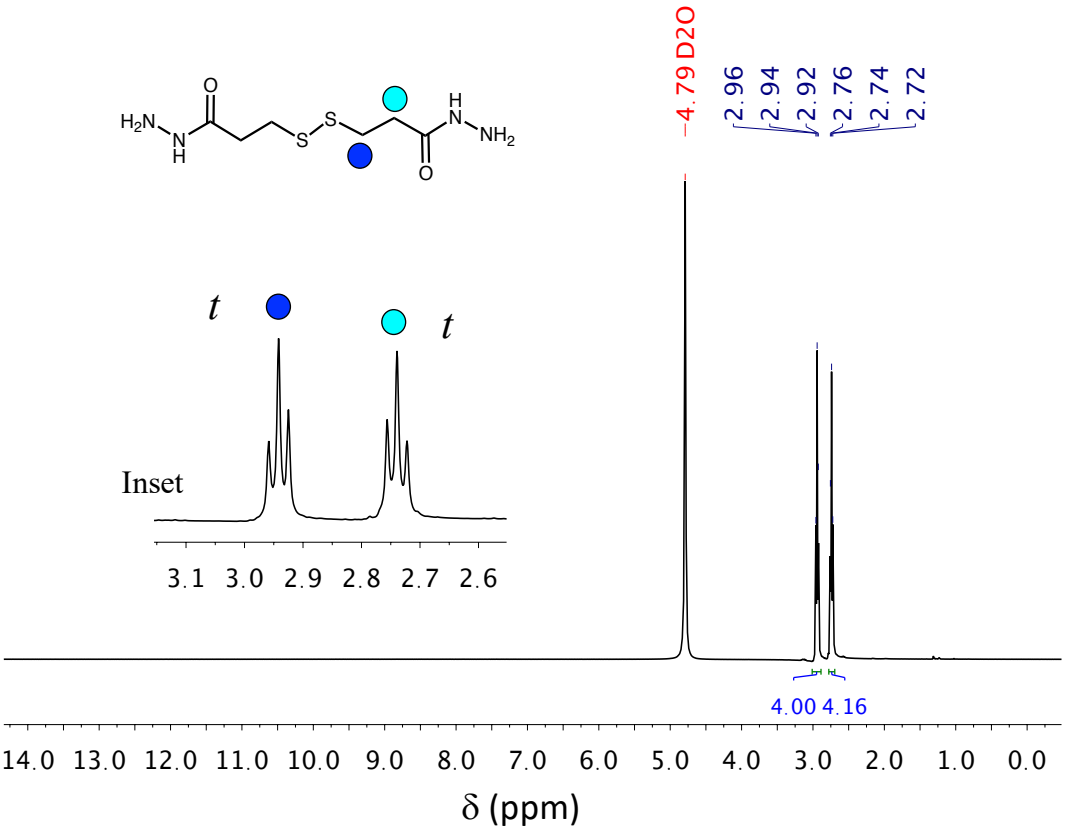


Figure 5.7. ^{1}H-NMR spectrum (300 MHz, D_2O) of DPA-HD. The figure shows the expected triplets of the methylenes of **28** whilst the hydrazides' protons are not observable at low-field due to chemical exchange with the solvent of the sample. The triplet at about 2.95 ppm (deep blue spot) was used to normalise the integrals.

B. Modification of Au(poly) Electrodes with Self-assembled monolayers of 3,3'-Disulfanediyldi(propanehydrazide)

With DPA-HD synthesised, the next step was to analyse the capacity of the species to adsorb on Au(poly) electrodes and form SAMs. To produce SAMs from solution it is crucial to obtain good dissolutions of the molecules to be used. EtOH was the initial choice for various reasons: it had already brought good results when used with another disulphide, LA; it had been successfully employed in the preparation of SAMs of thiols in the electrochemistry group[203] where the thesis was being done; and,

although several solvents could be utilised, EtOH is the preferred in the literature[139, 186, 549].

However, because DPA-HD was not soluble in absolute EtOH, water had to be used instead. CV was employed to characterise SAMs of DPA-HD, albeit no reproducible results could be attained in the region corresponding to the stripping of adsorbed molecules[203, 217, 527]. Since DPA-HD has two functional groups capable of interacting with Au, *i.e.* the disulphide and the hydrazide group, there was the possibility that the assembly of molecules was being affected by the competition between them. Indeed, the interaction between Au and the amine group has been reported[550, 551]. Consequently, a chemical equivalent of DPA-HD, AcHD, was used to investigate if the disulphide could also attach to the electrodes through the hydrazide group. CV on a Au(poly) electrode functionalised in a 5 mM solution of AcHD for 20 min. produced a reproducible reductive stripping peak at *ca.* -0.4 V *vs* Ag/AgCl **(Figure 5.8)**, confirming the adsorption of this species.

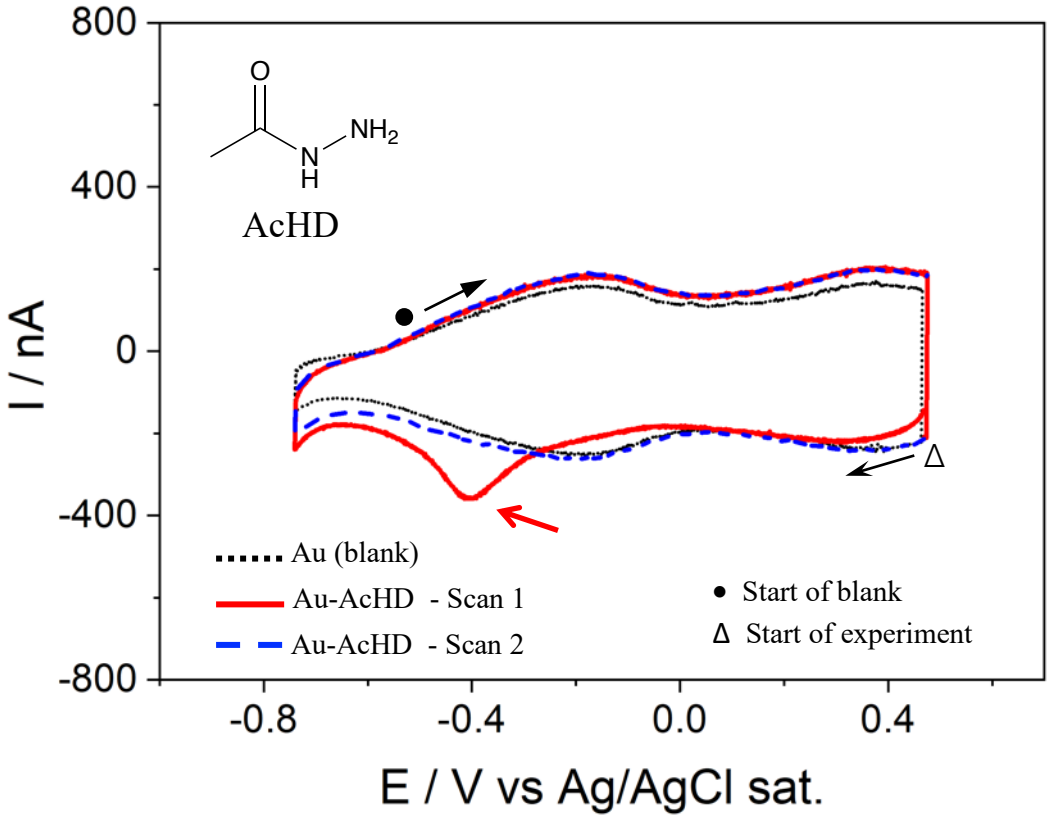


Figure 5.8. CV scans between -0.75 and +0.45 V to study the adsorption of hydrazides on Au surfaces; scan rate 50 $mV \cdot s^{-1}$, in-house DPBS electrolyte. (Dotted black line) CV on a Au(poly) electrode in phosphate buffer previous modification; (solid red line) first CV scan on a Au(poly) electrode modified in an AcHD solution (5 mM, 20 min., room temperature); (blue dashed line) second CV scan on the functionalised electrode. (•) Start of the blank; (Δ) start of the experiment with the modified surface. The red arrow indicates the desorption of molecules of AcHD from the Au(poly) electrode during Scan 1.

The results also showed the weak adsorption of this molecule on Au(poly), since habitually the desorption of organosulfides under these electrochemical conditions takes place at lower potentials, from -0.70 V. In the second scan (dashed blue curve), the original profile of a clean, bare electrode was recovered. This indicated that a single cycle was enough to remove all the AcHD molecules from the electrode surface.

Furthermore, unlike with LA **(Scan 3, Figure 5.5-B)**, the total absence of a stripping process in the second scan evidenced the inexistence of a fast readsorption of the hydrazide.

C. Investigation of the Adsorption of 3,3'-Disulfanediyldi(propanehydrazide) on Au(poly)

The lack of reproducibility of the desorption of SAMs of DPA-HD from Au(poly) electrodes was investigated during a research visit of 2 months to the Universitat d'Alacant. *In situ* ATR-SEIRAS was utilised to unveil some aspects of the SAMs' formation mechanism and the molecules' final arrangement on the surface, trying to establish which groups of the molecule interact and how with a Au surface. First, the kinetics of SAM formation were examined: the changes of FTIR absorbance on a sputtered Au surface after setting it into contact with a 10 mM aqueous dissolution of DPA-HD proved that, within approximately 20 min., the adsorption process had been practically completed **(Figure 5.9)**.

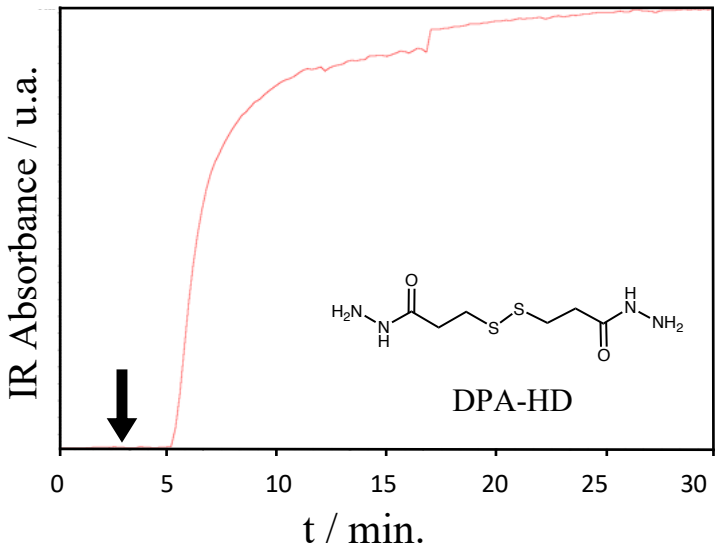


Figure 5.9. Kinetics curve of the DPA-HD adsorption on a sputtered Au surface obtained with *in situ* SEIRAS-ATR. The face of a Si prism was sputtered with Au, put into contact with an aqueous solution of DPA-HD (10 mM) for *ca*. 25 min., and then the SEIRAS-ATR signal was recorded. The black arrow indicates the moment when the disulphide dissolution started to be in contact with the Au surface.

This outcome ruled out that the period of functionalisation of the electrode employed in previous experiments, 30 min., was the cause behind the poor reproducibility obtained in the reductive stripping of DPA-HD SAMs. The analysis of the *in situ* and *in operando* absorption spectra at different wavelengths of the SAM formation **(Figure 5.10)** revealed the characteristic vibrational bands of the hydrazide group, as expected if DPA-HD had adsorbed on the Au surface through S atoms: a very intense peak at 1,677 cm^{-1}, known as 'band I' of amides, corresponding to C=O stretching [υ_s(CO)]; the signal at 1,542 cm^{-1} resulting from the N-H bending [β(NH)], the 'band II of amides' in the literature; and the band at 1,261 cm^{-1} caused by the C-N stretching [υ_s(CN)]. Other bands related to the rest of the backbone of the molecule could be seen: peak at 1,369 cm^{-1} linked to bending of CH [$\beta(CH_2)$], and a peak at

1,407 cm^{-1} perhaps produced by other vibrational modes of CH from the ethylene group[552]. Most of these resonances in the region between 1,000 cm^{-1} and 2,000 cm^{-1}, the fingerprint of a molecule, found a correspondent in the ATR-FTIR spectrum of AcHD **(Figure 5.11)**, chemical equivalent of the head group of DPA-HD. The shift differences, though, might be explained because the hydrazide group was part of a larger molecule in DPA-HD and was also adsorbed on a Au surface. Moreover, the ATR-SEIRA spectra of **Figure 5.10** also revealed the presence of bands of the trifluoroacetate anion (annotated in red) when adsorbed on Au[553]: the symmetric mode of C-F stretching [$\upsilon_s(CF_3)$] at 1,203 cm^{-1}; the broad band at 1,677 cm^{-1} most probably contained the υ_s(CO) of the anion overlapped with the amide I band[554] of DPA-HD; and the weak 1,407 cm^{-1} peak, earlier assigned to ethylene groups of the disulphide, could instead arise from the asymmetric stretching of O-C-O [υ_a(OCO)]. Besides, the tiny resonance at 1.739 cm^{-1} could be ascribed to the unidentate adsorption to a specific phase of Au, according to Delgado *et al.*[553] At the pH of the DPA-HD solution (pH 2.7 at 24 ˚C) it had to be expected that TFA was dissociated (pK_a 0.52 at 25 ˚C)[555], favouring the presence of the trifluoroacetate anion and allowing its adsorption on Au.

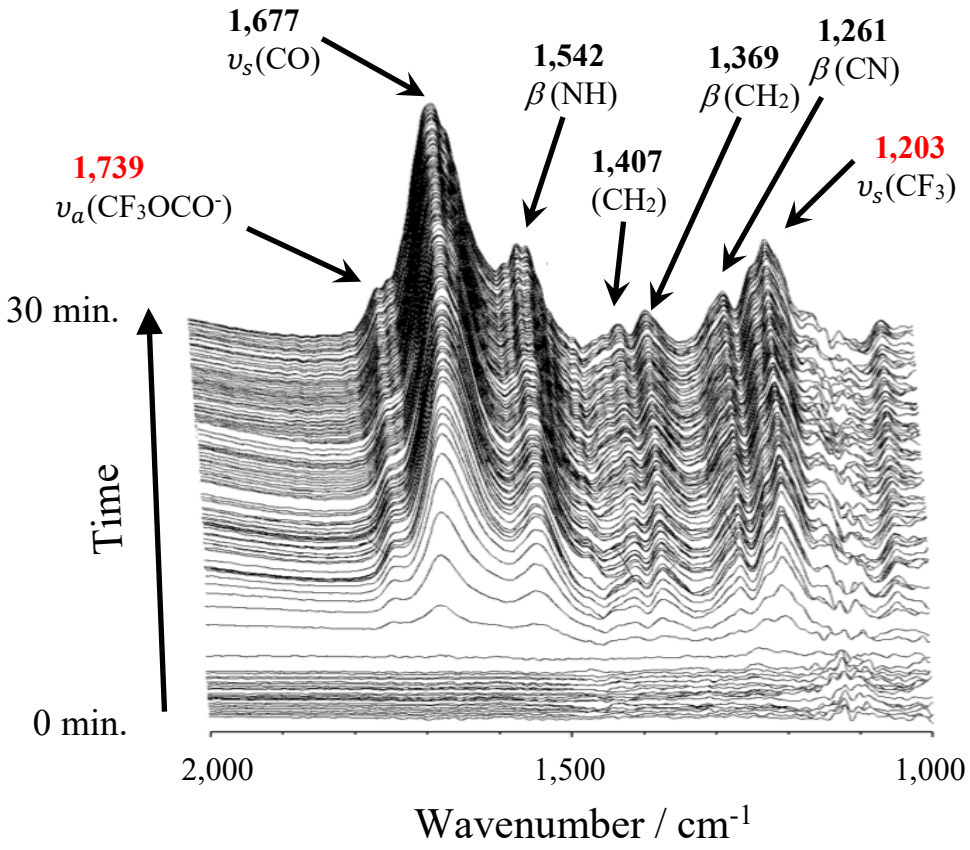


Figure 5.10. ATR-SEIRAS spectra obtained during the formation of a SAM of DPA-HD from an aqueous solution on a sputtered Au surface. Characteristic modes of vibration expected from the di-hydrazide can be seen annotated in black, like the 'amide I band' at 1,677 cm^{-1} and the 'amid II band' at 1,542 cm^{-1}. Peaks related to the adsorption of trifluoroacetate appear in red. The band's intensity increase over time confirmed the adsorption of molecules of DPA-HD and TFA anion.

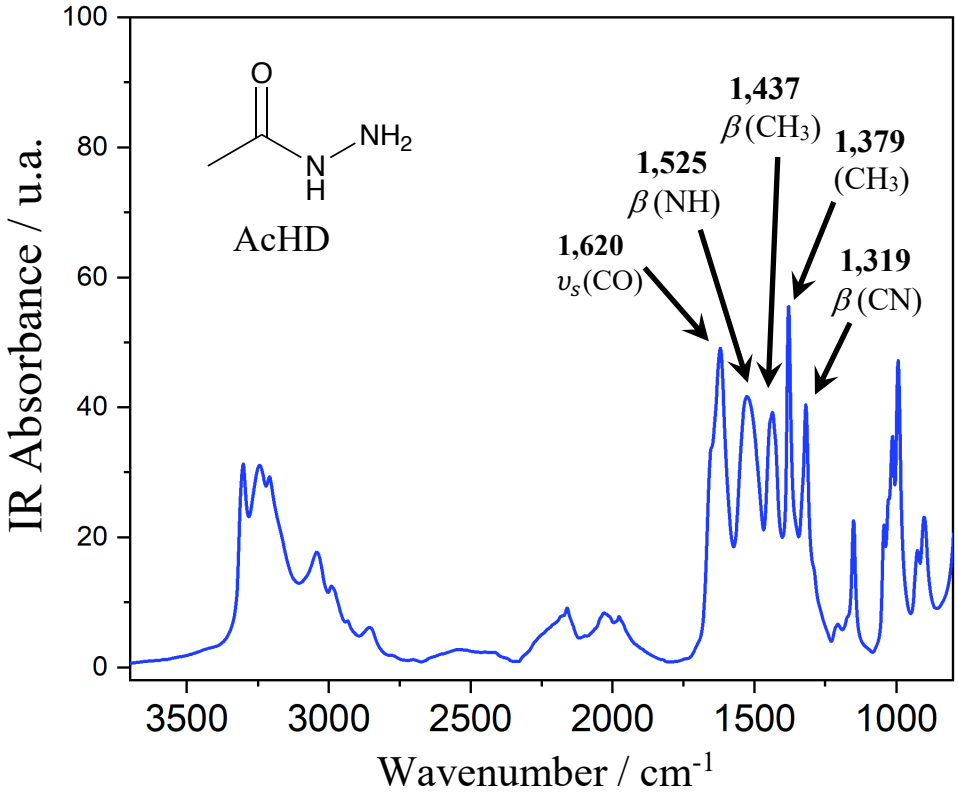


Figure 5.11. ATR-FTIR spectrum of AcHD with some of its most characteristic vibrational bands annotated. The close correspondence of some of these vibrations, like 'band I of amides' (1,620 cm^{-1}) and 'band II of amides' (1,525 cm^{-1}), with those present in **Figure 5.10** confirmed the adsorption of DPA-HD on the sputtered Au surface. The small vibrational shifts observed between both spectra may be associated with structural differences between the two species analysed and also the adsorption of DPA-HD.

After finishing the ATR-SEIRAS measurement, the Au surface was used as an electrode to conduct CV **(Figure 5.12)** and prove that the spectra in **Figure 5.10** originated from adsorbed disulphide molecules and not just in solution near the surface. Two reduction processes (purple arrow) at between -0.3 and -0.6 V *vs* Ag/AgCl (sat.), characteristic of disulphide or thiol stripping from Au, confirmed it.

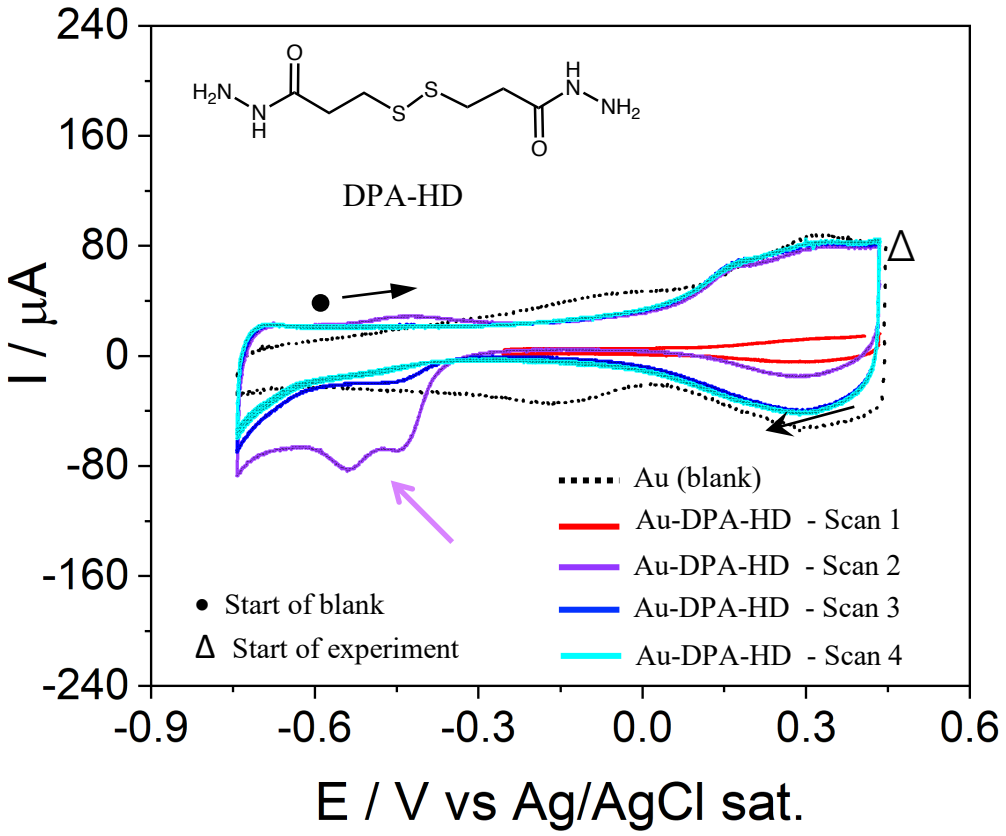


Figure 5.12. CV on a face of a Si prism sputtered with Au before and after modification with DPA-HD. (Black, dotted curve) Scan between -0.75 and +0.45 V on the Au surface before modification (blank); (solid red curve) first scan (between -0.20 and +0.45 V) after surface functionalisation with DPA-HD; (solid purple curve) second scan after surface modification with a new low limit potential of -0.80 V; (solid deep blue line) third scan after Au modification; (solid light blue line) fourth scan after surface functionalisation. (•) Beginning of the blank; (Δ) start of scans on the modified surface. All sweeps were run at a scan rate of 50 $mV \cdot s^{-1}$ in an in-house DPBS electrolyte. The purple arrow points at the 2 reductive peaks resulting from the electrochemical desorption of molecules from the electrode in Scan 2.

Transmission FTIR **(Figure 5.13)** of the stock solution used to prepare the SAM of DPA-HD investigated in **Figure 5.10** confirmed the presence of TFA, or the trifluoroacetate anion acting as counterion of the disulphide[552, 556, 557]: peak at 1,674

cm^{-1} resulting from υ_s(CO); band at 1,639 cm^{-1} from υ_s(CF$_3$COO$^-$); signal at 1,203 cm^{-1} originating from υ_s(CF$_3$); and the vibration at 1,149 cm^{-1} corresponding to υ_s(CO) and υ_s(CC)[558].

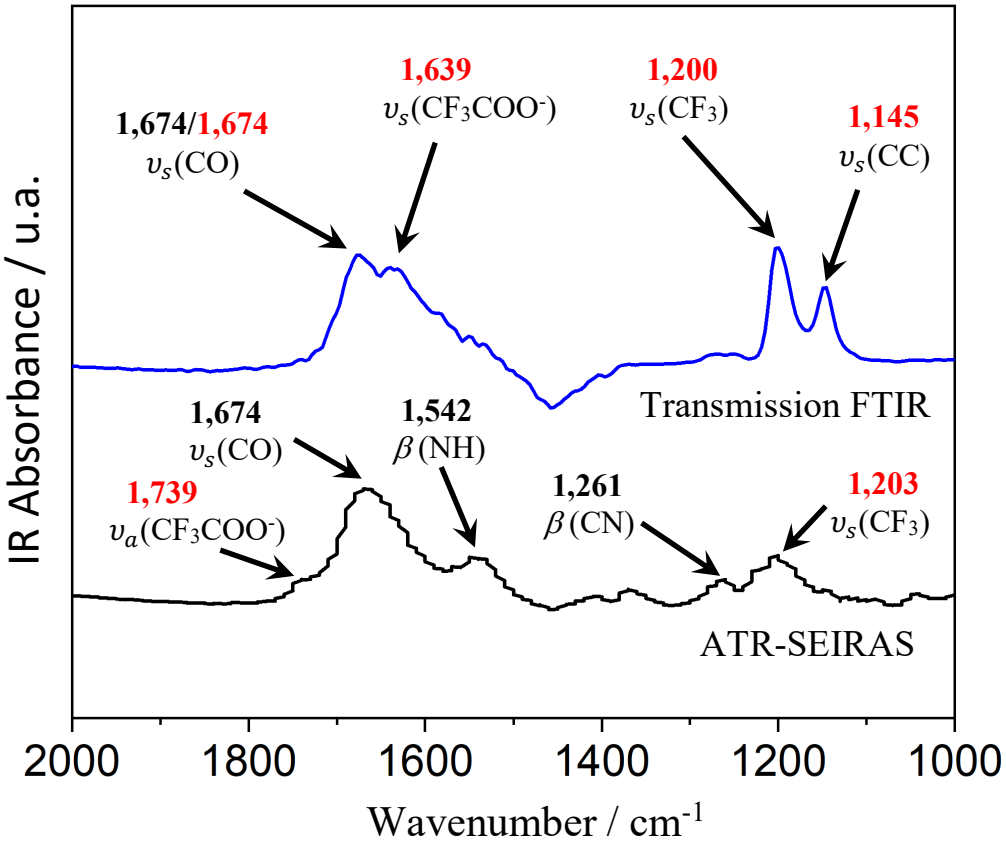
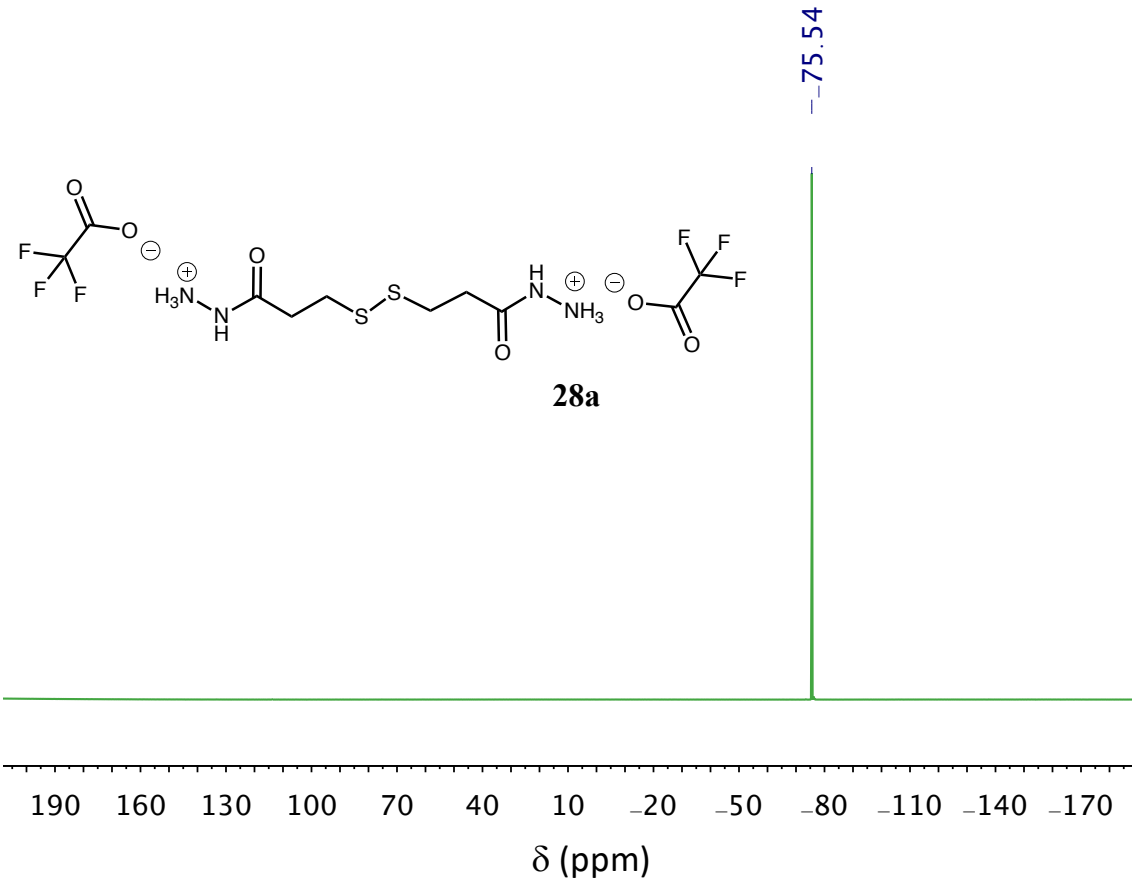


Figure 5.13. FTIR transmission spectrum (top, blue) of a 50 mM aqueous solution of DPA-HD; and ATR-SEIRAS spectrum (bottom, black) of a SAM formed from a 10 mM aqueous solution of DPA-HD on a sputtered Au surface; the absorbances of the two spectra were normalised; bands from TFA are annotated in red and those from DPA-HD in black. The presence of TFA adsorbed on the Au surface besides DPA-HD molecules, suggested by the presence of some characteristic bands of the anion in ATR-SEIRAS (*i.e.* at 1,739 cm^{-1} and 1,203 cm^{-1}), was supported by the transmission FTIR analysis of the DPA-HD stock solution used to prepare the SAM studied in **Figure 5.10**, which presented very intense TFA peaks.

Some of the characteristic bands of the hydrazide, like band II at 1540 cm^{-1} or the one at 1260 cm^{-1}, were difficult to observe in transmission FTIR. This may indicate the high quantities of trifluoroacetate in the sample; or perhaps, the interaction of DPA-HD with the TFA anion and the formation of a salt, cancelled these vibrations. ^{19}F-NMR confirmed the presence of the trifluoroacetate anion in the sample used to prepare SAMs of DPA-HD **(Figure 5.14)**.



28a

Figure 5.14. ^{19}F-NMR spectrum (400 MHz, D_2O) of the DPA-HD sample used for the ATR-SEIRAS and transmission FTIR experiments. The presence of a singlet at *ca.* -76 ppm evidenced the existence of trifluoroacetate[559].

In summary, the use of TFA for the deprotection of the Boc group of **27** to obtain DPA-HD resulted problematic since trifluoroacetate cannot be easily removed from organic samples[560] and it could affect the formation of DPA-HA SAMs.

To bypass this problem, the next step was to couple DPA-HD with Gal (DPA-HD-Gal) and then form SAMs of DPA-HD-Gal on a Au(poly) electrode **(Scheme 5.3-B)**. This way, DPA-HD-Gal would incorporate the BRE on the position of the hydrazide group, averting its interaction with Au and allowing the formation of sound SAMs. Furthermore, it would facilitate the removal of TFA by breaking up the TFA salt of DPA-HD.

D. Coupling of 3,3'-Disulfanediyldi(propanehydrazide) with Galactose

The procedure followed to link Gal with DPA-HD to obtain Galactose 3,3'-disulfanediyldi(propanehydrazide) (DPA-HD-Gal, **29**) was based on the results published by Godula et *al.*[519] and work previously done by Creese[561] in the Fernández-Trillo Group. The condensation reaction **(Scheme 4.8)** efficiently proceeded under slightly acidic conditions (phosphate buffer 0.1 M, pH 5.4) and mild temperature (60 ˚C). The starting material, the TFA salt of DPA-HD (**28a**), was not soluble in the buffer at room temperature. After adding *ca.* 4 equivalents of Gal and stirring, the initial cloudy suspension became an even more opaque crude within a few hours, hinting at a successful coupling. The white, sticky solid recovered after lyophilisation proved to be insoluble in water, organic solvents, and mixtures thereof, including MeOH, EtOH, isopropanol, DMF, $CHCl_3$, THF, hexane, acetone, EtOAc, DCM, Et_2O, AcCN, toluene;

this made its characterisation difficult. Nonetheless, MS of a sample without purification **(Figure 5.15)** seemed to confirm the linkage between DPA-HD and Gal. Still, due to the lack of solubility of the product, ^{1}H-NMR could not be used to determine the degree of coupling achieved by calculating the intensity reduction of the peaks of the anomeric carbon proton (red proton in **Scheme 5.2**) in the pyranoside forms[562].

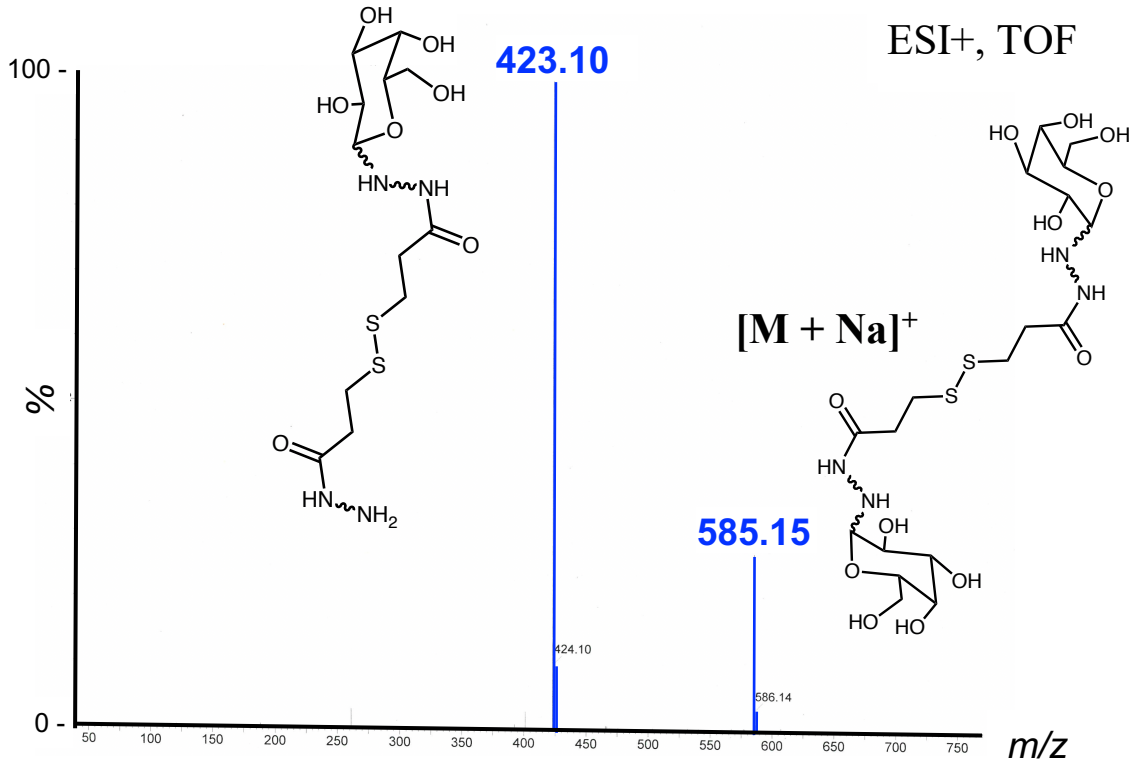


Figure 5.15. MS spectrum of the crude product of the condensation reaction between DPA-HD (TFA salt) and Gal. The presence of a Na adduct (585.15 m/z) of the molecular ion (M^+) appeared to confirm the coupling of the 2 hydrazide groups of DPA-HD with the sugar. Nevertheless, the base peak (423.10 m/z) might have also pointed towards the presence of monosubstituted molecules.

To accomplish NMR analysis, the sample had to be dissolved in DMSO at high temperature (80 ˚C). Nevertheless, the use of DMSO introduced other issues beyond chemical identification, like making this compound purification very challenging (*e.g.*

HPLC and extractions); or raising questions about the feasibility of preparing SAMs from dissolutions because DMSO adsorbs on Au surfaces[563] **(Figure 5.16)**.

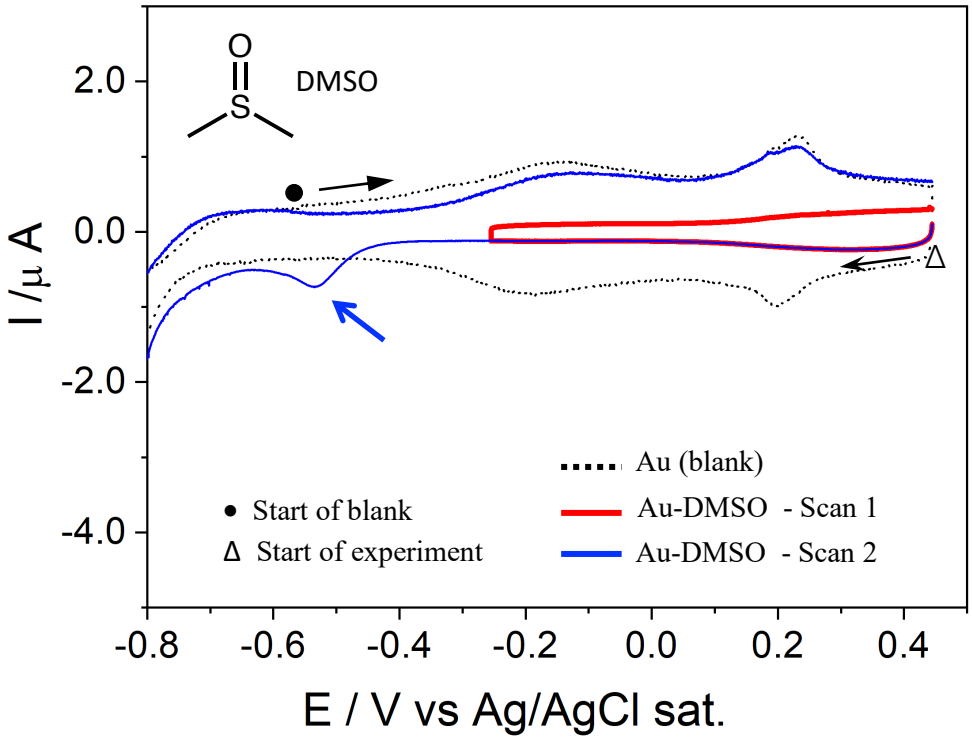


Figure 5.16. CV characterisation of a Au(poly) electrode modified in DMSO: electrode dipped in pure DMSO-d_6 for 30 min. at room temperature; a 0.1 M phosphate buffer (pH 7.4) electrolyte and a scan rate of 50 $mV \cdot s^{-1}$ were used. The sweep of the clean Au electrode surface (blank) between +0.45 and -0.9 V (dotted black line) presented the characteristic electrochemical profile of Au in phosphate buffer electrolyte at pH 7.4. Following electrode modification with DMSO, the first scan (solid red curve, from +0.45 to -0.25 V) showed the loss of the clean Au profile and a reduction of the EDL, attesting the blockage of the surface by DMSO molecules. The second scan (solid blue line, from +0.45 to -0.90 V) confirmed the adsorption of the sulfoxide with a reductive stripping peak occurring at -0.53 V (blue arrow). (•) Start of the blank; (Δ) start of CV scans on the modified electrode. At low potentials, sweeps are shown only till -0.80 V to omit the hydrogen evolution reaction signal.

At this stage, it seemed that the possibility of using DPA-HD as a linker in the project had reached a dead end. On the one hand, the impracticality of forming good SAM of DPA-HD on the electrodes ruled out the possibility of first having SAMs of DPA-HD and then chemically reacting them with Gal **(Scheme 5.3-A)**. On the other, the condensation of DPA-HD with Gal produced an insoluble species (DPA-HD-Gal) that made impractical to pursue the modification of electrodes from solution **(Scheme 5.3-B)**. However, one last attempt was made synthesising the HCl salt of DPA-HD.

E. 3,3'-Disulfanediyldi(propanehydrazide) Deprotected with HCl

Since the deprotection of the Boc group can be accomplished under several acidic conditions[564], HCl was chosen **(Scheme 4.6, conditions b)** as an alternative to TFA[565]. Although the formation of the HCl salt of DPA-HD was expected, removing the counterion during purification (HPLC) was more feasible. Besides, Cl^- is a much smaller counterion than trifluoroacetate and it was assumed that it would be less problematic to form SAMs if still present. All of it opened the possibility of immobilising DPA-HD on Au first and then coupling Gal.

The initial conditions tried to deprotect **27** (HCl 1 M, room temperature overnight) did not work. The same acid concentration at 100 ˚C proved to be too harsh: it did not only cleavage the Boc group but also hydrolysed the hydrazide group back into dicarboxylic acid **25**. Eventually, HCl 1 M at 40 ˚C overnight yielded dihydrazide **28**. Unlike when TFA was used, ^{1}H-NMR **(Figure 5.17)** and HPLC **(Figure 4.2)** showed the presence of byproducts. This was probably caused by the severe acidic conditions, which removed the Boc group but also transformed some hydrazide groups into acids.

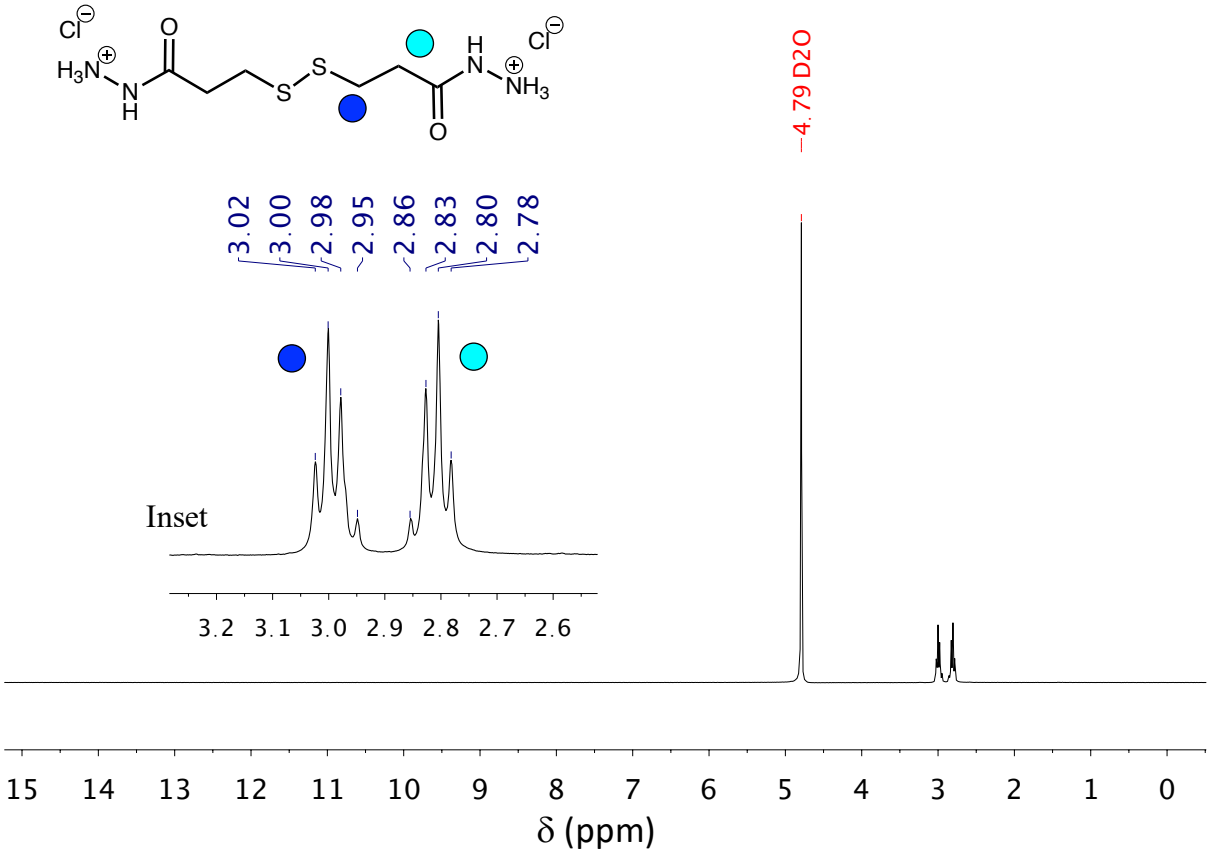


Figure 5.17. ^{1}H-NMR spectrum (400 MHz, D_2O) of DPA-HD synthesised with HCl before purification. According to its chemical structure, the pure disulphide should produce 2 neat triplets at high field in ^{1}H-NMR. Therefore, the sample required purification.

The HCl salt was purified with HPLC in a preparative column **(Figure 4.2)** and characterised with ^{1}H-NMR **(Figure 5.18)**, ^{13}C-NMR, and MS.

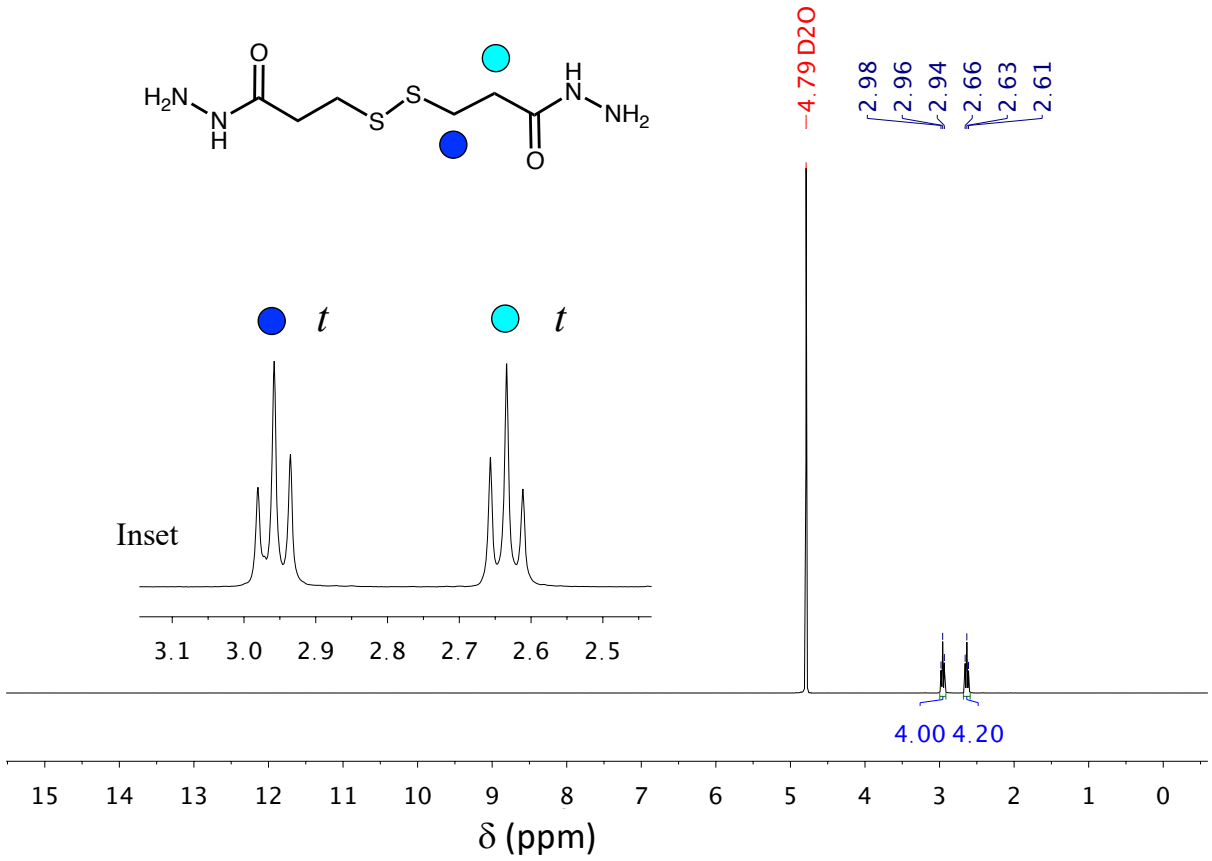


Figure 5.18. ^{1}H-NMR spectrum (400 MHz, D_2O) of pure DPA-HD with the expected 2 triplets (inset) at high-field from the aliphatic region of the disulphide. The protons of the hydrazide group were not observable at low-field due to the fast exchange with the solvent. The purification of **28** probably also meant the remova of the chloride counterion. The normalisation of the integrals (bottom, blue digits) was done taking the triplet at about 3.00 ppm as a reference.

The use of HCl to deprotect DPA-HD did not improve the reproducibility of the desorption of the DPA-HD SAMs. Perhaps due to the adsorption of the DPA-HD salt counterion, Cl^-, onto Au[566, 567], as it had happened with trifluoroacetate; but most probably, as previously shown **(Figure 5.8)**, by the hydrazide group interacting with the electrode. This latter case may be especially true since Cl^- had probably been removed during the purification with HPLC. Whatever the reason, it dismissed the

possibility of modifying electrodes with the linker and then attaching Gal **(Scheme 5.3-A)**. The last option to use this molecule, coupling DPA-DH (or its Cl^- salt) with Gal and then immobilising DPA-HD-Gal on the electrodes **(Scheme 5.3-B)**, was thus tried.

DPA-DH was completely soluble in the reaction conditions **(Scheme 4.8)**, unlike its TFA salt, with 4 equivalents of Gal being employed. ^{1}H-NMR was used to track the reaction and the changes observed in the spectral region between 3.40 and 4.20 ppm **(Figure 5.19)** seemed to confirm the coupling of monosaccharide and disulphide (no variations in this region were observed in the blank containing only Gal). ^{1}H-NMR determined that after 6 h. at 60 ˚C the condensation reaction had reached completion.

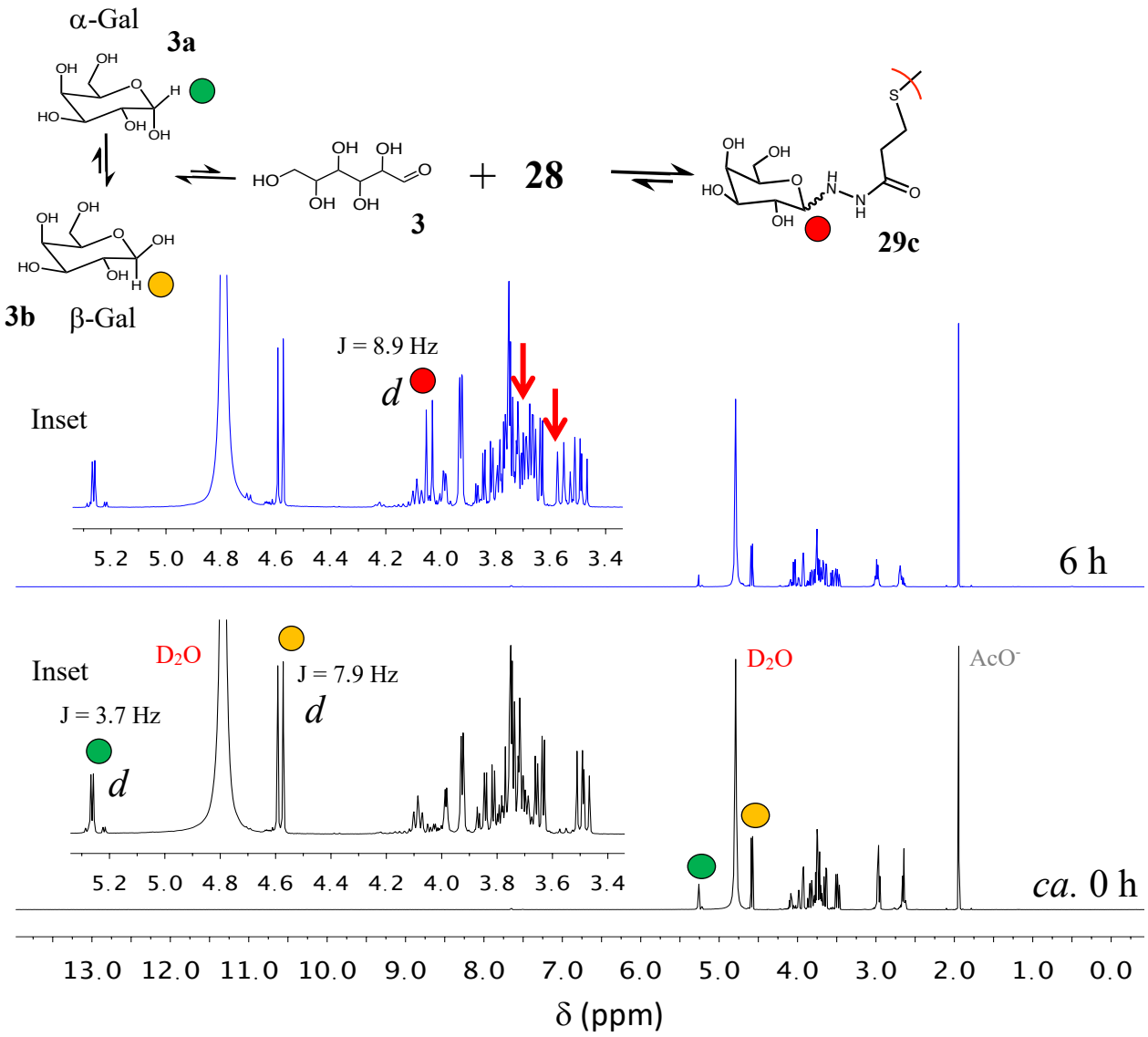


Figure 5.19. ^{1}H-NMR (400 MHz, D_2O) spectra of the crude of the reaction of DPA-DH with Gal (4 equivalents) at *ca.* 0 h. and 6 h. Green and yellow dots correspond to signals produced by the proton of the anomeric carbon of the galactopyranoside isomers. Due to the mutarotation of Gal, this proton can occupy the equatorial position ($^{\alpha}$H, α-Gal) or the axial position ($^{\beta}$H, β-Gal). The electron-withdrawing effect of the 2 atoms of O next to the anomeric C explains the reduction of electron density around its proton and its resonance at a lower radiofrequencies (lower field, higher chemical shift) than the rest of the Gal protons (resonance between 3.40 and 4.20 ppm[568]). The coupling of Gal with DPA-HD after 6 h. induced changes in this same region (*e.g.*, red arrows and red dot) by modifying the chemical environment of the protons and how they interact with the readiofrequencies applied by the NMR spectrometer.

In the low-field region **(Figure 5.20)**, at *ca.* 7.66 ppm, the doublet of the hydrazone proton (black star) could also be seen. Its intensity was small because the equilibrium was displaced towards the formation of isomers where the saccharide part of DPA-HD-Gal was cycled. This signal was also duplicated (another small doublet at 7.51 ppm, red star) due to the presence of linear stereoisomers of DPA-HD-Gal. In principle, this duplication could be attributed to E/Z geometric isomers or to syn/antiperiplanar conformational isomers[569] (rotamers) (top of **Figure 5.20**). However, because of the molecule's structure, it was assumed a small rotational barrier in the N-N bond, making it less likely to observe the syn and antiperiraplanar rotamers in the spectra. Therefore, the peak at 7.66 ppm was associated with the formation of the E isomer during Gal cyclisation (more stable and, thus, intense); and the signal at 7.51 with the Z isomer. The tiny singlet at 9.70 ppm (yellow triangle) could pertain to the proton on the N atom of the linear isomers.

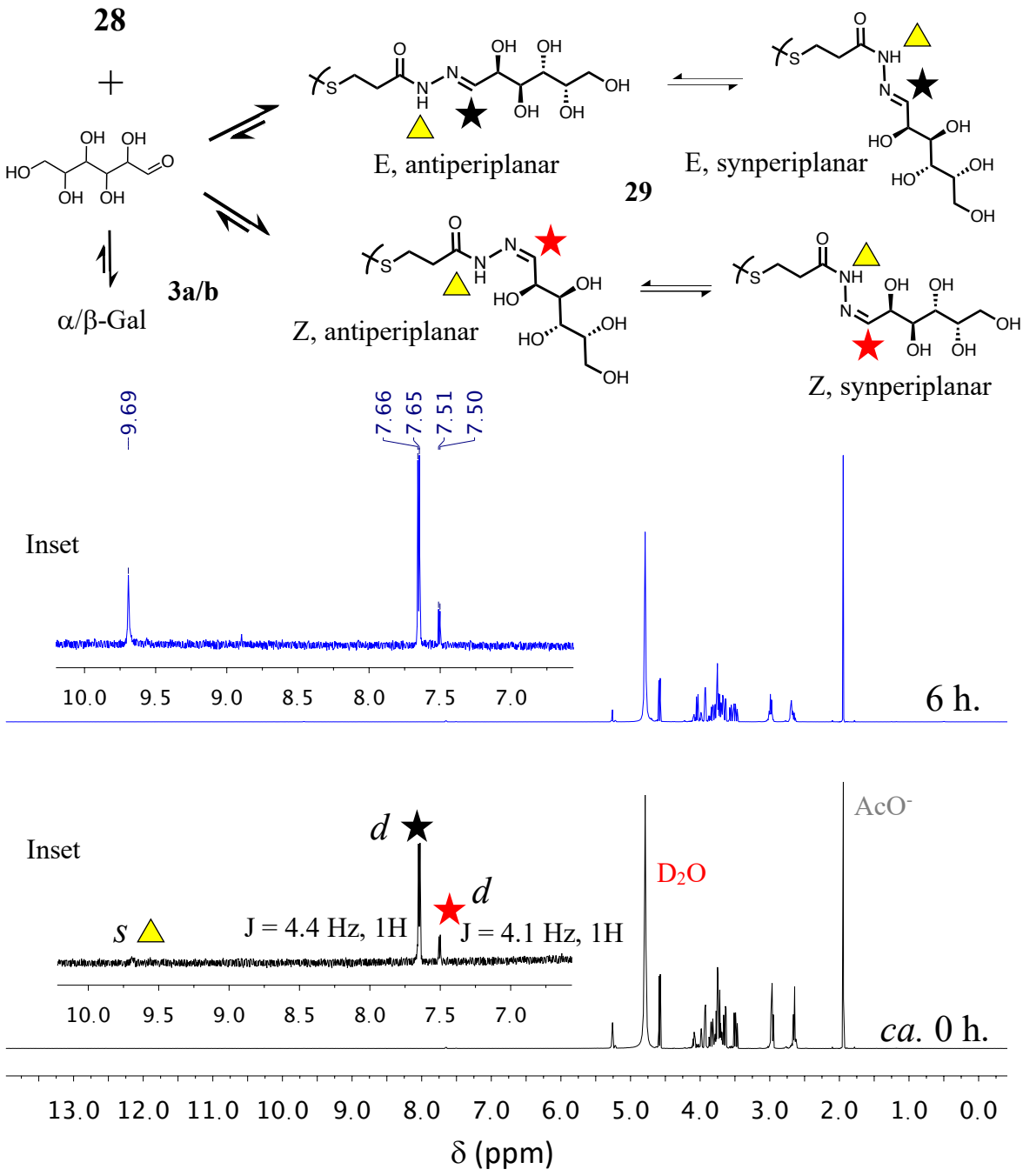


Figure 5.20. ^{1}H-NMR spectra (400 MHz, D_2O) from the crude of the condensation between DPA-DH and Gal at *ca.* 0 h. and after 6 h.; the insets show the low-field region of the spectra. The doublet at 7.65 ppm (black star) signalled the formation of the hydrazone (E isomers) and the success of the reaction. A weaker doublet at 7.50 ppm (red star) was identified with less thermodynamically favoured Z isomers. The small singlet (yellow triangle) at 9.70 ppm probably pertained to the NH group of the hydrazone.

At high-field, the complexity of the multiplicity of the spectra after 6 h. **(Figure 5.21),** in the region of the DPA-HD-Gal methylenes (between 2.50 and 3.10 ppm, inset B), could be explained by the aforementioned isomers; but also by the highly probable formation of the mono and di-substituted DPA-HD-Gal.

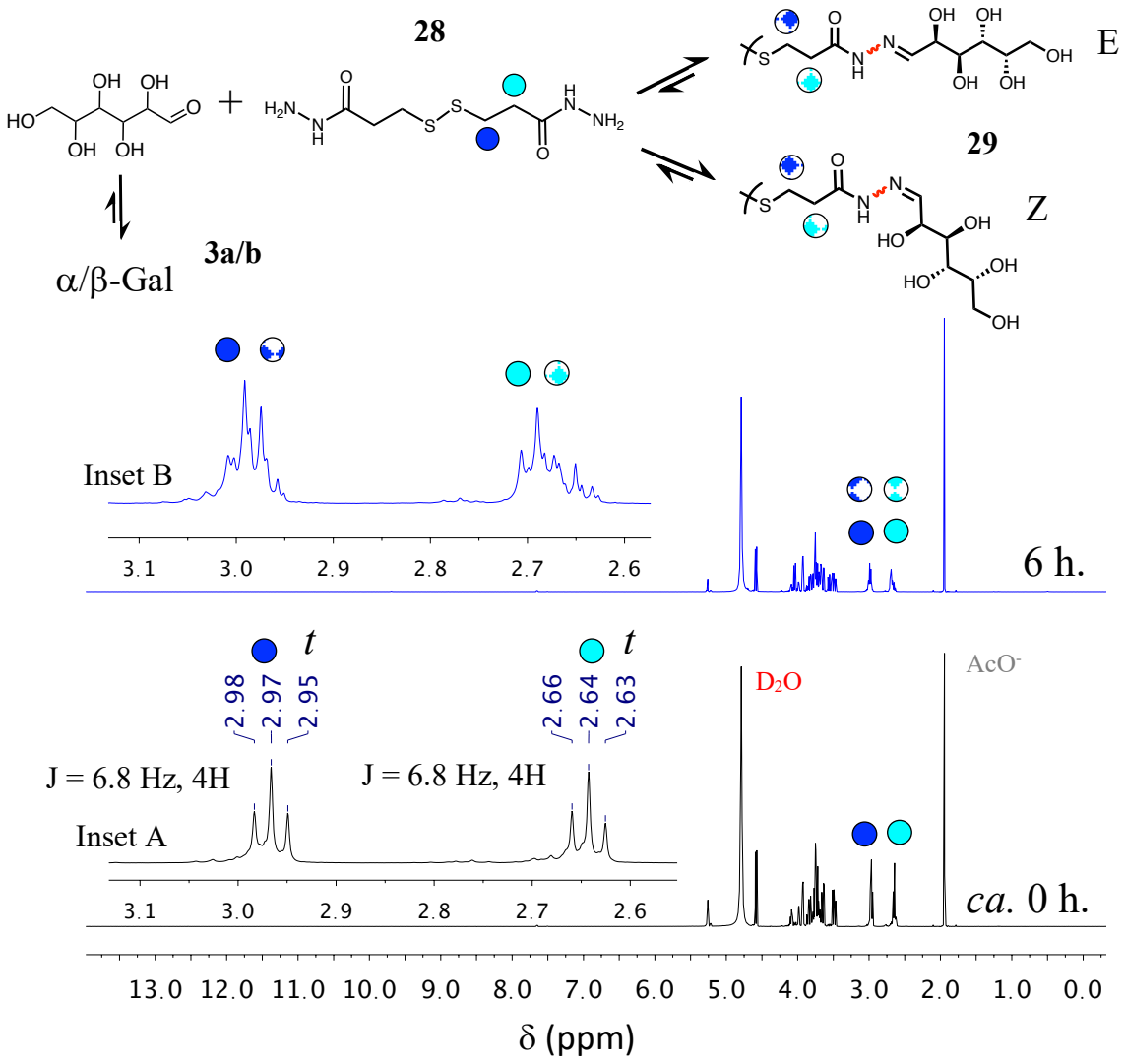


Figure 5.21. ^{1}H-NMR spectra (400 MHz, D_2O) of the reaction crude of the coupling of DPA-DH with Gal; the insets show the high-field region. The multiplicity change of the methylene peaks after 6 h. (chequered dots) evidenced the formation of DPA-HD-Gal. Their new complexity probably also implied the presence of isomers, including the mono and disubstituted products.

The integration of the anomeric proton signals of free Gal allowed an approximate calculation of the yield of the condensation reaction **(Figure 5.22)**. All the peaks from free Gal were integrated (bottom, blue digits) for 7 (Gal has 7 protons) in the spectrum recorded soon after the reaction started (*ca.* 0 h). As expected, the integration of the peaks of the anomeric proton at that time was approximately 1 (0.36 + 0.58). However, after 6 h., this sum was only 0.59 (0.20 + 0.39) indicating that 41% of the free saccharide had disappeared from the reaction medium by coupling with the dihydrazide. Because the equivalents of Gal used in this synthesis were double what was needed for a complete reaction with the hydrazide groups of DPA-HD, the estimated yield was 82%, per previous work of Creese[570] and the literature[519].

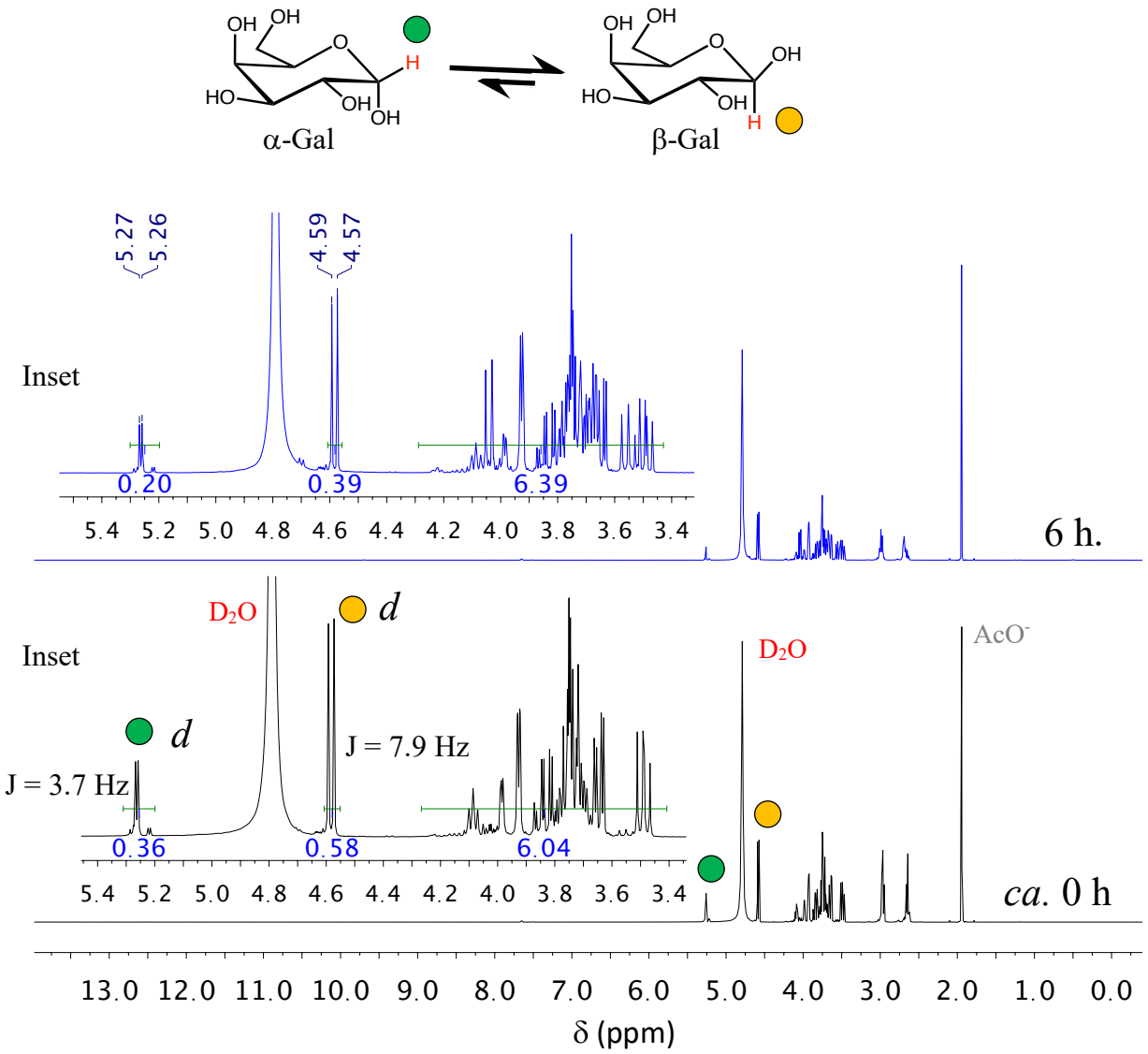


Figure 5.22. Calculation of the yield of the condensation reaction between DPA-HD and Gal (4 equivalents) with ^{1}H-NMR (400 MHz, D_2O). The signals in the sugar region (from 3.40 to 5.40 ppm) were integrated (blue digits) for 7, the total number of protons of Gal. The sum of the integrals of the anomeric carbon proton (yellow and green dots) was around 1 (0.36 + 0.58) at *ca.* 0 h., since almost no Gal molecule could have reacted by then. After 6 h. it was only 0.59 (0.20 + 0.39), illustrating that 41% of the free Gal had coupled to the disulphide. Considering that 4 equivalents of Gal were used in this synthesis, double what was needed for the full reaction of the 2 hydrazide groups of DPA-HD, the yield was estimated at 82%.

Different times of reaction and concentrations of Gal were used to optimise the synthesis by forcing the equilibrium towards the hydrazone. With all equivalents tested, the maximum conversion of DPA-HD had been reached after approximately 20 min. When 6 or 8 equivalents of monosaccharide were employed, the calculated conversion was over 100% according to ^{1}H-NMR. This could be explained by the formation of a precipitate, an emulsion, already observable in condensations with only 1 equivalent of Gal. As happened with the DPA-HD-Gal obtained from the TFA salt of the dihydrazide, the product was insoluble in all solvents tried, except for hot (80 ˚C) DMSO. The same occurred when Glc and Man were linked to DPA-HD. The explanation to this phenomenon was found in the literature: a type of molecule called bolaamphiphile had formed[571, 572].

Bolaamphiphiles **(Figure 5.23)** are characterised by a hydrophobic skeleton - typically an alkane chain- with two hydrophilic groups attached to its ends. These species can self-assemble, giving rise to complex structures in aqueous media like vesicles[573], fibres[574] or gels[575]. The presence of a hydrophilic and a hydrophobic region would also explain the difficulties to dissolve these species.

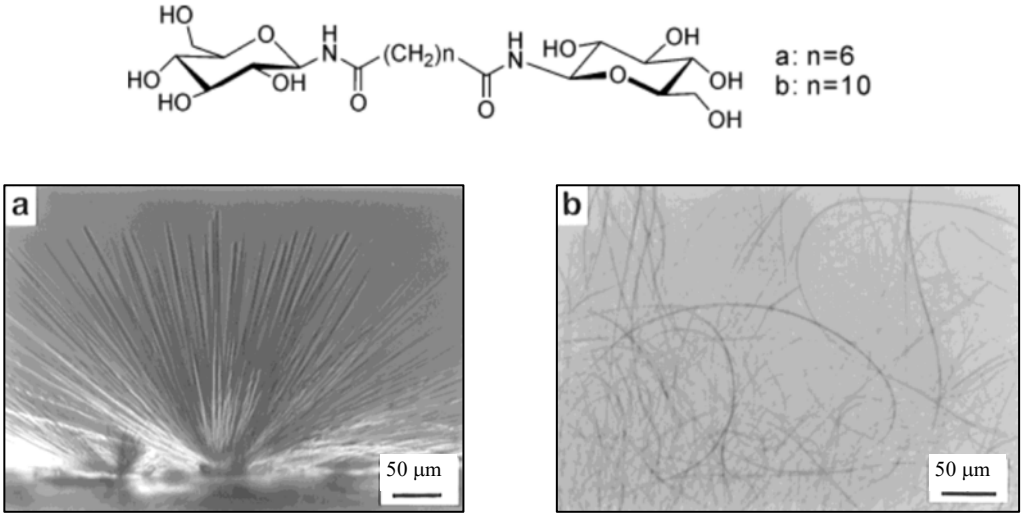
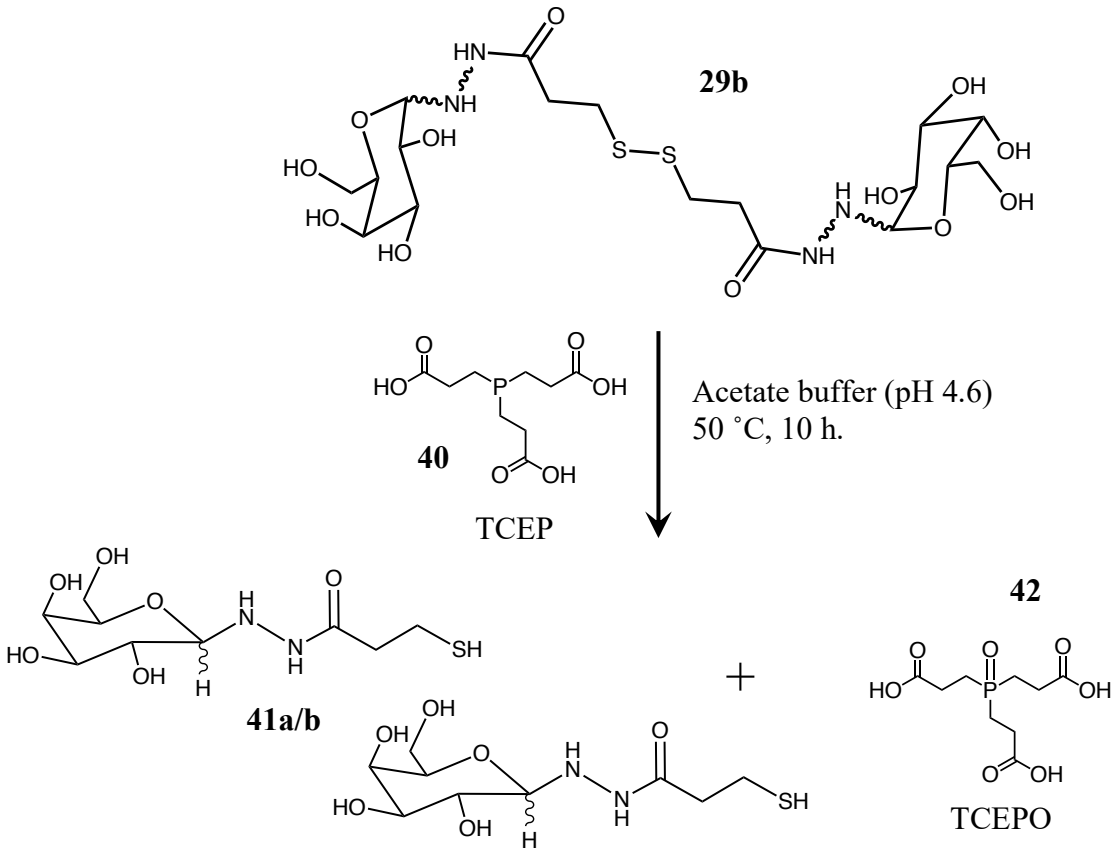


Figure 5.23. TEM images (**a** and **b**) of the structures produced by two bolaamphiphiles through self-assembling (Fuhrhop *et al.*[572]); the molecular structures of both bolaamphiphiles are on top of the pictures. Image **a** shows the bundles of needles formed after the crystallisation of an α,ω-bis-1-aminoglucoside, with a connecting chain $(CH_2)_6$. Picture **b** presents the chain twisted ribbons generated by another α,ω-bis-1-aminoglucoside but with a slightly longer connecting chain, $(CH_2)_{10}$.

At this point, a possibility was reducing the disulphide bridge of the DPA-HD-Gal bolaamphiphile: the splitting of the S-S bond would halve the molecule's hydrophobic chain, reducing the amphiphilic nature that makes it so insoluble. The reduction of this bond through different methods is commonly found in the literature[576-578] given the importance of studying the composition, structure and functionality of proteins[579, 580]. The effectiveness of TCEP as reducer was tested by adding 0.14 mg (0.055 mmol) of the phosphine to a white, opaque suspension of DPA-HD-Gal (20 mg, 0.036 mmol) in acetate buffer (20 mM, pH 4.6). The appearance of the crude did not change when the suspension was stirred overnight at room temperature. However, when the reaction temperature was increased up to 50 ˚C **(Scheme 5.5)**, the suspension transformed

into a colourless dissolution within 10 h. This probably indicated the splitting of DPA-HD-Gal and the formation of 3-mercapto-*N'*-galactopropanehydrazide (**41**).



Scheme 5.5. Reaction scheme for the reduction of the disulphide bridge of DPA-HD-Gal with TCEP to produce 3-mercapto-N'-galactopropanehydrazide (**41a/b**), a more soluble molecule. The change of the crude apearance after 10 h. at 50 ˚C, passing from an opaque suspension to a dissolution, seemed to confirm an increase of the solubility of its molecules and, thus, the splitting of the disulphide DPA-HD-Gal to afford **41a/b**.

These promising results were backed by ^{1}H-NMR analysis of the crude, which still corroborated the presence of a galactohydrazone **(Figure 5.24)** through a doublet at *ca.* 7.50 ppm (magenta star). However, unlike in the ^{1}H-NMR spectra of DPA-HD-Gal **(Figure 5.19)**, there was a doublet at *ca.* 4.62 (chequered grey dot) that could

pertain to the α isomer (anomer) of **41**, **41a**. Instead, the doublet at 4.08 ppm (chequered red dot), which would relate to the β anomer (**41b**), was also present in the DPA-HD-Gal spectrum (red dot, **Figure 5.19**). If confirmed by further investigations, it would mean that during the formation of DPA-HD-Gal the anomeric effect is quite significant and only one of the two possible isomers is formed. All in all, because little is known about the anomeric effect in hydrazides and how its two contributions - electrostatic and stereoelectronic effects- affect them[581], a case by case study would be necessary to determine the predominant isomers.

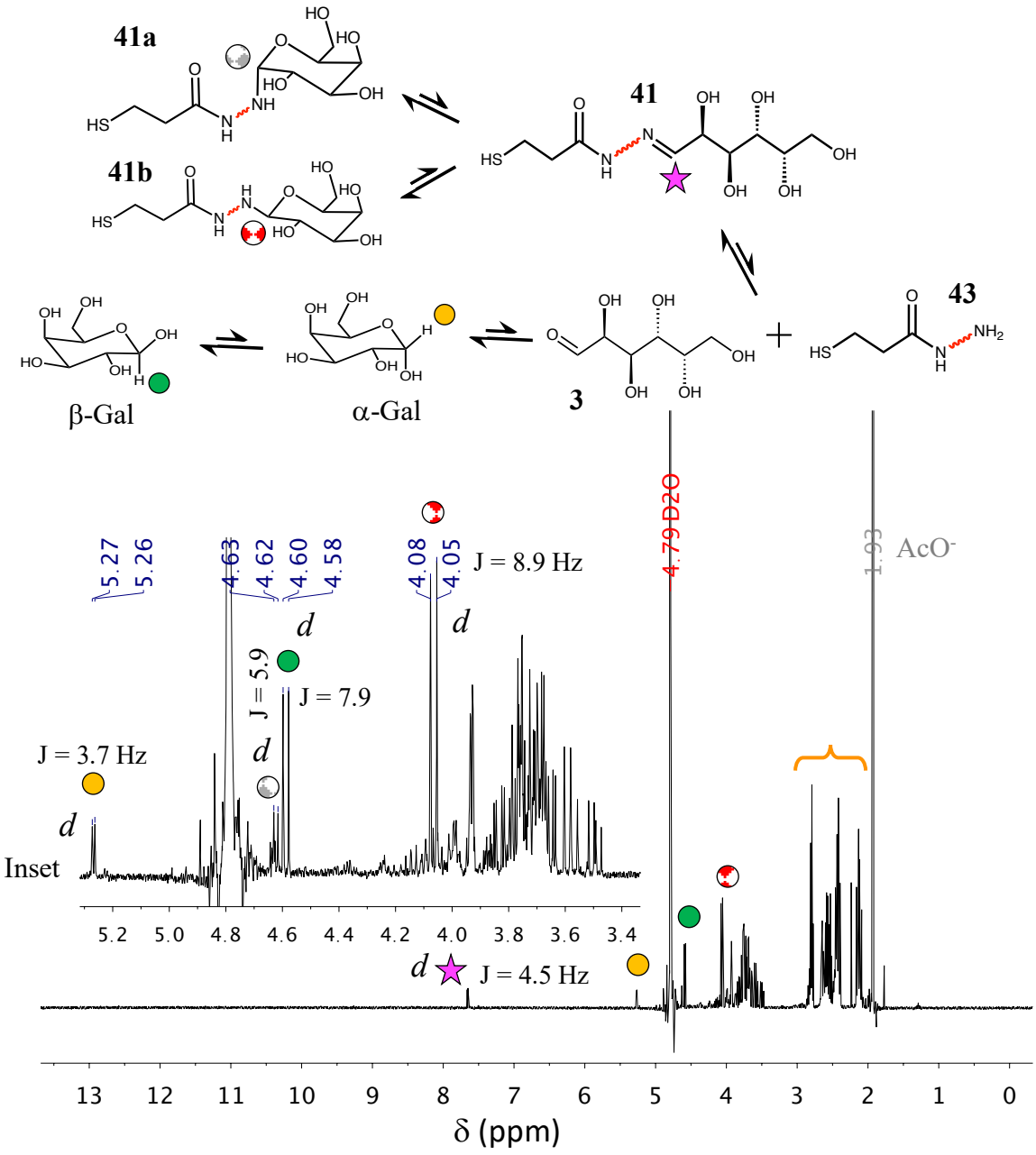


Figure 5.24. ^{1}H-NMR spectrum (400 MHz, D_2O) of the lyophilised crude product obtained after reducing DPA-HD-Gal into 3-mercapto-*N'*-galactopropanehydrazide (**41**) with TCEP in acetate buffer (pH 4.7) at 50 ˚C. At high-field were observed (orange key) the signals of the methylenes of **41**, **41a** and **41b**, rests of TCEP and the byproduct TCEPO; further downfield (inset), resonated the peaks of the anomeric proton of the non-reacted free Gal (yellow and green dots) and of the products **41a** (α anomer, chequered grey dot) and **41b** (β anomer, chequered red dot). The proton of the hydrazone isomers (**41**) was detected at around 7.66 ppm (magenta star).

Because of the prospect of a complex and time-consuming purification of **41** due to the presence of TCEP and 3,3',3''-(oxo-λ^5-phosphanetriyl)tripropionic acid (TCEPO), oxidised TCEP, it was decided to try another type of linker to immobilise Gal on Au(poly) electrodes: polymers. The Fernández-Trillo Group, one of the research groups where the project was being done, were dedicated to the synthesis and application of polymers. One of the macromolecules produced and available in the group was recognised as a potentially suitable linker: it contained a thiol group in one of its ends and many hydrazide groups to link with Gal.

5.3 Conclusions

The attempt to synthesise asparagusic acid as a potential linker of Gal for developing an electrochemical glycosensor to detect the cholera toxin failed. The different conditions tried in the second step of the synthesis to forward an S_N2 reaction did not work, most probably because of the neopentyl effect. Indeed, the x-ray spectrum of the starting material of this step showed how a high steric hindrance around the reaction centre could have been blocking the nucleophile.

A linear dihydrazide disulphide (DPA-HD) was synthesised as an alternative. However, according to CV characterisation, difficulties emerged to obtain good-quality SAMs on Au(poly) electrodes from where Gal could be linked. CV experiments with AcHD demonstrated that the hydrazide group adsorbs on Au. Therefore, the formation of poor DPA-HD SAMs may had been caused by this molecule's interaction with Au through two different regions (hydrazide groups and S atoms), producing a disordered

orientation and assembling of molecules on the electrode. Nevertheless, since different FTIR spectroscopic techniques laid bare the presence of trifluoroacetate in the DPA-HD sample used to generate SAMs, and since this anion also adsorbs on Au, it could have been that the true source of disruption of self-assembling was the anion. To avoid this impurity, a different synthetic route to afford pure DPA-HD using HCl was undertaken. But SAM formation issues continued, so their most probable origin was indeed the hydrazide group adsorption.

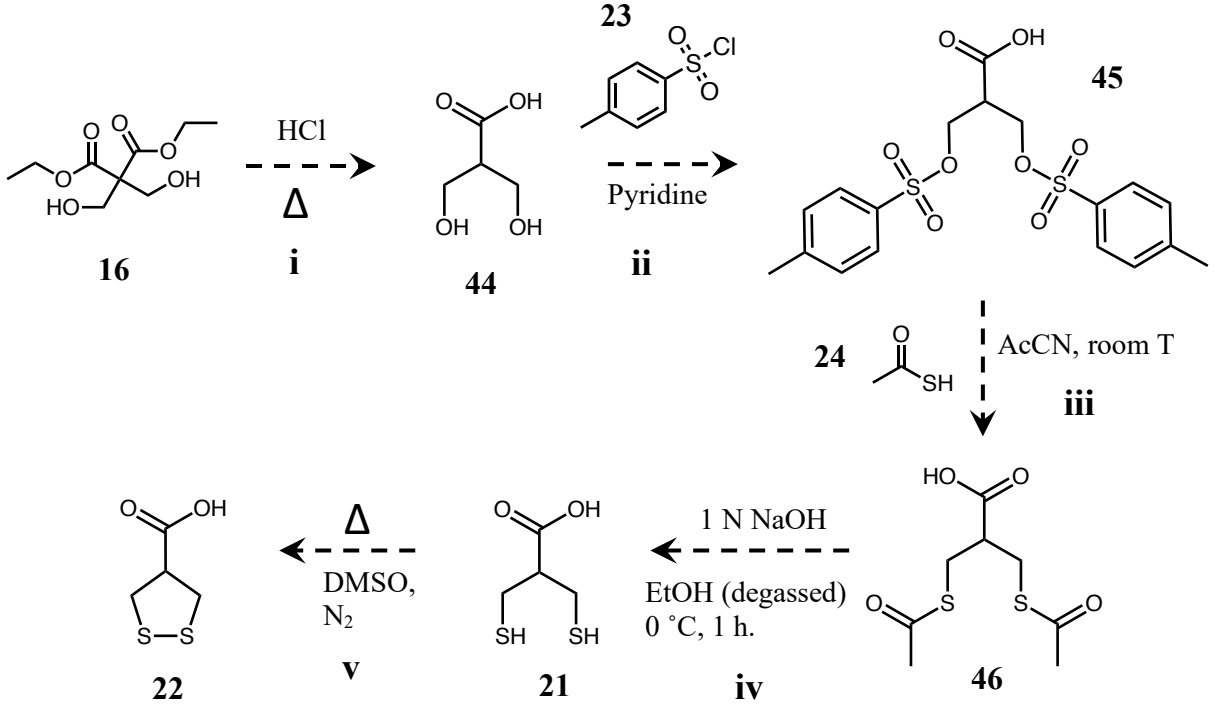
To circumvent this situation, DPA-HD was coupled with Gal previous adsorption on the electrode. However, in this case, the bolaamphiphile DPA-HD-Gal was synthesised. Bolaamphiphiles have very poor solubility in most solvents, precluding the obtainment of monolayers from solution.

In summary, the efforts to synthesise or use a small molecule as a linker to adsorb Gal on Au(poly) electrodes were unsuccessful, despite logical approaches to bypass the problems.

5.4 Future work

The synthesis of asparagusic acid with the synthetic route proposed in **Scheme 4.1** may be still possible using in **step ii** some of the conditions described by Tuber *et al.*[478] for a similar S_N2 reaction with the same starting material: DMSO as a solvent and 6 days of reaction at room temperature (60% yield). An alternative would be a new synthetic route. The best choice considered **(Scheme 5.6)** would transform **16** into **44**

in **step i**, converting the β carbon of the reaction centre of the starting material of **step ii** (**16**) from a tertiary to a secondary carbon in (**44**). This would reduce the steric hindrance faced by nucleophile **24** in **step iii** when attempting to substitute the tosylate group of electrophile **45**.



Scheme 5.6. Alternative synthetic route to afford asparagusic acid (**22**): **(i)** hydrolysis and decarboxylation of dihydroxymethyl malonate (**16**); **(ii)** nucleophilic substitution of Cl^- from **23** by 3-hydroxy-2-(hydroxymethyl)propanoic acid (**44**); **(iii)** S_N2 substitution of the tosylate groups of **44** by thioacetic acid (**24**); **(iv)** nucleophilic acyl substitution in **46** for obtaining dithiol **21**; **(v)** intramolecular cyclisation to afford **22**.

Regarding the use of DPA-HD as a linker, work should be done to purify compound **41** obtained from the reduction of DPA-HD-Gal with TCEP **(Figure 5.24)** and study the formation of SAMs on Au(poly) electrodes.

Chapter 6

Synthesis of Polymer Linkers and Functionalisation of Polycrystalline Au Electrodes with Galactose

6.1 Introduction

Integrating the BRE and the transducer of an electrochemical biosensor constitutes one of the most essential and challenging stages for its development. Examples of SAMs of small molecules as integrating platforms are ubiquitous in literature but in biosensing have a fundamental caveat: their bi-dimensional character. In chemical and biological systems, recognition processes greatly depend on 3D structures. The recognition of an analyte, typically in a liquid, by a BRE fixed on a SAM can be limited in various ways. For example, the orientation of the BRE can be constrained, making it more difficult to interact effectively with the analyte **(Figure 6.1-A)**. Closely packed SAMs can also restrict the movements of the BRE, preventing it from reaching an optimal position for analyte identification **(Figure 6.1-B)**. With only part of the molecules holding BREs[582], heterogeneous SAMs can address this issue by generating room around the BRE to move and interact with the analyte. Nevertheless, they lower the BRE density on the sensing surface and the signal/noise ratio of the device. Besides, controlling the molecular distribution in heterogeneous SAMs is *de facto* impossible, complicating an adequate surface modification. If the analyte engaged in a beyond one-to-one interaction with the BRE, these limitations are aggravated. Polymers can contribute to solving some of these issues.

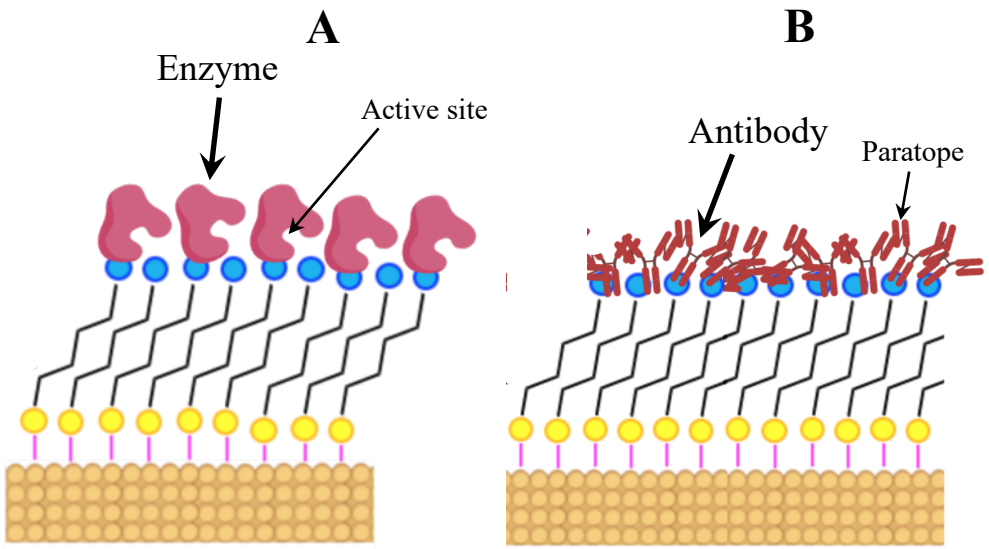


Figure 6.1. Constraints of using SAMs of small molecules to integrate BRE and transducer in an electrochemical sensor. **(A)** Example of the immobilisation of a BRE (enzyme) on a SAM where the BRE active region is hindered by the orientation and rigidity of the platform. **(B)** Too closely arranged molecules in a SAM can produce an agglomeration of the BRE that limits the interaction with the analyte, for instance the recognition of an antigen by the paratope of an antibody.

6.1.1 Polymers in Sensing

Polymers are of great use in sensing because they can mimic well natural systems. The glycosensor developed in this project is based on imitating the infection mechanism of *V. cholerae*, which significantly depends on the identification of the host's intestinal cells by the pentamer CTB of the bacterium's toxin **(Figure 6.2)**. The recognition is based on a one-to-one interaction between a pocket of each subunit of the CTB pentamer and the sugary end of GM1 molecules present in the cell membrane **(Figure 5.2)**. The binding, significantly strong[583], is enhanced by the simultaneous attachment of several subunits (up to 5) to different GM1 molecules on the cell[584] and a cooperative process[506, 585]. The phenomenon of cooperativity, common in nature,

occurs when a system constituted by several identical units sees a change in its avidity towards another system as more of its units bind it[586]. It plays a fundamental role in the interaction of many proteins[587] and increases the CTB affinity towards GM1 by a factor of between 1.7 and 2.9[585].

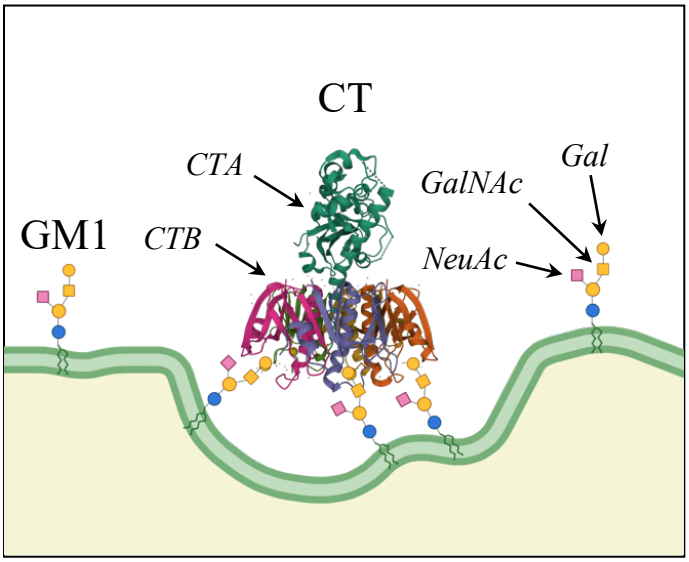


Figure 6.2. Recognition of a human intestinal cell by CT. The toxin recognition is based on the interaction of the pentamers of its CTB subunit with the sugary end of GM1 molecules anchored in the cell membrane. In this figure, 3 out of 5 pentamers of the CTB of a CT molecule interact with the ending of 3 different GM1 molecules.

Polymeric linkers can facilitate the multivalent interactions that define many recognition processes in nature by producing 3D architectures, increasing the BRE surface density on the electrode, and providing greater freedom of movement for the BRE. If one of the main difficulties in developing electrochemical sensors is achieving good selectivity, polymers' antifouling properties are advantageous. Indeed, many biosensors incorporate a spacer in the linker, like poly(ethylene glycol)[588] (PEG), to avoid fouling, the blocking of the electrode surface by unspecific interactions with

species other than the analyte. Some polymers are good antifouling agents thanks to their structure, surface grafting (how they adsorb on the electrode) and pendant groups' chemical composition[589]. Hydrophilic polymers, like pAH_n, are particularly effective against protein fouling given their reduced number of electrostatic interactions with the charged domains of these biomolecules[590].

6.1.2 Glycopolymers

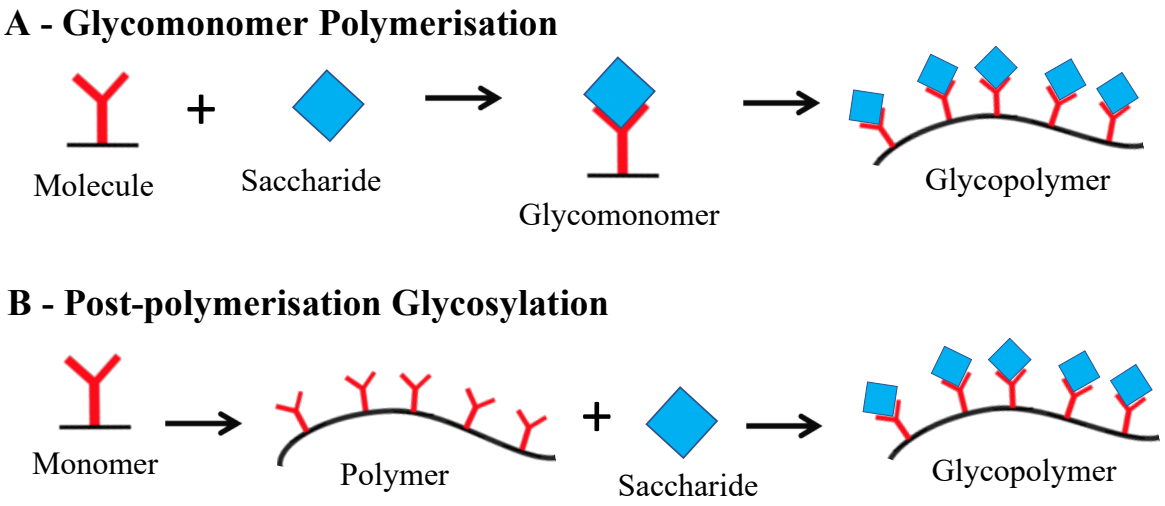
Glycopolymers are synthetic macromolecules whose pendant groups, at least some, are saccharides[591]. Given the importance of sugars in many biological functions[109, 592, 593], glycopolymers are used to mimic biological systems. The functionality of saccharides depends on most occasions upon weak forces like hydrogen bonds, van der Waals forces or hydrophilic/hydrophobic forces[594]. Therefore, their effectiveness is actually based on a multivalent interaction. Several features of glycopolymers make them very convenient to replicate the mode of action of sugars: first, the possibility of synthesising biocompatible, soluble, and polar glycopolymers permits their biomedical and biotechnological use[595, 596]. Second, because the backbone of a polymer can carry many saccharide pendant groups, they can replicate the multivalency character of many saccharides interactions[597]. Sometimes this multivalency depends not only on the number of carbohydrates but also on the space between them[598]; polymerisation can also control this. Furthermore, when more than one saccharide is responsible for the biological activity, they can be accommodated in a polymer to produce better analogs[599].

6.1.3 Synthesis of Glycopolymers

Most polymers are synthesised with living polymerisation methods because it allows high structural control. Although they generally only require a monomer and an initiator, they can have important drawbacks[600, 601,602]: use of organic solvents to dissolve the initiator or difficulties to remove a catalyst or having to protect the sugary monomer to avoid side-reactions. Reversible addition-fragmentation chain transfer polymerisation, RAFT polymerisation[603, 604], a living polymerisation method, has become very popular for glycopolymers synthesis thanks to the possibility of employing a wide range of functionalities, solvents and reaction conditions whilst maintaining a great polydispersity[603]. Besides an initiator, it also requires a chain transfer agent[605-608], a species to control the growth of the macromolecules. An advantage of RAFT polymerisation is the possibility of chemically transforming one of the ends of the polymers (the ω end) to endow them with more capacities through selective chain extension, labelling (*e.g.* fluorescent labelling) or incorporation of other functional groups. The scientific literature informs of glycopolymers of Gal obtained with this method[609, 610].

The effectiveness of glycopolymers to bind a target depends on the nature of the sugar moiety and other structural factors: length, saccharide density, arm length of the pendant group, and others[600]. Two main strategies are employed to prepare well-defined glycopolymers: polymerisation of monomers containing sugars (glycomonomers) **(Scheme 6.1-A)**; and post-polymerisation modification where sugars are added to a polymer *a posteriori*[611-613] **(Scheme 6.1-B)**. Glycomonomer

polymerisation guarantees a high degree of functionalisation. If a complete functionalisation is not necessary, though, post-polymerisation glycosylation[601] offers some advantages: avoidance of complex reactions (*e.g.* synthesis of monomer), elimination or simplification of purification (*e.g.* no catalysts used), obtainment of difficult architectures[601], greater control of glycans loading. The chemistry used in post-polymerisation glycosylation is very rich[600, 601]; for example, amino saccharides coupled with pendant groups containing acyl chlorides[614] or the amino functionality of pendant groups coupled to the aldehyde group of carbohydrates[615].

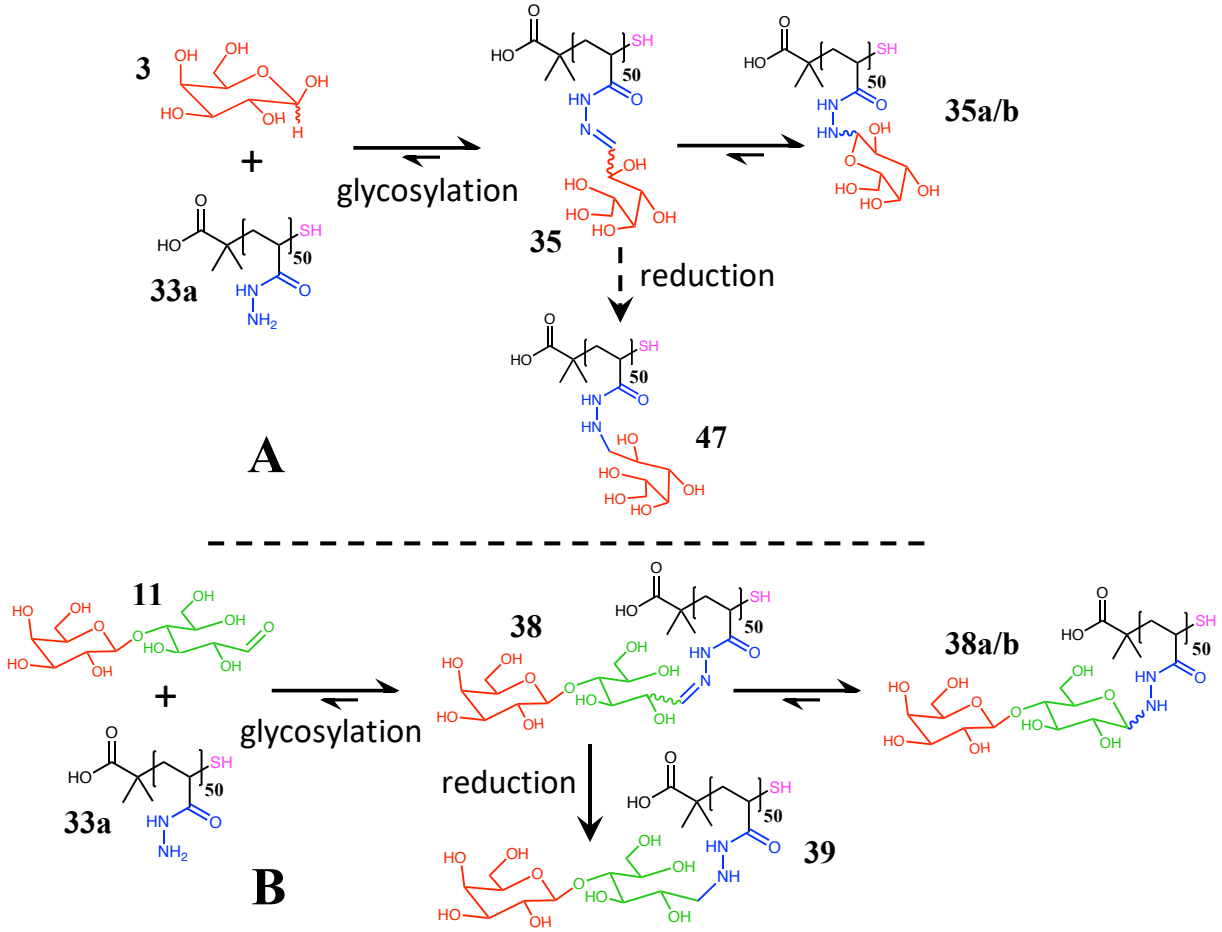


Scheme 6.1. Different strategies for the synthesis of glycopolymers. **(A)** Glycomonomer polymerisation consists of synthesising monomers containing sugars and then polymerising them. **(B)** In post-polymerisation glycosylation, saccharides are incorporated into the pendant groups of already synthesised macromolecules.

6.1.4 Glycopolymers with Galactose and Lactose

Due to the interaction between CTB and Gal, the sugar has been incorporated into glycopolymers to mimic this interplay[93]; and different configurations, *e.g.* monosaccharide loading, have been tried to optimise it. Lac, composed of Glc and Gal,

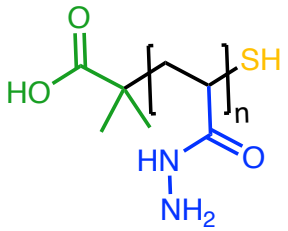
has also been linked to polymers through Glc, leaving Gal free to interact with CTB. This may even be more effective since the sugar is further apart from the polymer backbone and may help the pentamer approximation. Using Lac also offers the possibility of reducing the hydrazone formed for a more stable linkage **(Scheme 6.2)**. Although Gal was initially used in this chapter, the prospect of having to do a research visit to Portugal resulted in employing Lac to obtain more stable glycopolymers less problematic to transport.



Scheme 6.2. Two different strategies to link Gal to pAH_n. **(A)** Glycosylation of pAH_{50} with Gal; an eventual reduction of the product **35** would prevent the cyclisation of Gal (**47**), necessary for detecting CTB. **(B)** pAH_{50} glycosylation with Lac (**38**) followed by the reduction of the hydrazones formed; this second option permits the generation of a more stable bond whilst preserving the cyclic form of Gal in aqueous media (**39**), essential for its interaction with CTB.

6.1.5 Modification of Au(poly) Electrodes with Galactose

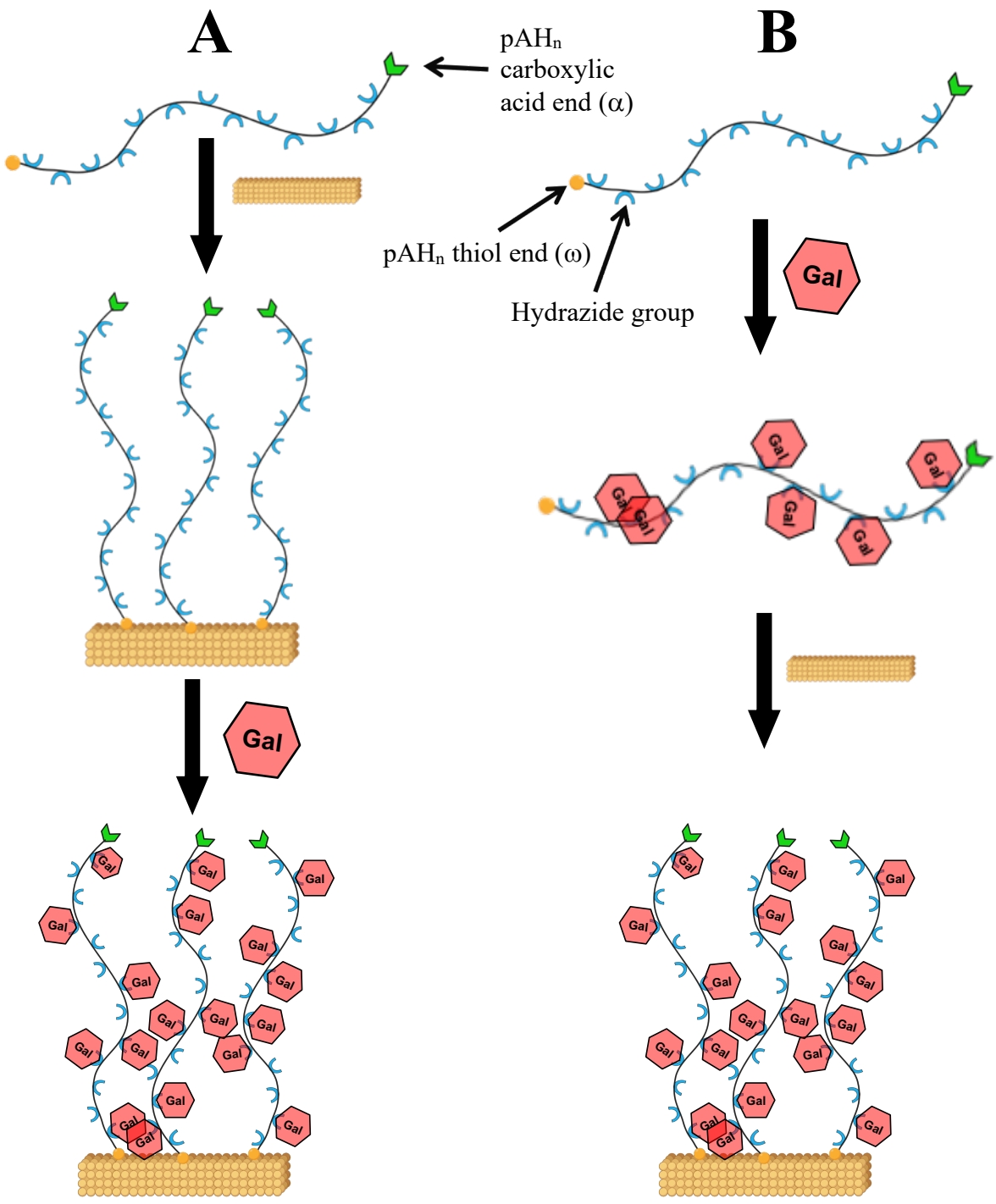
In this chapter, pAH_n **(Figure 6.3)** was synthesised as a chemical linker for the immobilisation of Gal on Au(poly). The presence of a thiol group on one of its ends, and the possibility of attaching Gal on this polymer through its hydrazide groups, made it a good candidate as a linker of the glycosensor. Modified electrodes (Au-pAH_n) were characterised with CV to determine the platform's potential window, stability, and feasibility.



33

Figure 6.3. General structure of poly(acryloyl) hydrazide polymers (pAH_n) used as chemical linkers for the immobilisation of Gal (BRE) onto Au(poly) electrodes. The pendant groups (blue) of the polymers are hydrazide groups that can be coupled to sugars; in green it appears the α end of the macromolecules, and in yellow the ω end, a thiol group that can adsorb the polymers on Au surfaces.

Next, two different strategies to immobilise Gal on a Au(poly) electrode through pAH_n were attempted: chemical coupling of Gal on the adsorbed pAH_n **(Scheme 6.3-A)**; and chemical linkage of pAH_n with the monosaccharide (pAH_n-Gal) followed by pAH_n-Gal immobilisation onto the electrode **(Scheme 6.3-B)**. Finally, pAH_n was linked to Lac and the ensuing hydrazones were reduced as a better, more stable way of attaching the Gal monosaccharide onto the Au transducer. CV was employed to determine the success of both electrode modifications.



Scheme 6.3. Two different strategies to immobilise sugars (*e.g.* Gal) on a Au(poly) electrode using pAH_n as a linker. **(A)** Adsorption of pAH_n on the electrode and then coupling with saccharides. **(B)** Linkage of pAH_n with saccharides followed by the adsorption of the glycosylated polymer on an electrode.

6.2 Results and Discussion

At this stage of the project, the main goal was still finding a stable linker to immobilise Gal on a Au electrode and establish the best way to detect CTB. After the difficulties encountered in **Chapter 5** using small molecule linkers, the synthesis of the macromolecule pAH_n was successfully achieved following the procedure described by Crisan *et al.*[472] **(Scheme 4.9)**. After the production and purification of the monomer *tert*-butyl-2-acryloylhydrazine-1-carboxyalte (**31**), RAFT polymerisation was performed using an in-house CTA, 2-((ethylthio)carbonothioyl)thio-2-methylpropanoic acid (**34**), to control the molecular weight of the macromolecules[605, 616, 617]. Finally, pAH_n was afforded by removing the Boc group from the pendant groups under acidic conditions.

Because CTB is not an electrochemically active species, the initial strategy was to use a redox mediator, a redox probe, to detect it **(Chapter 7)**. Fearing that the polymer adsorption could completely block the electrode surface, preventing any ET with the mediator, moderately long macromolecules of pAH_n with 20 pendant groups (pAH_{20}) were initially used for electrode modification.

6.2.1 Modification of Au(poly) Electrodes with Poly(acryloyl) Hydrazide

The first step was to assess with CV if pAH_{20} adsorbed on Au(poly) electrodes and its stability. **Figure 6.4** shows the characteristic electrochemical features of a clean (polished and flame-annealed) bare Au(poly) disk electrode in phosphate electrolyte (0.1 M, pH 7.4) during a first (solid green) and a second (solid black) CV sweep. The characteristic signals of the adsorption and desorption of the oxoanions of the

phosphate buffer were seen as a reversible process at between -0.30 and +0.05 V[618] (red keys); whilst the lifting of the reconstruction[619, 620] could be observed in the form of peaks in the forward sweeps, between +0.10 and +0.30 V (red arrow). During electrode flame-annealing, at high temperatures, the Au atoms move and arrange in determined packings to reach the most thermodynamically stable configuration. This order was lost (lifting) when high potentials were applied to the electrode and recovered (reconstruction) at low potentials. In the second scan, the lifting of the reconstruction peaks were smaller because the rearrangement of atoms achieved while applying negative potentials at the end of the first scan was not enough to match the high order achieved with flame-annealing. The onset of the hydrogen evolution reaction (HER) appeared at around -0.70 V (red star).

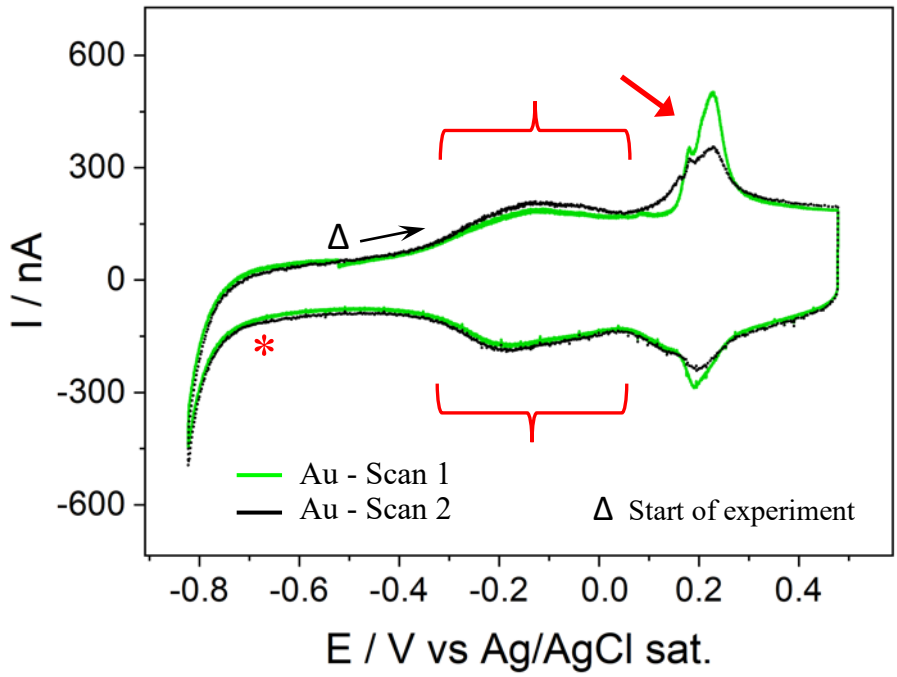


Figure 6.4. CV between -0.85 and +0.45 V on a clean bare Au(poly) electrode in a phosphate buffer solution (0.1 M, pH 7.4) at a 50 $mV \cdot s^{-1}$ scan rate. The sweeps were registered after polishing and flame-annealing the electrode. Scan 1 (solid green line) presented the reversible adsorption (forward) and desorption (backward) of phosphate anions at between -0.30 and +0.05 V; also, during the forward sweep, between +0.10 and +0.30 V, the intense peaks associated with the lifting of the reconstruction were observed. Scan 2 (solid black line) revealed weaker lifting of the reconstruction signals because, after the lifting of the flame-annealed surface in Scan 1, a less-well reconstructed Au(poly) surface was attained at lower potentials (between -0.40 and -0.80 V) at the end of Scan 1. (Δ) Start of the CV experiment.

Because of the composition and structure of pAH_n, it was expected that it would mainly adsorb on a Au electrode through the thiol end, changing scans' profile on bare Au(poly) surfaces. So for electrode modification **(section 4.2.3-D)**, the same procedure used with the small molecules of **Chapter 5** was employed. The concentration of the thiol group in the aqueous polymer solutions used was 20 mM (40 mg/mL of pAH_{20}).

According to CV, pAH_{20} adsorbed on the electrode because scans at high potentials **(Figure 6.5-A)**, between +0.45 and -0.30 V, showed the loss of the characteristic electrochemical features of a Au(poly) bare surfaced displayed in **Figure 6.4**. Besides, at lower potentials, down to -0.90 V, the characteristic reductive stripping of molecules adsorbed through Au-S bonds[203] was visible at approximately -0.70 V **(Figure 6.5-B)**.

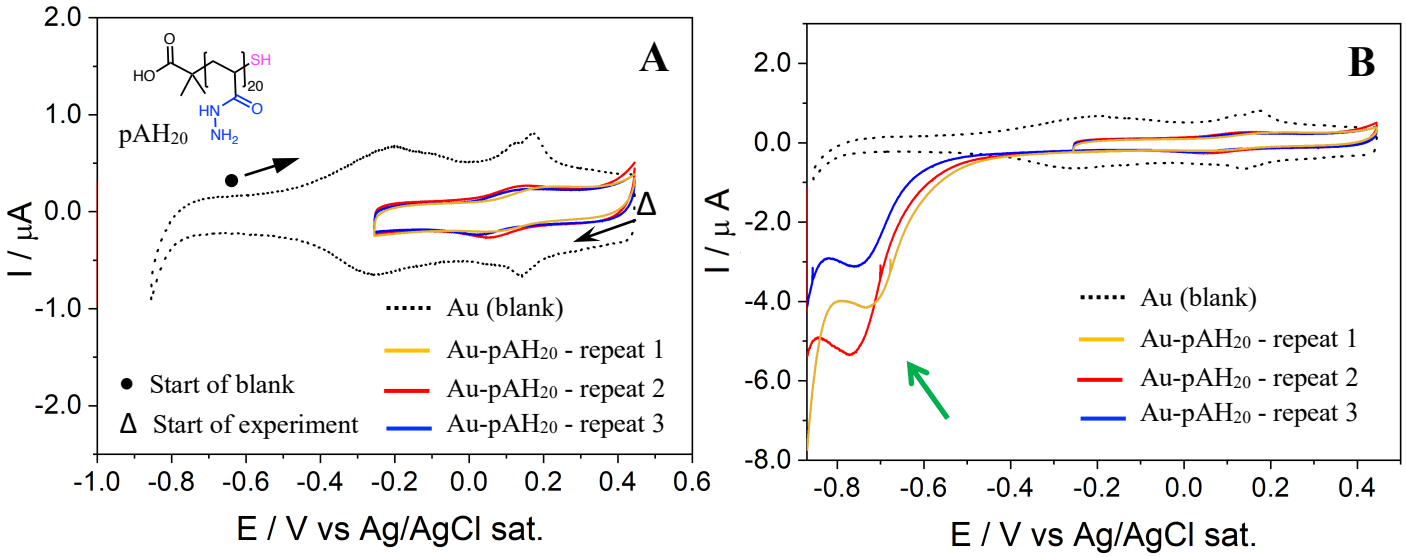


Figure 6.5. CV experiments in 0.1 M phosphate buffer electrolyte (pH 7.4) at a 50 $mV \cdot s^{-1}$ san rate to determine the adsorption and stability of pAH_{20} on a Au(poly) disk electrode. The black dotted line corresponds to a CV scan done on a clean bare electrode (blank); meanwhile, each of the 3 coloured, solid lines pertains to a CV repeat done on an electrode modified with the polymer (Au-pAH_{20}). In **Figure 6.5-A** are shown the scans at high potentials (between +0.45 and -0.30 V), whilst **Figure 6.5-B** displays the opening of the potential window of the scans (below -0.80 V) to observe the desorption of macromolecules (green arrow). (•) Beginning of the blank; (Δ) start of the CV scans carried out on functionalised electrodes.

The above experiments proved that the desorption of pAH_{20} macromolecules would start at not less than -0.40 V, so the system was stable in a wide potential range in physiological media and could be used for sensing CT. However, there were

significant differences between the 3 repeats regarding position and intensity of the reduction peak. They could be explained due to the inherent complexity of the system. On the one hand, the electrode employed was polycrystalline, meaning that its surface was made of different faces with different adsorption energies[621]. That also meant that grain boundaries could disturb the arrangement of macromolecules on each functionalisation. Besides, in between repeats, the Au(poly) disk was flame-annealed and cooled down to clean its surface. It is to be expected variations in the roughness and surface atom arrangements (*e.g.* adatoms and terraces) due to this process that, at atomic level, may prove determinant during polymer adsorption. Above all, pAH_{20} is a very complex species. As a synthetic polymer, it presents a dispersity in the size of its molecules[622]. Furthermore, although its macromolecules adsorbed through the thiol end, some interaction must be expected via the hydrazide pendant groups according to the results from the previous chapter **(Figure 5.8)**. Even though a higher reproducibility was desirable, the issue could be addressed in later stages of the development of the sensor; so the next step was to attach Gal onto the electrode via pAH_{20}.

6.2.2 Polymer Adsorption and Glycosylation

As shown earlier, two possible alternatives could be utilised to immobilise Gal on a Au(poly) electrode using pAH_n as a linker: the adsorption of pAH_n on the electrode followed by its chemical coupling with the sugar **(Scheme 6.3-A)**; or the coupling of pAH_n with the saccharide followed by their adsorption onto the electrode **(Scheme 6.3-B)**. Examples of modification of surfaces -including electrodes- through chemical reactions involving functional groups on those surfaces abound in the scientific

literature[502, 623-625]. In many instances, this procedure has been employed in polymeric surfaces or surfaces modified with polymers[626-628] . So after the adsorption of pAH_n on a Au(poly) electrode, the goal was to link its hydrazide groups to Gal; this reaction had already been successfully conducted in **Chapter 4** in homogeneous conditions. Therefore, a Au(poly) electrode modified with pAH_{20} (Au-pAH_{20}) was dipped in a 1.4 M buffered solution of Gal (acetate buffer 0.1 M, pH 5.6) for 24 h. at 60 ˚C to condensate polymer and monosaccharide. Afterwards, the electrode was abundantly rinsed with water and its surface was characterised with CV.

Displayed in **Figure 6.6-A** is the response obtained on the electrode at high potentials (between -0.30 and +0.40 V) before Gal coupling (solid blue line, Au-pAH_{20}). As expected for a modified Au surface, the reduction of the EDL and the loss of the characteristic profile of a bare electrode are observed. After glycosylation of Au-pAH_{20} with Gal (solid red line, Au-pAH_{20}-Gal) there was still an evident attenuation of the EDL and no sign of the lifting of the reconstruction, indicating that the polymer remained adsorbed after the 24 h. of the condensation reaction. Nevertheless, the outline differed with broad peaks in the forward (*ca.* 0.00 V) and backward (*ca.* +0.15 V) sweeps. Although this could indicate a successful linkage of Gal to the polymer, it could also be the result of adsorbed pAH_n macromolecules rearranging on the surface through time; for example, due to the reaction conditions used (acidic) or just because of the partial desorption of some of them. When scanning at more negative potentials (below -0.40 V), on Au-pAH_{20} and Au-pAH_{20}-Gal a reduction peak appeared at around -0.70 V **(Figure 6.6-B)**; this was the anticipated response if polymer molecules were adsorbed through the thiol group. Unlike at high potentials, both looked very similar in

terms of peak position and intensity, not allowing the confirmation of the sugar coupling.

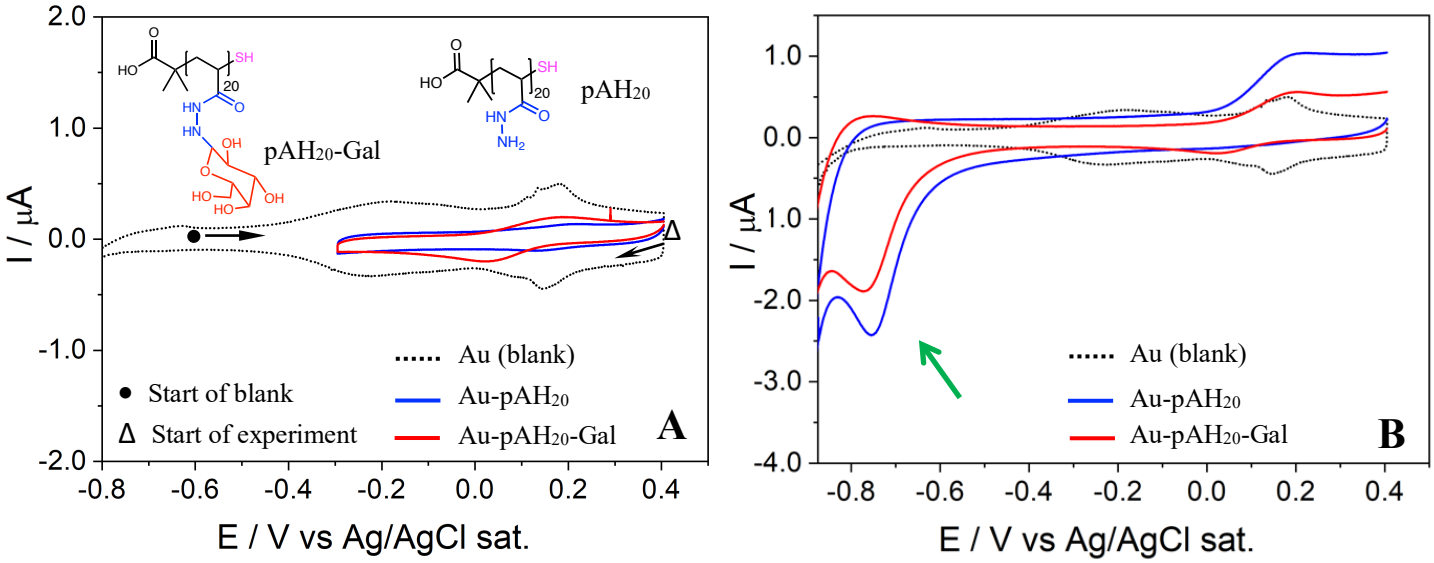


Figure 6.6. CV on a Au(poly) electrode modified with pAH_{20} (solid blue line, Au-pAH_{20}) or pAH_{20}-Gal (solid red line, Au-pAH_{20}-Gal); 0.1 M phosphate buffer electrolyte (pH 7.4) and 50 $mV{\cdot}s^{-1}$ scan rate. The black dotted line corresponds to a CV on a clean electrode previous modification (blank). **(A)** At high potentials (between -0.30 and +0.40 V), both functionalisations (Au-pAH_{20} and Au-pAH_{20}-Gal) produced a reduction of the EDL and the disappearance of the characteristic features of a clean Au(poly) electrode, confirmation of polymer adsorption. For Au-pAH_{20}-Gal, a quasi-reversible peak may prove the presence of Gal and, thus, the successful coupling of the sugar after 24 h. of reaction. **(B)** After opening the potential window below -0.40V, in both modifications, it appeared a stripping reduction peak at *ca.* -0.70 V (green arrow), characteristic of molecules adsorbed via a Au-S bond. No significant differences for the Au-pAH_{20} and Au-pAH_{20}-Gal peaks were observable in this potential range. (•) Start of the blank; (Δ) start of sweeps on functionalised electrodes.

CV demonstrated that pAH_{20} did not desorb under the glycosylation conditions. Nevertheless, the variations seen in CV after 24 h. of reaction, both at high and low potentials, did not permit to assure that Gal had been successfully coupled to pAH_{20}. Furthermore, it would be difficult to assess with this technique the percentage of sugar

linked. Given the difficulties in establishing the extent of modification of the electrode surface with Gal, an alternative functionalisation method was tried: the post-polymerisation glycosylation of pAH_n with Gal (pAH_n-Gal) followed by the adsorption of the resulting glycopolymer.

6.2.3 Post-polymerisation Glycosylation and Adsorption

Polymer glycosylation previous adsorption on an electrode has various advantages. First and foremost, it allows a much easier characterisation of the glycosylated pAH_n to determine saccharide loading. Studying surfaces at the micro or nanometric scale is, in most cases, a very complex task that often requires various techniques; so studying pAH_n-Gal once adsorbed would be very challenging. On the other hand, instead of pAH_{20}, a longer polymer with a DP of 50 (pAH_{50}) was chosen to optimise the use of the CTA, the RAFT agent. The preparation of very small macromolecules, like pAH_{20}, requires large quantities of RAFT agent **34**, a very toxic compound whose synthesis is very time-consuming. Longer polymers could also have advantages, like better anti-fouling properties and an increased number of Gal molecules attached to the electrodes to interact with CTB.

For coupling polymer and sugar **(section 4.1.3-F)**, 2.1 equivalents of Gal were employed (calculated with respect to the pendant groups of pAH_{50}) and the reaction was monitored with ^{1}H-NMR **(Figure 6.7)**. A few minutes after adding Gal to pAH_{50} (*ca.* 0 h, bottom spectrum) some features of the condensation product were already observed: a couple of peaks at around 7.50 ppm (purple star) related to hydrazone

formation; the reduction of the intensity of the α (yellow dot) and β (green dot) peaks (0.34 + 0.53 = 0.87), whose sum should have integrated for a total of 1 if there had been only free Gal; and the integration increase of the region of the rest of the sugary protons (light green hexagon, 6.11) that with only free monosaccharide should have integrated for 6. After 24 h. (top spectrum) the percentage of Gal linked to the polymer had increased with the anomeric signals of free Gal only integrating for 0.67 (0.25 + 0.42). From this intensity drop, a loading of *ca.* 66% was inferred (pAH_{50}-Gal_{33}). The hydrazone peak (purple star) appeared in duplicate, probably due to the presence of the E and Z hydrazones. The small doublet at around 7.30 ppm (grey dot) may have corresponded to a new hydrazone resulting from the hydrolysis of hydrazone groups of the glycosylated polymer, per the mechanism proposed by Crisan *et al*.[472].

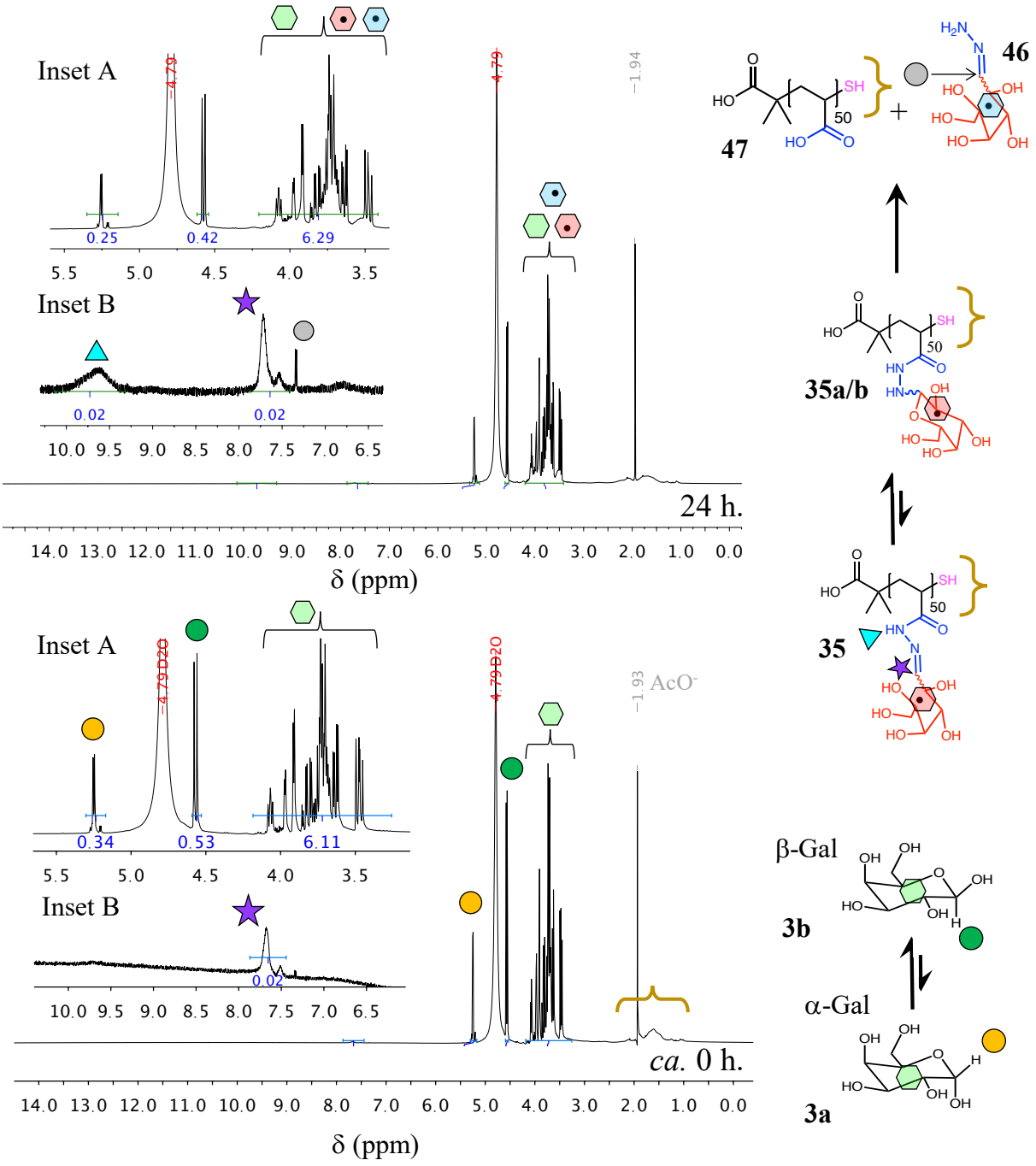


Figure 6.7. ^{1}H-NMR spectra (400 MHz, D_2O) of the crude of the reaction between pAH_{50} and Gal (polymer hydrazide group/Gal, 1:2.1) after *ca.* 0 h. (bottom) and 24 h. (top). Due to Gal coupling to pAH_{50}, there was a reduction of the integration of the free-Gal anomeric proton peaks (yellow and green dots) over time which signaled a sugar loading of approximately 66% (pAH_{50}-Gal_{33}) after 24 h. The most relevant parts of the spectra for analysis are amplified in the insets.

The standard method for the purification of glycosylated pAH_n is dialysis in water. However, the bond between Gal and pAH_n, a hydrazone bond, is prone to hydrolysis as the pH increases[629]. Although hydrazones are relatively stable at physiological pH, to avoid any risk of losing part of the saccharide loaded onto the macromolecules, no purification was done. Therefore, the crude product containing pAH_{50}-Gal_{33} and an excess of Gal was directly used to modify a Au(poly) electrode with dips of 30 min. at room temperature.

In **(Figure 6.8),** CV was employed to characterise the electrode functionalised with the glycosylated polymer (Au-pAH_{50}-Gal_{33}) and compare its response when modified with just the polymer (Au-pAH_{50}). At potentials between +0.45 and -0.15 V **(Figure 6.8-A)**, the CV signals of both systems looked the same: reduction of the EDL and the absence of the lifting of the reconstruction features at *ca.* +0.15 V. This was a clear indication of the blockage of the surface by polymeric molecules. However, when the potential window was opened and the scans were run between +0.45 and -0.9 V **(Figure 6.8-B)**, the reductive stripping was significantly different. In Au-pAH_{50} (solid blue line) a single, very intense (near -2 μA) peak was registered at about -0.70 V (blue arrow). Instead, 2 broad peaks were recorded in Au-pAH_{50}-Gal_{33} (solid red line): one at -0.45 V (red arrow) and the other, less well defined, at -0.70 V (purple arrow). The first peak may have been related to the desorption of less well-arranged pAH_{50}-Gal_{33} molecules on the surface, perhaps caused by the presence of the big Gal molecule in many of their pendant groups; or to the desorption of other functional groups other than the polymers' thiol end. The second process, at -0.70 V, had to be associated with the Au-S bond reduction.

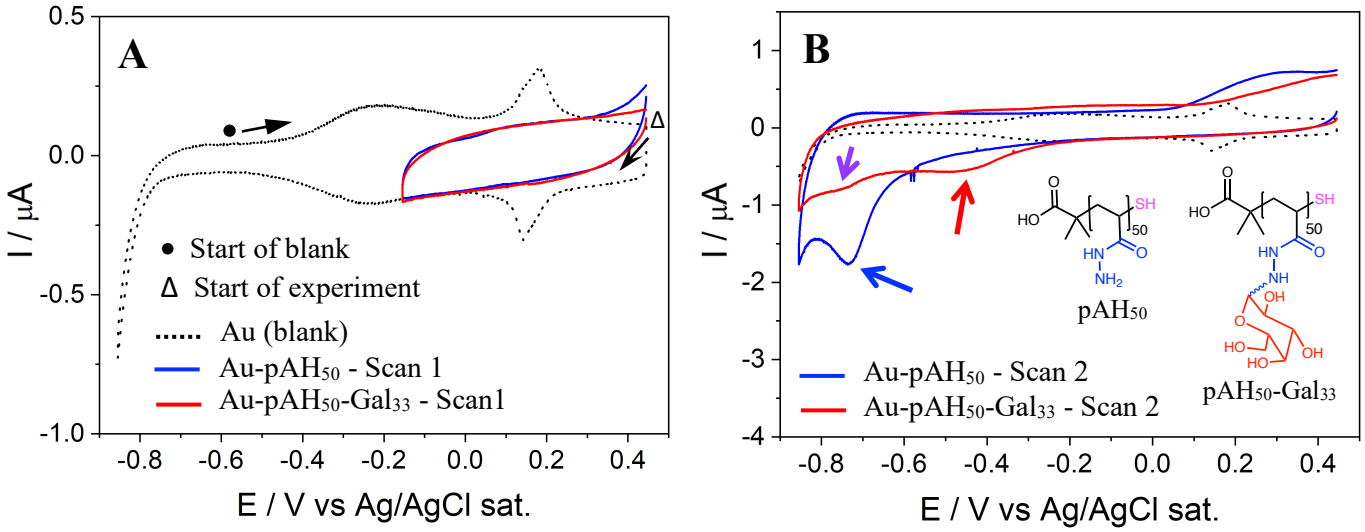


Figure 6.8. CV scans on Au-pAH_{50} (solid blue line) and Au-pAH_{50}-Gal_{33} (solid red line) in phosphate buffer electrolyte (pH 7.4) at a 50 $mV \cdot s^{-1}$ scan rate. **(A)** CV sweeps looked very similar at high potentials (between +0.45 V and -0.15 V) in both modified surfaces. **(B)** At lower potentials (from +0.45 to -0.90 V), Au-pAH_{50} produced a single, prominent stripping reduction peak (-0.73 V, blue arrow) due to the Au-S bond reduction; whilst Au-pAH_{50}-Gal_{33} presented two peaks: a broad peak at -0.45 V (red arrow), probably from the desorption of less-stable adsorbed glycosylated polymers; and also an almost imperceptible peak at around -0.73 V (purple arrow). (•) Beginning of the blank; (Δ) beginning of experiments on modified electrodes.

As mentioned, the origin of the reduction event at -0.45 V on Au-pAH_{50}-Gal_{33} could have been associated with chemical groups -other than the thiol group- adsorbed on Au(poly): *i.e.* Gal from the pendant groups of pAH_{50}-Gal_{33} or its free hydrazide groups. Although **Figure 5.8** showed that hydrazides could adsorb on Au, there was no clear evidence of their desorption from Au-pAH_{50} (blue scan of **Figure 6.8-B**). Therefore, hydrazides were rejected as the cause of the -0.45 V peak. When a clean Au(poly) electrode was modified for 30 min. at room temperature. in a Gal solution equivalent to that used for polymer glycosylation (1.4 M Gal in 0.1 M acetate buffer, pH 5.4), CV scans between +0.45 and -0.25 V **(Figure 6.9-A)** registered a drastic

reduction of the EDL (solid orange curve). The same submersion in 0.1 M acetate buffer (pH 5.4) also produced a narrowing of the EDL (solid blue line), although more attenuated. This was proof of the adsorption of both Gal and acetate anion on Au(poly), despite the latter inducing a less significant blockage of the surface. In the sweeps at more negative potentials (from +0.45 to -0.90 V) displayed in **Figure 6.9-B**, a slight reductive stripping peak (orange arrow) was detected at -0.65 V after incubation in the Gal dissolution; contrarywise, this feature did not appear when the dissolution used to modify the electrode only contained the acetate anion (solid blue curve). This outcome suggested that glycosylated polymers may also adsorbed to some extent through their functionalised pendant groups; and that this circumstance could result in less well-arranged layers of macromolecules on the surface and a lower stripping energy (-0.45 V), as observed in **Figure 6.8-B** (red arrow).

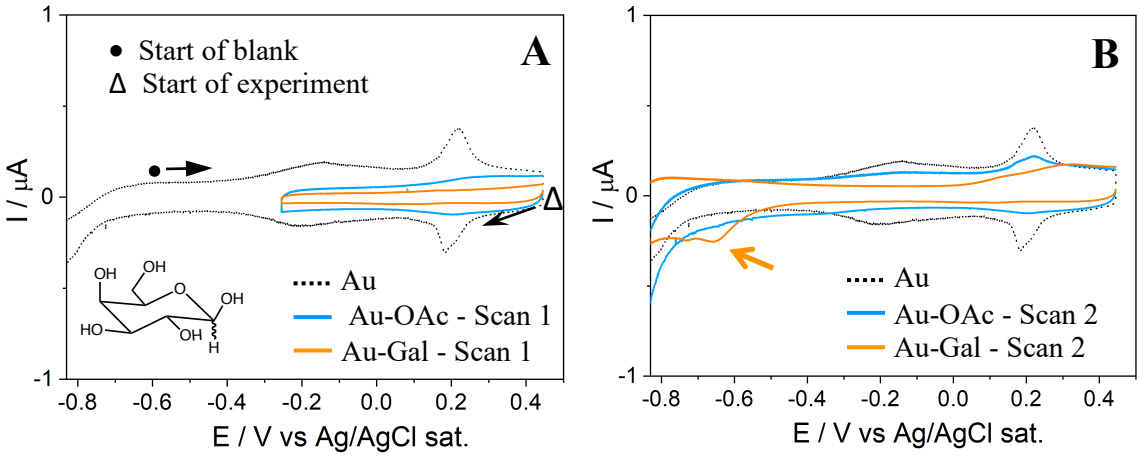


Figure 6.9. CV scans on a Au(poly) electrode after immersion for 30 min at 60 ˚C in either a 1.4 M Gal dissolution prepared in acetate buffer 0.1 M, pH 5.4 (solid orange curves); or only in the buffer (solid blue curves). **(A)** Scans between +0.45 and -0.25 V displayed a narrowing of the DLR, which was more acute when the solution contained Gal. **(B)** In scans reaching more negative potentials (from +0.45 to below -0.80 V), a peak at *ca.* -0.65 V (orange arrow) was observed only when the electrode was modified in the Gal-containing dissolution. (•) Start of the blank sweep; (Δ) start of CVs on a modified Au(poly) electrode. All experiments were carried out in phosphate buffer electrolyte (pH 7.4) with a 50 $mV \cdot s^{-1}$ scan rate.

To further explore interactions between pendant groups of pAH_{50}-Gal and the electrode, pAH_{50} was glycosylated with only 0.2 equivalents of Gal **(section 4.1.3-F)**, instead of the 2.1 employed for the synthesis of the pAH_{50}-Gal_{33} used in **Figure 6.8**. To determine the degree of condensation of this reaction, the integrals of the ^{1}H-NMR signals of the monosaccharide **(Figure 6.10)** -green hexagon, yellow dot, green dot, and purple star- were assigned a total value of 7. At *ca.* 0 h. (bottom spectrum in **Figure 6.10**) most Gal remained still unreacted and free, so the integration of the α (yellow dot) and β (green dot) peaks stood close to 1 (0.41 + 0.45 = 0.86) as they pertained to the anomeric proton. However, after 24 h. (top spectrum in **Figure 6.10**), the 2 peaks were integrated only by 0.22 (0.08 + 0.14). Therefore, it was estimated that only 22% of the monosaccharide in the crude remained free and the rest (78%) was loaded onto the polymer. The broadening of the peaks after 24 h. in the range between 3.00 and 4.50 ppm (inset A), where the rest of the saccharide protons resonate, was further proof of the condensation. In polymers, the repetition of functional groups in the same molecule leads to a spatial closeness equivalent of a high concentration, producing broad NMR signals. In this part of the spectra, this effect was evident after 24 h. when compared to the sharp peaks at *ca.* 0 h. A tiny signal at about 7.60 ppm (inset B, purple star) pertained to the hydrazone, the open form resulting from the coupling of Gal and hydrazide pendant groups of pAH_{50}. As already mentioned in this thesis, its duplicity (there is also a tiny peak at *ca.* 7.55 ppm) was interpreted as the presence of the E (more prominent signal) and Z isomers. Due to the number of equivalents of Gal used (0.2), the 78% sugar conversion meant a polymer loading of approximately 16% (pAH_{50}-Gal_8), considering that with 0.2 equivalents of monosaccharide a maximum of 20% could have been achieved.

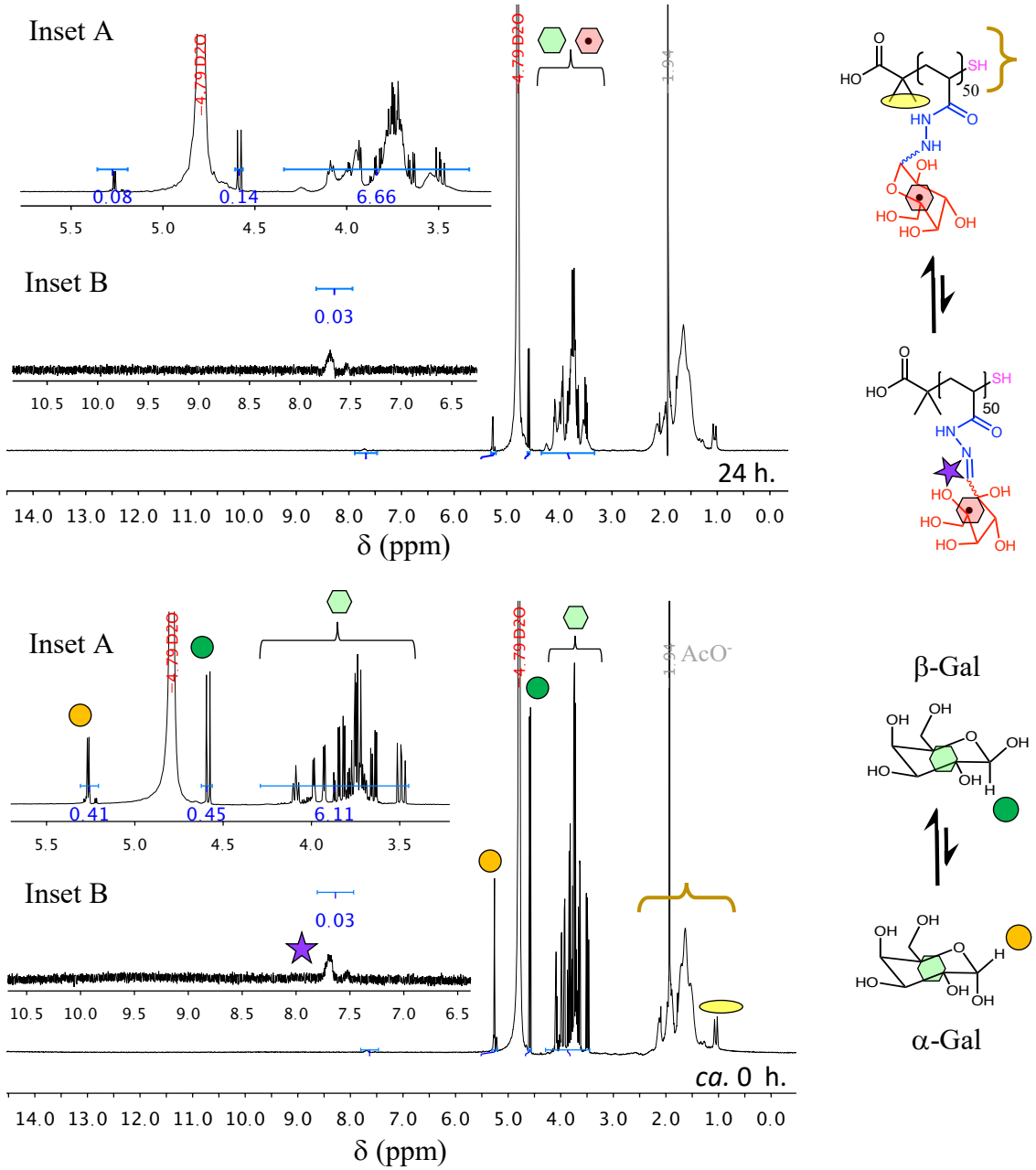


Figure 6.10. ^{1}H-NMR spectra (400 MHz, D_2O) of the reaction crude of the condensation between pAH_{50} and Gal (polymer hydrazide group/Gal, 1:0.2) after *ca.* 0 h. (bottom) and 24 h. (top). After 24 h., a substantial part (78%) of the integration of the anomeric proton of free Gal (α plus β peaks, yellow and green dots) had disappeared because of the coupling with the polymer, indicating an approximate loading of 16% (pAH_{50}-Gal_8). The broadening of the other sugar peaks (between 3.00 and 4.50 ppm) confirmed the condensation. Insets are amplifications of the most relevant parts of the spectra.

A Au(poly) electrode was modified with pAH_{50}-Gal_8 (16% Gal loading) by immersing it in the crude product (**Figure 6.10**, top spectrum) for 30 min. at room temperature. Then, CV was used to characterise its surface **(Figure 6.11)**. At high potentials **(Figure 6.11-A)**, from +0.45 to -0.15 V, the electrochemical response from Au-pAH_{50} and Au-pAH_{50}-Gal_8 was almost identical and demonstrated the adsorption of the polymers: EDL narrowing and disappearance of the lifting of the reconstruction peaks. When the potential window was opened till -0.85 V **(Figure 6.11-B)**, the desorption of macromolecules from Au-pAH_{50}-Gal_8 (pink arrow) had an onset at about -0.25 V (pink star), earlier than the desorption from Au-pAH_{50} (blue arrow) that commenced at *ca.* -0.60 V (blue star). This result coincided with that in **Figure 6.8**, possibly indicating that polymers carrying saccharides adsorb weaklier since they detached at lower energies, lower applied potentials. Also, as in **Figure 6.8**, the reductive peak from the glycosylated polymer (Au-pAH_{50}-Gal_{33}) at around -0.70 V (magenta arrow) was smaller and less well-defined than the one from the non-modified polymer (Au-pAH_{50}, blue arrow). It probably meant that the previous broad peak at *ca.* -0.45 V (pink arrow), not present in the desorption from Au-pAH_{50}, was caused by the early desorption of pAH_{50}-Gal_{33} macromolecules with a weaker attachment to the Au surface than pAH_{50}. Although SAMs formation critically depends on the interaction between a surface and the head group of molecules, much of their stability relies upon weak interactions between the molecules' backbone. Therefore, it is possible that the incorporation of bulky Gal molecules to pAH_{50} disturbed the chain-to-chain forces between macromolecules, driving the system towards a less stable state.

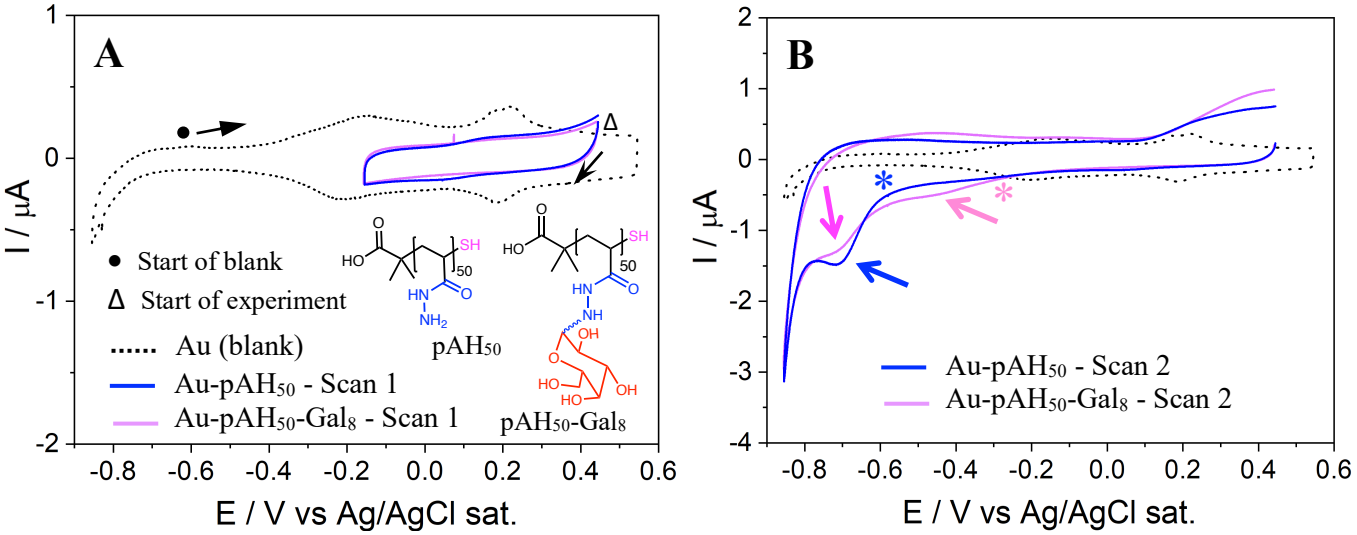


Figure 6.11. CV study of a Au(poly) electrode modified with pAH_{50} (Au-pAH_{50}, solid blue scan) or glycosylated pAH_{50} (Au-pAH_{50}-Gal_{33}, solid pink scan). **(A)** At high potentials (between +0.45 and -0.15 V) the adsorption of polymer and glycopolymer produced very similar electrochemical responses: reduction of the EDL and disappearance of the lifting of the reconstruction signals. **(B)** In sweeps till lower potentials (from +0.45 to -0.85 V), both modifications presented an intense reductive stripping peak at *ca.* -0.70 V (magenta and blue arrows). Nevertheless, the CV on Au-pAH_{50}-Gal_{33} also registered a broad peak at around -0.45 V (pink arrow). (•) Start of the scan on the bare electrode; (Δ) start of sweeps on the modified electrode. The experiments were conducted in phosphate buffer electrolyte (pH 7.4) with a 50 $mV \cdot s^{-1}$ scan rate.

The previously presented CV experiments confirmed that Gal molecules, the BRE of the glycosensor, had been immobilised on the transducer. Besides, they were stable in a potential range where electrochemical detection of CT could be possible. However, questions arose about the robustness of the bond between Gal and pAH_n, as the hydrazone bond is a reversible one. These misgivings led to an electrode modification with non-purified glycopolymers, using the condensation reaction's crude product. Therefore, various factors could have negatively affected the process

of macromolecule adsorption, like the acidic pH of the crude, the non-reacted molecules of Gal or the presence of acetate anions.

Seeking to work with a more robust platform to immobilise Gal on Au electrodes, the coupling of pAH_n with Lac was considered. The decision was also driven by an upcoming overseas research visit that required the transport of glycosylated polymers.

6.2.4 Post-polymerisation Glycosylation with Lactose

The main advantage of coupling pAH_n and Lac, instead of Gal, is the possibility of reducing the resulting hydrazone bond to make it irreversible and more stable **(Scheme 6.2-B)**. Because the disaccharide reacts with the hydrazide of the polymer through its Gal moiety, the cyclic conformation of Gal remains intact at all times, ready to bind CTB. Another potential gain is the presence of a longer spacer between Gal and the polymer's backbone, giving the sugar more room to recognise CTB. The most significant disadvantage would be extending the synthesis one step -reduction of the hydrazone bond- and introducing a purification stage, augmenting the chemicals and time spent.

A. Coupling of Acetohydrazide with Lactose

The synthesis of pAH_n is quite costly in terms of laboratory time. Therefore, before synthesising pAH_n-Lac, a chemical equivalent of the pAH_n pendant group, AcHD, was used to test the best reaction conditions to couple it with Lac and the optimal chemical

agent to reduce the hydrazone bond formed. Because the condensation of pAH_n with Lac is very similar to that with Gal, the same reaction conditions were used as starting point: acetate buffer (0.1 M, pH 5.4), 2.1 equivalents of the sugar (with respect to hydrazide pendant groups) and room temperature. The use of D_2O to prepare the buffer allowed an easy follow-up of the reaction with ^{1}H-NMR **(Figure 6.12)**. Like in previous coupling reactions of this chapter, variations of intensity of the anomeric proton (α and β peaks, yellow and green dots) permitted to estimate at 42% the disappearance of free Lac from the reaction medium after 7 days (1 – 0.26 – 0.46 = 0.28). Hence, around 56% of the AcHD had been converted (AcHD/Lac, 1:2.1). Right at the start of the reaction (*ca.* 0 h., bottom spectrum), at about 7.50 ppm (orange star), already appeared a duplicated doublet associated with the open Z and E isomers of the Lac hydrazone. The same feature was observed in this chapter when Gal was linked to the hydrazides of pAH_n **(*e.g.* Figure 6.7, purple star)**. Further downfield and after 7 days. (top spectrum), a new little duplicated peak emerged at 9.50 ppm (magenta and violet triangles), identified as the proton on the N atom of the open hydrazone (E and Z isomers). As per why it was not observable at the start of the reaction (*ca.* 0 h) like the two doublets at around 7.60 ppm (orange star), it may have to do with the complexity of this type of proton that can exchange with the solvent. At 4.44 ppm (light blue dot, bottom spectrum, Inset C) resonated the proton of the acetal carbon of free Lac (a doublet); after 7 days, practically at the same position, appeared another doublet (dark blue spot) corresponding to the same proton of Lac but when the sugar was linked to AcHD. The best evidence of the successful condensation, though, was the emergence after 7 days of a new doublet at *ca.* 4.10 ppm (violet dot). According to its chemical shift and coupling constant (J = 9.1 Hz) it related to the proton

of the anomeric carbon of the product in axial position (β product, β-AcHD-Lac). There is no evidence of an equivalent peak for the α product, which should appear further down the lower-field according to the relative positions of the $^{\alpha}$H and $^{\beta}$H signals in free Lac. In principle, this would indicate the formation of only one product and the absence of an anomeric effect. Nevertheless, the doublet from α-AcHD-Lac could had been overlapped by the broad D_2O peak at 4.79 ppm. This circumstance was not studied using a different solvent, like DMSO-d_6, because it was not essential for the project, since the product had to be reduced. Finally, the decrease over time of the signal of the acetyl group (bottom Inset A, brown dot, 1.92 ppm) and the appearance of a new one at 1.96 ppm after 7 days (top Inset A, chequered, brown dot) further confirmed the linkage between AcHD and Lac.

After 24 h. of reaction, ^{1}H-NMR had already shown a *ca.* 50% yield. This percentage was considered enough to test the reduction of the hydrazone bond in AcHD-Lac. Therefore, to save time, a crude of the condensation reaction after 24 h. was employed for this investigation.

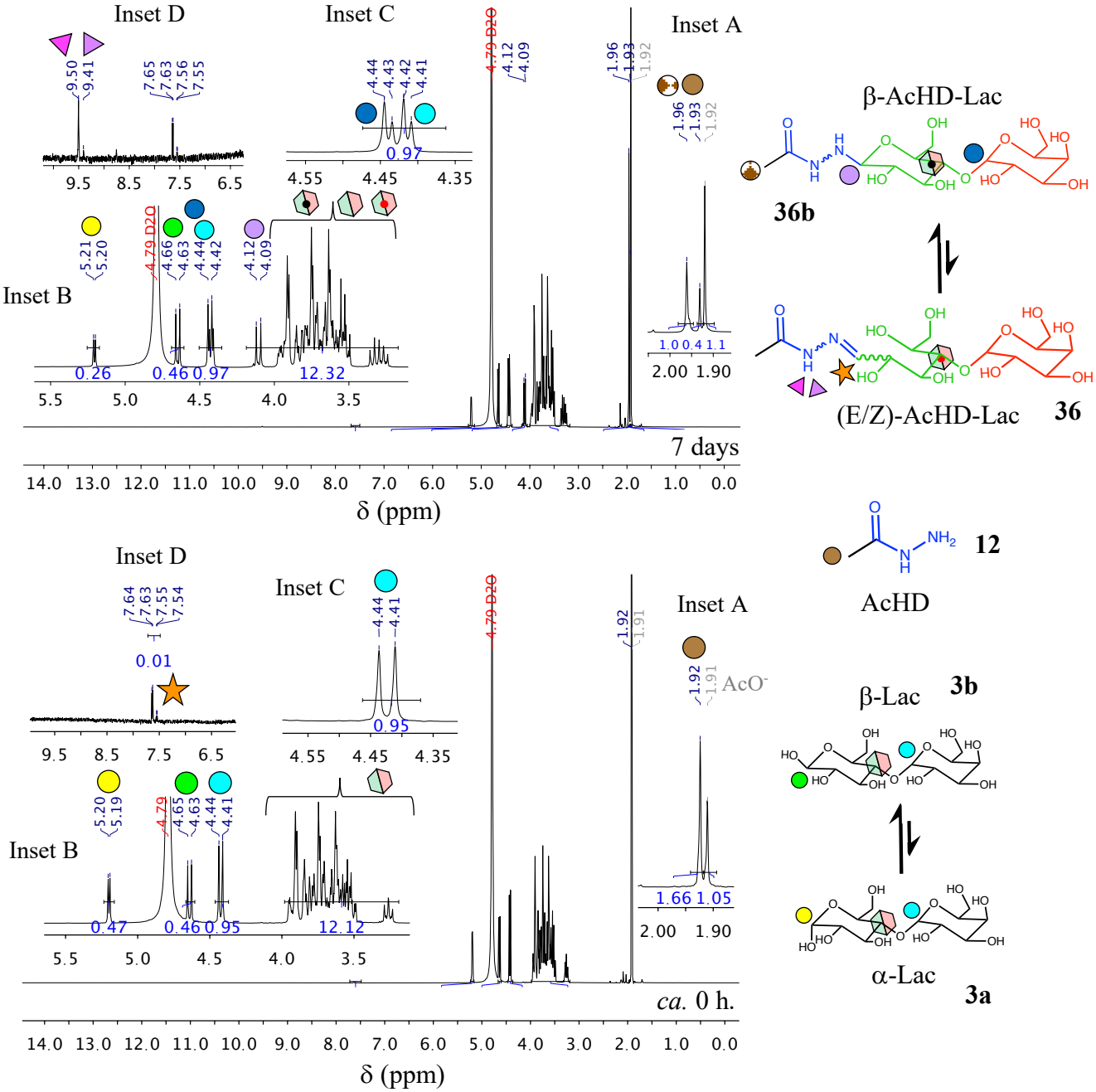


Figure 6.12. ^{1}H-NMR spectra (400 MHz, D_2O) of the reaction crude for linking AcHD and Lac (AcHD/Lac, 1:2.1) after *ca.* 0 h. (bottom) and 7 days. (top). The emergence of new signals, for example, at *ca.* 7.60 ppm (orange star) and 4.10 ppm (violet dot), confirmed the successful linkage of the two species. The integration decrease of the $^{\alpha}$H and $^{\beta}$H peaks (yellow and green dots) of free Lac allowed estimating a yield of 56%. Integrals were calculated assigning a value of 14 (Lac contains 14 protons) to the Lac signals (insets B and D).

B. Reduction of Hydrazones of Lactose into a Galactose-containing Acetohydrazide

The next step was to determine the best reducing agent for the hydrazone bond. Three reagents available in the laboratory were considered as candidates: $NaBH_4$, $PyBH_3$ and $NaBH_3CN$. The three species were added to the crude product of the coupling between AcHD and Lac under the conditions specified in **section 4.1.3-G**; ^{1}H-NMR was used to assess their effectiveness. In the case of $NaHB_4$, the addition produced foam, an indication of a vigorous reaction. The spectra in **Figure 6.13** showed that the most characteristic signals of the unreacted Lac, the anomeric proton (yellow and green dots, inset), had disappeared entirely after 3 h., confirming the reduction of the disaccharide into an alcohol, lactitol. Fearing these conditions were too harsh and could also break up the hydrazone bond or negatively affect the glycosylated polymers, this reducer was ruled out.

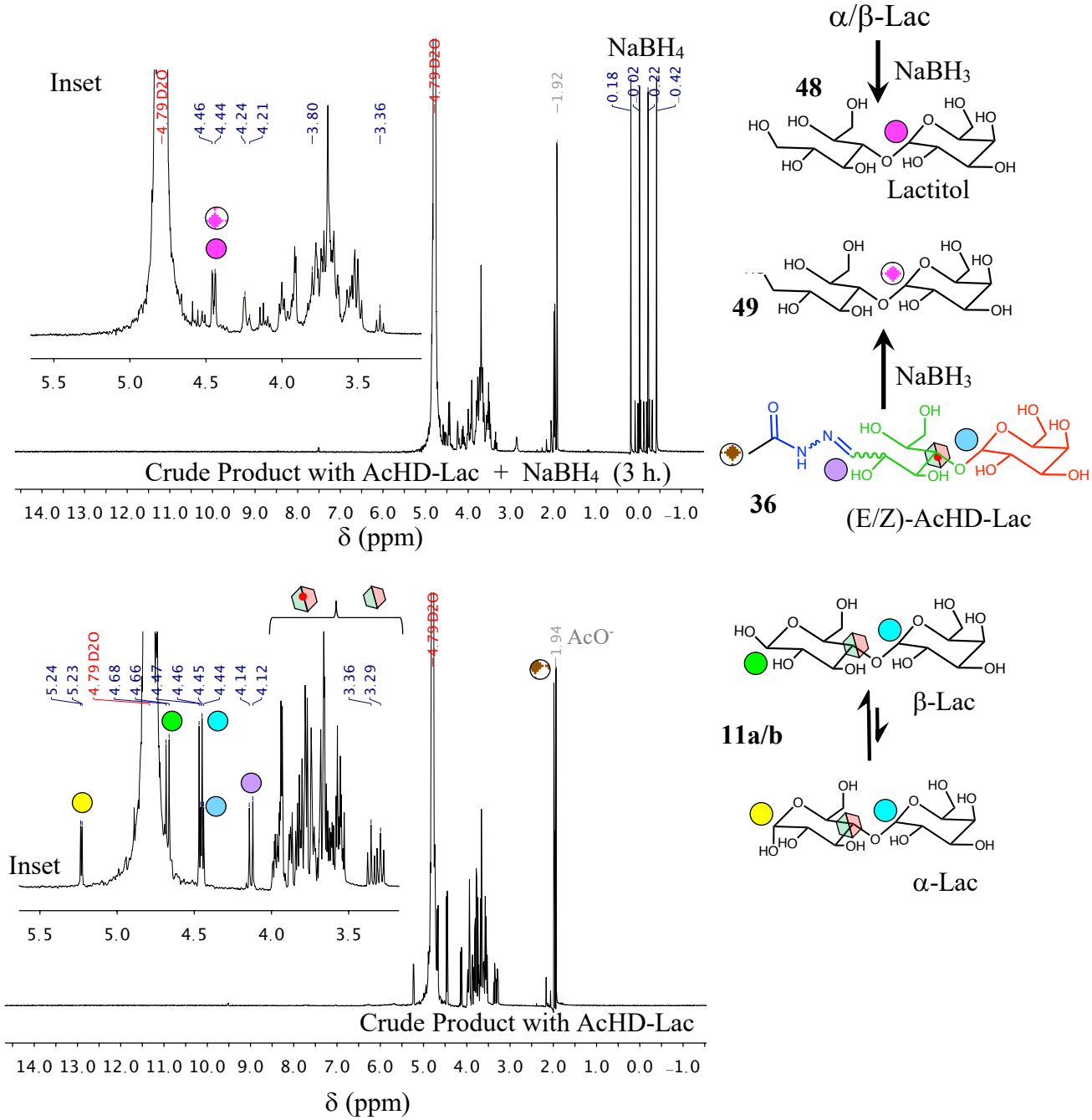


Figure 6.13. ^{1}H-NMR spectra (400 MHz, D_2O) of the reduction of lactose hydrazone of acetohydrazide (AcHD-Lac, **36**) with $NaBH_4$. At the bottom, the spectrum of the crude product of the condensation between AcHD and Lac. On top, the same crude after 3 h. of adding the reducer $NaBH_4$: the $^{\alpha}$H and $^{\beta}$H peaks (yellow and green dots) of free Lac completely disappeared after the disaccharide had converted into an alcohol (**48**).

When $PyBH_3$ complex was used **(Figure 6.14)**, the ^{1}H-NMR peaks attributed to the condensation product AcHD-Lac lost intensity after 4 h. For instance, the anomeric proton in axial orientation (Inset A, violet dot, 4.13 ppm), the protons on the N (Inset B, magenta triangle, 9.51 ppm), the hydrogen of the hydrazone bond (Inset B, orange star, *ca.* 7.72 ppm) and the proton marked with a stripped violet dot (Inset A, 3.35 ppm). The attenuation of the anomeric proton signal at 4.13 ppm is explained because, after the reduction of the hydrazone bond, the Glc moiety of Lac lost the possibility of closing up **(Scheme 6.2-B)** and the two cyclic isomers disappeared. Since the integrated intensity of the anomeric proton of β-AcHD-Lac fell *ca.* 50% (from 0.30 to 0.16) the reduction efficiency with $PyBH_3$ could be estimated at 50%. Contrary to when $NaBH_4$ was employed, the signals of non-reacted Lac still present in the crude product (*e.g.* yellow and green dots) did not change, suggesting a much less vigorous process. Further tests proved that the reaction was very fast, almost instantaneous, and that the yield remained the same when a higher pH (a smaller volume of HCl) was used.

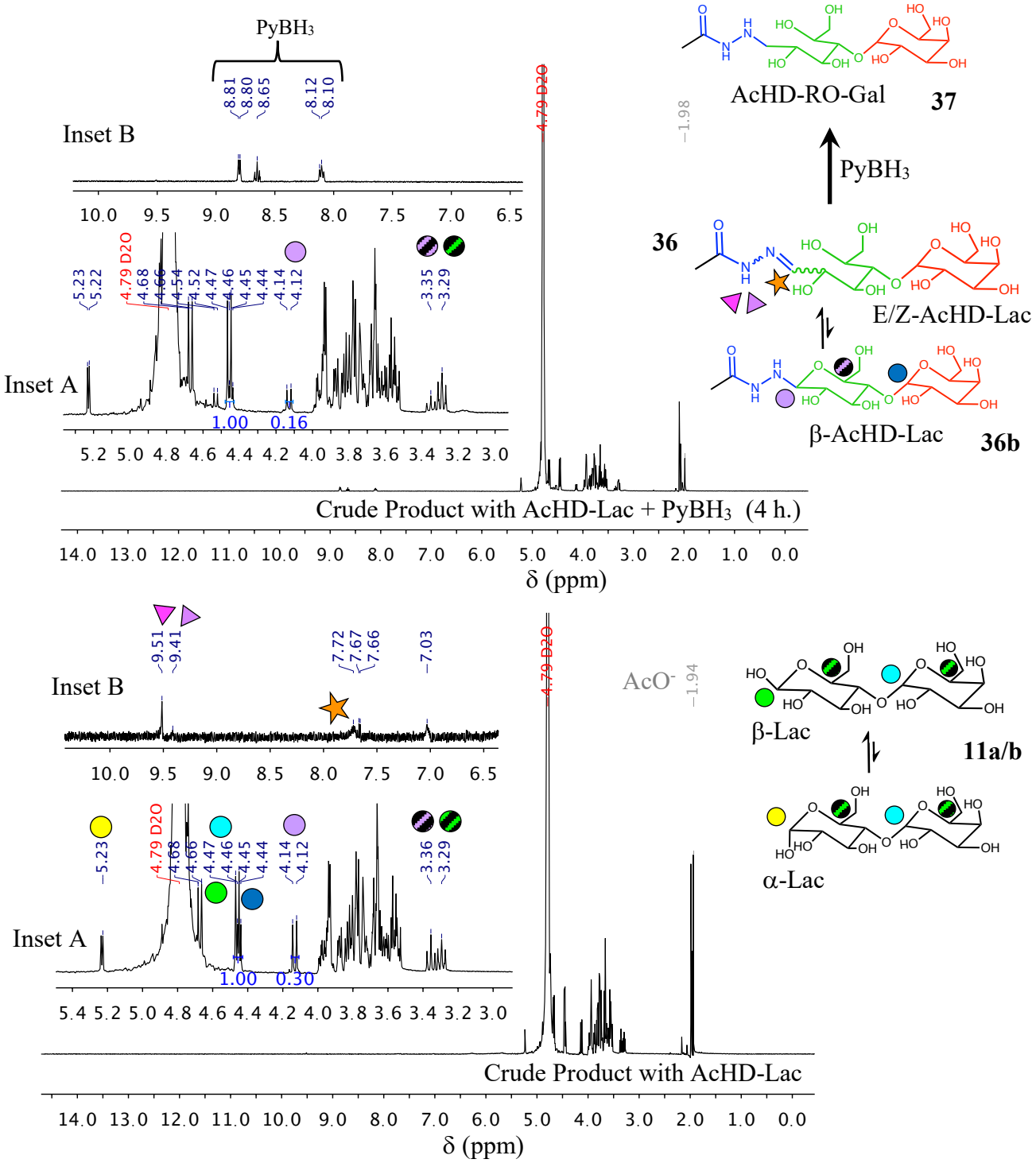


Figure 6.14. ^{1}H-NMR spectra (400 MHz, D_2O) to monitor the reduction of AcHD-Lac with $PyBH_3$. At the bottom, spectrum of the crude product used as starting material containing AcHD-Lac and free Lac. On top, the same crude after 4 h. of having added $PyBH_3$: resonance signals correspondent to AcHD-Lac either lost intensity (violet dot, stripped violet dot) or disappeared (orange star, magenta triangle) as a result of the reduction of the hydrazone bond.

$Na(CN)BH_3$ was also employed to reduce AcHD-Lac **(Figure 6.15)**. However, in this case, nuclear magnetic resonance seemed to indicate that no reaction occurred, with some of the characteristic peaks of AcHD-Lac mostly unchanged after 3 h.: anomeric proton at 4.12 ppm (violet dot), proton at 3.36 ppm (stripped violet dot). Therefore, after these results, $PyBH_3$ was considered the best of the 3 options to reduce the hydrazones formed from coupling Lac and pAH_n.

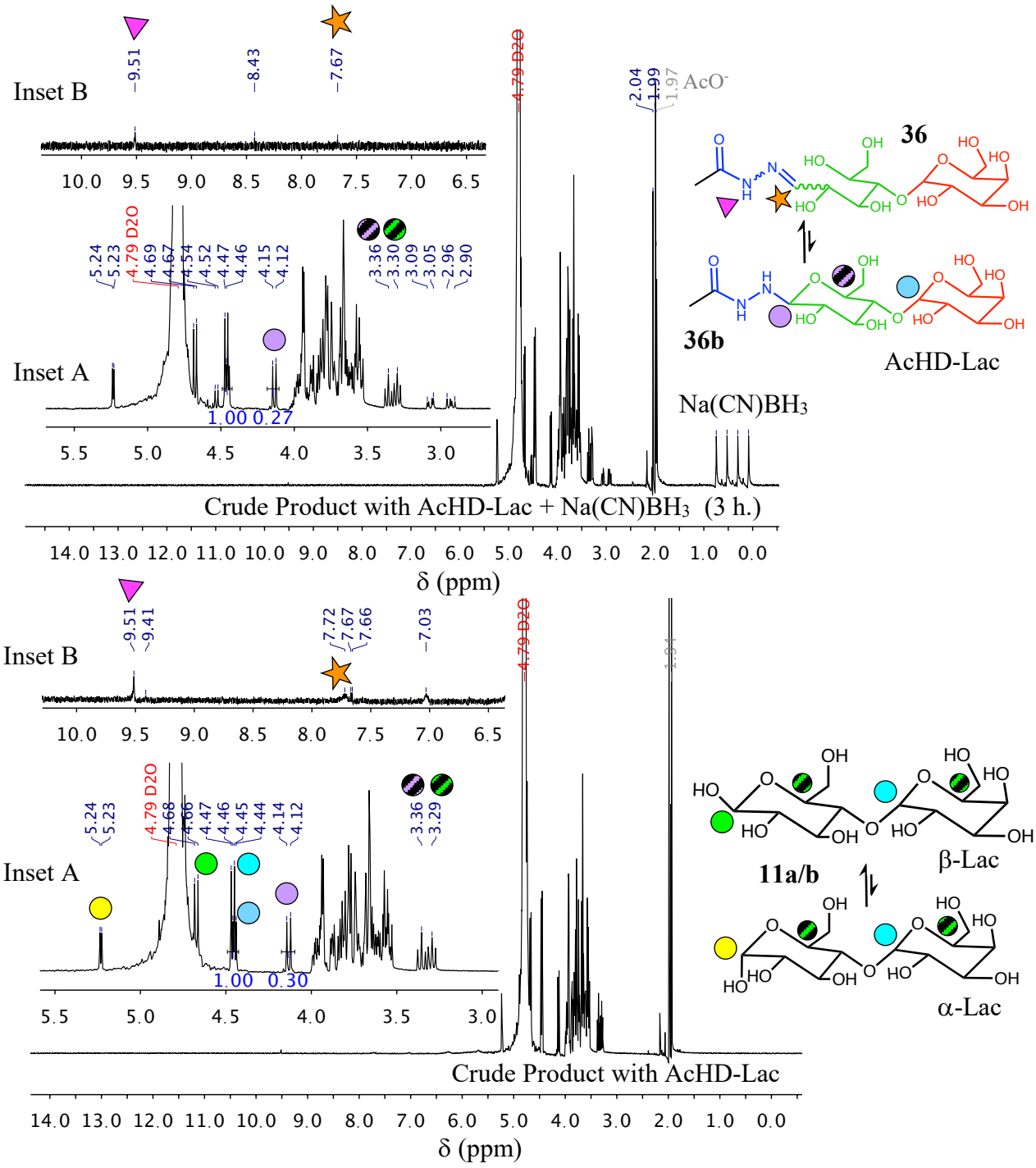


Figure 6.15. ^{1}H-NMR spectra (400 MHz, D_2O) of the reaction to reduce AcHD-Lac with $Na(CN)BH_3$. The spectrum at the bottom corresponds to the crude product of AcHD-Lac (starting material) with also free Lac before adding the borane. On top, the same crude 3 h. after $Na(CN)BH_3$ was added. The small or null drop of the intensity of the characteristic peaks of AcHD-Lac after adding $Na(CN)BH_3$, *e.g.* anomeric proton at 4.14 ppm (Inset A, violet dot, 4.13 ppm), suggests minimal or no reduction of AcHD-Lac.

C. Glycosylation of Poly(acryloyl) Hydrazide with Lactose and Reduction

pAH_{50} was glycosylated with 2.1 equivalents of Lac (calculated over the total number of pendant groups) in acetate buffer (0.1 M, pH 5.4) at room temperature for 24 h., as explained in **section 4.1.3-H**. The presence of broad peaks -characteristic of the resonance of polymers- in the saccharide region of the ^{1}H-NMR spectrum **(top of Figure 6.16, Inset B)** confirmed the incorporation of the disaccharide into the polymer. The signals of the anomeric carbon of free Lac ($^{\alpha}$H yellow dot and $^{\beta}$H green dot) were integrated (0.30 + 0.56) after 24 h., demonstrating a reduction of the quantity of free sugar in the medium of reaction of *ca.* 14% (1 – 0.30 – 0.56). Since 2.1 equivalents of Lac were used for this synthesis, approximately 30% of the hydrazide pendant groups of pAH_{50} were loaded with the saccharide (pAH_{50}-Lac_{15}). The 30% binding, smaller than that afforded with AcHD after 24 h. (56%), could be explained by some steric hindrance caused by the backbone of the macromolecules and other pendant groups nearby. After 24 h., no further loading was detected. As expected, in the reaction control containing only Lac **(bottom of Figure 6.16)**, the sum of the integrations of $^{\alpha}$H and $^{\beta}$H signals after 24 h. was *ca.* 1 (0.37 + 0.59) because there was no reaction.

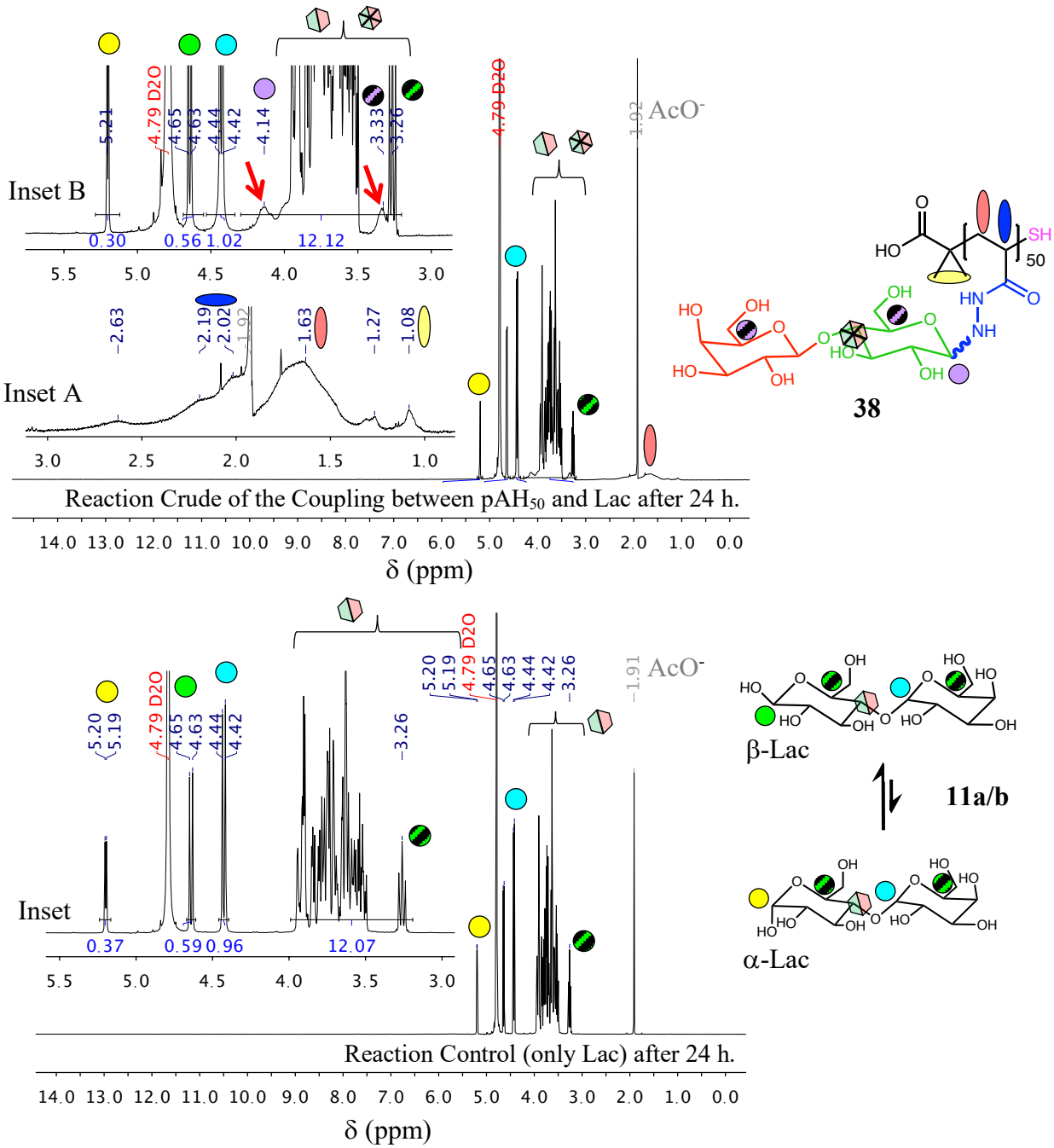


Figure 6.16. (Top) ^{1}H-NMR spectrum (400 MHz, D_2O) of the crude product of the condensation between pAH_{50} and Lac after 24 h. Lac protons were integrated for a total of 14 (number of H in Lac). In Inset A are seen the polymer's backbone signals. In Inset B, broad peaks in the saccharide region (red arrows) confirmed the formation of a glycopolymer with an estimated 30% loading (pAH_{50}-Lac_{15}) per the intensity drop of the anomeric proton peaks of free Lac (yellow and green dots). (Bottom) In the reaction control, containing only Lac, a value of *ca.* 1 (0.37 + 0.59) of the peaks of the anomeric proton of free Lac proved the lack of condensation.

Next, the glycosylated pendant groups of pAH_{50} were reduced with $PyBH_3$ ***(vid. 4.1.3-H)***. After purification with dialysis and lyophilisation, magnetic resonance analysis confirmed the reduction of pAH_{50}-Lac_{15} into pAH_{50}-RO-Gal_{15} **(Figure 6.17)** with the appearance of a new doublet (green oval, 2.92 and 3.06 ppm). Besides, the signal at 4.51 ppm (light blue oval) indicated that the glycosidic bond linking Gal and Glc in Lac remained intact and part of the pendant group of the new polymer. The broadness of all the compound's signals suggested an excellent product purification with the complete elimination of the acetate anion and the excess of Lac present in the reaction crude.

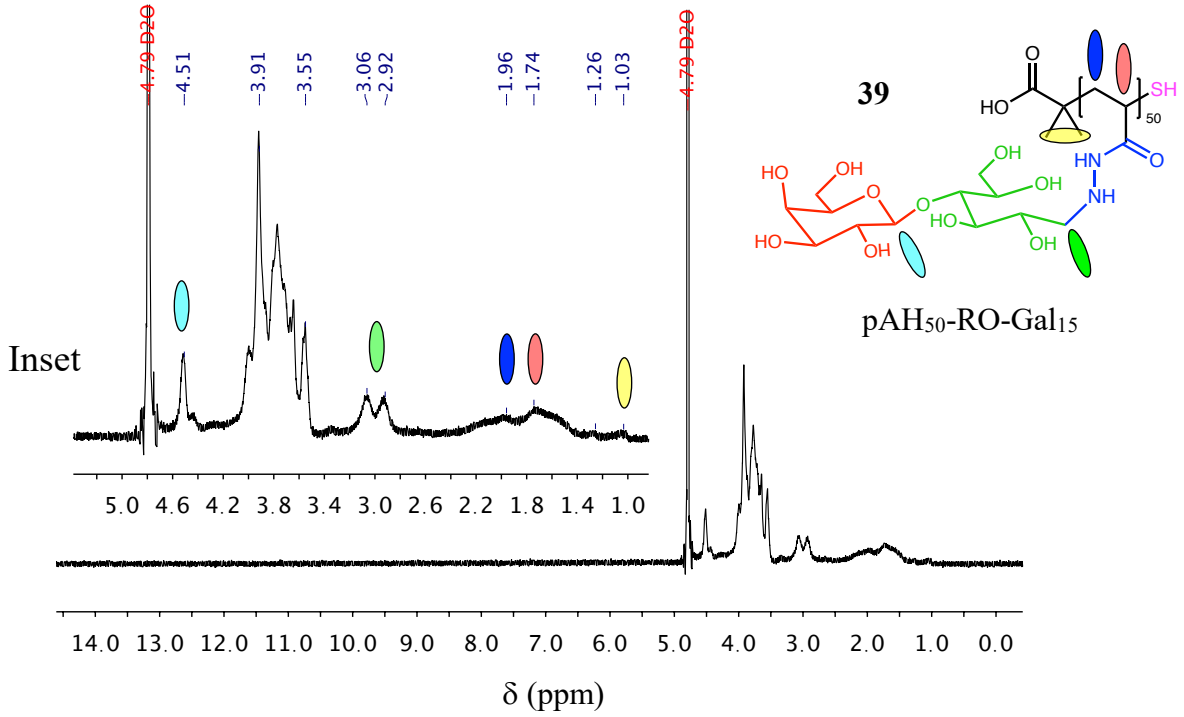


Figure 6.17. ^{1}H-NMR spectrum (400 MHz, D_2O) of the pure polymer pAH_{50}-RO-Gal_{15}, obtained after reducing pAH_{50}-Lac_{15} with $PyBH_3$. The broadness of all peaks demonstrated a successful dialysis purification of the polymer with the complete elimination of the excess of Lac of the crude product **(top Figure 6.16)**. The two peaks at 2.92 and 3.06 ppm (green oval), a doublet, would confirm the reduction of the hydrazone bond. The 4.51 ppm peak (light blue oval) indicated that the glycosidic bond of the Lac moiety remained unaffected by the reduction.

CV was utilised to probe the adsorption of pAH_{50}-RO-Gal_{15} on a Au(poly) electrode **(Figure 6.18)** and compare it with that of pAH_{50}. The electrode was modified by immersing it in dissolutions of pAH_{50}-RO-Gal_{15} (31.20 mg of polymer in 0.3 mL of water) or pAH_{50} (13.63 mg of polymer in 0.3 mL of water) for 30 min. at room temperature. As it happened with all previous pAH_n macromolecules used in this project (*i.e.* pAH_{20}, pAH_{50}, pAH_{50}-Gal_{33} and pAH_{50}-Gal_8), pAH_{50}-RO-Gal_{15} adsorbed on the Au(poly) electrode (solid red scan) according to the electrochemical response obtained between +0.45 and -0.15 V **(Figure 6.18-A)**: reduction of the EDL and disappearance of the lifting of the reconstruction (peak at *ca.* +0.23 V in the blank, dotted black arrow). When a more negative limit potential was set (-0.85 V), the characteristic reductive stripping of sulphur-containing molecules appeared peaking at *ca.* -0.70 V **(Figure 6.18-B)**. Compared to the desorption of pAH_{50} (solid blue curve) two traits appeared different: the onset region of the desorption process and the intensity of the peak. Although the intensities of the peaks were significantly different, it is difficult to assign those disparities to the presence or not of Gal in the polymer's pendant group. Because, as shown in **Figure 6.5-B**, the peak intensity between different experiments, even when the same polymer is used, can significantly differ. Regarding the start of the stripping from Au-pAH_{50}-RO-Gal_{15}, as noticed when other glycopolymers were desorbed (**Figures 6.8-B** and **6.11-B**), there seemed to be an early onset (violet star) at around -0.25 V, with a seemingly significant number of molecules detaching from -0.40 V (violet arrow). At about -0.55 V (red star) the process accelerated before peaking at -0.70 V (red arrow). This phenomenon was not observed in the sweep on Au-pAH_{50}, with a single reductive process starting at -0.55 V (blue star) that reached its maximum at -0.67 V (blue arrow). The early desorption of pAH_{50}-

RO-Gal$_{15}$ may have been associated with less-well adsorbed macromolecules: the presence of a sugar, a big molecule, in their pendant groups would have interfered in their attachment, leading to less-stable arrangements of molecules on the electrode surface. It may also be related to the desorption of other functional groups other than the thiol of the polymer (*i.e.* hydroxyls of the Gal), as studied in **Figure 6.9**.

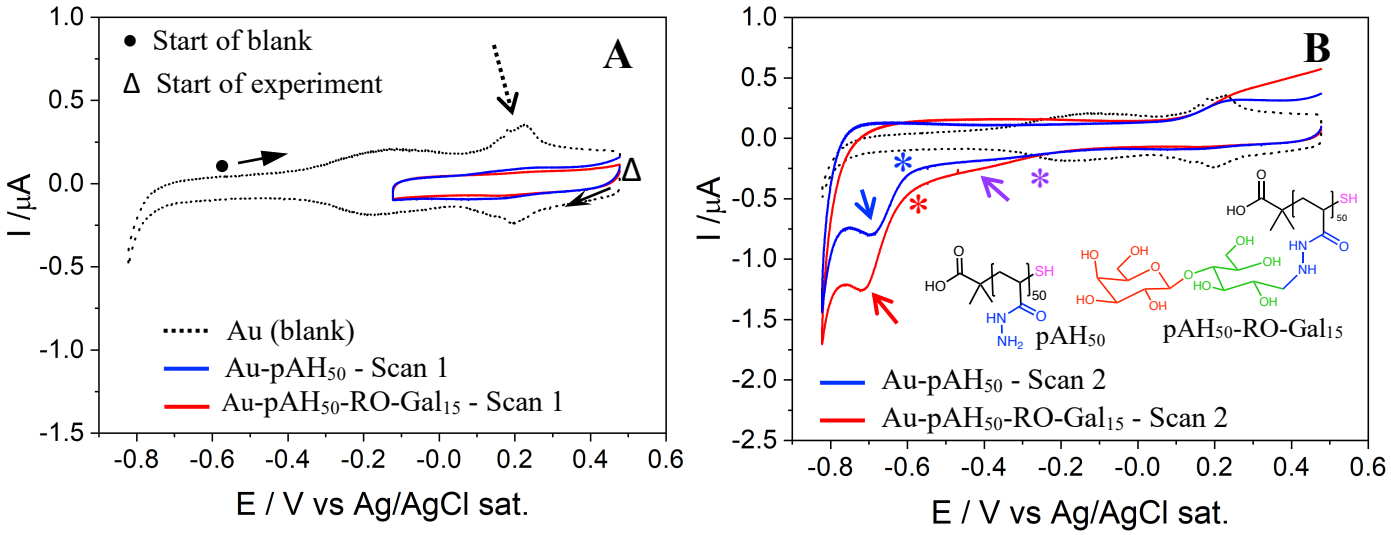


Figure 6.18. CV analysis in phosphate buffer electrolyte (0.1 M, pH 7.4) at a scan rate of 50 mV·s^{-1}of a Au(poly) electrode modified with pAH$_{50}$ (Au-pAH$_{50}$, solid blue line) and pAH$_{50}$-RO-Gal$_{15}$ (Au-pAH$_{50}$-RO-Gal$_{15}$, solid red line). **(A)** Scans at high potentials (from +0.45 V till -0.15 V) looked very similar for both modified surfaces. **(B)** In scans reaching more negative potentials (from +0.45 to -0.85 V), the CV response of Au-pAH$_{50}$ was a single, prominent stripping reduction peak at *ca.* -0.68 V (blue arrow) with onset at approximately -0.55 V (blue star). Instead, for Au-pAH$_{50}$-RO-Gal$_{15}$, a reduction process seemed to start at -0.25 V (purple star) and accentuate at -0.55 V (red star) to produce also a prominent reduction peak with a maximum at around -0.72 V (red arrow). (•) Start of the blank sweep; (Δ) start of CV scans on modified electrodes.

Despite CV proving to be helpful to determine the modification of Au(poly) electrodes, and even differentiate when the polymers adsorbed contained a

saccharide, it seemed unfeasible to detect CTB with this technique: it was difficult to foresee how the adsorption of CTB on Au-pAH$_n$-RO-Gal$_{15}$ would sufficiently modify the electrochemical signal, either at high or at low potential, to allow for its recognition. Therefore, using an electrochemical mediator seemed to be necessary to achieve the project's main goal, the detection of CTB.

6.3 Conclusions

The results presented in **Chapter 6** show that pAH$_n$ is a suitable linker to immobilise Gal onto Au(poly) surfaces.

pAH macromolecules adsorbed fast on Au(poly) electrodes and demonstrated excellent stability in a wide potential range, making them useful as immobilisation platforms for electroanalysis. The outstanding solubility of pAH$_n$ in water facilitated the modification of electrodes from solution and permitted the avoidance of more expensive and environmentally hazardous organic solvents. Furthermore, RAFT polymerisation conferred a high control of macromolecule synthesis, allowing the obtainment of polymers with different sizes according to necessity. Moreover**,** the high reactivity between the hydrazide group and aldehyde-containing molecules, like Gal and Lac, permitted an easy post-polymerisation in mild conditions.

The results in **Chapter 6** also illustrate that, although CV is a valuable technique to determine the adsorption and stability of macromolecules on Au electrodes, it lacks the accuracy to study other features that may be interesting when developing a sensor:

degree of BRE coverage, macromolecular arrangement, differentiation between species adsorbed. For example, it would be very challenging to distinguish between adsorbed pAH_{50}-OR-Gal_{15} **(Figure 6.18-B)** and pAH_{50}-Gal_8 **(Figure 6.11-B)**. This exposed something more critical, the lack of accuracy of CV to detect CT.

Finally, although hydrazones formed between Gal or Lac and hydrazides are stable over pH 7[630], reducing the bond between the linker and the sugar made it irreversible and improved the chances of getting a more robust sensor. This work contains an easy procedure for reducing the hydrazone bond between the pendant groups of pAH_n and Lac to obtain a Gal-baring glycopolymer. It must be highlighted that the scaling up of the glycopolymer synthesis would be facilitated by its simple dialysis purification.

In summary, the Gal monosaccharide was immobilised on a Au(poly) electrode using pAH_n as a linker. Due to its high chemical flexibility and good electrochemical stability, the polymer is a good choice for its use in electroanalysis.

Chapter 7

Electrochemical Detection of the Subunit B of Cholera Toxin

7.1 Introduction

Following the results of **Chapter 6**, where the Gal moiety was successfully immobilised on a Au(poly) electrode through a polymer, this section reports on the efforts made to electrochemically detect CTB, the subunit of CT which recognises the surface of human cells to start an infection. Although CV had proven to be a helpful technique for determining the modification of electrodes with Gal, to improve the sensitivity to detect CTB, and electrochemical mediator and other electrochemical techniques (*i.e.* SWV, EIS) were used.

Most electrochemical techniques are based on the ET process, the exchange of electrons between an electrode and some species in the bulk of the electrolyte. This limits electrochemical sensing under certain circumstances: if the analyte is not electroactive, so it cannot be directly oxidised or reduced by the electrode; if the process is too slow, for which the signal is too weak; or if the required applied potential to force the ET disturbs the system. Electroanalysis has found ways to bypass these drawbacks using electrochemical mediators. Redox probes, species with reversible states of oxidation and fast ET, are a common choice for a mediator **(Figure 7.1)**. The diversity of redox probes available regarding their nature -organic, inorganic, biological-, redox potential, solubility, charge[631, 632], ET mechanism -inner/outer-

sphere-, and other features, makes it relatively easy to find the most convenient for each need. Although usually dissolved in the electrolyte, the possibility of attaching electrochemical mediators to the electrode has become an increasingly popular option[633, 634]. Their incorporation onto the BRE or the analyte can also be used[635, 636].

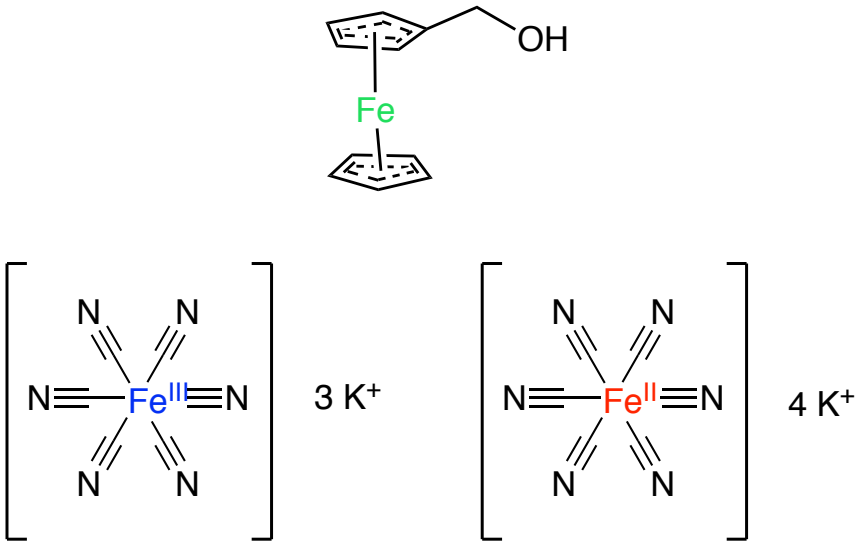


Figure 7.1. Electrochemical mediators utilised in this thesis. On top, ferrocenemethanol, a neutral molecule. At the bottom, the redox couple potassium ferro/ferricyanide ($K_3[Fe(CN)_6]$ / $K_4[Fe(CN)_6]$), one of the most popular redox mediators in electroanalysis.

Two main reasons made necessary the employment of a mediator in this project. First, the electrochemical signals obtained with CV from electrodes modified with pAH_n and glycosylated pAH_n were not distinctive or reproducible enough; so it would have been complicated to obtain significant qualitative or quantitative data trying to detect CTB. Second, CTB is a non-electroactive species. The selection of a redox probe must consider many issues: nature of the electrode (can affect the kinetics and reversibility of the probe), solubility in the electrolyte, concentration, ET rate and, of course,

potential window. Moreover, once the electrode surface has been modified, another essential question arises: how the chemical probe interacts with the new interface. $K_4Fe(CN)_6$, previously used in this project, was initially a good candidate: its redox potential was within the potential window of stability of glycosylated pAH_n adsorbed on a Au electrode **(Chapter 6)**; and its response was only relatively attenuated on those modified electrodes (unlike on SAMs of LA, **Figure 5.5**). In this chapter, though, the redox couple $Fe(CN)_6^{3-/4-}$ was used instead to increase the system's stability,

Despite the widespread use of $Fe(CN)_6^{3-/4-}$ in sensing, there were a series of concerns about its behaviour on a Au-pAH_{50}-RO-Gal_{15} electrode. For a start, the presence of hydrazide groups in the linker, a highly coordinating metal-ligand **(Figure 7.2)**, raised questions about potential strong interactions between polymers and the probe that may affect the analytical signal. Furthermore, using a charged molecule could generate electrostatic forces with the electrode surface, again affecting measurements. Finally, there is a debate[637] within the electrochemical community about the effect that the adsorption of this redox couple and the cyanide group on Au can have on electrochemical processes.

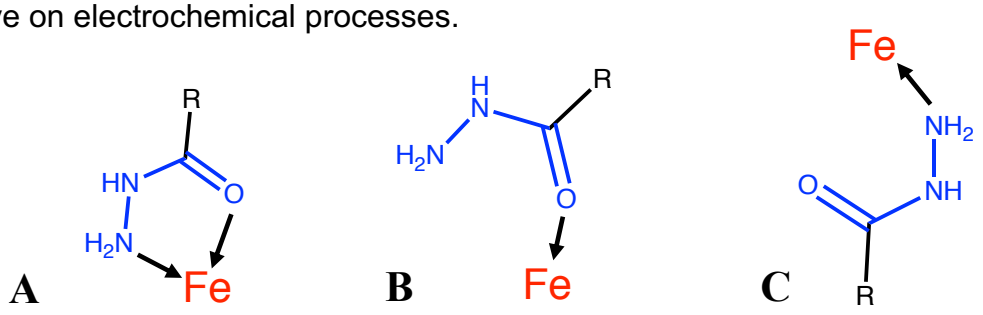


Figure 7.2. Possible forms of coordination between the hydrazide groups of pAH_n and Fe nuclei of redox mediators[638, 639]. The presence of several atoms with lone pair of electrons in the hydrazide group (O and N) can prompt the formation of coordination bonds between polymers and Fe nuclei (**A** bidentate coordination, **B** and **C** monodentate coordination).

To increase the chances of success, the behaviour of a second probe, FcMeOH, with similar redox potential but different chemical features **(Table 7.1)**, was also tested. FcMeOH, a neutral molecule, would reduce potential ionic interactions with the electrode and the glycosylated polymer. On the topic of interactions between free hydrazide groups of pAH_{50}-RO-Gal_{15} and the probe, the very stable penta-coordination of the FcMeOH ligands (2 ferrocene rings) would minimise the prospects of polymer coordination that could affect the analytical signal.

Table 7.1. Physical and chemical properties of FcMeOH and $[Fe(CN)_6^{3-/4-}]$.

Feature	$[Fe(CN)_6^{3-/4-}]$	FcMeOH
Relative size	Small	Big
Charge	Negative	Neutral
Coordination	Monodentate	Chelate
Interaction with Au	Good	Poor
Ligand polarity	High	Low
Solubility	Very good	Good
ET	Inner-sphere	Outer-sphere

After assessing both redox probes on modified electrodes (Au-pAH_{50} and Au-pAH_{50}-RO-Gal_{15}) to ascertain their behaviour in measuring conditions, $[Fe(CN)_6]^{-3/-4}$ was deemed the best to attempt the detection of CTB. The sensor's analytical signal would consist of the electrochemical response variation caused by CTB blocking the electrode surface after interacting with the Gal immobilised on the electrode **(Figure 7.3)**. The signal attenuation of a redox mediator is a standard procedure to characterise

modified electrode surfaces[640, 641] and has also been extended to sense analytes, including CT[55, 642].

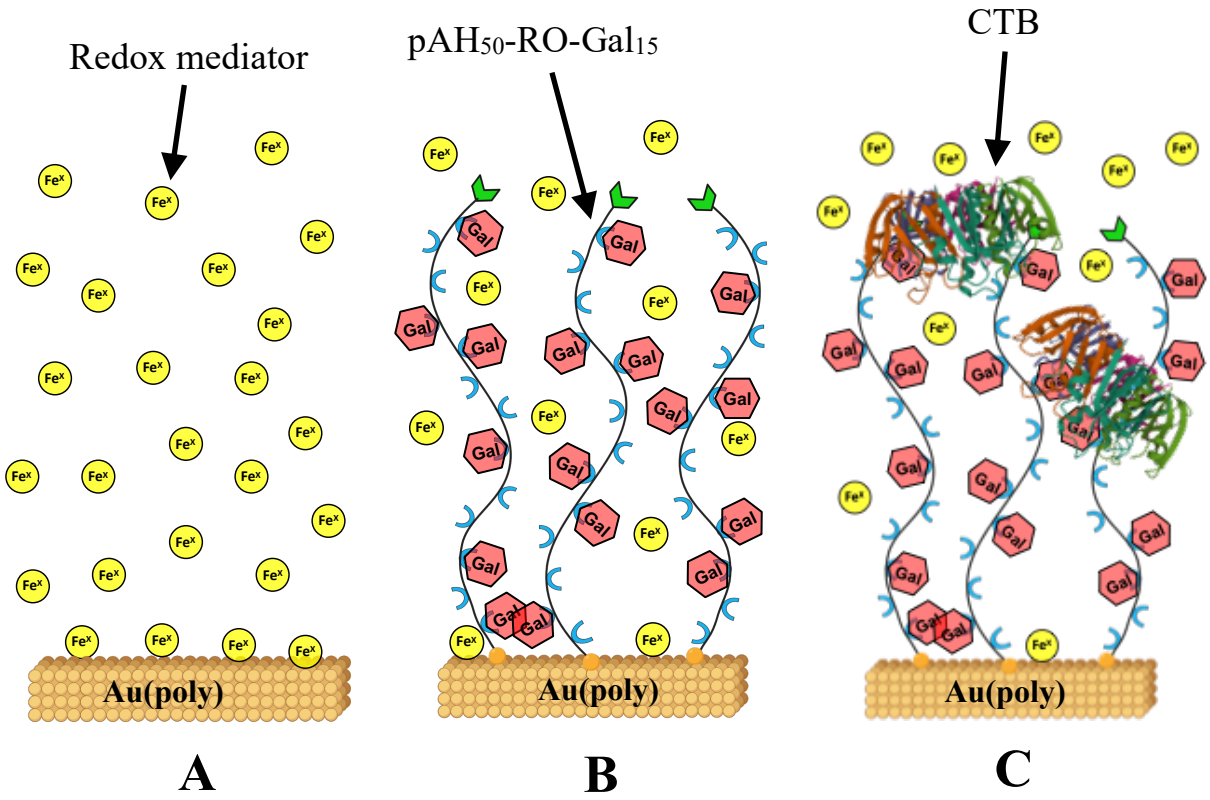


Figure 7.3. Diagram showing the different accessibility of the molecules of a redox mediator (yellow dots) to an electrode's surface to explain the attenuation of a probe's signal, which is the analytical signal of the biosensor of this thesis. **(A)** On a bare Au(poly) electrode, the probe's molecules have free access to the surface of the electrode producing a maximum electrochemical response. **(B)** When the electrode is modified with a polymer (*e.g.* pAH_{50}-RO-Gal_{15}), the surface is partially blocked: the mediator's signal is attenuated because the number of possible ET episodes is smaller or slower. **(C)** The interaction between CTB and an electrode modified with Gal further limits the ET between the mediator's molecules and the electrode, reducing the probe's signal even more.

CV is the best-known and most popular electrochemical technique because it is very simple and facilitates the study of the mechanism of chemical transformations. Nevertheless, because the intensity of current obtained from a CV is the sum of

faradaic and non-faradaic currents, it is significantly limited for quantitative analysis: the contribution of non-faradaic phenomena alters the dependency between redox species concentration and current intensity. Typically, the limits of detection of CV are found at around $1 \cdot 10^{-4}$ to $1 \cdot 10^{-5}$ M[463].

Pulse (or impulse) voltammetry techniques, like SWV, entailed an advance towards decoupling faradaic and non-faradaic currents. SWV occupies a prominent place in electroanalysis due to its fastness, selectivity, and high sensitivity, which can reach detection limits down to $1 \cdot 10^{-7}$ M.

EIS is an electrochemical technique employed to study the electrode/electrolyte interface. In the two previous voltammetry techniques, CV and SWV, the application of changing potentials on a system produces variations in intensity that are recorded. Instead, in EIS, a sinusoidal voltage perturbation is applied to a system leading to a current response whose amplitude and phase angle with respect to the perturbation are measured. The role of EIS in sensing has increased in the last two decades thanks to technological advances, *e.g.* the integration and miniaturisation of potentiostats and frequency response analysers or the development of software to analyse the complex EIS data[643]. EIS can be used to detect the effect that the interaction between the BRE of a sensor and an analyte can have on the current passing through the sensor's interface. The enormous sensitivity achievable with EIS, with limits of detection well below $1 \cdot 10^{-8}$ M, is one of the most attractive features of this technique in quantitative analysis. However, there are also caveats since its application requires careful control of the measurement conditions to avoid disturbances. In this chapter, after using CV

with two redox probes (FcMeOH and $[Fe(CN)_6]^{-3/-4}$) to characterise modified Au(poly) electrodes, SWV and EIS were employed with $[Fe(CN)_6]^{-3/-4}$ to try the detection of CTB.

7.2 Results and Discussion

Before attempting the detection of CTB, the two candidates to be used as electrochemical mediators were characterised: the redox couple $[Fe(CN)_6]^{-3/-4}$ **(Figure 7.4)**, an inner sphere redox probe and FcMeOH **(Figure 7.5)**, an outer-sphere redox probe[644-647]. Because the electrochemical oxidation and reduction of the two species occurred in a potential range rom -0.10 to +0.50 V, where glycosylated pAHs are stable on Au(poly) electrodes, both probes were initially considered helpful for detecting CTB. As expected in species with fast and reversible ET on metallic electrodes, the current intensity increased with the scan rate according to the Randles-Sevćik Equation **(Chapter 3, equation 12)**.

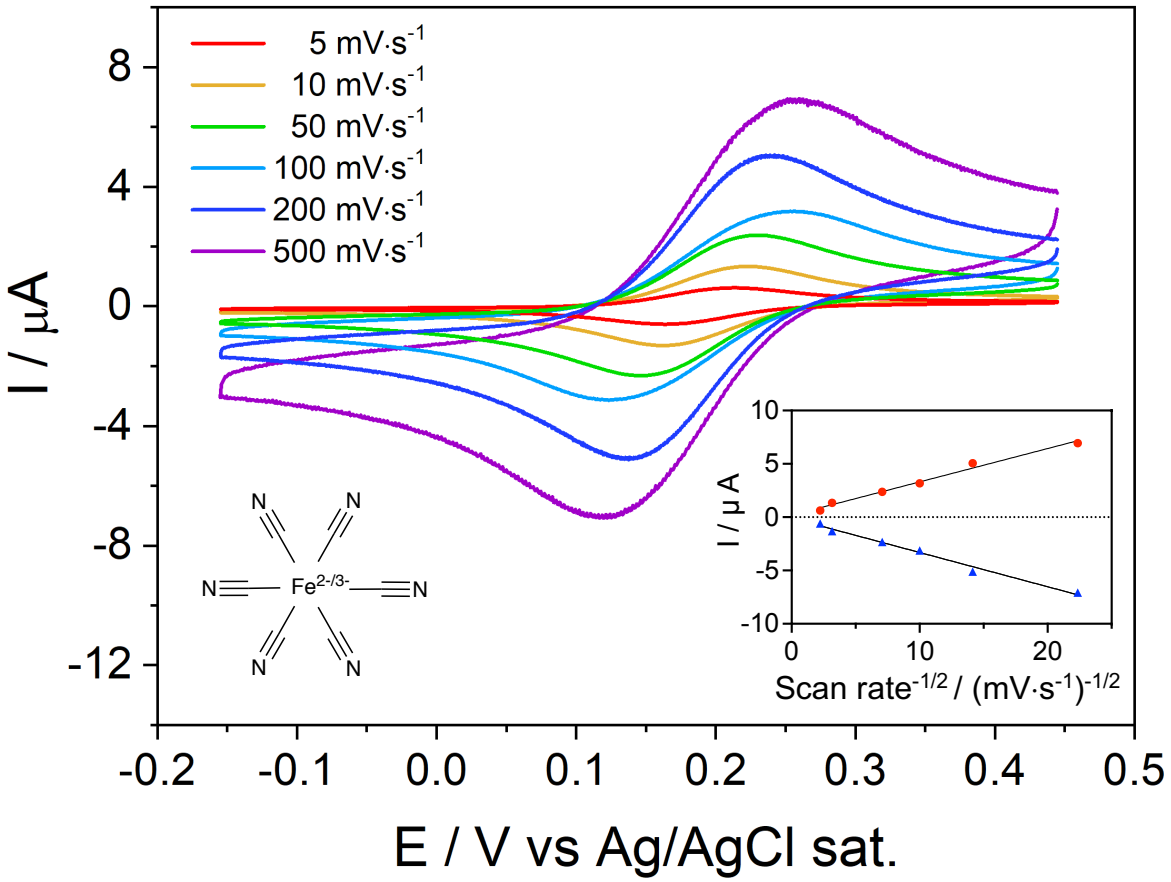


Figure 7.4. Electrochemical characterisation of the redox couple $K_4Fe(CN)_6$ / $K_3Fe(CN)_6$ on a bare Au(poly) electrode in phosphate buffer electrolyte (0.1 M, pH 7.4). CV at different scan rates (5, 10, 50, 100, 200 and 500 $mV{\cdot}s^{-1}$) were conducted in an electrolyte containing 0.5 mM of $K_3Fe(CN)_6$ / $K_2Fe(CN)_6$. In the inset, the linear regressions of the peak intensities in the oxidation (red) and reduction (blue) sweeps *versus* the square root of the scan rate demonstrated the high reversibility of this redox mediator in these electrochemical conditions.

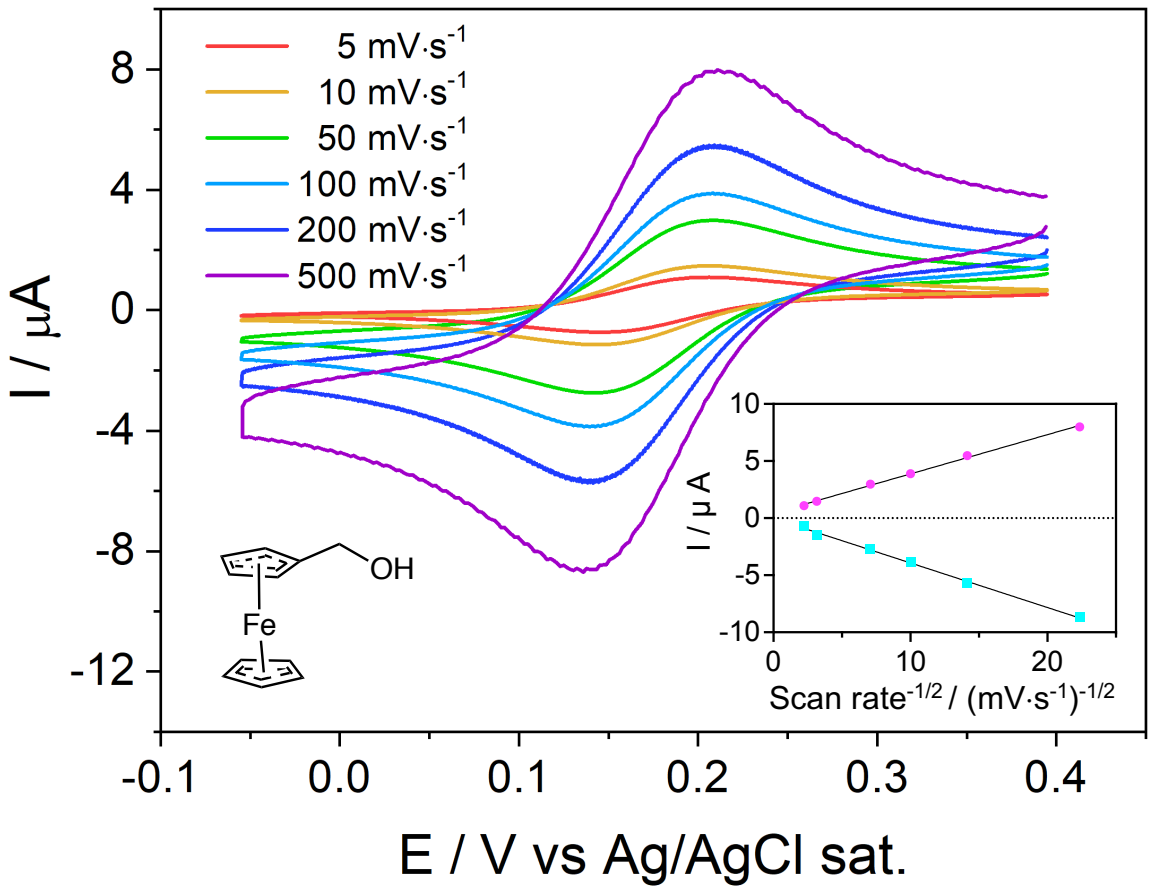


Figure 7.5. Electrochemical characterisation of the redox mediator FcMeOH on a bare Au(poly) electrode in phosphate buffer electrolyte (0.1 M, pH 7.4). CV scans at several rates (5, 10, 50, 100, 200 and 500 $mV \cdot s^{-1}$) were run in the electrolyte containing 0.5 mM of FcMeOH. In the inset, the linear regressions of the peak intensities of the oxidation (purple) and reduction (cyan) sweeps versus the square root of the scan rates proved the reversible character of this probe in these electrochemical conditions.

Next, CTB detection was attempted by comparing the electrochemical response of these two mediators on a Gal-modified electrode (Au-pAH_{50}-RO-Gal_{15}) before and after being incubated in a CTB solution.

7.2.1 FcMeOH as Electrochemical Mediator

FcMeOH was used first as a mediator because it has some characteristics that, *a priori*, made it the best option. The first consideration was the arrangement of macromolecules on the surface of the electrode and how they may block the electrode surface **(Figure 7.6)**. As FcMeOH is an outer-sphere probe, there were better chances of still obtaining a sensing signal in case of a significant blocking of the Au surface by the polymer **(Figure 7.6-B)**. In the opposite scenario, if the adsorbed polymer allowed ferrocene molecules to easily access the surface of the electrode **(Figure 7.6-A)**, because FcMeOH is a neutral molecule, it would experience fewer electrostatic interactions which, at least in the case of EIS, could affect the electrochemical response. Besides, the hydrazide group is an excellent coordinating ligand **(Figure 7.2)** and pAH_{50}-RO-Gal_{15}, with many free hydrazide groups, could interact with Fe nuclei of the probe. Therefore, it was thought that FcMeOH would be more stable since displacing its ferrocene ligands (chelate) would be more difficult than displacing the cyanide groups (monodentate) of $[Fe(CN)_6]^{-3/-4}$.

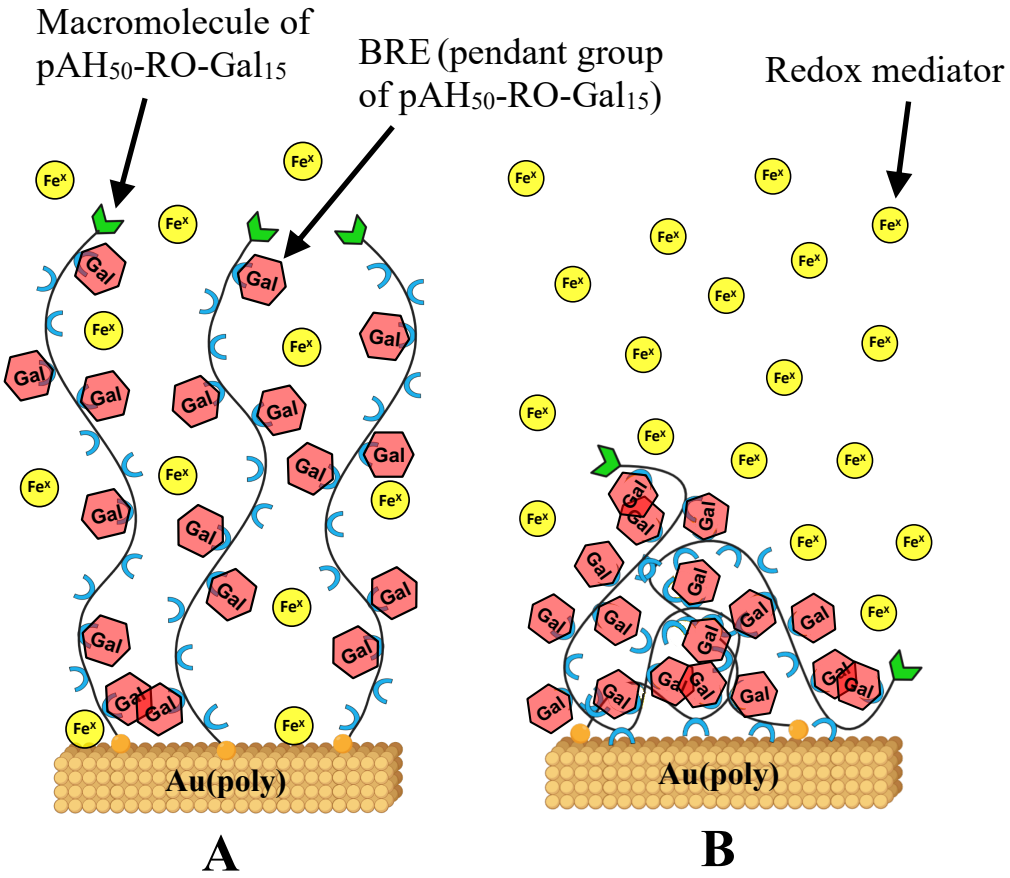


Figure 7.6. Representation of potential arrangements of adsorbed pAH_{50}-RO-Gal_{15} on a Au(poly) electrode and how they may affect the access of the redox mediator molecules to the electrode surface and its electrochemical response. In an ordered, stand-up arrangement of polymeric macromolecules **(A)** the mediator molecules enjoy an easier approach to the electrode surface than if the polymer presents a disordered, coiled configuration **(B)**.

CV and SWV were initially used to study the effect of pAH_{50}-RO-Gal_{15} and CTB adsorbed on a Au electrode on the ET of FcMeOH. The expectation was that the species adsorbed would attenuate the probe signal (solid yellow curves). Moreover, their attachment needed not to completely block the ET to have an analytical signal to detect CTB. With both electrochemical techniques, the oxidation and reduction currents of FcMeOH increased on an electrode modified in an aqueous dissolution of

the polymer (Au-pAH$_{50}$-RO-Gal$_{15}$, blue scans) during 30 min. **(Figure 7.7)**. The same happened after Au-pAH$_{50}$-RO-Gal$_{15}$ was incubated for 30 min. in a 4.33 ·10^{-5} M CTB aqueous dissolution (Au-pAH$_{50}$-RO-Gal$_{15}$-CTB, solid red curves); and also when an unmodified, bare Au(poly) electrode was submerged for 1 h. in the just mentioned CTB solution (dashed red curves).

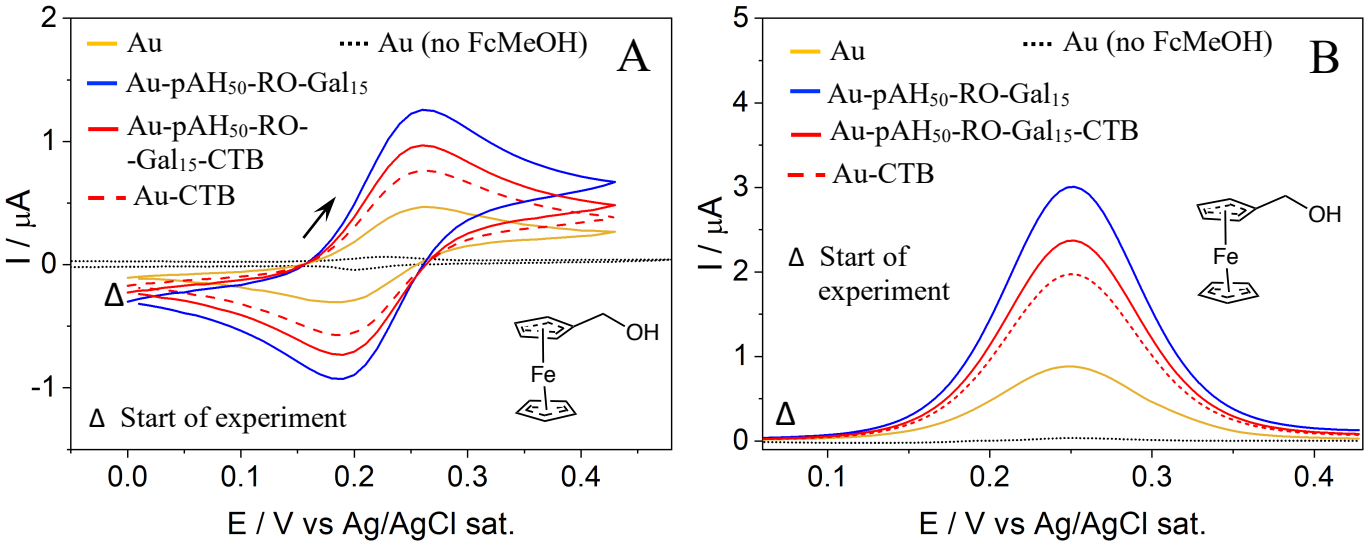


Figure 7.7. Electrochemical experiments (CV and SWV) studying the viability of using modified electrodes Au-pAH$_{50}$-RO-Gal$_{15}$ and the redox probe FcMeOH (0.5 mM) to detect CTB. **(A)** In CV, there was an increment of the intensity of the FcMeOH signal on modified electrodes, suggesting an interaction between the redox probe and the functional groups of pAH$_{50}$-OR-Gal$_{15}$ or CTB. **(B)** The results of the SWV sweeps were concordant with the equivalent CV experiments. Electrochemical conditions: phosphate buffer (0.1 M, pH 7.4) electrolyte; CV sweeps at 50 mV·s^{-1}; SWV scans done at a frequency of 5 Hz, a step E of 5 mV and an amplitude of 25 mV.

The above results did not match the expected reduction of the mediator's signal after electrode modification. This could be explained if FcMeOH molecules had adsorbed on some pendant groups of pAH$_{50}$-RO-Gal$_{15}$ or side chains of CTB, something already reported by Zheng *et al.*[648] **(Figure 7.8)**.

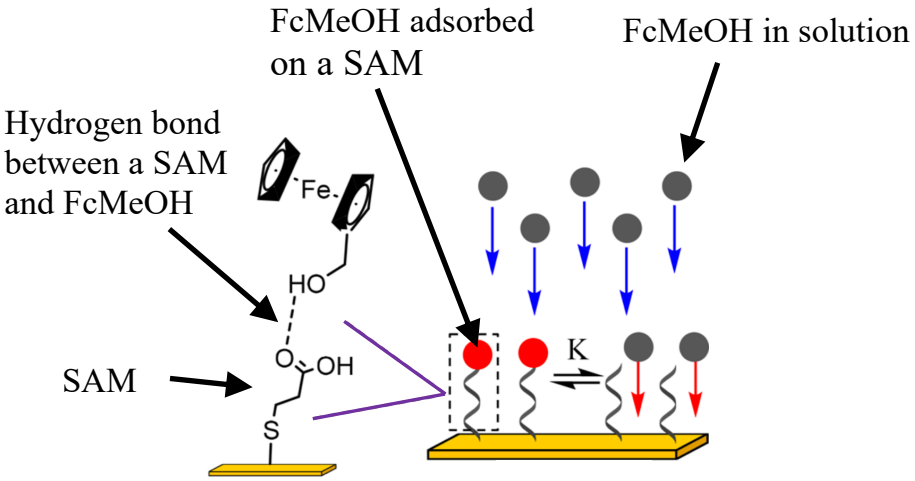


Figure 7.8. Electrochemical effect of the interaction between FcMeOH molecules and carboxylic groups of a SAM adsorbed on Au[648]. When the molecules of a redox probe (grey dots) like FcMeOH adsorb (red circles) on a SAM, the total registered faradaic current can become the sum of contributions from bulk and adsorbed molecules. Thus, an increment of current intensity, caused by the adsorbed molecules of the mediator, may be observed.

The adsorption of electroactive species on electrodes is a significant phenomenon that affects the ET and, thus, has a profound impact on the outcome of electrochemical reactions[649]. For example, Wopschall *et al.*[650] described how the weak adsorption of an electroactive reactant leads towards an increase of the intensity peak during the forward scan. Because in our case the enhancement was also noted in the backward sweep, the oxidation product $[FcMeOH]^+$ may have also adsorbed on Au-pAH_{50}-RO-Gal_{15}. Beyond the interaction of FcMeOH with pAH_{50}-RO-Gal_{15} and CTB, the experiments of **Figure 7.7** hinted at an outer-sphere ET of the probe under the experimental conditions employed: the presence of macromolecules on the interface (Au-pAH_{50}-RO-Gal_{15} and Au-CTB) did not altogether cancel the probe's signal. There also was confirmation of the CTB adsorption on Au(poly) electrodes. This did not come

as a surprise since protein adsorption on Au has been widely reported in the literature[651, 652]: thiol and amine groups on the side chains of the peptides facilitate this process. Indeed, a popular strategy to block the uncovered areas of a modified electrode surface is using proteins[653, 654] like BSA. Since the interactions between the polymeric layer modifying the electrode and FcMeOH could complicate and make less accurate the analytical signal to detect CTB, it was decided to try the alternative probe, $[Fe(CN)_6]^{-3/-4}$.

7.2.2 $[Fe(CN)_6]^{-3/-4}$ as Electrochemical Mediator

The behaviour of $[Fe(CN)_6]^{-3/-4}$ in the presence of pAH_{50}-RO-Gal_{15} or CTB on the surface of a Au(poly) electrode **(Figure 7.9)** was also studied with CV and SWV. According to CV **(Figure 7.9-A)**, there was a small increment of current intensity after a bare electrode (solid yellow scan) was functionalised (Au-pAH_{50}-RO-Gal_{15}, solid blue scan). However, this variation was not confirmed by SWV **(Figure 7.9-B)**, with which an apparent attenuation occurred. The divergence could be explained because a CV signal originates from faradaic and non-faradaic processes. Therefore, charge transfer not related to the redox probe was probably registered and its contribution produced the unexpected intensity augment. Instead, SWV permits the elimination of most non-faradaic currents and, thus, is a much more reliable source when comparing current intensities. In this case, there was an evident drop of the signal from Au(poly) bare electrode (solid yellow curve) to Au-pAH_{50}-OR-Gal_{15} (solid blue curve). When Au-pAH_{50}-RO-Gal_{15} was incubated for 1 h. at room temperature in a $4.33 \cdot 10^{-5}$ M CTB dissolution, both techniques recorded a reduction of the maximum intensity. These results suggested that the pentamer adsorbed on the electrode's surface through the

interaction with the glycosylated polymer, increasing the blockage of the ET. Finally, the incubation of a bare electrode in the same CTB dissolution led to an almost disappearance of the redox couple signal (dashed red scan), evidence that CTB had adsorbed on Au and had almost completely blocked the interface. This circumstance would also confirm the inner-sphere character of the ET of $[Fe(CN)_6]^{-3/-4}$ in this particular electrochemical system, unlike FcMeOH **(Figure 7.7)**.

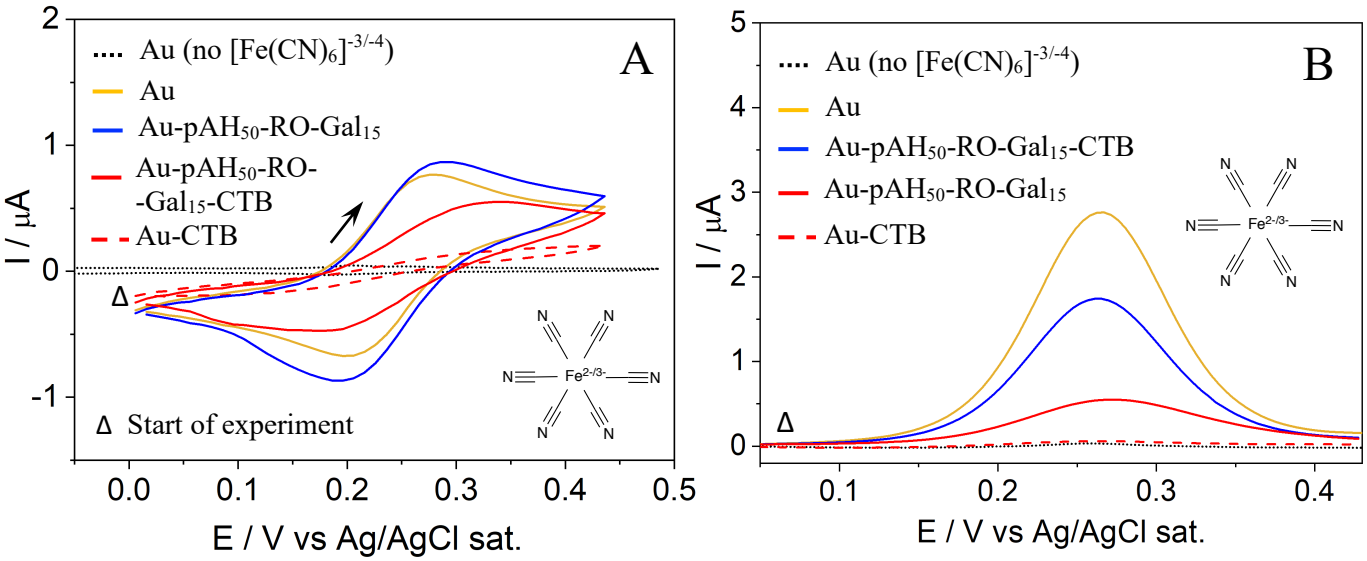


Figure 7.9. Electrochemical experiments testing $[Fe(CN)_6]^{-3/-4}$ (0.5 mM) on a Au-pAH$_{50}$-RO-Gal$_{15}$ electrode to detect CTB. **(A)** With CV, Au-pAH$_{50}$-RO-Gal$_{15}$ (solid blue scan) slightly enhanced the probe's signal (solid yellow curve); after its incubation in CTB (Au-pAH$_{50}$-RO-Gal$_{15}$-CTB, solid red scan), there was a significant signal drop. Finally, the surface of the bare electrode was effectively blocked after CTB incubation (Au-CTB, dashed red scan). **(B)** SWV experiments, run immediately after the corresponding CV scans, showed that Au-pAH$_{50}$-RO-Gal$_{15}$ significantly cancelled the probe. After CTB incubation, further reduction of the redox couple response was observed. When an unmodified electrode was incubated in CTB, the probe was totally blocked from its surface. Electrochemical conditions used: phosphate buffer (0.1 M, pH 7.4) electrolyte; CV scans done at 50 mV·s^{-1}; SWV sweeps run at a frequency of 5 Hz, step E of 5 mV and an amplitude of 25 mV.

After examining FcMeOH and $[Fe(CN)_6]^{-3/-4}$ as redox mediators, it was decided that the latter was the best option for the project since it appeared to interact exclusively with the Gal of pAH_{50}-RO-Gal_{15} and not with its free hydrazide groups or CTB.

7.2.3 Optimisation of the Functionalisation of Au(poly) Electrodes with Glycosylated Poly(acryloyl) Hydrazide (pAH_{50}-RO-Gal_{15}) for the Detection of Cholera Toxin Subunit B

Before trying the detection of CTB, an optimisation of the process of modification of electrodes with pAH_{50}-RO-Gal_{15} was performed. Up until now, in all the experiments of this chapter, clean bare Au(poly) electrodes had been modified by dipping them in a dissolution of the glycopolymer (thiol group end at a concentration of 10 mM) for 30 min. at room temperature. Now, Au-pAH_{50}-RO-Gal_{15} electrodes were characterised with SWV and EIS after 5, 10, 15, 20, 30, 40 and 60 min. functionalisation **(Figure 7.10)**. The attenuation of the SWV signal or the increase in the impedance (EIS) in all cases confirmed the glycopolymer adsorption on the electrode. Nevertheless, there was no correlation between the electrode's immersion time and the probe's electrochemical response. Therefore, 5 min. appeared to be enough to obtain an electrode modified with Gal and apt for sensing CTB.

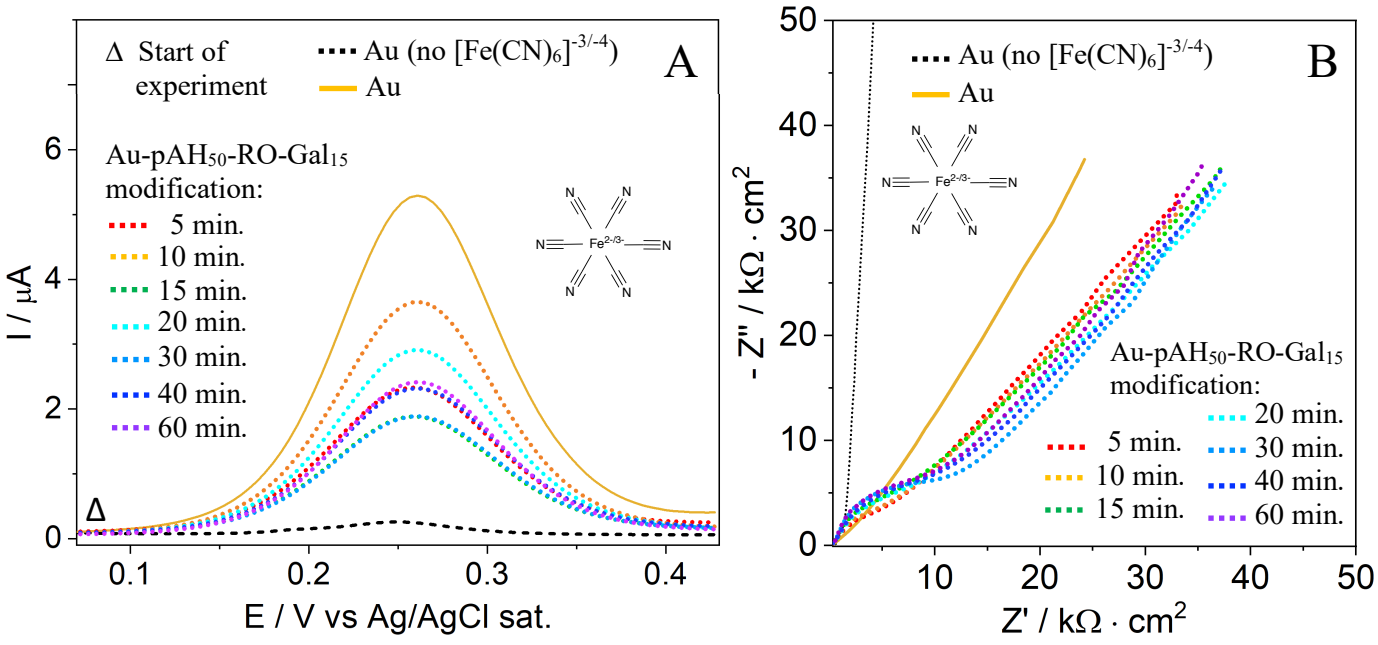


Figure 7.10. Study of the effect of the functionalisation time of a Au(poly) electrode with pAH_{50}-RO-Gal_{15} on the $[Fe(CN)_6]^{-3/-4}$ (0.5 mM) response. **(A)** According to SWV, there was no correlation between time of electrode modification and the probe's response. The reduction of the intensity in all cases (dotted scans), though, confirmed the polymer's adsorption. **(B)** EIS measurements, performed immediately after the corresponding SWV scan, verified the lack of correlation between modification time and electrochemical signal. Electrochemical conditions: phosphate buffer (0.1 M, pH 7.4) electrolyte; SWV scans done at a frequency of 5 Hz, a step E of 5 mV and an amplitude of 25 mV; EIS sweeps were conducted between 65,353 and 1 Hz with a set E of 148 mV and an amplitude of 10 mV.

Although SWV and EIS could not establish any relation between time of functionalisation and electrode response, to assess if this factor had any influence on sensing CTB, the detection of the protein from a $4.33 \cdot 10^{-5}$ M aqueous dissolution was attempted after electrode modifications of 5, 15, 30, 45 and 60 min. The time of incubation of Au-pAH_{50}-RO-Gal_{15} in the CTB solution was 5 min. in all instances. With SWV, as shown in **Figure 7.11**, there was always a further decrease of the

electrochemical signal after CTB incubation (solid lines), although no apparent correlation with the functionalisation time (dotted lines). This was in correspondence with a more significant blockage of the interface caused by the adsorption of the large CTB protein onto Au-pAH$_{50}$-RO-Gal$_{15}$ and confirmed the possibility of using this design to detect CTB.

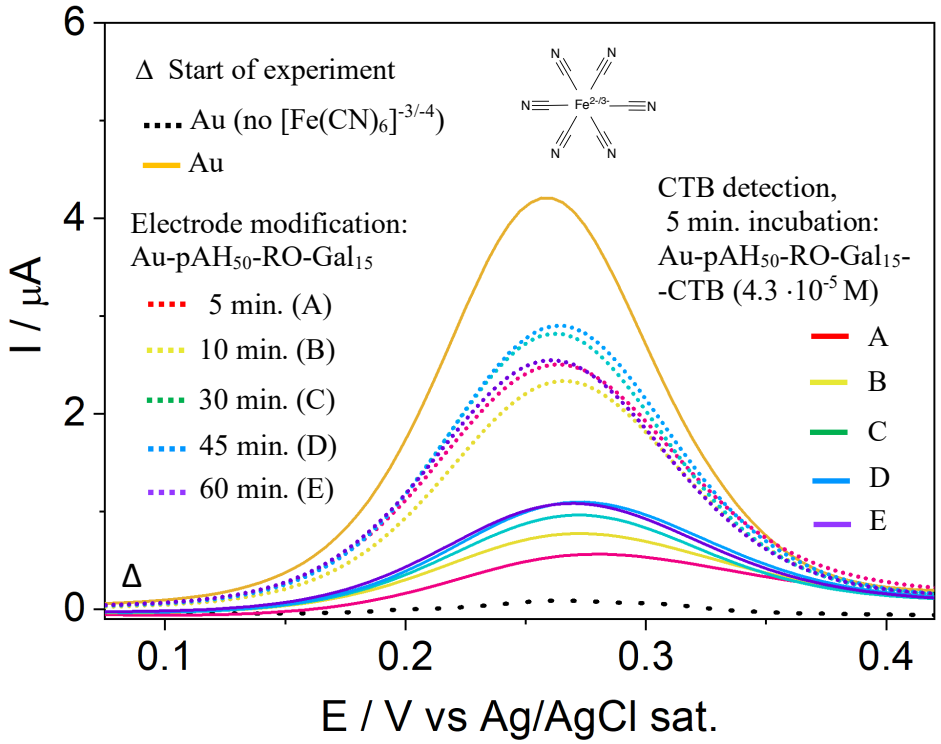


Figure 7.11. SWV study of the capacity of a Au-pAH50-RO-Gal$_{15}$ electrode to detect CTB from a 4.33 ·10^{-5} M dissolution (5 min. incubation) after several times of functionalisation; the phosphate buffer electrolyte contained 0.5 mM [Fe(CN)$_6$]$^{-3}$/$^{-4}$. SWV showed no apparent correlation between electrode modification time with the glycosylated polymer (dotted scans) and the detection of CTB after 5 min. incubation (solid curves). In all instances, the electrode incubation in CTB led to a drop of the probe's signal. SWV scans were done in phosphate buffer (0.1 M, pH 7.4) electrolyte with a frequency of 5 Hz, a step E of 5 mV and an amplitude of 25 mV.

All EIS scans **(Figure 7.12)**, obtained immediately after running each of the corresponding SWV sweeps of **Figure 7.11**, registered similar spectra of Au-pAH$_{50}$-RO-Gal$_{15}$ notwithstanding functionalisation time **(Figure 7.12-A)**. Nevertheless, the ensuing attempts to detect CTB from a 4.33 ·10^{-5} M aqueous dissolution **(Figure 7.12-B)** after 5 min. of incubation seemed to find a correlation between modification time and impedance. In this way, the most significant response change **(Figure 7.12-B, scan A)** was observed after 5 min. electrode modification **(Figure 7.12-A, scan A)**. When the time of functionalisation increased, the EIS response appeared to decrease.

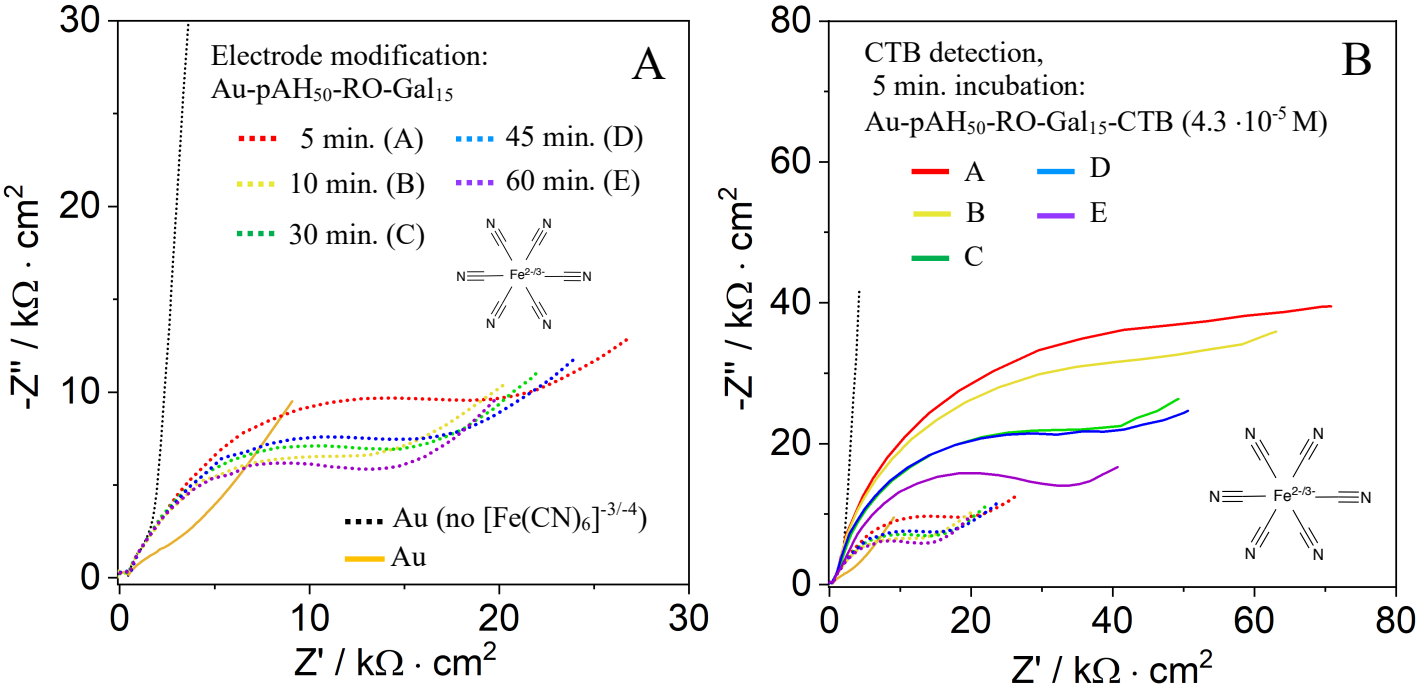


Figure 7.12. EIS analysis of the modification at different times of a Au(poly) electrode with the glycopolymer pAH$_{50}$-RO-Gal$_{15}$ and its performance detecting CTB from a 4.33 ·10^{-5} M aqueous dissolution (5 min. incubation) using 0.5 mM of [Fe(CN)$_6$]$^{-3}$/$^{-4}$ as electrochemical mediator. **(A)** EIS investigation of the modification of a Au(poly) electrode with pAH$_{50}$-RO-Gal$_{15}$ during various periods of time: 5, 10, 30, 45, and 60 min. **(B)** EIS spectra obtained after incubating the aforementioned modified electrode (dotted curves) in a CTB aqueous dissolution (solid curves). EIS experiments were performed in phosphate buffer (0.1 M, pH 7.4) electrolyte between 65,353 and 1 Hz with a set E of 148 mV and an amplitude of 10 mV.

After these experiments it was concluded that the best procedure to modify a Au(poly) electrode with pAH_{50}-RO-Gal_{15} macromolecules for detecting CTB was immersing it in an aqueous polymer dissolutions for 5 min. at room temperature.

7.2.4 Detection of Cholera Toxin Subunit B at Different Concentrations

The previous results showed a distinguishable SWV and EIS electrochemical signal when a modified electrode was incubated in a $4.33 \cdot 10^{-5}$ M CTB aqueous dissolution. The next goal was detecting the presence of the pentamer at different concentrations. When a freshly prepared CTB stock solution was used, the electrochemical response obtained after the incubation of Au-pAH_{50}-RO-Gal_{15} **(Figure 7.13)** was weaker than earlier. With SWV **(Figure 7.13-A)**, the attenuation of the probe's signal observed from Au-pAH_{50}-RO-Gal_{15}-CTB was less significant than when the previous CTB stock solution was used **(Figure 7.11)**. Regarding EIS **(Figure 7.13-B)**, although there was an impedance increment after the electrode incubation in the fresh CTB dissolution, the variation was much smaller than that observed in **Figure 7.12-B**.

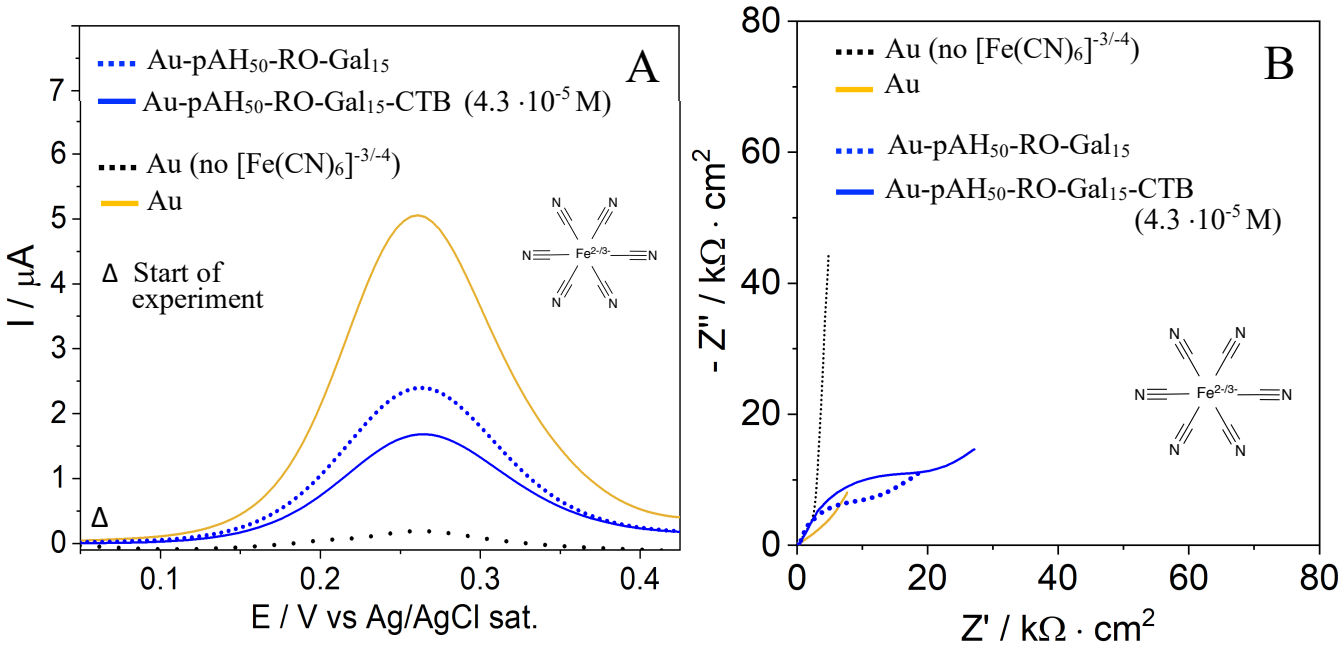


Figure 7.13. SWV and EIS responses of $[Fe(CN)_6]^{-3/-4}$ (0.5 mM) on a Au(poly) electrode modified with a glycosylated polymer (Au-pAH$_{50}$-RO-Gal$_{15}$) before (dotted blue scans) and after (solid blue scans) its incubation in a 4.33 ·10^{-5} M CTB fresh dissolution. **(A)** SWV showed the reduction of the probe's signal (solid yellow curve) after polymer modification (dotted blue scan) and a further dampening after 5 min. incubation in CTB (solid blue curve). **(B)** In the EIS experiments, done immediately after the equivalent SWV scans, there was an impedance increment after the modified electrode was incubated in the CTB dissolution. Electrochemical conditions: phosphate buffer (0.1 M, pH 7.4) electrolyte; SWV sweeps run at 5 Hz frequency, 5 mV step E and an amplitude of 25 mV; EIS scans were operated between 65,353 and 1 Hz with a set E of 148 mV and an amplitude of 10 mV.

Despite the smaller analytical signal acquired with the newly-prepared CTB stock solution, it was deemed still significant to attempt the detection of the protein at concentrations below 4.3 ·10^{-5} M. Dilutions of fresh CTB dissolution were made and SWV and EIS were used to try to sense the protein at 4.3 ·10^{-5} M, 7.2 ·10^{-6} M, 3.6 ·10^{-6} M, 3.6 ·10^{-7} M and 3.6 ·10^{-8} M **(Figure 7.14)**.

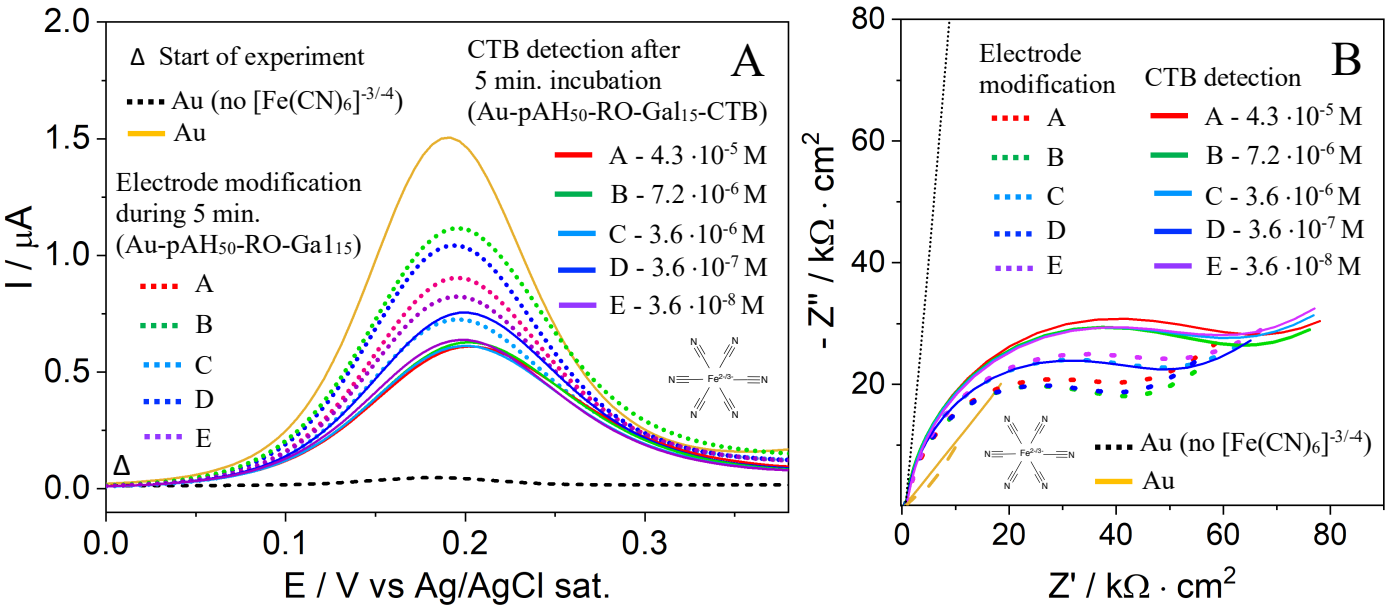


Figure 7.14. Detection with SWV **(A)** and EIS **(B)** of CTB in aqueous dissolutions at different concentrations (4.3 ·10^{-5}, 7.2 ·10^{-6}, 3.6 ·10^{-6}, 3.6 ·10^{-7} and 3.6 ·10^{-8} M) using $[Fe(CN)_6]^{-3/-4}$ (0.5 mM) as a redox mediator. Before measuring each concentration, the electrode was cleaned and modified with the pAH_{50}-RO-Gal_{15} glycopolymer. On both panels, dotted curves pertain to the SWV and EIS experiments done to characterise the modified electrode, which preceded the corresponding measurements of CTB concentrations (solid lines). In all instances, a SWV scan was conducted first and was immediately followed by its equivalent EIS sweep. Electrochemical conditions: phosphate buffer (0.1 M, pH 7.4) electrolyte; SWV scans performed with a frequency of 5 Hz, a step E of 5 mV and an amplitude of 25 mV; EIS experiments run between 65,353 and 1 Hz with a set E of 148 mV and an amplitude of 10 mV.

Controls with water **(Figure 7.15)** were done to verify the results obtained with different concentrations of CTB. First, the electrode was functionalised with the glycopolymer (Au-pAH_{50}-RO-Gal_{15}) and characterised with SWV and EIS, in this order as customary in this thesis. Then, the electrode was immersed in pure water for 5 min. and SWV and EIS were again recorded (Au-pAH_{50}-RO-Gal_{15} + H_2O). Finally, the electrode was incubated in two CTB dissolutions (4.3 ·10^{-5} M or 3.6 ·10^{-8} M) for another 5 minutes (Au-pAH_{50}-RO-Gal_{15}-CTB) before conducting SWV and EIS. As previously

in this work, the electrode modification with the polymer reduced the mediator's signal in SWV (dotted red and blue scans, **Figure 7.15-A**) and increased the impedance in EIS (dotted red and blue overlapping scans, **Figure 7.15-B**). The posterior dipping in water (dashed red curves and dashed blue curves) provoked a further drop of current intensity in SWV, while in EIS divergent results were observed: in one experiment impedance increased (dashed red scan) and in the other not (dashed blue scan). The intensity drop of the $[Fe(CN)_6]^{-3/-4}$ SWV signal after water immersion may have been caused by a rearrangement of macromolecules on the electrode's surface that increased its blockage. But the results obtained in EIS could not fully support this explanation given the mismatch of outcomes. After the water submersion measurements, the electrode was dipped in a $4.3 \cdot 10^{-5}$ M or in a $3.6 \cdot 10^{-8}$ M CTB aqueous dissolution and the electrochemical responses were recorded. When the electrode was incubated in the most concentrated dissolution, the interaction of protein molecules with the polymer further blocked the access of the probe to the electrode's surface, reducing the SWV intensity signal (solid red curve, **Figure 7.15-A**) and increasing the impedance (solid red curve, **Figure 7.15-B**). However, these effects were not observed when the concentration was $3.6 \cdot 10^{-8}$ M (solid blue scans). Perhaps, in this case, CTB-glycopolymers interaction was not big enough to block the probe as before and, instead, somehow, disturbed the arrangement of macromolecules facilitating the access of the mediator to the electrode surface.

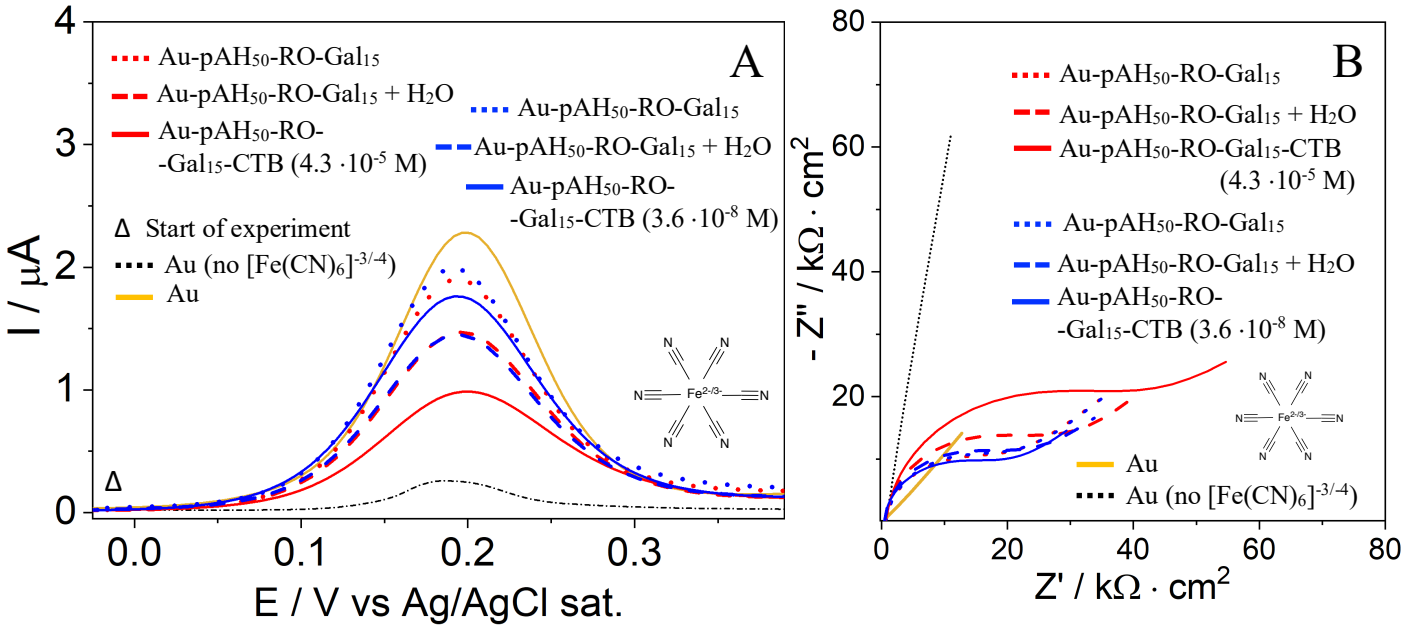


Figure 7.15. Study with SWV **(A)** and EIS **(B)** of the effect of submerging in water an electrode modified with pAH_{50}-RO-Gal_{15} before attempting the detection of CTB with the redox mediator $[Fe(CN)_6]^{-3/-4}$ (0.5 mM). The outcome was examined with two different concentrations of CTB: $4.3 \cdot 10^{-5}$ M (red scans) and $3.6 \cdot 10^{-8}$ M (deep blue scans). In both cases, the electrode was first modified with the glycosylated polymer (Au-pAH_{50}-RO-Gal_{15}, dotted scans); then immersed in pure water for 5 min. (Au-pAH_{50}-RO-Gal_{15} + H_2O, dashed scans); and finally incubated in the CTB dissolution (Au-pAH_{50}-RO-Gal_{15}-CTB, solid scans). Each SWV experiment was immediately followed by the correspondent EIS sweep. Electrochemical conditions: phosphate buffer (0.1 M, pH 7.4) electrolyte; SWV experiments completed at a 5 Hz frequency with a step E of 5 mV and an amplitude of 25 mV; EIS sweeps were carried out between 65,353 and 1 Hz, setting a E of 148 mV and an amplitude of 10 mV.

When the incubation was performed after water immersion and with an even lower concentration of CTB, $3.6 \cdot 10^{-9}$ M, SWV **(Figure 7.16-A)** was unable to detect the presence of the protein: there was an almost perfect overlapping of the scans carried out after water immersion (dashed, light blue curve) and CTB incubation (solid, light blue curve). Contrary to SWV, where the dipping of Au-pAH_{50}-RO-Gal_{15} in water

significantly attenuated the probe's signal (dashed, light blue curve), the results of EIS analysis **(Figure 7.16-B)** did not show a meaningful variation of signal, impedance. And, as it happened with SWV, EIS was also unable to detect CTB after incubation in the 3.6 $\cdot 10^{-9}$ M CTB dissolution (solid, light blue scan). The results in **Figure 7.15 and Figure 7.16** suggested that the Au-pAH$_{50}$-RO-Gal$_{15}$ platform for detecting CTB had a detection limit, after water immersion, of between 4.3 $\cdot 10^{-5}$ and 3.6 $\cdot 10^{-8}$ M with SWV and EIS.

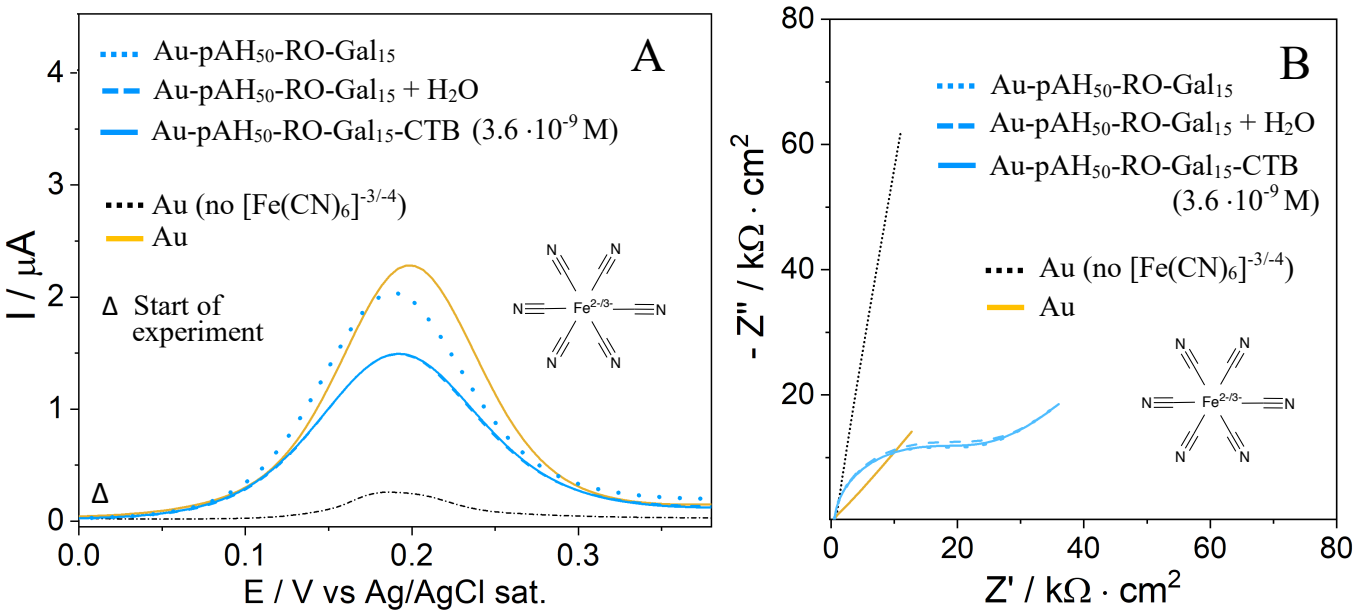


Figure 7.16. SWV **(A)** and EIS **(B)** electrochemical investigation with $[Fe(CN)_6]^{-3/-4}$ 0.5 mM of the effect caused by the submerging a modified electrode (Au-pAH$_{50}$-RO-Gal$_{15}$) in water before using it for detecting CTB in a 3.6 $\cdot 10^{-9}$ M aqueous dissolution. First, the electrode was modified with the glycosylated polymer (Au-pAH$_{50}$-RO-Gal$_{15}$, dotted light blue scans) and electrochemically analysed. Then, the functionalised transducer was dipped in pure water for 5 min. (Au-pAH$_{50}$-RO-Gal$_{15}$ + H_2O, dashed light blue outlines) and characterised again. Lastly, the electrode was incubated for a further 5 min. in a 3.6 $\cdot 10^{-9}$ M CTB dissolution (Au-pAH$_{50}$-RO-Gal$_{15}$-CTB, solid light blue curves) and electrochemically examined. Each SWV sweep was immediately followed by its corresponding EIS scan. Electrochemical conditions: phosphate buffer (0.1 M, pH 7.4) electrolyte; SWV sweep run with a 5 Hz frequency, step E of 5 mV and amplitude of 25 mV; EIS was operated between 65,353 and 1 Hz with a set E of 148 mV and an amplitude of 10 mV.

Thinking of a commercial impedimetric device based on this design, data were plotted to visualise the possibility of applying a single or a shorter range of frequencies to detect CT with simpler measurements. **Figure 7.17** displays the imaginary part of impedance *versus* applied frequency. In all measurements done with an electrode modified with the polymer pAH_{50}-RO-Gal_{15}, including some to detect CTB, emerged a peak between 10 and 20 Hz that could be used for sensing purposes and opened the possibility of shortening the frequency range applied to reduce the analysis time.

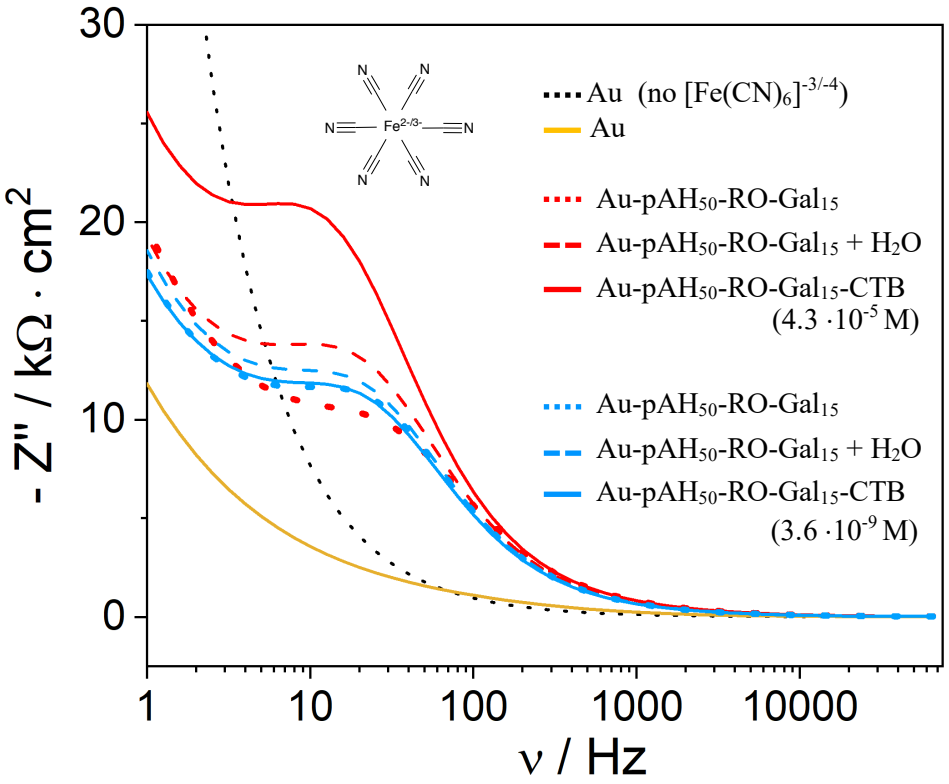


Figure 7.17. Bode plot (from 1 to 65,535 Hz) of the imaginary part (-Z'') of several EIS experiments where $[Fe(CN)_6]^{-3/-4}$ 0.5 mM was used as an electrochemical mediator. In scans obtained with an electrode modified with pAH_{50}-RO-Gal_{15}, including experiments for the detection of CTB, a peak appeared at approximately 20 Hz. Therefore, a short frequency range may be used to impedimetrically detect CTB. Electrochemical conditions: phosphate buffer (0.1 M, pH 7.4) electrolyte; EIS experiments performed in a 65,353 to 1 Hz frequency range with a 148 mV set E and 10 mV amplitude.

7.3 Conclusions

The results presented in **Chapter 7** suggest the possibility of electrochemically detecting CTB in aqueous solutions with Au(poly) electrodes functionalised with glycosylated polymers (pAH_n-OR-Gal_{15}).

SWV and EIS were selected to study the modification of Au(poly) electrodes and attempt the detection of CTB in aqueous dissolutions given their better sensitivity than CV. Of the two electrochemical mediators employed to enhance the analytical signal, $[Fe(CN)_6]^{-3/-4}$ appeared to be best suited owing to lesser interactions with the modified electrodes. Throughout the experiments of this chapter, SWV and EIS results appeared to agree.

When SWV was used to scan Au-pAH_{50}-RO-Gal_{15}, a noticeable decrease of the $[Fe(CN)_6]^{-3/-4}$ signal was detected compared to a bare electrode; in EIS, an increment of the impedance was seen. Nevertheless, neither response seemed to be correlated with the time of modification of the electrode **(Figure 7.10)**. However, it appeared that with shorter electrode modification times (*e.g.* 5 min.), the electrochemical signal after CTB incubation was higher. This effect was observed in EIS **(Figure 7.12-B)** and, to a minor extent, in SWV **(Figure 7.11)**.

Regarding the detection of CTB, the incubation of Au-pAH_{50}-RO-Gal_{15} in $4.3 \cdot 10^{-5}$ M concentrations of the protein for 5 min. produced a change in the analytical signals: attenuation of the current intensity peak in SWV and a rise of a semi-circle

resistance in EIS. However, when lower concentrations were used, the SWV response seemed not to change according to **Figure 7.14-A**, whilst the EIS data may allow quantitative analysis per **Figure 7.14-B**. Besides, water incubation of the modified electrode previous CTB measurements may have a negative effect on the analytical signal **(Figure 7.15)**. Lastly, EIS detection at different concentrations should be further explored just in a frequency range between 5 and 30 Hz, where the appearance of a characteristic peak **(Figure 7.17)** may help to simplify the measurements.

To conclude, the glycosensor presented in this thesis appeared to be capable of detecting CTB in aqueous dissolutions at concentrations of at least $3.6 \cdot 10^{-8}$ M with SWV and EIS **(Figure 7.14)**, although further work is necessary to determine the effect of water in the impedimetric response **(Figure 7.15)**. Besides, it is still indispensable to assess the sensing capacities of the system in the presence of potential interferents, such as other proteins.

Chapter 8

Main Conclusions and Perspectives

This thesis summarises the efforts to develop a new electrochemical sensor to detect CT, the toxin of the bacterium *V. cholerae*. Cholera, the disease caused by this microorganism's toxin, is still endemic in many countries and affects tens of millions of people. Unfortunately, current methods for detecting *V. cholerae* are not particularly suitable or effective in those regions most affected by the disease due to their cost, complexity, or time of analysis. Many biosensors have been proposed as substitutes but they all present significant shortcomings, such as complex layouts that make their use in these areas difficult.

Consequently, this work has described the first stages of the construction of an electrochemical glycosensor as a better alternative. The device tries to mimic the mechanism through which CT recognises human cells of the intestine to infect a host. One of the main advantages of the proposed design is using simple and inexpensive saccharides, *i.e.* Gal and Lac, as BRE. In addition, the employment of polymers as linkers of the BRE endows more flexibility for constructing the biosensor.

8.1 Main Conclusions

Herein are the main findings of this thesis.

Chapter 5 was devoted to using small molecules as linkers between the BRE (Gal) and the transducer (a Au(poly) disk electrode) of the new electrochemical glycosensor for detecting CTB. The first molecule utilised was DPA-HD. Although attempts were made to form SAMs of DPA-HD on a Au(poly) electrode to link Gal on them afterwards, the adsorption of hydrazide groups on Au per CV **(Figure 5.8)** made infeasible the obtainment of homogeneous SAMs on this metal. Furthermore, it could compromise the linkage between the hydrazide groups and sugars. An alternative could have been chemically linking DPA-HD with Gal and then producing SAMs of DPA-HD-Gal. But the coupling produced amphiphilic molecules (**Scheme 4.7** and **Figure 5.15**) very difficult to dissolve. Therefore, it made the modification of a Au electrode from solution very challenging, if not impossible. Finally, the endeavours to employ DPA-HD as a linker uncovered the importance of considering the formation of salts during the synthesis of hydrazides. The presence of a counter-anion can profoundly affect their chemical properties and electrochemical behaviour.

Experiments in **Chapter 6** demonstrated that pAH_n polymers adsorb fast and efficiently on Au(poly) electrodes from aqueous dissolution. The polymeric layers obtained were electrochemically stable in a wide potential window, from -0.20 to +0.50 V *vs* Ag/AgCl (*e.g.* **Figure 6.5-A**), which allows their use as sensing platforms. The macromolecules still maintained that same stability after pAH_n glycosylation with Gal

and Lac, *e.g.* **Figure 6.8-A** and **Figure 6.18-A**. Cyclic voltammograms hinted that pAH_n macromolecules -glycosylated or not- adsorbed on a Au electrode through the thiol group of one of their ends, according to the position of the reductive stripping in several plots (*e.g.* **Figure 6.18-B**). Nevertheless, it could not be ruled out the possibility of further interactions through hydrazide groups **(Figure 5.8)** or even sugar groups **(Figure 6.9)**. Throughout **Chapter 6**, it was also evidenced that CV is not an ideal characterisation technique to study adsorbed polymeric layers. Beyond some information about surface blockage and electrochemical potential stability, it did not explain the arrangement of macromolecules, the surface coverage of the electrode or the quantity of BRE (Gal) chemically attached to it.

In **Chapter 7**, SWV and EIS were employed to detect CTB from aqueous dissolutions given their higher sensitivity. Throughout this chapter the results obtained with both techniques were almost always in good agreement. It was demonstrated that the redox probe FcMeOH significantly interacted with the glycosylated polymer pAH_{50}-OR-Gal_{15} adsorbed on Au **(Figure 7.7)**, compromising its use as an electrochemical mediator for the detection of CTB. Contrariwise, this did not seem to occur with the redox couple $[Fe(CN)_6]^{-3/-4}$ **(Figure 7.9)**.

The best analytical signal for the detection of CTB with $[Fe(CN)_6]^{-3/-4}$ as redox mediator was obtained when Au(poly) electrodes were modified with pAH_{50}-OR-Gal_{15} for a short period of time (5 min.), especially when EIS was utilised **(Figure 7.12)**. The incubation of Au-pAH_{50}-Gal_{15} in CTB dissolutions for 5 min. produced a SWV response that allowed the detection of CTB at concentrations of at least $3.6 \cdot 10^{-8}$ M

(Figure 7.14-A). But these results also appeared to indicate that this technique would not allow quantitative analysis. Instead, EIS may enable it= at an even lower concentration **(Figure 7.14-B).**

There also seemed to be an effect in dipping a modified electrode (Au-pAH$_{50}$-RO-Gal$_{15}$) in water before attempting CTB detection. It probably produced a rearrangement of the adsorbed polymers, which further blocked the electrode surface. This was observed in current intensity drops in SWV experiments and impedance increases **(Figures 7.15 and 7.16)** and appeared to affect the sensor's sensitivity. Lastly, the impedimetric detection of CTB looked to be feasible applying a single or a small range of frequencies around 20 Hz **(Figure 7.17)**, which would help to reduce the time of analysis substantially.

8.2 Perspectives

Despite SAMs of small molecules being the most common platform to immobilise BRE on Au(poly) electrodes, this work has shown that polymers containing a thiol end group can be an excellent alternative. Nevertheless, several experiments revealed a notable lack of reproducibility that should be addressed. For example, in scans related to electrode modification with polymers, like the reductive stripping of Au-pAH$_n$ (*e.g.* **Figure 6.5-B**), the SWV current intensity decrease of $[Fe(CN)6]^{-3/-4}$ (*e.g.* **Figure 7.10-A**) or the EIS Nyquist plots (*e.g.* **Figure 7.12-A**). Easy steps to improve this issue could be using monocrystals to eliminate the inhomogeneities produced by grain boundaries and the presence of different faces of Au on the electrode surface. Or the employment

of sheathed electrodes to reduce the inaccuracies of a surface area dependent on the formation of a hanging meniscus. Besides, it would be helpful to use techniques such as AFM, ATR-SEIRAS or scanning electrochemical microscopy (SECM) to characterise the adsorption of the polymers adequately. This may help understand the final arrangement of the macromolecules on the electrode, unveil some of the sources of irreproducibility, and better comprehend the electrochemical response of the platform.

Once it has been demonstrated that pAH_n can be employed to immobilise Gal on Au electrodes, work could be done to optimise the glycosylation of the polymer, for example, establishing any dependence between polymer sugar loading and CTB detection. Tests could also be performed with different sizes of polymer. Another significant step aiming to enhance the sensitivity of the sensor could be incorporating other sugars to pAH_n, like N-acetylneuraminic acid, to improve the mimicry of the GM1 structure.

Although SWV and EIS have demonstrated that Au-pAH_5 -Gal_{15} can detect CTB in aqueous dissolutions of at least $3.6 \cdot 10^{-8}$ M, it is essential to study the effect of interferents on the selectivity of the sensor, for example with other proteins like BSA.

Finally, micro or macroelectrodes with AuNP functionalised with pAH_n-Gal polymers could be tried to increase the device's sensitivity.

References

1. WHO, https://bit.ly/foodbornediseaseWHO, (accessed April 2020).
2. M. B. Batz, S. Hoffmann and J. G. Morris, Jr., *J. Food Prot.*, 2012, **75**, 1278-1291.
3. T. Bintsis, *AIMS Microbiol.*, 2017, **3**, 529-563.
4. WHO, https://bit.ly/GlobalHungerWHO, (accessed April 2020).
5. World Bank, https://bit.ly/Percentage-Open-Defecation--World-Bank, (accessed April 2020).
6. WHO, https://bit.ly/CausesofFoodborne_WHO, (accessed April 2020).
7. J. L. Smith, *J. Food Prot.*, 1999, **62**, 818-829.
8. S. M. C. E. Scallan, A. Runkle, O. L. Henao, B. E. Mahon, R. M. Hoekstra, and P. M. Griffin, *Foodborne Pathog. Dis.*, 2015, **12**, 492-499.
9. B. M. Lund and S. J. O'Brien, *Foodborne Pathog. Dis.*, 2011, **8**, 961-973.
10. WHO, https://bit.ly/FoodborneChildrenDeaths_WHO, (accessed April 2020).
11. A. K. Jones, P. Cross, M. Burton, C. Millman, S. J. O'Brien and D. Rigby, *PLoS One*, 2017, **12**, e0175816.
12. FSA, https://bit.ly/FoodborneDiseaseBurdenUK, (access April 2020).
13. University of Liverpool, https://bit.ly/FoodborneUKestimates, (accessed April 2020).
14. R. L. Scharff, *J. Food Prot.*, 2012, **75**, 123-131.
15. J. A. Roberts, P. Cumberland, P. N. Sockett, J. Wheeler, L. C. Rodrigues, D. Sethi, P. J. Roderick and E. Infectious Intestinal Disease Study, *Epidemiol. Infect.*, 2003, **130**, 1-11.
16. J. C. Buzby and T. Roberts, *World Health Statistics Quarterly*, 1997, **50**, 57-66.
17. WHO, https://bit.ly/TerroristThreatstoFood, (accessed April 2020).
18. FSA, https://bit.ly/FoodborneDiseaseBurdeninUK, (accessed April 2020).

19. Government of Alberta, https://bit.ly/FoodSafetyDefinition, (accessed April 2020).

20. FSA, https://www.food.gov.uk/, (accessed April 2020).

21. FDA, https://www.fda.gov/, (accessed April 2020).

22. EFSA, https://www.efsa.europa.eu/en/aboutefsa, (accessed April 2020).

23. S. Kalyoussef and K. N. Feja, *Adv. Pediatr.*, 2014, **61**, 287-312.

24. WHO, https://bit.ly/FoodborneDiseaseBurden, (accessed April 2020).

25. M. Addis and D. Sisay, *J. Trop. Dis.*, 2015, **4**.

26. FSA, https://bit.ly/FoodborneUK2018, (accessed April 2020).

27. D. Holland, L. Thomson, N. Mahmoudzadeh and A. Khaled, *BMJ Open Gastroenterol*, 2020, **7**, e000377.

28. BBC, https://bit.ly/CampylobacterUK, (accessed April 2020).

29. S. J. O'Brien, T. L. Larose, G. K. Adak, M. R. Evans and C. C. Tam, *BMJ Open*, 2016, **6**, e011119.

30. BBC, https://bbc.in/3pidNVI, (accessed May 2020).

31. J. Hoorfar, *Rapid Detection, Characterization, and Enumeration of Foodborne Pathogens*, American Society for Microbiology, APMIS, 2011.

32. P.-G. Lantz, B. Hahn-Hägerdal and P. Rådström, *Trends Food Sci. Technol.*, 1994, **5**, 384-389.

33. CDC, https://www.cdc.gov/cholera/diagnosis.html, (accessd May 2020).

34. H. J. Chung, C. M. Castro, H. Im, H. Lee and R. Weissleder, *Nat. Nanotechnol.*, 2013, **8**, 369-375.

35. M. Alam, N. A. Hasan, M. Sultana, G. B. Nair, A. Sadique, A. S. G. Faruque, H. P. Endtz, R. B. Sack, A. Huq, R. R. Colwell, H. Izumiya, M. Morita, H. Watanabe and A. Cravioto, *J. Clin. Microbiol.*, 2010, **48**, 3918.

36. S. J. Krebs and R. K. Taylor, *Microbiology*, 2011, **157**, 2942-2953.

37. K. H. Keddy, A. Sooka, M. B. Parsons, B. M. Njanpop-Lafourcade, K. Fitchet and A. M. Smith, *J. Infect. Dis.*, 2013, **208**, S23-S31.

38. D. C. Griffith, L. A. Kelly-Hope and M. A. Miller, *Am. J. Trop. Med.*, 2006, **75**, 973-977.

39. M. Ali, A. R. Nelson, A. L. Lopez and D. A. Sack, *PLOS Negl. Trop. Dis.*, 2015, **9**, e0003832.

40. J. W. Law, N. S. Ab Mutalib, K. G. Chan and L. H. Lee, *Front. Microbiol.*, 2014, **5**, 770.

41. A. K. B. P. K. Mandal, K. Choi and U. K. Pal, *Am. J. Food Technol.*, 2011, **6**, 87-102.

42. Y. Wang and J. K. Salazar, *Compr. Rev. Food Sci. Food Saf.*, 2016, **15**, 183-205.

43. S. Ayyash, W.-I. Wu and P. R. Selvaganapathy, *Sensors*, 2016, **16**, 1879.

44. L. Garibyan and N. Avashia, *J. Invest. Dermatol.*, 2013, **133**, 1-4.

45. J. Maurer, *PCR methods in foods*, Springer Science & Business Media, USA, 2006.

46. P. I. Fields, T. Popovic, K. Wachsmuth and O. Olsvik, *J. Clin. Microbiol.*, 1992, **30**, 2118.

47. A. J. Gubala, *J. Microbiol. Methods*, 2006, **65**, 278-293.

48. A. C. Wennberg, Master Thesis, Norwegian University of Science and Technology, 2009.

49. T. Notomi, H. Okayama, H. Masubuchi, T. Yonekawa, K. Watanabe, N. Amino and T. Hase, *Nucleic Acids Res.*, 2000, **28**, E63-E63.

50. K. Okada, S. Chantaroj, T. Taniguchi, Y. Suzuki, A. Roobthaisong, O. Puiprom, T. Honda and P. Sawanpanyalert, *Diagn. Microbiol. Infect. Dis.*, 2010, **66**, 135-139.

51. M. Severgnini, P. Cremonesi, C. Consolandi, G. De Bellis and B. Castiglioni, *Food Bioproc. Tech.*, 2011, **4**, 936-953.

52. E. Engvall and P. Perlmann, *Protides Biol. Fluids*, 1971, 553-556.

53. E. Engvall and P. Perlmann, *J. Immunol.*, 1972, **109**, 129.

54. C.-W. L. Xihong Zhao, Jun Wang, Deog Hwan Oh, *J. Microbiol. Biotechnol.* , 2014, **24**, 297 - 312.

55. M. M. Archibald, B. Rizal, T. Connolly, M. J. Burns, M. J. Naughton and T. C. Chiles, *Biosens. Bioelectron.*, 2015, **74**, 406-410.

56. B. K. Kumar, P. Raghunath, D. Devegowda, V. K. Deekshit, M. N. Venugopal, I. Karunasagar and I. Karunasagar, *Int. J. Food Microbiol.*, 2011, **145**, 244-249.

57. Abingdon, https://bit.ly/Lateralflowtestexplained, (accessed May 2020).

58. B. Flower, J. C. Brown, B. Simmons, M. Moshe, R. Frise, R. Penn, R. Kugathasan, C. Petersen, A. Daunt, D. Ashby, S. Riley, C. J. Atchison, G. P. Taylor, S. Satkunarajah, L. Naar, R. Klaber, A. Badhan, C. Rosadas, M. R. Khan, N. Fernandez, M. Sureda-Vives, H. M. Cheeseman, J. Hara, G. Fontana, S. J. C. Pallett, M. Rayment, R. Jones, L. S. P. Moore, M. O. McClure, P. Cherepanov, R. Tedder, H. Ashrafian, R. Shattock, H. Ward, A. Darzi, P. Elliot, W. S. Barclay and G. S. Cooke, *Thorax*, 2020, **75**, 1082.

59. B. B. Dzantiev, N. A. Byzova, A. E. Urusov and A. V. Zherdev, *Trends Analyt. Chem.*, 2014, **55**, 81-93.

60. M. Sajid, A.-N. Kawde and M. Daud, *J. Saudi Chem. Soc.*, 2015, **19**, 689-705.

61. U. Tuteja, S. Kumar, J. Shukla, J. Kingston and H. V. Batra, *J. Med. Microbiol.*, 2007, **56**, 1340-1345.

62. T. Ramamurthy, B. Das, S. Chakraborty, A. K. Mukhopadhyay and D. A. Sack, *Vaccine*, 2020, **38**, A73-A82.

63. S. Hosseini, P. Vázquez-Villegas, M. Rito-Palomares and S. O. Martinez-Chapa, in *Enzyme-linked Immunosorbent Assay (ELISA): From A to Z*, eds. S. Hosseini, P. Vázquez-Villegas, M. Rito-Palomares and S. O. Martinez-Chapa, Springer Singapore, Singapore, ch. 5, pp. 67-115.

64. J. R. Couchman, *Journal of J. Histochem. Cytochem.Cytochemistry*, 2009, **57**, 7-8.

65. Labome, https://www.labome.com/method/PCR-Machines.html, (accessed May 2020).

66. S. Neethirajan, V. Ragavan, X. Weng and R. Chand, *Biosensors*, 2018, **8**, 23.

67. D. R. Matthews, E. Bown, A. Watson, R. R. Holman, J. Steemson, S. Hughes and D. Scott, *Lancet*, 1987, **329**, 778-779.

68. B. M. Paddle, *Biosens. Bioelectron.*, 1996, **11**, 1079-1113.

69. R. Reyes, R. Ahn, K. Thurber and T. F. Burke, in *Challenges in Infectious Diseases*, ed. I. W. Fong, Springer Science and Business Media, New York, 2013, ch. 4, pp. 123-146.

70. E. K. Silbergeld, J. Graham and L. B. Price, *Annu. Rev. Public Health*, 2008, **29**, 151-169.

71. E. Hartnett, A. Adkin, M. Seaman, J. Cooper, E. Watson, H. Coburn, T. England, C. Marooney, A. Cox and M. Wooldridge, *Risk Anal.*, 2007, **27**, 187-202.

72. F. L. Bryan, *J. Food Prot.*, 1988, **51**, 663-673.

73. C. P. D. Sousa, *Braz. Arch. Biol. Technol.*, 2008, **51**, 615-623.

74. G. Constantin de Magny, R. Murtugudde, M. R. Sapiano, A. Nizam, C. W. Brown, A. J. Busalacchi, M. Yunus, G. B. Nair, A. I. Gil, C. F. Lanata, J. Calkins, B. Manna, K. Rajendran, M. K. Bhattacharya, A. Huq, R. B. Sack and R. R. Colwell, *PNAS USA*, 2008, **105**, 17676-17681.

75. S. Paz, *Ecohealth*, 2009, **6**, 340-345.

76. R. Reyburn, D. R. Kim, M. Emch, A. Khatib, L. von Seidlein and M. Ali, *Am. J. Trop. Med. Hyg.*, 2011, **84**, 862-869.

77. E. K. Lipp, A. Huq and R. R. Colwell, *CMR*, 2002, **15**, 757.

78. New York Times, https://nyti.ms/32WJuet, (accessed May 2020).

79. M. A. Morales and J. M. Halpern, *Bioconjugate Chem.*, 2018, DOI: 10.1021/acs.bioconjchem.8b00592.

80. R. Monošík, M. Streďanský and E. Šturdík, *Acta Chim. Slov.*, 2012, **5**, 109-120.

81. N. Bhalla, P. Jolly, N. Formisano and P. Estrela, *Essays Biochem.*, 2016, **60**, 1-8.

82. D. R. Thévenot, K. Toth, R. A. Durst and G. S. Wilson, *Biosens. Bioelectron.*, 2001, **16**, 121-131.

83. N. Olson and J. Bae, *Sensors*, 2019, **19**, 2615.

84. M. A. Alonso-Lomillo, O. Dominguez-Renedo and M. J. Arcos-Martinez, *Talanta*, 2010, **82**, 1629-1636.

85. J. Monzo, I. Insua, F. Fernandez-Trillo and P. Rodriguez, *Analyst*, 2015, **140**, 7116-7128.

86. P. Arora, A. Sindhu, N. Dilbaghi and A. Chaudhury, *Biosens. Bioelectron.*, 2011, **28**, 1-12.

87. L. C. Clark and C. Lyons, *Ann. N.Y. Acad. Sci.*, 2006, **102**, 29-45.

88. J. Lago, L. P. Rodríguez, L. Blanco, J. M. Vieites and G. Cabado, *Mar. Drugs*, 2015, **13**.

91. M. S. Chiriacò, E. Primiceri, E. D'Amone, R. E. Ionescu, R. Rinaldi and G. Maruccio, *Lab Chip*, 2011, **11**, 658-663.

90. S. A. Khan, J. A. DeGrasse, B. J. Yakes and T. R. Croley, *Anal. Chim. Acta*, 2015, **892**, 167-174.

91. J. G. Bruno and J. L. Kiel, *BioTechniques*, 2002, **32**, 178-183.

92. T. Kubo, M. Nomachi, K. Nemoto, T. Sano, K. Hosoya, N. Tanaka and K. Kaya, *Anal. Chim. Acta*, 2006, **577**, 1-7.

93. D. Jeong, K.-S. Ahn and W.-Y. Lee, *J. Electroanal. Chem.*, 2017, **806**, 123-129.

94. S.-H. Tark, A. Das, S. Sligar and V. P. Dravid, *Nanotechnology*, 2010, **21**, 435502.

95. S. Viswanathan, L.-c. Wu, M.-R. Huang and J.-a. A. Ho, *Anal. Chem.*, 2006, **78**, 1115-1121.

96. J. J. Pan and D. Charych, *Langmuir*, 1997, **13**, 1365-1367.

97. C. Byeungsoo, E. Hideaki, H. Tetsuhito, N. Yuuji and W. Etsuo, *Biosens. Bioelectron.*, 1996, **11**, 1185-1191.

98. H. J. Lin, P. T. Charles, J. D. Andreadis, A. M. Churilla, D. A. Stenger and J. J. Pancrazio, *Anal. Chim. Acta*, 2002, **457**, 97-108.

99. M. L. Frisk, W. H. Tepp, E. A. Johnson and D. J. Beebe, *Anal. Chem.*, 2009, **81**, 2760-2767.

100. M. Tolba, M. U. Ahmed, C. Tlili, F. Eichenseher, M. J. Loessner and M. Zourob, *Analyst*, 2012, **137**, 5749-5756.

101. P. D. Skottrup, M. Nicolaisen and A. Justesen, *Biosens. Bioelectron.*, 2008, **24**, 339-348.

102. N. Bojorge Ramírez, A. M. Salgado and B. Valdman, *Braz. J. Chem. Eng.*, 2009, **26**, 227-249.

103. B. Lu, M. R. Smyth and R. O'Kennedy, *Analyst*, 1996, **121**, 29R-32R.

104. J. Credou and T. Berthelot, *J. Mater. Chem. B.*, 2014, **2**, 4767-4788.

105. M. P. Arora, in *Biomolecules*, Himalaya Pub. House, Mumbai, 2009, ch. 9, pp. 124-134.

106. H.-J. Gabius, S. André, J. Jiménez-Barbero, A. Romero and D. Solís, *Trends Biochem. Sci.*, 2011, **36**, 298-313.

107. J. D. Esko, K. Kimata and U. Lindahl, in *Essentials of glycobiology*, ed. A. Varki, R. D. Cummings, J. D. Esko, H. H. Freeze, P. Stanley, C. R. Bertozzi, G. W. Hart and M. E. Etzler, Cold Spring Harbor Laboratory Press, Cold Spring Harbor (NY), 3rd edn, 2009, ch. 7.

108. G. A. Rabinovich and M. A. Toscano, *Nat. Rev. Immunol.*, 2009, **9**, 338-352.

109. A. Varki, *Glycobiology*, 2016, **27**, 3-49.

110. C. R. Bertozzi and L. L. Kiessling, *Science*, 2001, **291**, 2357.

111. J. D. Esko, K. Kimata and U. Lindahl, in *Essentials of glycobiology*, ed. A. Varki, R. D. Cummings, J. D. Esko, H. H. Freeze, P. Stanley, C. R. Bertozzi, G. W. Hart and M. E. Etzler, Cold Spring Harbor Laboratory Press, Cold Spring Harbor (NY), 3rd edn, 2009, ch. 2.

112. Z. J. Witczak, in *Glycoscience: Chemistry and Chemical Biology*, ed. B. O. Fraser-Reid, K. Tatsuta and J. Thiem, Springer Berlin Heidelberg, Berlin, Heidelberg, 2008, ch. 18, pp. 815-840.

113. P. H. Seeberger, in *Essentials of Glycobiology [internet]*, ed. A. Varki, R. D. Cummings, J. D. Esko, P. Stanley, G. W. Hart, M. Aebi, A. G. Darvill, T. Kinoshita, N. H. Packer and J. H. Prestegard, Cold Spring Harbor Laboratory Press, Cold Spring Harbor (NY), 2015, ch. 2.

114. R. U. Lemieux, *Pure Appl. Chem.*, 1971, **25**, 527-548.

115. G. P. Moss, *Pure Appl. Chem.*, 1996, **68**, 2193-2222.

116. E. Juaristi and G. Cuevas, *Tetrahedron*, 1992, **48**, 5019-5087.

117. K. B. Wiberg, W. F. Bailey, K. M. Lambert and Z. D. Stempel, *J. Org. Chem.*, 2018, **83**, 5242-5255.

118. A. Varki, R. D. Cummings, J. D. Esko, P. Stanley, G. W. Hart, M. Aebi, A. G. Darvill, T. Kinoshita, N. H. Packer and J. H. Prestegard, in *Essentials of Glycobiology [internet]*, Cold Spring Harbor Laboratory Press, 2015, ch. 2.

119. O. Blixt, S. Head, T. Mondala, C. Scanlan, M. E. Huflejt, R. Alvarez, M. C. Bryan, F. Fazio, D. Calarese, J. Stevens, N. Razi, D. J. Stevens, J. J. Skehel, I. van Die, D. R. Burton, I. A. Wilson, R. Cummings, N. Bovin, C.-H. Wong and J. C. Paulson, *PNAS USA*, 2004, **101**, 17033-17038.

120. R. D. Cummings, R. L. Schnaar, J. D. Esko, K. Drickamer and M. E. Taylor, in *Essentials of glycobiology [Internet]*, eds. A. Varki, R. D. Cummings, J. D. Esko and e. al., Cold Spring Harbor Laboratory Press, Cold Spring Harbor (NY), 2017, ch. 29.

121. V. L. Tesh and A. D. O'Brien, *Mol. Microbiol.*, 1991, **5**, 1817-1822.

122. N. Verma and A. Bhardwaj, *Appl. Biochem. Biotechnol.*, 2015, **175**, 3093-3119.

123. O. Lazcka, F. J. Del Campo and F. X. Munoz, *Biosens Bioelectron*, 2007, **22**, 1205-1217.

124. N. J. Ronkainen, H. B. Halsall and W. R. Heineman, *Chem. Soc. Rev.*, 2010, **39**, 1747-1763.

125. H. Chen, Q.-Y. Hu, Z. Yue, J.-H. Jiang, G.-L. Shen and R.-Q. Yu, *Anal. Chim. Acta*, 2010, **657**, 204-209.

126. K. Ramanathan and B. Danielsson, *Biosens. Bioelectron.*, 2001, **16**, 417-423.

127. B. Danielsson, *J. Biotechnol.*, 1990, **15**, 187-200.

128. S. X. Wang and G. Li, *IEEE Trans. Magn.*, 2008, **44**, 1687-1702.

129. F. S. Ligler, C. R. Taitt, L. C. Shriver-Lake, K. E. Sapsford, Y. Shubin and J. P. Golden, *Anal. Bioanal. Chem.*, 2003, **377**, 469-477.

130. P. Damborský, J. Švitel and J. Katrlík, *Essays Biochem.*, 2016, **60**, 91-100.

131. W. Zhang, S. Zhu, R. Luque, S. Han, L. Hu and G. Xu, *Chem. Soc. Rev.*, 2016, **45**, 715-752.

132. C. Berggren, B. Bjarnason and G. Johansson, *Electroanalysis*, 2001, **13**, 173-180.

133. M. K. Patel, M. Azahar Ali, V. V. Agrawal, Z. A. Ansari, S. G. Ansari and B. D. Malhotra, *Appl. Phys. Lett.*, 2013, **102**, 144106.

134. J. M. Pingarrón, P. Yáñez-Sedeño and A. González-Cortés, *Electrochim. Acta*, 2008, **53**, 5848-5866.

135. Y. Wang, S. Sun, J. Luo, Y. Xiong, T. Ming, J. Liu, Y. Ma, S. Yan, Y. Yang, Z. Yang, J. Reboud, H. Yin, J. M. Cooper and X. Cai, *Microsyst. Nanoeng.*, 2020, **6**, 32.

136. W. Putzbach and N. J. Ronkainen, *Sensors*, 2013, **13**, 4811-4840.

137. LibreTexts;, Working Electrodes, https://bit.ly/WorkingElectrode, (accessed May 2020).

138. L. D. Burke and P. F. Nugent, *Gold Bull.*, 1997, **30**, 43-53.

139. J. C. Love, L. A. Estroff, J. K. Kriebel, R. G. Nuzzo and G. M. Whitesides, *Chem. Rev.*, 2005, **105**, 1103-1170.

140. M. D. Porter, T. B. Bright, D. L. Allara and C. E. D. Chidsey, *JACS*, 1987, **109**, 3559-3568.

141. J. Monzó, Y. Malewski, F. J. Vidal-Iglesias, J. Solla-Gullon and P. Rodriguez, *ChemElectroChem*, 2015, **2**, 958-962.

142. F. Patolsky, G. Zheng, O. Hayden, M. Lakadamyali, X. Zhuang and C. M. Lieber, *PNAS*, 2004, **101**, 14017-14022.

143. S. Dzyadevych and N. Jaffrezic-Renault, in *Biological Identification*, ed. R. P. Schaudies, Woodhead Publishing, 2014, ch. 6, pp. 153-193.

144. O. Kanoun, *Impedance Spectroscopy: Advanced Applications: Battery Research, Bioimpedance, System Design*, PB - De Gruyter, 2019.

145. J. Gonzalo Ruiz, PhD thesis, Universitat Autònoma de Barcelona, 2006.

146. A. Ahluwalia, D. De Rossi, C. Ristori, A. Schirone and G. Serra, *Biosens. Bioelectron.*, 1992, **7**, 207-214.

147. M. Labib, A. S. Zamay, O. S. Kolovskaya, I. T. Reshetneva, G. S. Zamay, R. J. Kibbee, S. A. Sattar, T. N. Zamay and M. V. Berezovski, *Anal Chem*, 2012, **84**, 8966-8969.

148. X. Li, L. Shen, D. Zhang, H. Qi, Q. Gao, F. Ma and C. Zhang, *Biosens. Bioelectron.*, 2008, **23**, 1624-1630.

149. I.-S. Park and N. Kim, *Biosens. Bioelectron.*, 1998, **13**, 1091-1097.

150. B. Ortiz, C. Saby, G. Y. Champagne and D. Bélanger, *J. Electroanal. Chem.*, 1998, **455**, 75-81.

151. Z. Bagheryan, J. B. Raoof, M. Golabi, A. P. F. Turner and V. Beni, *Biosens. Bioelectron.*, 2016, **80**, 566-573.

152. A.-E. Radi, X. Muñoz-Berbel, M. Cortina-Puig and J.-L. Marty, *Electroanalysis*, 2009, **21**, 696-700.

153. Y. Jung, J. Y. Jeong and B. H. Chung, *Analyst*, 2008, **133**, 697-701.

154. S. Dong and J. Li, *Bioelectrochem. Bioenerg.*, 1997, **42**, 7-13.

155. W. Schuhmann, *Biosens. Bioelectron.*, 1995, **10**, 181-193.

156. J. Q. Brown, R. Srivastava and M. J. McShane, *Biosens. Bioelectron.*, 2005, **21**, 212-216.

157. J. Wang, L.-H. Wu, Z. Lu, R. Li and J. Sanchez, *Anal. Chim. Acta*, 1990, **228**, 251-257.

158. J. Wang, L. Fang and D. Lopez, *Analyst*, 1994, **119**, 455-458.

159. D. Iveković, S. Milardović and B. S. Grabarić, *Biosens. Bioelectron.*, 2004, **20**, 872-878.

160. B. R. Eggins, *Chemical Sensors and Biosensors*, John Wiley & Sons, Incorporated, New York, UK, 2002.

161. A. Harper and M. R. Anderson, *Sensors*, 2010, **10**.

162. S. Liébana and Guido A. Drago, *Essays Biochem.*, 2016, **60**, 59-68.

163. M. Álvarez-Icaza and U. Bilitewski, *Anal. Chem.*, 1993, **65**, 525A-533A.

164. L. Asturias Arribas, PhD thesis, Universidad de Burgos, 2014.

165. A. Arabzadeh and A. Salimi, *Biosens. Bioelectron.*, 2015, **74**, 270-276.

166. H. Y. Song, J. Hobley, X. Su and X. Zhou, *Plasmonics*, 2014, **9**, 851-858.

167. M. T. Neves-Petersen, T. Snabe, S. Klitgaard, M. Duroux and S. B. Petersen, *Protein Sci.*, 2006, **15**, 343-351.

168. A. K. Trilling, J. Beekwilder and H. Zuilhof, *Analyst*, 2013, **138**, 1619-1627.

169. K. Hajizadeh, H. B. Halsall and W. R. Heineman, *Talanta*, 1991, **38**, 37-47.

170. V. K. Gade, D. J. Shirale, P. D. Gaikwad, P. A. Savale, K. P. Kakde, H. J. Kharat and M. D. Shirsat, *React. Funct. Polym.*, 2006, **66**, 1420-1426.

171. ThermoScientific, https://bit.ly/CrosslinkingHandbook, (accessed May 2020).

172. R. F. Garmann, A. M. Goldfain and V. N. Manoharan, *PNAS*, 2019, **116**, 22485-22490.

173. D. L. Caspar and A. Klug, in *Cold Spring Harbor symposia on quantitative biology*, Cold Spring Harbor Laboratory Press, 1962, vol. 27, pp. 1-24.

174. G. M. Whitesides and B. Grzybowski, *Science*, 2002, **295**, 2418.

175. B. A. Grzybowski, C. E. Wilmer, J. Kim, K. P. Browne and K. J. Bishop, *Soft Matter*, 2009, **5**, 1110-1128.

176. J. N. Israelachvili, D. J. Mitchell and B. W. Ninham, *Biochim. Biophys. Acta Biomembr.*, 1977, **470**, 185-201.

177. J. J. McManus, P. Charbonneau, E. Zaccarelli and N. Asherie, *COCIS*, 2016, **22**, 73-79.

178. Y. Timsit, *Int. J. Mol. Sci.*, 2013, **14**, 8252-8270.

179. M. H. Lash, M. V. Fedorchak, J. J. McCarthy and S. R. Little, *Soft Matter*, 2015, **11**, 5597-5609.

180. A. C. Mendes, E. T. Baran, R. L. Reis and H. S. Azevedo, *WIREs Nanomed. Nanobiotechnol.* , 2013, **5**, 582-612.

181. F. Schreiber, *Prog. Surf. Sci.*, 2000, **65**, 151-257.

182. A. Ulman, *An Introduction to Ultrathin Organic Films: From Langmuir--Blodgett to Self--Assembly*, Academic Press Limited, London, 2013.

183. A. Ulman, *Chem. Rev.*, 1996, **96**, 1533-1554.

184. O. P. Dimitriev, K. P. Grytsenko, P. M. Lytvyn, T. P. Doroshenko, J. L. Briks, A. I. Tolmachev, Y. L. Slominskii, M. A. Kudinova, S. Schrader, R. D. Schulze and J. Friedrich, *Thin Solid Films*, 2013, **539**, 127-133.

185. G. B. Jones, PhD thesis, University of Warwick, 2015.

186. C. D. Bain, E. B. Troughton, Y. T. Tao, J. Evall, G. M. Whitesides and R. G. Nuzzo, *JACS*, 1989, **111**, 321-335.

187. T. W. Schneider and D. A. Buttry, *JACS*, 1993, **115**, 12391-12397.

188. O. Dannenberger, J. J. Wolff and M. Buck, *Langmuir*, 1998, **14**, 4679-4682.

189. M. A. Daza Millone, H. Hamoudi, L. Rodríguez, A. A. Rubert, G. A. Benítez, M. E. Vela, R. C. Salvarezza, J. E. Gayone, E. A. Sánchez, O. Grizzi, C. Dablemont and V. A. Esaulov, *Langmuir*, 2009, **25**, 12945-12953.

190. E. Delamarche, B. Michel, H. Kang and C. Gerber, *Langmuir*, 1994, **10**, 4103-4108.

191. R. Yamada, H. Wano and K. Uosaki, *Langmuir*, 2000, **16**, 5523-5525.

192. C. Vericat, M. E. Vela, G. Benitez, P. Carro and R. C. Salvarezza, *Chem. Soc. Rev.*, 2010, **39**, 1805-1834.

193. Y. Xue, X. Li, H. Li and W. Zhang, *Nat Commun*, 2014, **5**, 4348.

194. M. Bougrini, A. Baraket, T. Jamshaid, A. E. Aissari, J. Bausells, M. Zabala, N. E. Bari, B. Bouchikhi, N. Jaffrezic-Renault, E. Abdelhamid and N. Zine, *Sens. Actuators B Chem.*, 2016, **234**, 446-452.

195. M. Cohen-Atiya, A. Nelson and D. Mandler, *J. Electroanal. Chem.*, 2006, **593**, 227-240.

196. G. M. Whitesides and P. E. Laibinis, *Langmuir*, 1990, **6**, 87-96.

197. H. Häkkinen, *Nat. Chem.*, 2012, **4**, 443-455.

198. M. S. Inkpen, Z. F. Liu, H. Li, L. M. Campos, J. B. Neaton and L. Venkataraman, *Nat. Chem.*, 2019, **11**, 351-358.

199. L. L. Rouhana, M. D. Moussallem and J. B. Schlenoff, *JACS.*, 2011, **133**, 16080-16091.

200. M. Hasan, D. Bethell and M. Brust, *JACS*, 2002, **124**, 1132-1133.

201. F. Tielens and E. Santos, *J. Phys. Chem. C*, 2010, **114**, 9444-9452.

202. C. D. Bain, H. A. Biebuyck and G. M. Whitesides, *Langmuir*, 1989, **5**, 723-727.

203. A. Kołodziej, F. Fernandez-Trillo and P. Rodriguez, *J. Electroanal. Chem.*, 2017, DOI: 10.1016/j.jelechem.2017.07.039.

204. R.-F. Dou, X.-C. Ma, L. Xi, H. L. Yip, K. Y. Wong, W. M. Lau, J.-F. Jia, Q.-K. Xue, W.-S. Yang, H. Ma and A. K. Y. Jen, *Langmuir*, 2006, **22**, 3049-3056.

205. M. Sprik, E. Delamarche, B. Michel, U. Roethlisberger, M. L. Klein, H. Wolf and H. Ringsdorf, *Langmuir*, 1994, **10**, 4116-4130.

206. Y. Zhou, C. W. Chiu and H. Liang, *Sensors (Basel)*, 2012, **12**, 15036-15062.

207. R. Chelmowski, D. Käfer, S. D. Köster, T. Klasen, T. Winkler, A. Terfort, N. Metzler-Nolte and C. Wöll, *Langmuir*, 2009, **25**, 11480-11485.

208. J. Lahiri, L. Isaacs, J. Tien and G. M. Whitesides, *Anal. Chem.*, 1999, **71**, 777-790.

209. S. Herrwerth, T. Rosendahl, C. Feng, J. Fick, W. Eck, M. Himmelhaus, R. Dahint and M. Grunze, *Langmuir*, 2003, **19**, 1880-1887.

210. M. N. Yousaf and M. Mrksich, *JACS*, 1999, **121**, 4286-4287.

211. W. S. Dillmore, M. N. Yousaf and M. Mrksich, *Langmuir*, 2004, **20**, 7223-7231.

212. J. Noh, H. S. Kato, M. Kawai and M. Hara, *J. Phys. Chem. B*, 2006, **110**, 2793-2797.

213. Y. Liu and V. Ozolins, *J. Phys. Chem. C*, 2012, **116**, 4738-4747.

214. G. E. Poirier, *Chem. Rev.*, 1997, **97**, 1117-1128.

215. H. Kondoh, C. Kodama, H. Sumida and H. Nozoye, *J. Chem. Phys.*, 1999, **111**, 1175-1184.

216. C. D. Bain and G. M. Whitesides, *Science*, 1988, **240**, 62.

217. H. Azehara, S. Yoshimoto, H. Hokari, U. Akiba, I. Taniguchi and M. Fujihira, *J. Electroanal. Chem.*, 1999, **473**, 68-74.

218. E. B. Troughton, C. D. Bain, G. M. Whitesides, R. G. Nuzzo, D. L. Allara and M. D. Porter, *Langmuir*, 1988, **4**, 365-385.

219. R. G. Jones. International Union of Pure and Applied Chemistry. Polymer Division and E. S. Wilks, in *Compendium of polymer terminology and nomenclature : IUPAC recommendations*, RSC Publishing, 2008, ch. 1, p. 443.

220. A. Yacynych, US Pat., US005540828A, 1996

221. B. Adhikari and S. Majumdar, *Prog. Polym. Sci.*, 2004, **29**, 699-766.

222. J. Ashley, M.-A. Shahbazi, K. Kant, V. A. Chidambara, A. Wolff, D. D. Bang and Y. Sun, *Biosens. Bioelectron.*, 2017, **91**, 606-615.

223. P. A. G. Cormack and A. Zurutuza Elorza, *J. Chromatogr. B*, 2004, **804**, 173-182.

224. X. Qin, H. Xiao-Ya and H. Shi-Rong, *Electropolymerization*, 2011, 187.

225. M. Gerard, A. Chaubey and B. D. Malhotra, *Biosens. Bioelectron.*, 2002, **17**, 345-359.

226. S. Prakash, T. Chakrabarty, A. K. Singh and V. K. Shahi, *Biosens. Bioelectron.*, 2013, **41**, 43-53.

227. P. P. Joshi, S. A. Merchant, Y. Wang and D. W. Schmidtke, *Anal. Chem.*, 2005, **77**, 3183-3188.

228. S. Geetha, C. R. K. Rao, M. Vijayan and D. C. Trivedi, *Anal. Chim. Acta*, 2006, **568**, 119-125.

229. T. Ahuja, I. A. Mir, D. Kumar and Rajesh, *Biomaterials*, 2007, **28**, 791-805.

230. S. Cosnier, *Electroanalysis*, 1997, **9**, 894-902.

231. M. Badoux, M. Billing and H.-A. Klok, *Polym. Chem.*, 2019, **10**, 2925-2951.

232. T.-P. Huynh, P. S. Sharma, M. Sosnowska, F. D'Souza and W. Kutner, *Prog. Polym. Sci.*, 2015, **47**, 1-25.

233. W. Schuhmann, R. Lammert, B. Uhe and H. L. Schmidt, *Sens. Actuators B Chem.*, 1990, **1**, 537-541.

234. A. P. Grekov and V. Y. Veselov, *Russ. Chem. Rev.*, 1978, **47**, 631.

235. J. O. Edwards and R. G. Pearson, *JACS*, 1962, **84**, 16-24.

236. S. Hoz, *J. Org. Chem.*, 1982, **47**, 3545-3547.

237. Y. Ren and H. Yamataka, *Chem. Eur. J.*, 2007, **13**, 677-682.

238. D. K. Kölmel and E. T. Kool, *Chem. Rev.*, 2017, **117**, 10358-10376.

239. E. H. Cordes and W. P. Jencks, *JACS*, 1963, **85**, 2843-2848.

240. J. B. Conant and P. D. Bartlett, *JACS*, 1932, **54**, 2881-2899.

241. G. Stempel Jr and G. S. Schaffel, *JACS*, 1944, **66**, 1158-1161.

242. R. Nguyen and I. Huc, *ChemComm.*, 2003, 942-943.

243. K. Qvortrup, V. V. Komnatnyy and T. E. Nielsen, *Org. Lett.*, 2014, **16**, 4782-4785.

244. E. Lattová and H. Perreault, *Mass Spectrom. Rev.*, 2013, **32**, 366-385.

245. G. M. Eldridge and G. A. Weiss, *Bioconjugate Chem.*, 2011, **22**, 2143-2153.

246. G. T. Hermanson, in *Bioconjugate Techniques*, Academic Press, Boston, 3rd edn., 2013, ch. 2, pp. 127-228.

247. W. L. Hoffman and D. J. O'Shannessy, *J. Immunol. Methods*, 1988, **112**, 113-120.

248. S. Raddatz, J. Mueller-Ibeler, J. Kluge, L. Wäss, G. Burdinski, J. R. Havens, T. J. Onofrey, D. Wang and M. Schweitzer, *Nucleic Acids Res.*, 2002, **30**, 4793-4802.

249. F. L. Thompson, T. Iida and J. Swings, *Microbiol. Mol. Biol. Rev.*, 2004, **68**, 403-431.

250. M. Vital, H. P. Füchslin, F. Hammes and T. Egli, *Microbiology*, 2007, **153**, 1993-2001.

251. Y. Senderovich, I. Izhaki and M. Halpern, *PLoS One*, 2010, **5**, e8607.

252. E. Barbieri, L. Falzano, C. Fiorentini, A. Pianetti, W. Baffone, A. Fabbri, P. Matarrese, A. Casiere, M. Katouli, I. Kühn, R. Möllby, F. Bruscolini and G. Donelli, *Appl. Environ. Microbiol.*, 1999, **65**, 2748-2753.

253. J. F. Heidelberg, K. B. Heidelberg and R. R. Colwell, *Appl. Environ. Microbiol.*, 2002, **68**, 5488-5497.

254. P. A. West, *Epidemiol. Infect.*, 1989, **103**, 1-34.

255. CDC, https://www.cdc.gov/vibrio/index.html, (accessed Juned, 2020).

256. M. K. Jones and J. D. Oliver, *Infect. Immun.*, 2009, **77**, 1723-1733.

257. R. Phetsouvanh, M. Nakatsu, E. Arakawa, V. Davong, M. Vongsouvath, O. Lattana, C. E. Moore, S. Nakamura and P. N. Newton, *Ann. Clin. Microbiol. Antimicrob.*, 2008, **7**, 10.

258. S. W. Lacey, *Clin. Infect. Dis.*, 1995, **20**, 1409-1419.

259. D. Hu, B. Liu, L. Feng, P. Ding, X. Guo, M. Wang, B. Cao, P. R. Reeves and L. Wang, *PNAS*, 2016, **113**, E7730.

260. R. R. Colwell, P. Brayton, D. Herrington, B. Tall, A. Huq and M. M. Levine, *World J. Microbiol. Biotechnol.* , 1996, **12**, 28-31.

261. I. M. Longini, Jr., M. Yunus, K. Zaman, A. K. Siddique, R. B. Sack and A. Nizam, *J. Infect. Dis.*, 2002, **186**, 246-251.

262. J. B. McAteer, S. Danda, T. Nhende, P. Manamike, T. Parayiwa, A. Tarupihwa, O. Tapfumanei, P. Manangazira, G. Mhlanga, D. B. Garone, A. Martinsen, R. D. Aubert, W. Davis, R. Narra, S. Balachandra, B. A. Tippett Barr and E. Mintz, *MMWR Morb. Mortal Wkly. Rep.*, 2018, **67**, 560-561.

263. M. Makoni, *Lancet*, 2018, **392**, e8-e8.

264. G. B. Nair, B. L. Sarkar, S. P. De, M. K. Chakrabarti, R. K. Bhadra and S. C. Pal, Microb. Ecol., 1988, **15**, 203-215.

265. J. T. Watson, M. Gayer and M. A. Connolly, *Emerg. Infect. Dis.*, 2007, **13**, 1-5.

266. A. K. Siddique, K. Akram, K. Zaman, S. Laston, A. Salam, R. N. Majumdar, M. S. Islam and N. Fronczak, *Lancet*, 1995, **345**, 359-361.

267. A. Camacho, M. Bouhenia, R. Alyusfi, A. Alkohlani, M. A. M. Naji, X. de Radiguès, A. M. Abubakar, A. Almoalmi, C. Seguin, M. J. Sagrado, M. Poncin, M. McRae, M. Musoke, A. Rakesh, K. Porten, C. Haskew, K. E. Atkins, R. M. Eggo, A. S. Azman, M. Broekhuijsen, M. A. Saatcioglu, L. Pezzoli, M.-L. Quilici, A. R. Al-Mesbahy, N. Zagaria and F. J. Luquero, *Lancet Glob. Health*, 2018, **6**, e680-e690.

268. A. Jutla, R. Khan and R. Colwell, *Curr. Environ. Health Rep.*, 2017, **4**, 99-107.

269. M. Enserink, *Science*, 2010, **330**, 738-739.

270. B. S. Schwartz, J. B. Harris, A. I. Khan, R. C. Larocque, D. A. Sack, M. A. Malek, A. S. G. Faruque, F. Qadri, S. B. Calderwood, S. P. Luby and E. T. Ryan, *Am. J. Trop. Med.*, 2006, **74**, 1067-1073.

271. F. R. Chowdhury, Z. Nur, N. Hassan, L. von Seidlein and S. Dunachie, *Ann. Clin. Microbiol. Antimicrob.*, 2017, **16**, 10-10.

272. J. N. Zuckerman, L. Rombo and A. Fisch, *Lancet Infect. Dis.*, 2007, **7**, 521-530.

273. WHO, http://www.who.int/en/news-room/fact-sheets/detail/cholera, (accessed June 2020).

274. R. Steffen, J. Acar, E. Walker and J. Zuckerman, *Travel. Med. Infect. Dis.*, 2003, **1**, 80-88.

275. WHO, https://bit.ly/GlobalBurdenCholera, (accessed May 2020).

276. WHO, https://www.who.int/health-topics/cholera#tab=tab_1, (accessed March 2020).

277. Mayo Clinic, https://mayocl.in/32mPmNF, (accessed February 2020).

278. D. A. Sack, R. B. Sack, G. B. Nair and A. K. Siddique, *Lancet*, 2004, **363**, 223-233.

279. WHO, https://bit.ly/CholeraVaccines, (accessed June 2020).

280. WHO, https://bit.ly/OralCholeraVaccines, (accessed June 2020).

281. J. G. Morris Jr and R. E. Black, *N. Engl. J. Med.*, 1985, **312**, 343-350.

282. J. Lindenbaum, W. B. Greenough and M. R. Islam, *Bull. World Health Organ.*, 1967, **36**, 871-883.

283. P. Garg, S. Chakraborty, I. Basu, S. Datta, K. Rajendran, T. Bhattacharya, S. Yamasaki, S. K. Bhattacharya, Y. Takeda, G. B. Nair and T. Ramamurthy, *Epidemiol. Infect.*, 2000, **124**, 393-399.

284. WHO, https://bit.ly/TreatmentDiarrhoea, (accessed June 2020).

285. S. Sawasvirojwong, P. Srimanote, V. Chatsudthipong and C. Muanprasat, *PLOS Negl. Trop. Dis.*, 2013, **7**, e2293-e2293.

286. R. I. Glass, P. A. Blake, R. J. Waldman, M. Claeson and N. F. Pierce, *Lancet*, 1991, **338**, 791-795.

287. C. Miller, R. Feachem and B. Drasar, *Lancet*, 1985, **325**, 261-263.

288. P. W. Lowry, Arch. Intern. Med., 1989, **149**, 2079.

289. WHO and United Nations Children's Fund (UNICEF), https://bit.ly/DrinkingWaterHygiene, (accessed June 2020).

290. P. R. Murray, K. S. Rosenthal and M. A. Pfaller, in *Medical microbiology*, Elsevier Health Services, 2020, ch. 26, pp. 271-277.

291. J. B. Harris and R. C. LaRocque, *Am. J. Trop. Med.*, 2016, **95**, 263-264.

292. C. T. Codeço, *BMC Infect. Dis.*, 2001, **1**, 1-1.

293. S. N. Chatterjee and K. Chaudhuri, *Biochim. Biophys. Acta Mol. Basis Dis.*, 2003, **1639**, 65-79.

294. M. H. Rahaman, T. Islam, R. R. Colwell and M. Alam, *Front. Microbiol.*, 2015, **6**.

295. A. J. Sabat, A. Budimir, D. Nashev, R. Sá-Leão, J. M. van Dijl, F. Laurent, H. Grundmann, A. W. Friedrich and o. b. o. t. E. S. G. o. E. Markers, *Eurosurveillance*, 2013, **18**, 20380.

296. J. B. Kaper, J. G. Morris and M. M. Levine, *CMR*, 1995, **8**, 48.

297. S. Keasler and R. Hall, *Lancet*, 1993, **341**, 1661.

298. V. J. DiRita, M. Neely, R. K. Taylor and P. M. Bruss, *PNAS*, 1996, **93**, 7991.

299. K. Lee, *GCHH*, 2001, **2**, 6-17.

300. A. S. Cross, *Crit. Care*, 2008, **12**, 197.

301. A. J. Silva and J. A. Benitez, *PLOS Negl. Trop. Dis.*, 2016, **10**, e0004330.

302. S. Almagro-Moreno, K. Pruss and R. K. Taylor, *PLoS Pathog.*, 2015, **11**, e1004787.

303. D. S. Merrell, D. L. Hava and A. Camilli, *Mol. Microbiol.*, 2002, **43**, 1471-1491.

304. D. S. Merrell, S. M. Butler, F. Qadri, N. A. Dolganov, A. Alam, M. B. Cohen, S. B. Calderwood, G. K. Schoolnik and A. Camilli, *Nature*, 2002, **417**, 642-645.

305. S. M. Faruque, K. Biswas, S. M. N. Udden, Q. S. Ahmad, D. A. Sack, G. B. Nair and J. J. Mekalanos, *PNAS*, 2006, **103**, 6350.

306. R. Tamayo, B. Patimalla and A. Camilli, *Infect. Immun.*, 2010, **78**, 3560-3569.

307. M. Alam, M. Sultana, G. B. Nair, A. K. Siddique, N. A. Hasan, R. B. Sack, D. A. Sack, K. U. Ahmed, A. Sadique, H. Watanabe, C. J. Grim, A. Huq and R. R. Colwell, *PNAS USA*, 2007, **104**, 17801-17806.

308. P. Louis and C. P. O'Byrne, *Sci. Prog.*, 2010, **93**, 7-36.

309. G. Kovacikova and K. Skorupski, *Infect. Immun.*, 2002, **70**, 5355-5362.

310. M. J. Kazmierczak, M. Wiedmann and K. J. Boor, *Microbiol. Mol. Biol. Rev.*, 2005, **69**, 527.

311. S. M. Butler and A. Camilli, *Nat. Rev. Microbiol.*, 2005, **3**, 611-620.

312. M. A. McGuckin, S. K. Lindén, P. Sutton and T. H. Florin, *Nat. Rev. Microbiol.*, 2011, **9**, 265-278.

313. Y. A. Millet, D. Alvarez, S. Ringgaard, U. H. von Andrian, B. M. Davis and M. K. Waldor, *PLoS Pathog.*, 2014, **10**, e1004405.

314. M. N. Guentzel, L. H. Field, E. R. Eubanks and L. J. Berry, *Infect. Immun.*, 1977, **15**, 539-548.

315. K. A. Syed, S. Beyhan, N. Correa, J. Queen, J. Liu, F. Peng, K. J. Satchell, F. Yildiz and K. E. Klose, *J. Bacteriol.*, 2009, **191**, 6555-6570.

316. S. J. Krebs and R. K. Taylor, *J. Bacteriol.*, 2011, **193**, 5260-5270.

317. D. Sun, J. J. Mekalanos and R. K. Taylor, *J. Infect. Dis.*, 1990, **161**, 1231-1236.

318. E. Wong, G. Vaaje-Kolstad, A. Ghosh, R. Hurtado-Guerrero, P. V. Konarev, A. F. M. Ibrahim, D. I. Svergun, V. G. H. Eijsink, N. S. Chatterjee and D. M. F. van Aalten, *PLoS Pathog.*, 2012, **8**, e1002373-e1002373.

319. R. Bhowmick, A. Ghosal, B. Das, H. Koley, D. R. Saha, S. Ganguly, R. K. Nandy, R. K. Bhadra and N. S. Chatterjee, *Infect. Immun.*, 2008, **76**, 4968-4977.

320. M. van den Berg Bernard, H. Vink and A. E. Spaan Jos, *Circ. Res.*, 2003, **92**, 592-594.

321. R. Freter, P. C. M. O'Brien and M. S. Macsai, *Infect. Immun.*, 1981, **34**, 234-240.

322. A. M. Krachler, H. Ham and K. Orth, *PNAS*, 2011, **108**, 11614-11619.

323. J. Haiko and B. Westerlund-Wikström, *Biology*, 2013, **2**, 1242-1267.

324. G. W. Jones and R. Freter, *Infect. Immun.*, 1976, **14**, 240-245.

325. S. R. Attridge and D. Rowley, *J. Infect. Dis.*, 1983, **147**, 864-872.

326. T. Proft and E. N. Baker, *Cell. Mol. Life Sci.*, 2008, **66**, 613.

327. D. A. Chiavelli, J. W. Marsh and R. K. Taylor, *Appl. Environ. Microbiol.*, 2001, **67**, 3220-3225.

328. C. J. Jones, A. Utada, K. R. Davis, W. Thongsomboon, D. Zamorano Sanchez, V. Banakar, L. Cegelski, G. C. L. Wong and F. H. Yildiz, *PLoS Pathog.*, 2015, **11**, e1005068.

329. K. L. Meibom, X. B. Li, A. T. Nielsen, C.-Y. Wu, S. Roseman and G. K. Schoolnik, *PNAS USA*, 2004, **101**, 2524.

330. P. A. Manning, in *Bacterial Pathogenesis of Plants and Animals*, ed. J. L. Dangl, Springer, Berlin, Heidelberg, 1994, pp. 265-281.

331. R. K. Taylor, V. L. Miller, D. B. Furlong and J. J. Mekalanos, *PNAS*, 1987, **84**, 2833.

332. O. Creese, PhD thesis, University of Birmingham, 2020.

333. J. Li, M. S. Lim, S. Li, M. Brock, M. E. Pique, V. L. Woods and L. Craig, *Structure*, 2008, **16**, 137-148.

334. C. C. Häse, *Microbiology*, 2001, **147**, 831-837.

335. L. Craig and J. Li, *Curr. Opin. Struct. Biol.*, 2008, **18**, 267-277.

336. M. S. Lim, D. Ng, Z. Zong, A. S. Arvai, R. K. Taylor, J. A. Tainer and L. Craig, *Mol. Microbiol.*, 2010, **77**, 755-770.

337. T. J. Kirn, N. Bose and R. K. Taylor, *Mol. Microbiol.*, 2003, **49**, 81-92.

338. T. J. Kirn, B. A. Jude and R. K. Taylor, *Nature*, 2005, **438**, 863-866.

339. J. W. Wilson, M. J. Schurr, C. L. LeBlanc, R. Ramamurthy, K. L. Buchanan and C. A. Nickerson, *Postgrad. Med. J.*, 2002, **78**, 216.

340. B. Henderson, M. Wilson and B. Wren, *Trends Microbiol.*, 1997, **5**, 454-458.

341. J. Moss and M. Vaughan, *Annu. Rev. Biochem.*, 1979, **48**, 581-600.

342. R.-G. Zhang, D. L. Scott, M. L. Westbrook, S. Nance, B. D. Spangler, G. G. Shipley and E. M. Westbrook, *J. Mol. Biol.*, 1995, **251**, 563-573.

343. D. M. Gill, *Biochemistry*, 1976, **15**, 1242-1248.

344. B. D. Spangler, *Microbiol. Rev.*, 1992, **56**, 622-647.

345. N. L. B. Wernick, D. J. F. Chinnapen, J. A. Cho and W. I. Lencer, *Toxins (Basel)*, 2010, **2**, 310-325.

346. C. J. O'Neal, M. G. Jobling, R. K. Holmes and W. G. Hol, *Science*, 2005, **309**, 1093-1096.

347. T. R. Hirst and J. Holmgren, *PNAS*, 1987, **84**, 7418-7422.

348. B. Tsai, C. Rodighiero, W. I. Lencer and T. A. Rapoport, *Cell*, 2001, **104**, 937-948.

349. T. R. Hirst, J. Sanchez, J. B. Kaper, S. J. Hardy and J. Holmgren, *PNAS*, 1984, **81**, 7752-7756.

350. J. Mekalanos, R. Collier and W. Romig, *J. Biol. Chem.*, 1979, **254**, 5855-5861.

351. W. I. Lencer, C. Constable, S. Moe, P. A. Rufo, A. Wolf, M. G. Jobling, S. P. Ruston, J. L. Madara, R. K. Holmes and T. R. Hirst, *J. Biol. Chem.*, 1997, **272**, 15562-15568.

352. B. A. Booth, M. Boesman-Finkelstein and R. A. Finkelstein, *Infect. Immun.*, 1984, **45**, 558.

353. H. A. Hansson, J. Holmgren and L. Svennerholm, *PNAS*, 1977, **74**, 3782.

354. S. van Heyningen, *Science*, 1974, **183**, 656-657.

355. W. I. Lencer and B. Tsai, *Trends Biochem. Sci.*, 2003, **28**, 639-645.

356. R. A. Finkelstein, in *Medical Microbiology*, ed. S. Baron, Texas Medical Branch, Galveston (USA), 4th edn., 1996, ch. 24.

357. C. A. King and W. E. van Heyningen, *J. Infect. Dis.*, 1973, **127**, 639-647.

358. P. Cuatrecasas, *Biochemistry*, 1973, **12**, 3558-3566.

359. B. J. Wisnieski and J. S. Bramhall, *Nature*, 1981, **289**, 319-321.

360. D. Cabral-Lilly, G. E. Sosinsky, R. A. Reed, M. R. McDermott and G. G. Shipley, *Biophys. J.*, 1994, **66**, 935-941.

361. E. A. Merritt, S. Sarfaty, F. V. D. Akker, C. L'Hoir, J. A. Martial and W. G. J. Hol, *Protein Sci.*, 1994, **3**, 166-175.

362. P. H. Fishman, J. Moss and J. C. Osborne, *Biochemistry*, 1978, **17**, 711-716.

363. E. A. Merritt, P. Kuhn, S. Sarfaty, J. L. Erbe, R. K. Holmes and W. G. J. Hol, *J. Mol. Biol.*, 1998, **282**, 1043-1059.

364. D. J. Chinnapen, H. Chinnapen, D. Saslowsky and W. I. Lencer, *FEMS Microbiol. Lett.*, 2007, **266**, 129-137.

365. M. L. Torgersen, G. Skretting, B. van Deurs and K. Sandvig, *J. Cell Sci.*, 2001, **114**, 3737-3747.

366. P. A. Orlandi and P. H. Fishman, *J. Cell Biol.*, 1998, **141**, 905-915.

367. M. Kirkham and R. G. Parton, *Biochim. Biophys. Acta*, 2005, **1745**, 273-286.

368. M. Kaksonen and A. Roux, *Nat. Rev. Mol. Cell Biol.*, 2018, **19**, 313-326.

369. L. Pelkmans and A. Helenius, *Traffic*, 2002, **3**, 311-320.

370. J. Rejman, V. Oberle, I. S. Zuhorn and D. Hoekstra, *Biochem. J.*, 2004, **377**, 159-169.

371. P. Bastiaens, I. V. Majoul, P. J. Verveer, H.-D. Söling and T. M. Jovin, *EMBO J.*, 1996, **15**, 4246-4253.

372. A. A. Wolf, M. G. Jobling, D. E. Saslowsky, E. Kern, K. R. Drake, A. K. Kenworthy, R. K. Holmes and W. I. Lencer, *Infect. Immun.*, 2008, **76**, 1476-1484.

373. Y. Fujinaga, A. A. Wolf, C. Rodighiero, H. Wheeler, B. Tsai, L. Allen, M. G. Jobling, T. Rapoport, R. K. Holmes and W. I. Lencer, *Mol. Biol. Cell*, 2003, **14**, 4783-4793.

374. Y. Feng, A. P. Jadhav, C. Rodighiero, Y. Fujinaga, T. Kirchhausen and W. I. Lencer, *EMBO Rep.*, 2004, **5**, 596-601.

375. B. Tsai, Y. Ye and T. A. Rapoport, *Nat. Rev. Mol. Cell Biol.*, 2002, **3**, 246-255.

376. W. I. Lencer, *Int. J. Med. Microbiol.*, 2004, **293**, 491-494.

377. A. Winkeler, D. Gödderz, V. Herzog and A. Schmitz, *FEBS Lett.*, 2003, **554**, 439-442.

378. A. Schmitz, H. Herrgen, A. Winkeler and V. Herzog, *JCB*, 2000, **148**, 1203-1212.

379. M. Taylor, F. Navarro-Garcia, J. Huerta, H. Burress, S. Massey, K. Ireton and K. Teter, *J. Biol. Chem.*, 2010, **285**, 31261-31267.

380. B. Hazes and R. J. Read, *Biochemistry*, 1997, **36**, 11051-11054.

381. G. Zhang, Y. Liu, A. E. Ruoho and J. H. Hurley, *Nature*, 1997, **386**, 247-253.

382. D. Cassel and T. Pfeuffer, *PNAS*, 1978, **75**, 2669-2673.

383. L. D. Vries, B. Zheng, T. Fischer, E. Elenko and M. G. Farquhar, *Annu. Rev. Pharmacol. Toxicol.*, 2000, **40**, 235-271.

384. D. M. Rosenbaum, S. G. F. Rasmussen and B. K. Kobilka, *Nature*, 2009, **459**, 356-363.

385. A. J. Venkatakrishnan, X. Deupi, G. Lebon, C. G. Tate, G. F. Schertler and M. M. Babu, *Nature*, 2013, **494**, 185-194.

386. W. M. Oldham and H. E. Hamm, *Nat. Rev. Mol. Cell Biol.*, 2008, **9**, 60-71.

387. J. R. Hepler and A. G. Gilman, *Trends Biochem. Sci.*, 1992, **17**, 383-387.

388. A. G. Gilman, *Cell*, 1984, **36**, 577-579.

389. Y. Salomon, C. Londos and M. Rodbell, *Anal. Biochem.*, 1974, **58**, 541-548.

390. P. C. Sternweis, *Trends Neurosci.*, 1990, **13**, 122-126.

391. B. Skalhegg and K. Tasken, *Front. Biosci.*, 2000, **5**, D678-D693.

392. R. K. Gill and G. A. Hecht, in *Physiology of the Gastrointestinal Tract*, ed. H. M. Said, Academic Press, Irvine (USA), 6th edn., 2018, ch. 64, pp. 1547-1577.

393. A. C. Chao, F. J. de Sauvage, Y. Dong, J. Wagner, D. Goeddel and P. Gardner, *EMBO J.*, 1994, **13**, 1065-1072.

394. S. H. Cheng, D. P. Rich, J. Marshall, R. J. Gregory, M. J. Welsh and A. E. Smith, *Cell*, 1991, **66**, 1027-1036.

395. P. Pongkorpsakol, N. Pathomthongtaweechai, P. Srimanote, S. Soodvilai, V. Chatsudthipong and C. Muanprasat, *PLOS Negl. Trop. Dis.*, 2014, **8**, e3119.

396. M. J. Stutts, C. M. Canessa, J. C. Olsen, M. Hamrick, J. A. Cohn, B. C. Rossier and R. C. Boucher, *Science*, 1995, **269**, 847-850.

397. S. E. Gabriel, K. N. Brigman, B. H. Koller, R. C. Boucher and M. J. Stutts, *Science*, 1994, **266**, 107-109.

398. K. E. Barrett and S. J. Keely, *Annu. Rev. Physiol.*, 2000, **62**, 535-572.

399. T. M. Vuong and M. Chabre, *Nature*, 1990, **346**, 71-74.

400. N. Watson, M. E. Linder, K. M. Druey, J. H. Kehrl and K. J. Blumer, *Nature*, 1996, **383**, 172-175.

401. D. M. Gill and R. Meren, *PNAS*, 1978, **75**, 3050-3054.

402. J. Holmgren, *Nature*, 1981, **292**, 413-417.

403. G. W. G. Sharp and S. Hynie, *Nature*, 1971, **229**, 266-269.

404. D. V. Kimberg, M. Field, J. Johnson, A. Henderson and E. Gershon, *J. Clin. Investig.*, 1971, **50**, 1218-1230.

405. R. Abbott, https://bit.ly/CholeraToxinAction, (accessed April 2020).

406. S. Kopic and J. P. Geibel, *Toxins (Basel)*, 2010, **2**, 2132-2157.

407. J. C. Azurin and M. Alvero, *Bull. World Health Organ.*, 1974, **51**, 19-26.

408. S. M. Faruque, M. J. Islam, Q. S. Ahmad, A. Faruque, D. A. Sack, G. B. Nair and J. J. Mekalanos, *PNAS*, 2005, **102**, 6119-6124.

409. R. H. Watten, F. M. Morgan, Y. N. Songkhla, B. Vanikiati and R. A. Phillips, *J. Clin. Investig.*, 1959, **38**, 1879-1889.

410. N. Pierce, R. Sack, R. Mitra, J. Banwell, K. Brigham, D. Fedson and A. Mondal, *Ann. Intern. Med.*, 1969, **70**, 1173.

411. M. M. Levine, J. B. Kaper, D. Herrington, G. Losonsky, J. G. Morris, M. L. Clements, R. E. Black, B. Tall and R. Hall, *Infect. Immun.*, 1988, **56**, 161-167.

412. E. J. Nelson, A. Chowdhury, J. B. Harris, Y. A. Begum, F. Chowdhury, A. I. Khan, R. C. LaRocque, A. L. Bishop, E. T. Ryan and A. Camilli, *PNAS*, 2007, **104**, 19091-19096.

413. J. C. N. Fong, K. A. Syed, K. E. Klose and F. H. Yildiz, *Microbiology (Reading, Engl.)*, 2010, **156**, 2757-2769.

414. R. A. Finkelstein, M. Boesman-Finkelstein, Y. Chang and C. Häse, *Infect. Immun.*, 1992, **60**, 472-478.

415. A. J. Silva, K. Pham and J. A. Benitez, *Microbiology*, 2003, **149**, 1883-1891.

416. M. Kitaoka, S. T. Miyata, D. Unterweger and S. Pukatzki, *J. Med. Microbiol.*, 2011, **60**, 397-407.

417. K. L. Cottingham, D. A. Chiavelli and R. K. Taylor, *Front. Ecol. Environ.*, 2003, **1**, 80-86.

418. A. J. Bard, Faulkner, L. R., in *Electrochemical Methods: Fundamentals and Applications*, ed. E. Swain, John Wiley & Sons, Inc., 2nd edn., 2001, ch. 1, p. 1.

419. C. K. Chung, and Chang, W. T., in *Handbook of Manufacturing, Engineering and Technology*, ed. A. Y. C. Nee, Springer, London, 2015, ch. 80, p. 2891.

420. A. Younis, Chu, D., and Li, S., in *Handbook of Manufacturing, Engineering and Technology*, ed. A. Y. C. Nee, Springer, London, 2015, ch. 79, p. 2851.

421. A. J. Bard, Faulkner, L. R., in *Electrochemical Methods: Fundamentals and Applications*, ed. E. Swain, John Wiley & Sons, Inc., 2nd edn., 2001, ch. 1, p. 2.

422. Á. Colina Santamaría, presented in Análisis Instrumental - Issue 9, Year 2 of BSci in Chemistry, University of Burgos, Burgos, 2012.

423. A. J. Bard, Faulkner, L. R., in *Electrochemical Methods: Fundamentals and Applications*, ed. E. Swain, John Wiley & Sons, Inc., 2nd edn., 2001, ch. 1, pp. 18-19.

424. A. D. McNaught, A. Wilkinson and S. J. Chalk, in *Compendium of chemical terminology*, Blackwell Science Oxford, 1997.

425. Shodor.org, https://bit.ly/Disproportionation, (accessed June 2020).

426. Á. Colina Santamaría, presented in Análisis Instrumental - Issue 10, Year 2 of BSci in Chemistry, University of Burgos, Burgos, 2012.

427. A. J. Bard, Faulkner, L. R., in *Electrochemical Methods: Fundamentals and Applications*, ed. E. Swain, John Wiley & Sons, Inc., 2nd edn., 2001, ch. 1, pp. 9-10.

428. S. Tan, PhD thesis, University of Warwick and Monash University, 2017, p. 2.

429. S. Tan, PhD, University of Warwick and Monash University, 2017, p. 6.

430. S. Tan, PhD, University of Warwick and Monash University, 2017, pp. 4-6.

431. A. J. Bard, Faulkner, L. R., in *Electrochemical Methods: Fundamentals and Applications*, ed. E. Swain, John Wiley & Sons, Inc., 2nd edn., 2001, ch. 1, pp. 28-29.

432. A. J. Bard, Faulkner, L. R., in *Electrochemical Methods: Fundamentals and Applications*, ed. E. Swain, John Wiley & Sons, Inc., 2nd edn., 2001, ch. 4, p. 146.

433. A. J. Bard, Faulkner, L. R., in *Electrochemical Methods: Fundamentals and Applications*, ed. E. Swain, John Wiley & Sons, Inc., 2nd edn., 2001, ch. 4, pp. 148-151.

434. A. Kołodziej, PhD thesis, University of Birmingham, 2019, pp 31-32.

435. A. J. Bard, Faulkner, L. R., in *Electrochemical Methods: Fundamentals and Applications*, ed. E. Swain, John Wiley & Sons, Inc., 2nd edn., 2001, ch. 1, pp. 11-14.

436. A. J. Bard, Faulkner, L. R., in *Electrochemical Methods: Fundamentals and Applications*, ed. E. Swain, John Wiley & Sons, Inc., 2nd edn., 2001, ch. 1, pp. 544-563.

437. R. A. Marcus, *Electrochim. Acta*, 1968, **13**, 995-1004.

438. R. A. Marcus, *J. Chem. Phys.*, 1956, **24**, 966-978.

439. A. J. Bard, Faulkner, L. R., in *Electrochemical Methods: Fundamentals and Applications*, ed. E. Swain, John Wiley & Sons, Inc., 2nd edn., 2001, ch. 3, pp. 115-117.

440. H. Taube, *Electron transfer reactions of complex ions in solution*, Elsevier, 2012.

441. E. Merzbacher, *Phys. Today*, 2002, **55**, 44-50.

442. A. J. Bard, Faulkner, L. R., in *Chapter 3 - Electrochemical Methods: Fundamentals and Applications*, ed. E. Swain, John Wiley & Sons, Inc., 2nd edn., 2001, ch. 3, pp. 130-132.

443. D. J. Wold, R. Haag, M. A. Rampi and C. D. Frisbie, *J. Phys. Chem. B*, 2002, **106**, 2813-2816.

444. W. Wang, T. Lee, I. Kretzschmar and M. A. Reed, *Nano Lett.*, 2004, **4**, 643-646.

445. F. Scholz, *ChemTexts*, 2015, **1**, 17.

446. A. J. Bard, G. Inzelt and F. Scholz, *Electrochemical Dictionary*, Springer, Berlin, Heidelberg, 2012.

447. A. J. Bard, Faulkner, L. R., in *Electrochemical Methods: Fundamentals and Applications*, ed. E. Swain, John Wiley & Sons, Inc., 2nd edn., 2001, ch. 5, pp. 156-157.

448. N. Elgrishi, K. J. Rountree, B. D. McCarthy, E. S. Rountree, T. T. Eisenhart and J. L. Dempsey, *J. Chem. Educ.*, 2018, **95**, 197-206.

449. D. S. Silvester, PhD thesis, University of Oxford, 2008, p. 21.

450. P. J. S. Richardt, R. W. Gable, A. M. Bond and A. G. Wedd, *Inorg. Chem.*, 2001, **40**, 703-709.

451. B. K. Ghosh and A. Chakravorty, *Coord. Chem. Rev.*, 1989, **95**, 239-294.

452. T. Matsubara and P. C. Ford, *Inorg. Chem.*, 1976, **15**, 1107-1110.

453. Y. B. Vogel, A. Molina, J. Gonzalez and S. Ciampi, *Anal. Chem.*, 2019, **91**, 5929-5937.

454. A. A. Carmona-Martínez, F. Harnisch, U. Kuhlicke, T. R. Neu and U. Schröder, *Bioelectrochemistry*, 2013, **93**, 23-29.

455. M. A. Murphy, G. D. Wilcox, R. H. Dahm and F. Marken, *Electrochem. commun.*, 2003, **5**, 51-55.

456. D. Mampallil, K. Mathwig, S. Kang and S. G. Lemay, *J. Phys. Chem. Lett.*, 2014, **5**, 636-640.

457. E. M. Geniès, M. Lapkowski and J. F. Penneau, *J. Electroanal. Chem. and Interfacial Electrochemistry*, 1988, **249**, 97-107.

458. S. Alehashem, F. Chambers, J. W. Strojek, G. M. Swain and R. Ramesham, *Anal. Chem.*, 1995, **67**, 2812-2821.

459. X. Kang, J. Wang, H. Wu, J. Liu, I. A. Aksay and Y. Lin, *Talanta*, 2010, **81**, 754-759.

460. G. A. Mabbott, *J. Chem. Educ.*, 1983, **60**, 697.

461. F. Malz and H. Jancke, *J. Pharm. Biomed. Anal.*, 2005, **38**, 813-823.

462. E. P. Randviir, J. P. Metters, J. Stainton and C. E. Banks, *Analyst*, 2013, **138**, 2970-2981.

463. S. P. Kounaves, in *Voltammetric Tecniques*, ed. F. A. Settles, Prentice Hall, 1997, 709-726.

464. A. Molina and J. González, in *Pulse voltammetry in physical electrochemistry and electroanalysis*, ed. F. Scholz, Springer, 2016, ch. 1, pp. 63-64.

465. C. Brett and A. M. O. Brett, in *Electroanalysis*, OUP Oxford, 1998, ch. 4, pp. 54-55.

466. Britannica, https://bit.ly/ElectricalImpedance, (accessed April 2021).

467. A. J. Bard, Faulkner, L. R., in *Electrochemical Methods: Fundamentals and Applications*, ed. E. Swain, John Wiley & Sons, Inc., 2nd edn., 2001, ch. 10, pp. 368-369.

468. A. J. Bard, Faulkner, L. R., in *Electrochemical Methods: Fundamentals and Applications*, ed. E. Swain, John Wiley & Sons, Inc., 2nd edn., 2001, ch. 10, pp. 368-388.

469. B.-Y. Chang and S.-M. Park, *Annual Review of Anal. Chem.*, 2010, **3**, 207-229.

470. J.-Y. Park, Y.-S. Lee, B. H. Kim and S.-M. Park, *Anal. Chem.*, 2008, **80**, 4986-4993.

471. N. Huang, M. M. Siegel, G. H. Kruppa and F. H. Laukien, *J. Am. Soc. Mass. Spectrom.*, 1999, **10**, 1166-1173.

472. D. N. Crisan, O. Creese, R. Ball, J. L. Brioso, B. Martyn, J. Montenegro and F. Fernandez-Trillo, *Polym. Chem.*, 2017, **8**, 4576-4584.

473. O. V. Dolomanov, L. J. Bourhis, R. J. Gildea, J. A. K. Howard and H. Puschmann, *J. Appl. Crystallogr.*, 2009, **42**, 339-341.

474. G. Sheldrick, *Acta Cryst. A.*, 2008, **64**, 112.

475. G. M. Sheldrick, *Acta Crystallogr. C Struct. Chem.*, 2015, **71**, 3-8.

476. R. Singh and G. M. Whitesides, *JACS*, 1990, **112**, 1190-1197.

477. H. Yanagawa, K. Tadahiro, H. Sagami and Y. Kitahara, *Synthesis*, 1973, **1973**, 607-608.

478. L. Teuber and C. Christophersen, *Acta. Chem. Scand*, 1988, **42**, 629.

479. V. Theodorou, K. Skobridis, A. G. Tzakos and V. Ragoussis, *Tetrahedron Lett.*, 2007, **48**, 8230-8233.

480. B. E. Hoogenboom, P. J. Ihrig, A. N. Langsjoen, C. J. Linn and S. D. Mulder, *J. Chem. Educ.*, 1991, **68**, 689.

481. J. Souza-Garcia, A. Berná, E. A. Ticianelli, V. Climent and J. M. Feliu, *J. Electroanal. Chem.*, 2011, **660**, 276-284.

482. J. M. Tarbell and L. M. Cancel, *J. Intern. Med.*, 2016, **280**, 97-113.

483. A. K. Bhunia, in *Foodborne Microbial Pathogens: Mechanisms and Pathogenesis*, ed. A. K. Bhunia, Springer, New York (USA), 2018, ch. 4, pp. 87-115.

484. N. Arabyan, D. Park, S. Foutouhi, A. M. Weis, B. C. Huang, C. C. Williams, P. Desai, J. Shah, R. Jeannotte, N. Kong, C. B. Lebrilla and B. C. Weimer, *Sci. Rep.*, 2016, **6**, 29525.

485. J. Martinez, J., M. A. Mulvey, J. D. Schilling, J. S. Pinkner and S. J. Hultgren, *EMBO J.*, 2000, **19**, 2803-2812.

486. N. Sharon and H. Lis, *Sci. Am.*, 1993, **268**, 82-89.

487. J. H. Seo, C. S. Kim, B. H. Hwang and H. J. Cha, *Nanotechnology*, 2010, **21**, 215101.

488. J. L. de Paz and P. H. Seeberger, *QSAR Comb. Sci.*, 2006, **25**, 1027-1032.

489. S. Fukui, T. Feizi, C. Galustian, A. M. Lawson and W. Chai, *Nat. Biotechnol.*, 2002, **20**, 1011-1017.

490. M. Lee and I. Shin, *Org. Lett.*, 2005, **7**, 4269-4272.

491. M. Mrksich, *Chem. Soc. Rev.*, 2000, **29**, 267-273.

492. T. Weber, V. Chandrasekaran, I. Stamer, M. B. Thygesen, A. Terfort and T. K. Lindhorst, *Angew. Chem. Int. Ed.*, 2014, **53**, 14583-14586.

493. J. H. Seo, K. Adachi, B. K. Lee, D. G. Kang, Y. K. Kim, K. R. Kim, H. Y. Lee, T. Kawai and H. J. Cha, *Bioconjugate Chem.*, 2007, **18**, 2197-2201.

494. M. Mrksich and G. M. Whitesides, *Annu. Rev. Biophys. Biomol. Struct.*, 1996, **25**, 55-78.

495. M. A. Cooper, M. T. Fiorini, C. Abell and D. H. Williams, *Bioorg. Med. Chem.*, 2000, **8**, 2609-2616.

496. A. Subramanian, J. Irudayaraj and T. Ryan, *Biosens. Bioelectron.*, 2006, **21**, 998-1006.

497. S. Hideshima, H. Hinou, D. Ebihara, R. Sato, S. Kuroiwa, T. Nakanishi, S. Nishimura and T. Osaka, *Anal. Chem.*, 2013, **85**, 5641-5644.

498. C. Cao, Y. Zhang, C. Jiang, M. Qi and G. Liu, *ACS Appl. Mater. Interfaces*, 2017, **9**, 5031-5049.

499. G. J. Zhang, M. J. Huang, J. J. Ang, E. T. Liu and K. V. Desai, *Biosens. Bioelectron.*, 2011, **26**, 3233-3239.

500. F. Davis and S. P. J. Higson, *Biosens. Bioelectron.*, 2005, **21**, 1-20.

501. M. Curreli, C. Li, Y. Sun, B. Lei, M. A. Gundersen, M. E. Thompson and C. Zhou, *JACS*, 2005, **127**, 6922-6923.

502. J. J. Gooding and S. Ciampi, *Chem. Soc. Rev.*, 2011, **40**, 2704-2718.

503. D. Echeverri, M. Garg, D. Varón Silva and J. Orozco, *Talanta*, 2020, **217**, 121117.

504. D. Jeong and W. Y. Lee, *J. Electroanal. Chem.*, 2020, **856**, 113735.

505. Z. Shen, M. Huang, C. Xiao, Y. Zhang, X. Zeng and P. G. Wang, *Anal. Chem.*, 2007, **79**, 2312-2319.

506. W. B. Turnbull, B. L. Precious and S. W. Homans, *JACS*, 2004, **126**, 1047-1054.

507. J. B. Heim, V. Hodnik, J. E. Heggelund, G. Anderluh and U. Krengel, *Sci. Rep.*, 2019, **9**, 12243.

508. N. Bunyakul, C. Promptmas and A. J. Baeumner, *Anal. Bioanal. Chem.*, 2015, **407**, 727-736.

509. N. Bunyakul, K. A. Edwards, C. Promptmas and A. J. Baeumner, *Anal. Bioanal. Chem.*, 2009, **393**, 177-186.

510. S. Karapetis, G.-P. Nikoleli, C. G. Siontorou, D. P. Nikolelis, N. Tzamtzis and N. Psaroudakis, *Electroanalysis*, 2016, **28**, 1584-1590.

511. L. Alfonta, I. Willner, D. J. Throckmorton and A. K. Singh, *Anal. Chem.*, 2001, **73**, 5287-5295.

512. E. Fan, E. A. Merritt, Z. Zhang, J. C. Pickens, C. Roach, M. Ahn and W. G. J. Hol, *Acta Crystallogr. D*, 2001, **57**, 201-212.

513. E. A. Merritt, T. K. Sixma, K. H. Kalk, B. A. M. van Zanten and W. G. J. Hol, *Mol. Microbiol.*, 1994, **13**, 745-753.

514. A. V. Gudmundsdottir, C. E. Paul and M. Nitz, *Carbohydr. Res.* 2009, **344**, 278-284.

515. F. Franks, P. J. Lillford and G. Robinson, *J. Chem. Soc., Faraday Trans. 1*, 1989, **85**, 2417-2426.

516. Y. Zhu, J. Zajicek and A. S. Serianni, *J. Org. Chem.*, 2001, **66**, 6244-6251.

517. C. J. McGill and P. R. Westmoreland, *J. Phys. Chem. A*, 2019, **123**, 120-131.

518. P. W. Wertz, J. C. Garver and L. Anderson, *JACS*, 1981, **103**, 3916-3922.

519. K. Godula and C. R. Bertozzi, *JACS*, 2010, **132**, 9963-9965.

520. S. Kuss, R. A. S. Couto, R. M. Evans, H. Lavender, C. C. Tang and R. G. Compton, *Anal. Chem.*, 2019, **91**, 4317-4322.

521. Z. Altintas, M. Akgun, G. Kokturk and Y. Uludag, *Biosens. Bioelectron.*, 2018, **100**, 541-548.

522. F. Arduini, S. Guidone, A. Amine, G. Palleschi and D. Moscone, *Sens. Actuators B Chem.*, 2013, **179**, 201-208.

523. S. C. Mitchell and R. H. Waring, *Phytochemistry*, 2014, **97**, 5-10.

524. H. Yang, H. Zhou, H. Hao, Q. Gong and K. Nie, *Sens. Actuators B Chem.*, 2016, **229**, 297-304.

525. D. Lin, R. G. Pillai, W. E. Lee and A. B. Jemere, *Microchim. Acta*, 2019, **186**, 169.

526. K. A. Peterlinz and R. Georgiadis, *Langmuir*, 1996, **12**, 4731-4740.

527. Y. Han and K. Uosaki, *Electrochim. Acta*, 2008, **53**, 6196-6201.

528. D. S. Karpovich and G. J. Blanchard, *Langmuir*, 1994, **10**, 3315-3322.

529. L. Schotte and H. Ström, 1956, **10**, 687-688.

530. E. Morera, F. Pinnen and G. Lucente, *Org. Lett.*, 2002, **4**, 1139-1142.

531. A. J. Morgan, S. Nguyen, V. Uttamsingh, G. Bridson, S. Harbeson, R. Tung and C. E. Masse, *J. Labelled Compd. Radiopharm.*, 2011, **54**, 613-624.

532. F. Denonne , S. Célanire, B. Christophe, S. Defays, C. Delaunoy, M.-L. Delporte, E. Detrait, V. Durieu, M. Gillard, Y. Lamberty, G. Lorent, J.-M. Nicolas, A. Vanbellinghen, N. Van Houtvin and L. Provins, *ChemMedChem*, 2011, **6**, 1559-1565.

533. S. Roy, S. Shinde, G. A. Hamilton, H. E. Hartnett and A. K. Jones, *Eur. J. Inorg. Chem.*, 2011, **2011**, 1050-1055.

534. A. Venditti, M. Mandrone, A. M. Serrilli, A. Bianco, C. Iannello, F. Poli and F. Antognoni, *J. Agric. Food Chem.*, 2013, **61**, 6848-6855.

535. D. G. van Greunen, W. Cordier, M. Nell, C. van der Westhuyzen, V. Steenkamp, J.-L. Panayides and D. L. Riley, *Eur. J. Med. Chem.*, 2017, **127**, 671-690.

536. E. Juaristi, F. Díaz, G. Cuéllar and H. A. Jiménez-Vázquez, *J. Org. Chem.*, 1997, **62**, 4029-4035.

537. S. Kłossowski, A. Muchowicz, M. Firczuk, M. Świech, A. Redzej, J. Golab and R. Ostaszewski, *J. Med. Chem.*, 2012, **55**, 55-67.

538. J. R. Rumble, in *CRC Handbook of Chemistry and Physics*, ed. J. R. Rumble, CRC Press/Taylor & Francis, Boca Raton (USA), 102nd (Internet Version 2021) edn., 2021.

539. J. P. Guthrie, *Can. J. Chem.*, 1978, **56**, 2342-2354.

540. G. W. Kabalka, M. Varma, R. S. Varma, P. C. Srivastava and F. F. Knapp, *J. Org. Chem.*, 1986, **51**, 2386-2388.

541. T. W. Bentley, M. Christl, R. Kemmer, G. Llewellyn and J. E. Oakley, *J. Chem. Soc., Perkin Trans. 2*, 1994, DOI: 10.1039/P29940002531, 2531-2538.

542. J. Ashenhurst, https://bit.ly/TosylatesMesylates, (accessed July 2020).

543. J. Clayden, N. Greeves and S. Warren, in *Organic Chemistry*, Oxford University Press, 2012, 2nd edn., ch. 10, pp. 344-346.

544. S. M. Mali and H. N. Gopi, *J. Org. Chem.*, 2014, **79**, 2377-2383.

545. C. H. De Puy, S. Gronert, A. Mullin and V. M. Bierbaum, *JACS*, 1990, **112**, 8650-8655.

546. J. Clayden, N. Greeves and S. Warren, in *Organic Chemistry*, Oxford University Press, 2012, 2nd edn., ch. 10, pp. 340-343.

547. G. Vayner, K. N. Houk, W. L. Jorgensen and J. I. Brauman, *JACS*, 2004, **126**, 9054-9058.

548. F. A. Carey and R. J. Sundberg, in *Advanced Organic Chemistry.*, Springer, 5th edn., 2007, vol. A: Structure and Mechanisms, ch. 7, p. 667.

549. J. Dai, Z. Li, J. Jin, J. Cheng, J. Kong and S. Bi, *J. Electroanal. Chem.*, 2008, **624**, 315-322.

550. E. de la Llave, R. Clarenc, D. J. Schiffrin and F. J. Williams, *J. Phys. Chem. C*, 2014, **118**, 468-475.

551. D. V. Leff, L. Brandt and J. R. Heath, *Langmuir*, 1996, **12**, 4723-4730.

552. L. E. Valenti, M. B. Paci, C. P. De Pauli and C. E. Giacomelli, *Anal. Biochem.*, 2011, **410**, 118-123.

553. J. M. Delgado, R. Blanco, J. M. Orts, J. M. Pérez and A. Rodes, *J. Phys. Chem. C*, 2009, **113**, 989-1000.

554. V. V. Andrushchenko, H. J. Vogel and E. J. Prenner, *J. Pept. Sci.*, 2007, **13**, 37-43.

555. J. R. Rumble, in *CRC Handbook of Chemistry and Physics*, ed. J. R. Rumble, CRC Press/Taylor & Francis, Boca Ratón (USA), 101 (Internet Version 2020) edn., 2020.

556. W. K. Surewicz, H. H. Mantsch and D. Chapman, *Biochemistry*, 1993, **32**, 389-394.

557. NIST, https://bit.ly/TFA_NIST, (accessed July 2020).

558. K. A. Kristoffersen, A. van Amerongen, U. Böcker, D. Lindberg, S. G. Wubshet, H. de Vogel-van den Bosch, S. J. Horn and N. K. Afseth, *Sci. Rep.*, 2020, **10**, 7844.

559. M. J. Little, N. Aubry, M.-E. Beaudoin, N. Goudreau and S. R. LaPlante, *J. Pharm. Biomed. Anal.*, 2007, **43**, 1324-1330.

560. H. Gaussier, H. Morency, M. C. Lavoie and M. Subirade, *Appl. Environ. Microbiol.*, 2002, **68**, 4803-4808.

561. O. Creese, PhD thesis, University of Birmingham, 2020, pp. 133-140.

562. J. E. Gurst, *J. Chem. Educ.*, 1991, **68**, 1003.

563. C. Schröter, B. Roelfs and T. Solomun, *Surf. Sci.*, 1997, **380**, L441-L445.

564. N. George, S. Ofori, S. Parkin and S. G. Awuah, *RSC Adv.*, 2020, **10**, 24017-24026.

565. G. Han, M. Tamaki and V. J. Hruby, *J. Pept. Res.*, 2001, **58**, 338-341.

566. Z. Shi and J. Lipkowski, *J. Electroanal. Chem.*, 1996, **403**, 225-239.

567. O. M. Magnussen, B. M. Ocko, R. R. Adzic and J. X. Wang, *Phys. Rev. B*, 1995, **51**, 5510.

568. LibreTexts, https://bit.ly/Chemical_Shift, (accessed October 2020).

569. A. B. Lopes, E. Miguez, A. E. Kümmerle, V. M. Rumjanek, C. A. Fraga and E. J. Barreiro, *Molecules*, 2013, **18**.

570. O. Creese, PhD thesis, University of Birmingham, 2020, pp. 131-140.

571. G. H. Escamilla and G. R. Newkome, *Angew. Chem. Int. Ed.*, 1994, **33**, 1937-1940.

572. J.-H. Fuhrhop and T. Wang, *Chem. Rev.*, 2004, **104**, 2901-2938.

573. J.-H. Fuhrhop and J. Mathieu, *Angew. Chem. Int. Ed.*, 1984, **23**, 100-113.

574. J. Schneider, C. Messerschmidt, A. Schulz, M. Gnade, B. Schade, P. Luger, P. Bombicz, V. Hubert and J.-H. Fuhrhop, *Langmuir*, 2000, **16**, 8575-8584.

575. H. Kobayashi, A. Friggeri, K. Koumoto, M. Amaike, S. Shinkai and D. N. Reinhoudt, *Org. Lett.*, 2002, **4**, 1423-1426.

576. J. Burns, J. C. Butler, J. Moran and G. M. Whitesides, *J. Org. Chem.*, 1991, **56**, 2648-2650.

577. J. McNulty, V. Krishnamoorthy, D. Amoroso and M. Moser, *Biorg. Med. Chem. Lett.*, 2015, **25**, 4114-4117.

578. K. S. Iyer and W. A. Klee, *J. Biol. Chem.*, 1973, **248**, 707-710.

579. W. Konigsberg, in *Methods in Enzymology*, Academic Press, 1972, vol. 25, pp. 185-188.

580. O. Smithies, *Science*, 1965, **150**, 1595.

581. J. M. Langenhan, R. P. McLaughlin, S. A. Loskot, L. M. Rozal, M. S. Clay and P. J. Alaimo, *J. Carbohydr. Chem.*, 2016, **35**, 106-117.

582. V. Chandrasekaran, H. Jacob, F. Petersen, K. Kathirvel, F. Tuczek and T. K. Lindhorst, *Chem. Eur. J.*, 2014, **20**, 8744-8752.

583. A. Schoen and E. Freire, *Biochemistry*, 1989, **28**, 5019-5024.

584. M. Mammen, S.-K. Choi and G. M. Whitesides, *Angew. Chem. Int. Ed.*, 1998, **37**, 2754-2794.

585. H. Lin, E. N. Kitova and J. S. Klassen, *J. Am. Soc. Mass. Spectrom.*, 2014, **25**, 104-110.

586. C. A. Hunter and H. L. Anderson, *Angew. Chem. Int. Ed.*, 2009, **48**, 7488-7499.

587. M. F. Perutz, *Q. Rev. Biophys*, 1989, **22**, 139-237.

588. S. I. Jeon, J. H. Lee, J. D. Andrade and P. G. De Gennes, *J. Colloid Interface Sci.*, 1991, **142**, 149-158.

589. S. Lowe, N. M. O'Brien-Simpson and L. A. Connal, *Polym. Chem.*, 2015, **6**, 198-212.

590. S. Chen, L. Li, C. Zhao and J. Zheng, *Polymer*, 2010, **51**, 5283-5293.

591. Y. Miura, *Polym. J.*, 2012, **44**, 679-689.

592. J. B. Lowe and J. D. Marth, *Annu. Rev. Biochem*, 2003, **72**, 643-691.

593. N. Sharon, *Complex carbohydrates, their chemistry, biosynthesis, and functions*, Addison-Wesley Pub. Co., Advanced Book Program, 1975.

594. Y. Miura, Y. Hoshino and H. Seto, *Chem. Rev.*, 2016, **116**, 1673-1692.

595. Y. Wang, R. Narain and Y. Liu, *Langmuir*, 2014, **30**, 7377-7387.

596. H.-T. Deng, Z.-K. Xu, Z.-W. Dai, J. Wu and P. Seta, *Enzyme Microb. Technol.*, 2005, **36**, 996-1002.

597. K. H. Mortell, R. V. Weatherman and L. L. Kiessling, *JACS*, 1996, **118**, 2297-2298.

598. B. D. Polizzotti and K. L. Kiick, *Biomacromolecules*, 2006, **7**, 483-490.

599. L. L. Kiessling and J. C. Grim, *Chem. Soc. Rev.*, 2013, **42**, 4476-4491.

600. S. R. S. Ting, G. Chen and M. H. Stenzel, *Polym. Chem.*, 2010, **1**, 1392-1412.

601. S. G. Spain, M. I. Gibson and N. R. Cameron, *J. Polym. Sci., Part A: Polym. Chem.*, 2007, **45**, 2059-2072.

602. M. Okada, *Prog. Polym. Sci.*, 2001, **26**, 67-104.

603. J. Chiefari, Y. K. Chong, F. Ercole, J. Krstina, J. Jeffery, T. P. T. Le, R. T. A. Mayadunne, G. F. Meijs, C. L. Moad, G. Moad, E. Rizzardo and S. H. Thang, *Macromolecules*, 1998, **31**, 5559-5562.

604. C. Barner-Kowollik, T. P. Davis, J. P. A. Heuts, M. H. Stenzel, P. Vana and M. Whittaker, *Journal of Polymer Science Part A: Polym. Chem.*, 2003, **41**, 365-375.

605. O. Creese, P. Adoni, G. Su, A. Romanyuk and P. Fernandez-Trillo, *Polym. Chem.*, 2019, **10**, 5645-5651.

606. D. J. Keddie, G. Moad, E. Rizzardo and S. H. Thang, *Macromolecules*, 2012, **45**, 5321-5342.

607. M. Benaglia, J. Chiefari, Y. K. Chong, G. Moad, E. Rizzardo and S. H. Thang, *JACS*, 2009, **131**, 6914-6915.

608. J. Bartels, S. Grajales, K. Patel, K. V. B. Josyula, G. Panambur and S. Batcheller, https://bit.ly/RAFT_Agent, (accessed April 2021).

609. Z. Deng, S. Li, X. Jiang and R. Narain, *Macromolecules*, 2009, **42**, 6393-6405.

610. A. Gregory and M. H. Stenzel, *Prog. Polym. Sci.*, 2012, **37**, 38-105.

611. M. A. Gauthier, M. I. Gibson and H.-A. Klok, *Angew. Chem. Int. Ed.*, 2009, **48**, 48-58.

612. P. Theato and H.-A. Klok, *Functional polymers by post-polymerization modification*, Wiley Online Library, 2012.

613. O. Creese, PhD thesis, University of Birmingham, 2020, pp. 127-162.

614. R. Bahulekar, T. Tokiwa, J. Kano, T. Matsumura, I. Kojima and M. Kodama, *Carbohydr. Polym.*, 1998, **37**, 71-78.

615. X. Zhu and R. R. Schmidt, *Angew. Chem. Int. Ed.*, 2009, **48**, 1900-1934.

616. J. Skey and R. K. O'Reilly, *Chem. Commun.*, 2008, DOI: 10.1039/B804260H, 4183-4185.

617. S. Perrier, *Macromolecules*, 2017, **50**, 7433-7447.

618. A. Cuesta, M. Kleinert and D. M. Kolb, *Phys. Chem. Chem. Phys.*, 2000, **2**, 5684-5690.

619. F. Silva and A. Martins, *Electrochim. Acta*, 1998, **44**, 919-929.

620. D. M. Kolb, *Prog. Surf. Sci.*, 1996, **51**, 109-173.

621. R. C. Salvarezza and P. Carro, *J. Electroanal. Chem.*, 2018, **819**, 234-239.

622. K. Tamada, T. Ishida, W. Knoll, H. Fukushima, R. Colorado, M. Graupe, O. E. Shmakova and T. R. Lee, *Langmuir*, 2001, **17**, 1913-1921.

623. W. H. Binder and R. Sachsenhofer, *Macromol. Rapid Commun.*, 2007, **28**, 15-54.

624. R. A. Decréau, J. P. Collman and A. Hosseini, *Chem. Soc. Rev.*, 2010, **39**, 1291-1301.

625. J. P. Collman, N. K. Devaraj and C. E. D. Chidsey, *Langmuir*, 2004, **20**, 1051-1053.

626. Y. Ikada, *Biomaterials*, 1994, **15**, 725-736.

627. G. K. Such, J. F. Quinn, A. Quinn, E. Tjipto and F. Caruso, *JACS*, 2006, **128**, 9318-9319.

628. S. Fleischmann, K. Hinrichs, U. Oertel, S. Reichelt, K.-J. Eichhorn and B. Voit, *Macromol. Rapid Commun.*, 2008, **29**, 1177-1185.

629. J. Kalia and R. T. Raines, *Angew. Chem. Int. Ed.*, 2008, **47**, 7523-7526.

630. S. C. Purcell and K. Godula, *Interface Focus*, 2019, **9**, 20180080.

631. C. Karman, N. Vilà and A. Walcarius, *ChemElectroChem*, 2016, **3**, 2130-2137.

632. S. Vogt, Q. Su, C. Gutiérrez-Sánchez and G. Nöll, *Anal. Chem.*, 2016, **88**, 4383-4390.

633. A. L. Eckermann, D. J. Feld, J. A. Shaw and T. J. Meade, *Coord. Chem. Rev.*, 2010, **254**, 1769-1802.

634. N. Liu, Z. Liu, H. Han and Z. Ma, *J. Mater. Chem. B*, 2014, **2**, 3292-3298.

635. M. Safavieh, M. U. Ahmed, A. Ng and M. Zourob, *Biosens. Bioelectron.*, 2014, **58**, 101-106.

636. M. U. Ahmed, S. Nahar, M. Safavieh and M. Zourob, *Analyst*, 2013, **138**, 907-915.

637. J. Lazar, C. Schnelting, E. Slavcheva and U. Schnakenberg, *Anal. Chem.*, 2016, **88**, 682-687.

638. A. Dutta Ahmed and N. Ray Chaudhuri, *J. Inorg. Nucl. Chem.*, 1971, **33**, 189-201.

639. K. K. Narang and V. P. Singh, *Synth. React. Inorg. Met.-Org. Chem.*, 1993, **23**, 971-989.

640. G. W. Bishop, B. K. Ahiadu, J. L. Smith and J. D. Patterson, *J. Electrochem. Soc.*, 2016, **164**, B23-B28.

641. C. Cannes, F. Kanoufi and A. J. Bard, *J. Electroanal. Chem.*, 2003, **547**, 83-91.

642. P. Tshikalaha and O. A. Arotiba, *Int. J. Electrochem. Sci.*, 2015, **10**, 10083-10092.

643. F. Lisdat and D. Schafer, *Anal. Bioanal. Chem*, 2008, **391**, 1555-1567.

644. M. C. Granger and G. M. Swain, *J. Electrochem. Soc.*, 1999, **146**, 4551-4558.

645. P. Chen and R. L. McCreery, *Anal. Chem.*, 1996, **68**, 3958-3965.

646. J. C. Zuaznabar-Gardona and A. Fragoso, *J. Electroanal. Chem.*, 2020, **871**, 114314.

647. J. Velmurugan, P. Sun and M. V. Mirkin, *J. Phys. Chem. C*, 2009, **113**, 459-464.

648. Q. Zheng, X. Huang, Y. Liu, X. Fang, J. Zhang and H. Shao, *J. Phys. Chem. C*, 2017, **121**, 22123-22129.

649. A. J. Bard, Faulkner, L. R., in *Electrochemical Methods: Fundamentals and Applications*, ed. E. Swain, John Wiley & Sons, Inc., 2nd edn., 2001, ch. 14, pp. 589-608.

650. R. H. Wopschall and I. Shain, *Anal. Chem.*, 1967, **39**, 1514-1527.

651. M. Hoefling, F. Iori, S. Corni and K.-E. Gottschalk, *Langmuir*, 2010, **26**, 8347-8351.

652. S. Nakata, N. Kido, M. Hayashi, M. Hara, H. Sasabe, T. Sugawara and T. Matsuda, *Biophys. Chem.*, 1996, **62**, 63-72.

653. M. V. Riquelme, H. Zhao, V. Srinivasaraghavan, A. Pruden, P. Vikesland and M. Agah, *Sens. Bio-Sens. Res.*, 2016, **8**, 47-54.

654. Y. Zhuo, R. Yuan, Y. Chai, Y. Zhang, X. Li, N. Wang and Q. Zhu, *Sens. Actuators B Chem.*, 2006, **114**, 631-639.